AUTOMATED METHODS DEVELOPMENT IN FLOW INJECTION ANALYSIS

by

PAUL MWANZA SHIUNDU

B.Sc., University of Nairobi, Kenya, 1986
CPGS, University of Cambridge, U.K., 1987

A THESIS SUBMITTED IN PARTIAL FULFILLMENT OF THE REQUIREMENTS FOR THE DEGREE OF DOCTOR OF PHILOSOPHY

in

THE FACULTY OF GRADUATE STUDIES

(Department of Chemistry)

We accept this thesis as conforming

to the required standard

THE UNIVERSITY OF BRITISH COLUMBIA

September 1991

In presenting this thesis in partial fulfilment of the requirements for an advanced degree at the University of British Columbia, I agree that the Library shall make it freely available for reference and study. I further agree that permission for extensive copying of this thesis for scholarly purposes may be granted by the head of my department or by his or her representatives. It is understood that copying or publication of this thesis for financial gain shall not be allowed without my written permission.

Department of CHEMISTRY

The University of British Columbia
Vancouver, Canada

Date OCTOBER 8, 1991

DE-6 (2/88)

ABSTRACT

A versatile computer-controlled flow injection analyzer has been constructed and used to develop and characterize five analytical methods using a variety of manifolds and modes of operation. (1) Palladium(II) was determined by its reaction with sulphochlorophenolazorhodanine monosodium salt (Na-SCPAR). The reagent was synthesized, purified and characterized. The rate constant and pre-exponential factor were then obtained by non-linear least-squares fitting. Potential interference from other ions (*e.g.*, Pt(II), Zn(II), Hg(II)) was quantified, and the pH dependence of the reaction and a masking agent used to improve specificity. Factor analysis helped determine the number of possible chemical reaction components in the mixture and elucidate the reaction mechanism. (2) Peroxydisulphate was determined via its previously unreported reaction with 3,3'-dimethoxybenzedine. The rate constant and pre-exponential factor were obtained, and potential organic and inorganic interferents assessed. Two "classical" chemistries used in comparative studies were the determination of (3) iron(II) with 1,10-phenanthroline and (4) orthophosphate by the molybdenum blue method. Finally, (5) selenium(IV) was determined via its catalytic effect on reaction of chlorate ion with phenylhydrazine: The intermediate product was coupled with 1,8-dihydroxynaphthalene-3,6-disulphonic acid to form the colored analytical species. Interference studies were undertaken and a masking agent used to improve the specificity. The pseudo-first order rate constant, pre-exponential factor and activation energy were obtained.

Automated optimization of each of these chemistries was achieved within 2 - 4 hours by the composite modified simplex algorithm. The apparatus ran replicate experiments under different chemical conditions in a sequential manner and without human intervention. This yielded significant sensitivity improvements *(e.g.*, palladium 58%; persulphate 197%), relative to initial operating conditions. The resulting analytical methods exhibited improved precision and accuracy, faster sample throughput, and decreased cost per analysis over existing manual procedures.

Previously, flow injection analysis (FIA) has almost exclusively been used to rapidly and reproducibly measure analyte concentrations. Automated FIA provides a powerful new tool by which chemical interactions (which govern analytical performance) may be thoroughly *characterized*. Reported here are the first uses of automated chemical response surface mapping in FIA. Selected surfaces were mathematically modelled. The interactions of chemical and/or physical FIA variables were investigated for all five methods; these each required 64 or 100 sets of experimental conditions, with at least four replicates. Response surface maps thus obtained were compared and contrasted with those from the simplex studies, and found to be more reliable. Also, surfaces obtained under conditions of constant and variable total flow rates were compared. Alternative responses were found to be useful for maximizing analytical performance: Examples included peak height repeatability, wavelength of maximum absorbance, and time to peak maximum. Data sets of higher dimensionality (*e.g.*, absorbance vs. time "peak shape curves" as a function of two chemical concentrations) were also generated, and are discussed.

The studies required implementation of four FIA modes of operation: Conventional, stopped flow, flow reversal and merging zones FIA. The ability of the instrument to precisely control timing of injection(s), and direction and rates of multiple flows was critical. Flow-reversal FIA provided a useful means to dynamically alter sample residence time. It allowed good control of sample dispersion and facilitated changes in "effective" reaction coil length, whilst maintaining a fixed geometry manifold. Stopped-flow FIA served to further limit sample dispersion, whilst allowing longer reaction times. The analytical performance of the first three modes was critically compared for the selenium chemistry: Flow reversal provided greatest sensitivity, but over the smallest linear dynamic range. Lastly, studies which combined merging zones and flow-reversal modes have attempted to characterize two-variable chemical interactions over a wide range of concentrations within a single complex experiment.

TABLE OF CONTENTS

LIST OF TABLES

LIST OF FIGURES

GLOSSARY

A	Absorbance
AAS	Atomic absorption spectrometry
A/D	Analog-to-digital
AC	Alternating current (amperes)
ACPS	2-amino-4-chlorophenol-6-sulphonic acid
adc	Analog-to-digital conversion (as in measurement units)
ADC	Analog-to-digital converter
AND	Digital AND-gate, as in (*e.g.*) the 74LS00 integrated circuit
AOI	Digital AND-OR-INVERT gate, as in (*e.g.*) the 74LS54 integrated circuit
ArNH	Arylamine radical
ArO	Aryloxy radical
ASCFA	Air segmented continuous flow analysis
a.u.	Absorbance units
BIOS	Basic input/output system
BI	Binary input (digital electronics; +5V = HI, 0V = = LO)
BO	Binary output (digital electronics; +5V = HI, 0V = = LO)
C	Concentration (M)
C^o	Initial sample concentration (M)
C^{max}	Maximum dispersed sample concentration
CF	Continuous flow
CFA	Continuous flow analysis
C_n	Normalized concentration (C / C^o)
CTA	Chromotropic acid
C_{total}	Total concentration of analyte present (M) in initial sample plug = C^o
D	Ruzicka's dispersion number, C^o / C^{max} (dimensionless)
$\underline{D}$	Axial diffusion coefficient ($cm^2\ s^{-1}$)
DC	Direct current (amperes)
D_m	Molecular diffusion coefficient ($cm^2\ s^{-1}$)
d	Tube diameter (mm)
δ	Dispersion number (dimensionless)
δ^2_{det}	Variance contribution of peak due to detection
D/A	Digital-to-analog
DAC	Digital-to-analog converter
DACA	Data acquisition and control adapter

DMA	Direct memory access
DMG	Dimethylglyoxime
DMGA	Dimethylglutaric acid
DOS	Disk operating system
E_a	Activation energy (Kcal/mol)
EDTA	Ethylenediamine tetraacetic acid
EGA	Enhanced graphics adapter
EVOP	Evolutionary operation (as in simplex procedure)
FIA	Flow injection analysis
FIDO	Flow injection development and optimization system
FRFIA	Flow reversal flow injection analysis
F_i	Velocity of individual streamlines (ml. min^{-1})
$\underline{F}$	Average flow velocity (ml. min^{-1})
H^o	Peak height of undiluted the dispersed sample plug
H^{max}	Peak height of dispersed sample plug
HETP	Height equivalent to a theoretical plate
HPIB	Hewlett-Packard interface bus (IEEE-488 standard parallel interface)
HPLC	High performance liquid chromatography
Hz	Hertz (s^{-1})
IC	Integrated circuit
i.d.	Internal diameter (mm)
IEEE	Institute of Electrical and Electronics Engineers
IEEE-488	General purpose interface bus; IEEE-standard high speed parallel interface
I/O	Input / Output
INH	Digital input-high (digital electronics, +5V)
k_u	Uncatalyzed pseudo-first-order rate constant (s^{-1})
L	Reactor coil length (mm)
LED	Light emitting diode
Mb	Megabyte
MHz	Megahertz
MSQB4	Microsoft QuickBasic programming language, version 4.0 (Microsoft Inc., Mississauga, ON)
MZFR-FIA	Merging zones-flow reversal FIA
m	Mass of injected sample material (g)
n	Number of simplex vertices
n	Number of experiments

N	Number of imaginary tanks-in-series between point of injection and detection
NOR	Digital Not-OR gate, as in (*e.g.*) the 74LS27 integrated circuit
Na-SCPAR	Sulphochlorophenolazorhodanine monosodium salt
ODA	*o*-dianisidine
OR	Digital OR gate, as in (*e.g.*) the 74LS32 integrated circuit
pCa	$-\log_{10}[Ca]$
pH	$-\log_{10}[H^+]$
PHDZ	Phenylhydrazine hydrochloride
ppb	Parts per billion (1 in 10^9)
ppm	Parts per million (1 in 10^6)
PTFE	Poly(tetrafluoroethylene)
PVC	Poly(vinyl chloride)
Q	Volumetric flow rate (ml. min^{-1})
R	Gas constant (8.3143 Joules K^{-1} mol^{-1})
RAM	Random access memory
ROM	Read only memory
RS-232	Serial interface
RSD%	Percent relative standard deviation
RWM	Random walk model
R_e	Reynolds number
r_i	Individual streamline's distance from the central streamline (mm)
r_o	Internal radius (mm) of flow manifold tubing
S/B	Signal-to-background ratio
S/N	Signal-to-noise ratio
SEE	Standard error of estimate
t	Time (s)
t_{mean}	Mean residence time (s)
T	Absolute temperature (Kelvin)
TMK	Thio-Michler's ketone
Δt	A small amount of time (s)
VCO	Voltage controlled oscillator output
W	Peak width - usually measured at some fraction (perhaps 50%) of the peak maximum height, H^{max}
x	Distance in the axial direction (cm)
XOR	Digital Exclusive-OR gate, as in (*e.g.*) the 74LS86 integrated circuit

ACKNOWLEDGEMENTS

I would like to express my deepest and sincere appreciation to my supervisor, Dr. A. P. Wade, whom I owe my utmost gratitude for introducing me to this exciting research, and for his tireless efforts in advice and encouragement. Many thanks also go to Dr. Peter D. Wentzell who contributed immensely by his computer programming and electronics feats during his postdoctoral work in the "laboratory for automated chemical analysis."

I would also like to thank many associates and colleagues for their useful discussions. My compliments also go to the technical staff of the department and the staff of the mechanical workshop, and electrical and electronic workshop, for their invaluable and excellent abilities. I especially thank Timothy J. Sly for the initial design and rugged construction of parts of the apparatus used and Mike J. Hatton for his assistance with the electronics hardware. Thanks are also due to Peter Borda of this department for assistance with elemental analysis. I also wish to greatly acknowledge the UBC-University Graduate Fellowship research program for three years of financial support which enabled me devote much more of my time to research.

In particular, I would like to express my greatest thanks to my parents for their continued belief in me. Last, but certainly not least, I am deeply grateful to my wife, Praxxie, for her patience and constant support.

CHAPTER ONE

INTRODUCTION

1.0 Introduction

This thesis describes the development of a fully computer-controlled research-grade flow injection analyzer, and its use in the development of several analytical schemes. In addition to implementation of conventional flow injection analysis (FIA) manifolds, the analyzer has been used for chemical and physical response surface mapping studies, flow-reversal flow injection analysis (FR-FIA), stopped-flow flow injection analysis, and merging zones - flow reversal flow injection analysis (MZFR-FIA) studies. The methods developed exhibit improved precision and accuracy, higher sample throughput rates, lower sample and reagent consumption rates, (and consequently a decreased cost per analysis) relative to manual procedures.

This thesis demonstrates that, given sufficiently versatile apparatus, the boundaries of flow injection analysis may be expanded beyond routine chemical analysis; indeed, FIA can be a highly efficient means for carrying out chemical research and characterizing chemical systems. The power of the approaches to be discussed is greatly enhanced by the multiple wavelength detection ability of the diode array spectrophotometer. Data analysis procedures reported here include mapping of multiple response surfaces for an improved FIA system characterization, factor analysis to establish chemical factor contributions to an observable, and chemical kinetic studies.

This chapter outlines the work undertaken and provides the reader with a brief but necessary discussion on the history, basic principles, some theoretical aspects specific to FIA, and applications of continuous flow techniques. A more detailed discussion on the theory of FIA may be found elsewhere. [1]

Chapter Two contains a description of the hardware of the computer-controlled apparatus and its corresponding control software. The apparatus has been referred to as a "flow injection development and optimization" system. Because of this, it has been given the acronym, FIDO (*c.f.* man's best friend). The system has the capability of controlling multiple peristaltic and syringe pumps, and valves. It can monitor several different types of

detectors. Its functions are controlled through an IBM PC-AT compatible computer. A brief discussion of each of these units is given and details of the interface circuitry are presented where appropriate. Also given is a concise overview of the major sub-units of the control algorithm, including a description of the optimization procedures.

Chapter Three demonstrates the utility of this apparatus for the automated development and characterization of analytical continuous flow methods. Details are given of methods for spectrophotometric determinations of (i) palladium using sulphochlorophenolazorhodanine monosodium salt (Na-SCPAR) reagent, and (ii) peroxydisulphate (persulphate) ions based on their oxidizing properties on dimethoxybenzidine (a substituted aromatic amine). For the palladium determination, details of the synthesis, purification and characterization of the complexing reagent (Na-SCPAR) are given. A possible reaction mechanism and reaction product(s) are postulated. A discussion on the use of the chemometric technique called factor analysis to determine possible chemical intermediates involved in this reaction is also given.

In most cases, automated simplex optimization and response surface mapping procedures were conducted to establish the optimum flow and chemical conditions. Results from these two optimization procedures are compared and contrasted. These studies also provide us with a much improved insight into the possible effects of the various chemical variables investigated. Reaction kinetics of these chemistries are also reported. In both cases, optimization and characterization studies were conducted only after a series of preliminary batch experiments were completed. Such studies include the establishment of suitable buffer systems, and working stock reagent concentrations, and the determination of the effect of ionic strength on reaction rates.

Chapter Four describes the application of the computer controlled analyzer in three advanced FIA modes of operation: (i) methods for the automated exploration and exploitation of FIA response surfaces, are proposed and demonstrated; (ii) conventional, stopped flow and flow reversal FIA methods are compared for the catalytic photometric

determination of Se(IV); (iii) proper operation of a MZFR-FIA system was established, and the characterization of this system attempted.

In the exploration and exploitation of flow injection response surface studies, three dimensional plots of instrumental responses as a function of chemical concentrations or flow parameters were obtained in an automated manner. The driving forces behind the study of these several alternative responses for FIA were; (i) to realize the experimental conditions which give best overall system performance and, (ii) to obtain a fundamental understanding of the flow and chemical interactions for these chemistries by characterizing them over the entire search space. The different response surfaces discussed are those for the palladium determination with Na-SCPAR, persulphate determination with *o*-dianisidine, phosphate determination in the molybdophosphate reaction and the determination of Fe(II) with 1,10-phenanthroline. The effects of individual experimental variables (reagent concentrations, pH, flow-rates, *etc.*), their interactions, and instrumental factors, on surface topography are discussed. The propriety of automated response surface mapping is demonstrated and the efficacies of simplex and grid search approaches to response surface exploration are contrasted. Response functions obtained include absorbance at peak maximum, percent relative standard deviation (RSD%) of maximum absorbance, time from injection to peak maximum, and wavelength of maximum absorbance. Higher dimensional response surface representations of peak shape and absorbance spectra as a function of both physical and chemical parameters are also presented. This approach to automated characterization of the chemical reactions in flow injection analysis is critically assessed.

The ability to perform high precision flow reversal and stopped-flow FIA experiments arises from the improved timing available on the hardware developed here, which is critical to the success of these studies. In the stopped-flow flow injection studies, the automatic generation of multiple stop times and establishment of optimum stop time is important. These results are compared with those from conventional flow injection studies.

Se(IV) is determined based on its catalytic effect on the oxidation of phenylhydrazine by potassium chlorate followed by a coupling reaction with chromotropic acid. It is evident from the present literature that the slow rates of color-forming reactions involving selenium have precluded wider use of conventional flow injection procedures for the determination of selenium. It is for this reason that use of flow reversal and stopped-flow modes of operation was investigated, with the intention of improving the sensitivity of the system over conventional FIA.

For the MZFR-FIA, both merging zones and flow reversal flow injection techniques are combined. Their individual and combined contributions to the dispersion characteristics are detailed, in addition to the interaction of the two overlapping chemical concentration gradients (*e.g.*, pH against concentration). Discussed are possible ways of exploiting such interactions, and how the FIDO hardware is used to facilitate the stringent timing of sequences of operations needed for such experimentation.

Chapter Five covers further work to be done on (and with) the FIDO system. Of immediate interest is the further development and characterization of the MZFR-FIA experiment to exploit its multivariate capabilities. This includes multicomponent analysis, speciation studies, and minimization of interference effects. Also important is the automation of the modelling of chemical response surfaces obtained with the FIDO apparatus; several different response functions should be considered. Development of an expert-system control and / or intelligent software for bad peak shape detection will also be important, and has been started by other members of this research group.

Chapter Six gives both specific and generic conclusions on these studies and a forecast into the future of FIA.

1.1 Automation in flow injection analysis (FIA)

Most measurements in an analytical laboratory involve samples in liquid form. These require a wide variety of solution handling processes (sampling, dilution, reagent addition, reagent solution mixing, phase separation, preconcentration, *etc.*), analyte detection, data collection and computation of results. These processes, while very tedious and time consuming, are still often performed manually. The analyte measurement stage has probably received the most attention and almost all measurement techniques used in chemical analysis have been partially or fully automated. More recently, attention has been focussed on the post-analysis stages, and data processing using computers has been extensively exploited. It is now cost-effective to use simple personal computers to control analyzer operation, calculate results, and prepare reports in a suitable format. However, by far the most demanding stages of the analytical process are sampling and sample preparation; far less work has so far been done in these areas.

Research into automation of analytical techniques is prompted by the need to produce cost-effective solutions to an ever-increasing demand for chemical analysis; this includes the growing concern for the quality of the environment, and rapid analysis of large numbers of samples with minimal labour expenses, reagent costs, waste disposal, *etc.* The latter has been believed by many people to be the sole purpose of automation. This is indeed the driving force in most clinical and many industrial laboratories where the increased precision, inherent to automated handling, is appreciated. The need for greater sample throughput rate and improved efficiency has been met by automating the apparatus and chemical processes used in classical wet chemistry. From a research or academic point of view, continuous flow automation is much more than a mere mechanization of existing procedures, since it offers much opportunity for innovation *e.g.*, several modes of the FIA experiment already exist for which there are no manual equivalents and others are being designed. Continuous flow systems are highly flexible: The flow of fluids and the mixing patterns between regions of different concentrations offer many new opportunities for

performing chemical analysis and for characterizing chemical interactions.

In general, continuous flow analysis refers to any prccess in which the concentration of analyte is measured intermittently in a stream of fluid (liquid or gas). Continuous flow analyzers can be considered as "conveyor belt" systems for wet chemical analysis. They share many of the throughput advantages of the "production line" approach in manufacturing. Continuous flow analysis (CFA) (of which FIA is an example) has proven to be an extremely versatile methodology that is simple to operate and amenable to automation. FIA has been demonstrated to be an ideal tool for the handling and pre-treatment of samples prior to their determination. Sample handling may be as simple as using FIA as a means to transport a sample to a detector or as complicated as a solvent extraction of an analyte followed by back extraction prior to reaction and detection. Application of FIA to automate chemical analysis yields a fast, precise, accurate and versatile system. This is important as large numbers of samples requiring precise and sometimes fast analysis are received in today's analytical laboratories. It is therefore no surprise that for industrial, clinical, environmental and other applications, CFA methods have replaced many previous manual methods.[2, 3] Improved repeatability, lower reagent and/or sample consumption,[4] and faster analysis times have been reported [1, 2, 5] compared with batch sample handling procedures. Typical CFA methods are capable of processing between 60 and 200 samples per hour. [1, 6] For simpler systems, rates as high as 360 samples per hour have been achieved. [7]

Fully computer-controlled flow injection methods development systems allow faster development of new analytical methods. Physical and chemical conditions which maximize sensitivity can be achieved in a minimum number of experiments. Such systems can carry out preprogrammed sequences of chemical experiments or make decisions to change their operating conditions "on the fly" (*e.g.*, simplex optimization). By using a number of proportioning pumps, each pumping a separate solution (reagent or inert carrier, buffer, *etc.*), it is possible for such systems to vary the overall pumping rate and the relative

concentration of each chemical species automatically, with minimal human intervention.

Also of prime importance is the reproducibility of timing for sequences of injections, stream switching, flow rate changes and detection operations. This enables reaction conditions to be carefully controlled; thereby, each sample is subjected to similar conditions. This has led to improved performance, particularly when the method includes stages in which reactions do not proceed to completion or where the analyte (or an intermediate) being measured is unstable. Separation techniques such as dialysis and solvent extraction, in which the recovery of the desired species is frequently incomplete, can give highly reproducible automatic performance when accurately sequenced. It is possible to employ colorimetric reactions where the stability of the colored species is inadequate for use in a manual analytical procedure. FIA offers advantages which include the possibility of increasing the range of potentially useful analytical reactions, provided that suitable standards, processed in exactly the same manner as samples, are available. An automated FIA system provides a means of carrying out an analysis in a closed system, such that materials which are toxic or unstable in air can be more conveniently analyzed than by a manual method.

1.2 Air segmented continuous flow analysis (ASCFA)

Development of FIA [1] was preceded by air-segmented continuous flow analysis (ASCFA). [8] If one excludes liquid chromatography, together these are presently the two main classes of wet chemical continuous flow methods. A brief review on ASCFA is now presented before a formal introduction of FIA.

Air segmented continuous flow analysis (ASCFA) was devised by Leonard Skeggs, a Cleveland biochemist with joint academic and hospital affiliations. The analytical technique was first developed commercially by the Technicon Corporation in 1957. Thus, ASCFA was a mature and widely applied technology well before FIA was proposed. Technicon's Auto Analyzer continuous flow system became the first widely used automated

equipment for clinical and other analyses.[8] Indeed, Technicon's practice of patenting practically every advance in this field made it difficult for other companies to compete. Technicon systems were developed mainly to handle clinical testing which required large sample throughput rates, *e.g.*, determination of glucose and urea in serum samples. Figure 1.1 is a general schematic representation of an apparatus for ASCFA.[2]

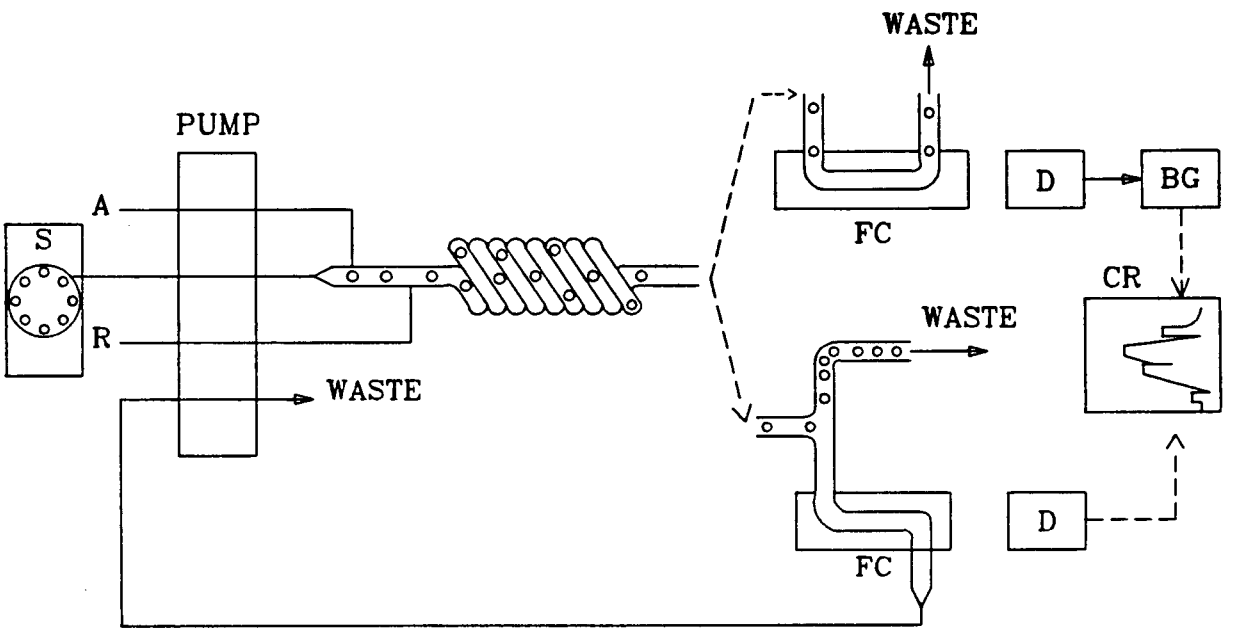

Figure 1.1 A schematic diagram for an air segmented continuous flow analyzer (ASCFA). The apparatus consists of an autosampler (typically of carousel design) containing samples (**S**), a flow manifold and a detection system. The stream marked **A** is of air (the segmenting fluid), and the stream **R** is of a color-forming reagent. The lower detection system illustrates a physical de-bubbler (**DB**) and flow cell (**FC**). The detector (**D**) sends its output directly to a chart recorder (**CR**). In the upper detection system, the de-bubbler is omitted, and its function is duplicated electronically by a bubble gate circuit (**BG**).

The hardware can essentially be divided into 3 basic subsections: the sample introduction system, the analytical cartridge (the portion between the pump and the detector) and the detector(s). Sample introduction can be via an autosampler, injection valve (usually associated with FIA) or by continuous aspiration. The sample withdrawal tube is connected to one of the peristaltic pump channels, which in turn is connected to the analytical cartridge. In ASCFA, fluid samples are intermittently aspirated at the sampler, with the resulting stream segmented with air bubbles (which act as an immiscible fluid) into many smaller, nominally identical sub units. Segmenting fluids other than air (*e.g.*, perfluorinated hydrocarbons) are also used.

The analytical cartridge, represented as a mixing coil in Figure 1.1, may be comprised of reagent addition tees, debubblers, dialyzers, reaction coils, gas diffusion cells, distillation heads, or phase separators in order to make the system more specific. Phase separation operations are not limited to ASCFA, but are also common to FIA (*e.g.*, ref. 9). In-line separation of constituents may also be achieved via coated tubes (*e.g.*, segmented-flow capillary liquid chromatography [10]).

A recording colorimeter is normally used as a detector, but many other types have been successfully interfaced to ASCFA analytical manifolds. However, with colorimetric detection systems, appropriate amounts of sample and reagent are mixed together until a "steady state" is reached at which point the absorbance is measured. Detection in ASCFA is usually complicated by the presence of air bubbles, which are compressible, highly reflective and electrically non-conductive. Because of these characteristics, their passage through most detectors is marked by artifacts that severely distort the analytical signal. Such artifacts can be removed in real time provided the response time of the detector is sufficiently fast and the volume of its measurement cell is less than that of an individual liquid segment. [11] The most frequently used option is to de-bubble the analytical stream just prior to detection. This approach has the inherent problem of pooling previously segregated liquid segments and thus decreasing the sampling rate. An alternative

procedure often used if maximum possible sampling frequency is to be achieved is by an analog or digital signal processing technique known as *bubble-gating*. This technique discriminates between air bubbles and liquid segments on the basis of conductivity, refractive index, (*etc.*) and timing, such that the air bubble artifacts are not seen at the output.

Air bubbles are included in the analytical stream of an ASCFA system to effect three primary functions:

(1) to limit sample dispersion,
(2) to promote mixing of the sample and reagents by generating turbulent flow and
(3) to scrub the inner walls of the analytical conduits.

Drawbacks of the presence of air bubbles in the flowing stream are well known [1]:

(1) air is compressible; thus, the stream tends to pulsate rather than flow regularly;
(2) the streams have to be either electronically bubble-gated or physically de-bubbled before they reach the flow cell or before being re-pumped;
(3) the size of the air bubbles has to be controlled and reproducible;
(4) different tubing materials experience different pressure drop and flow velocities in the presence of air;
(5) air bubbles in plastic tubes act as electrical insulators, which support a build up of static electricity that disturbs electrochemical sensors;
(6) the efficiency of dialysis, gas diffusion across a membrane, and solvent extraction is lowered as a result of a decrease in the effective transfer surfaces;
(7) the movement of the carrier stream cannot be exactly controlled or instantly stopped or re-started due to compressibility of gas bubbles;
(8) the apparatus is consequently rather complex and expensive.

Despite the seemingly large number of disadvantages that the presence of air bubbles have in ASCFA, it is fair to point out that ASCFA became, and to a large extent remains (on the basis of commercial success) the technique of choice for routine automated colorimetric analysis. The theoretical basis of ASCFA's operation is now well understood and the hardware required for its implementation is commercially available. The low dispersion and reproducible timing inherent in ASCFA have now facilitated automation of many manual procedures, even those that require long reaction times.

1.3 **Flow injection analysis (FIA)**

1.3.1 Brief History

The term flow injection analysis was proposed by Ruzicka and Hansen in 1975.[12] However, the concepts which underly flow injection analysis received earliest attention from electrochemists. Nagy *et al.* published their first work in a series of papers describing injection of a sample into a flowing stream of electrolyte in 1970. [13] Their system involved passage of the sample carrier stream through a magnetically stirred mixing chamber, followed by flow past a silicone-rubber based graphite electrode. The resulting analytical readout was in the form of transient peaks. The shared concepts of sample introduction, transport, and in-line detection mean that there have been obvious parallels with chromatography [14] and ASCFA.[8]

Ruzicka and Hansen [12] and Stewart *et al.*, [14] separately, were the first people to demonstrate the advantage of flow induced sample dispersion as the sample carrier stream is pumped through narrow bore tubing. This mechanism was used to effect *controlled* mixing of the sample with the stream and provide a transient response (this is in contrast with the gross mixing generated in the mechanically stirred chamber, and its potential for excessive sample dilution). These workers proved that continuous flow analysis without air

segmentation is possible and that the "steady state" assumption inherent to ASCFA is unnecessary.

Ruzicka and Hansen were the first to coin the term "flow injection analysis" and their names have since become inseparable from progress in this area. Flow injection analysis has also been referred to as unsegmented or non-segmented continuous flow analysis. Since its inception in 1974, FIA has become widely accepted as a convenient and very versatile form of continuous flow analysis. [1, 15-20] Over 3000 papers on this topic have now appeared in the literature. The majority of these deal with the development of FIA systems to replace conventional manual procedures.

1.3.2 Principles of FIA

Flow injection analysis may be defined as "a form of continuous flow analysis that utilizes an unsegmented analytical stream into which a known volume of sample is injected and transported, under highly reproducible chemical and flow conditions, to one or more detectors".

Figure 1.2 is a schematic representation of two different FIA configurations. A simple FIA system consists of a means of propelling the reagent stream, a single sample injector (a means of injecting sample directly into the reagent/carrier stream), a reaction manifold, and a detector. The injected sample is initially in the form of a plug. During transport, this then forms a well defined zone which has a parabolic leading edge. Reagents may be added while the sample plug is *en route* to the detector where the absorbance, electrode potential, or other physical parameter may be recorded continuously as it passes through the detector flow cell.

Multiple channel configurations are also possible. A more complex example, to illustrate the versatility of the FIA approach, is shown in Figure 1.3. This manifold incorporates a single solvent extraction step with a post-extraction reaction.

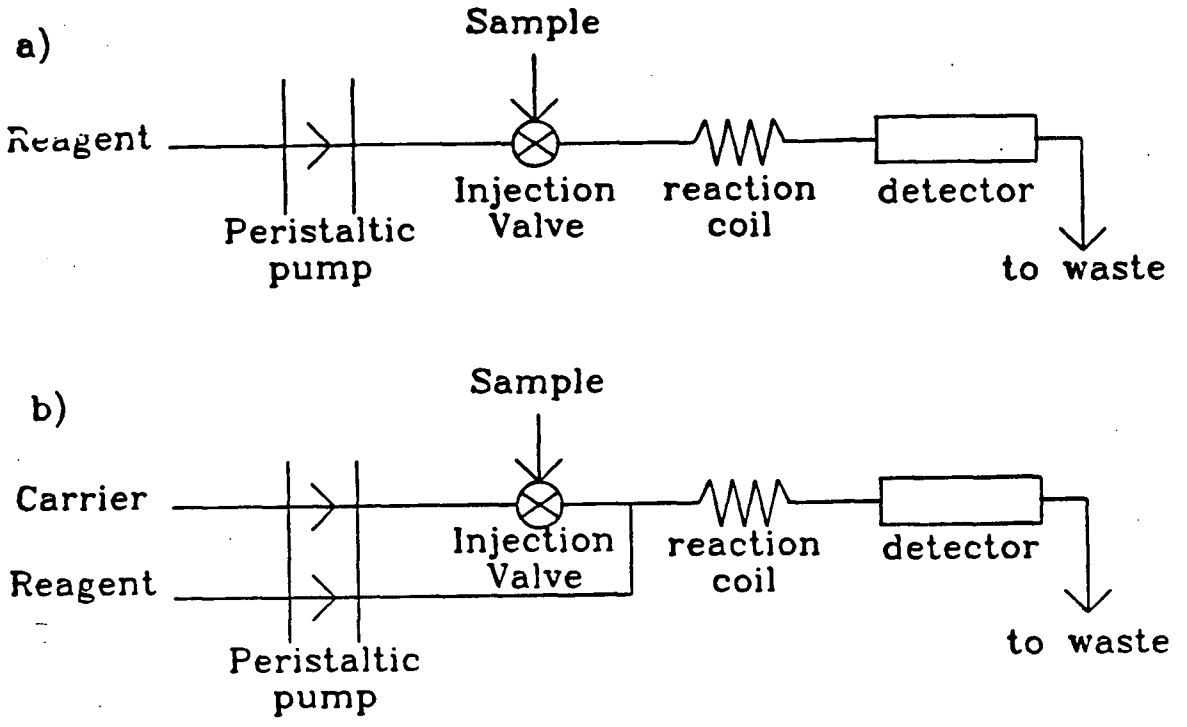

Figure 1.2 Simple FIA manifolds; (a) injection of sample directly into reagent carrier stream; (b) merging of sample (in an inert carrier) with reagent stream.

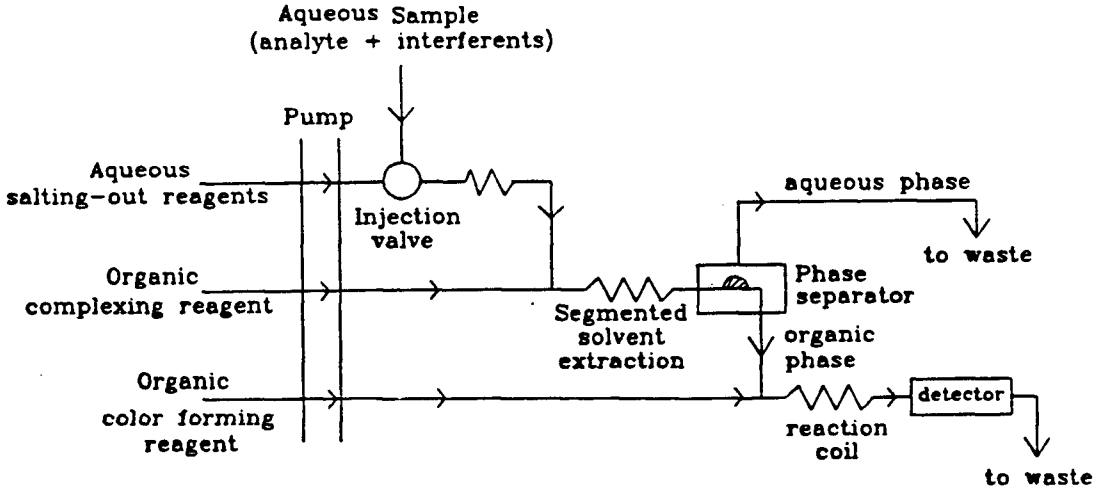

Figure 1.3 An FIA manifold incorporating solvent extraction and post-extraction reaction.

This shows an aqueous sample containing an interferent being merged with a stream containing a salting-out agent (this is meant to push as much of the analyte as possible out of the aqueous and into the organic phase). The resulting stream is then merged with a stream of an immiscible organic solvent, which may contain a complexing reagent for the analyte. The result of this is a segmented (aqueous-organic-aqueous-organic-...) stream in which solvent extraction occurs as the stream travels towards the phase separator. After extraction, both phases are separated in the phase separator, with the interferent-containing aqueous phase going to waste as the analyte in the organic phase is detected directly (usually spectrophotometrically) or subjected to a further color-forming reaction. [9]

FIA systems have also incorporated dialysis and gas diffusion cells, columns containing ion exchange resins and chelating agents, chromatographic separation steps, reactors with immobilized reagents, dilution systems, *etc.* Determinations of different analytes have been accomplished sequentially or in parallel. All these indicate the versatility of the FIA approach. A brief discussion of common FIA system components is given below.

1.3.2.1 *Pumps*

For most applications, flow rates of between 0.5 - 5 ml min^{-1} are employed. Such flow rates have been easily achieved by the use of multiple-roller peristaltic pumps or constant head systems. The most commonly used means of propulsion in CFA is the relatively inexpensive peristaltic pump. This design however has the inherent problem of pulsation of the flow pattern which causes poor baseline stability and decreased precision in measurements. For most systems pulsation is not a very serious problem and can be tolerated. However in more specialized studies such as in solvent extraction, where the relative proportions of solvents directly affect the absorbance measurements, pulsation must be minimized. Minimizing pulsation prevents pressure surges which would lead to irregular segmentation patterns, less efficient extraction, and unstable separator operation.

For systems where first derivatives of signals are measured,[21] pulsation must be minimized, otherwise high noise levels on the derivative signals would be recorded. The pulsation problem has been reduced (but not eliminated) by use of peristaltic pumps with more rollers and the insertion of "depulse coil(s)" (*e.g.*) of 2 m length between the pump and the injection valve(s). The extra length of these coils acts as a hydraulic buffer (damper). Since they are put prior to the injection valve(s), they make no contribution to dispersion of the sample.

Highly pressurized vessels have been used to propel reagent streams.[22, 23] These have used a pressure in the region of 500 psi and a very narrow bore tubing of 0.2 to 0.4 mm internal diameter to provide a constant flow of reagents. This technique is particularly useful in process control, due to the limited lifetime of the pump tubing for peristaltic pumps and the need for long periods of uninterrupted operation.

Syringe pumps offer almost pulse-free propulsion and have found increasing use in CF analyzers where pulse free studies are intended.

The simplest form of propulsion for CF methods is gravity feed. In this the carrier solution flows from a vessel placed at a level higher than the apparatus. Flow rate may be controlled by either the height of the reservoir relative to the manifold, or by a back-pressure-inducing flow constriction device at some point in the system.

1.3.2.2 *Tubing*

The material most often used for reaction manifolds is polytetrafluoroethylene (PTFE, Teflon^{R}) tubing. This is because of its chemical inertness and its lesser tendency (relative to polypropylene, polyethylene, or nylon) to become discolored. The tubing dimensions are chosen to produce the degree of mixing (between the sample and carrier stream - depending on system geometry) desired for particular applications. Coil lengths typically range from 5 to 300 cm, with internal dimensions from 0.2 mm to 1.0 mm. Tubing of 0.5 mm and 0.8 mm internal diameter (i.d.) are commonly used in our laboratory.

Larger diameter tubing causes increased dispersion while smaller internal diameter tubing can become easily clogged. The tubes may be coiled, knotted, or of a "figure of eight" design to enhance radial mixing and minimize axial dispersion.

1.3.2.3 *Sample introduction*

Samples may be injected via a manually operated syringe, flap valve, a manual or semi-automatic rotary valve, modified manual chromatography slide valve, or by multiple miniaturized solenoid valves. The flap and the rotary valves were first used by Ruzicka and Hansen. Stewart *et al.* [22] developed a fully automated sample injection system in which samples are drawn from an automatic sampler by a second pump into a slide valve, from which they enter the carrier stream.

For the flap valve, the sample volume used is between 100 - 200 μl. Because of pressure surges, it is desirable to have a length of tubing between the injection port and the carrier reservoir to act as a buffer. The precision of the flap valve however is dependent on the volume injected. The rotary valve typically dispenses 30 - 100 μl of sample. With chromatography slide valves, sample sizes of as little as 6 μl have been attained.

Most commonly used are six-port or four-port low pressure rotary valves. The operation of a six-port valve is shown in Figure 1.4. In this, a sufficient amount of sample solution is introduced into a fixed volume loop to completely displace its previous contents (using a syringe or a pump), while the valve is in the "fill" position. During this phase, the carrier stream by-passes the fixed volume loop and flows into the reaction manifold. On switching the valve to the "inject" position, the carrier stream then sweeps out the contents of the loop, transporting the sample plug downstream. The procedure can then be repeated as required.

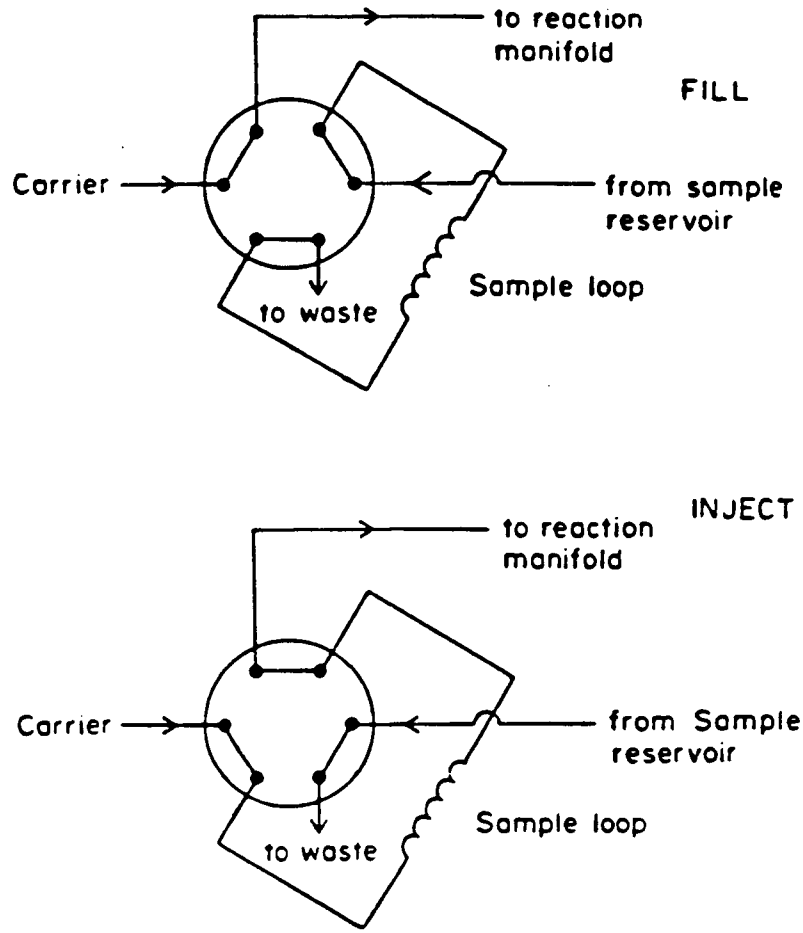

Figure 1.4 Internal workings of a six-port injection valve.

Figure 1.5 shows the internal workings of a dual four-port injection valve. The use of a very versatile twelve-port valve has also been reported.[23] Valve operation may be automated by using a solenoid-driven actuator to switch a compressed air stream, which turns the valve. Alternatively, motor-driven rotary valves and banks of miniature soleniod-driven flap valves have also been used. In our laboratory, 6-port air-driven solenoid-actuated injection valves equipped with a 70 μl sample loop are most commonly used.

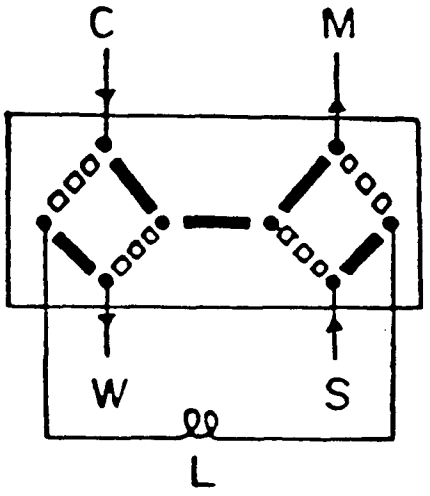

Figure 1.5 Internal workings of a dual four-port injection valve. The connections are: carrier stream (**C**), manifold (**M**), sample solution (**S**), waste (**W**) and sample loop (**L**).

1.3.2.4 *Detectors*

Different types of detectors have been used with FIA systems and these may be categorized as (spectro)photometric, spectrometric, electrochemical, or thermal. Examples of these are: UV-visible spectrophotometers, turbidimetric detectors, atomic absorption/emission spectrometers, ion-selective electrodes, conductivity cells, amperometric detectors, mass spectrometers, *etc.* Detectors such as UV-visible spectrophotometers, when used with FIA systems, utilize flow-through cells. The signals observed by the detectors are transient, rather than steady state. Some specific requirements, however, exist for FIA detectors; the considerations are similar to those for chromatography. The linearity of response, noise level, and peak broadening effects are all important. Peak broadening effects arise from flow velocity, the hold up volume of the

detector flow-through cell, speed of detector response, and time constant of the associated electronics. It is desirable that peak broadening caused by the detector, expressed as its variance δ^2_{det}, should be no more than 5% of the overall peak width.

The cell hold-up volume and its geometry have the greatest influence on the peak broadening contributed by the detector; the associated electronics are of lesser importance since they usually have a response time much shorter than 1 s. Generally, chromatographic detectors with cell volumes of below 20 μl are well suited for FIA work, although high pressure cells are unnecessary. The main difference between chromatographic and FIA detectors is that in FIA one prefers to use chemically selective detectors. In HPLC, separation occurs on the column, and it is better to use non-selective detectors that yield a readout for as many species as possible, preferably with the same sensitivity. A conductivity detector is ideal for ion chromatography, but has much more limited use in FIA since its response to different anions and cations is non-selective. Ion-selective electrodes, on the other hand, have been successfully used in FIA for the selective assays of individual cations or anions in mixtures, but find no real applications in chromatography. An exception to this rule in FIA is a case when a non-selective detector is coupled to a highly selective chemical reaction.

The other important aspect of the detection system is the cell geometry, which determines the way in which the dispersed sample zone is probed. Bulk sensing is used in optical detectors and surface sensing in the case of electrochemical detectors. In most optical sensors, the signal approximates the mean composition of the flowing stream present in the detector cell, and thus reflects the composition of the bulk of the solution. The beam penetrates the sample zone either axially (Fig. 1.6 a,b), or perpendicularly (Fig. 1.6 c) to the direction of flow. Electrochemical methods, however, rely on the transport of an electroactive species from the bulk solution through the double layer onto the electrochemically active surface.

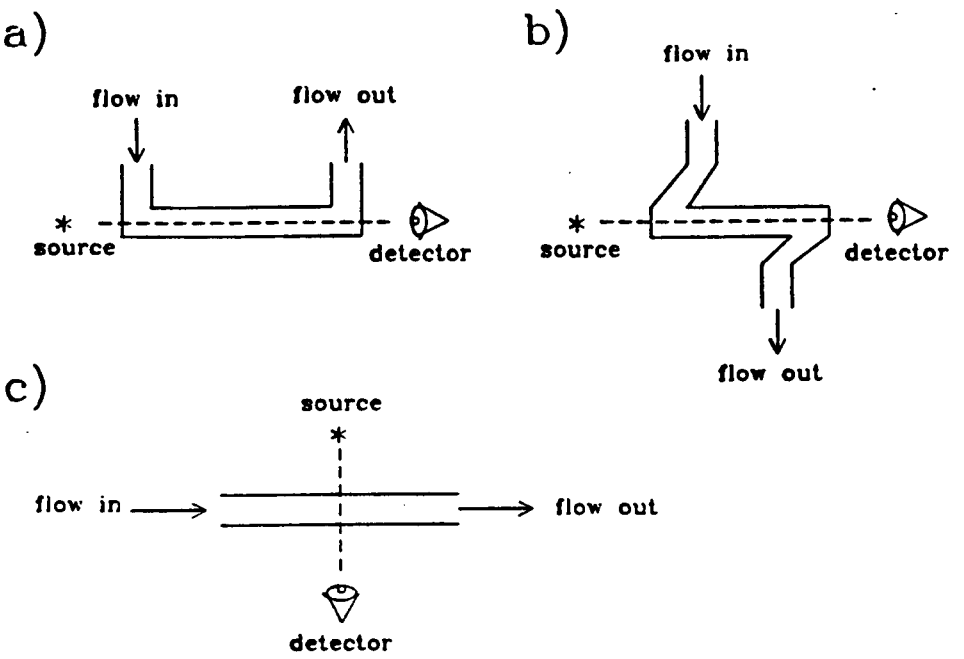

Figure 1.6 Flow-cell configurations for spectrophotometric measurements: a) U-cell, with path length 10-30 mm; b) Z-cell, as used in liquid chromatography; and c) transverse cell, with pathlength 0.8-1.0 mm.

1.3.2.5 *Signal recording*

Chart recorders have been the most common form of output devices. Other methods becoming common and more affordable include microcomputers equipped with data acquisition cards, and inexpensive digital readout systems. [25]

1.3.3 Theory of FIA

Flow injection analysis is a non-equilibrium technique since the transient signal observed does not attain a steady state (*i.e.*, neither steady state nor homogeneity are realized prior to detection). The distinctive feature of FIA is the existence of the interface zones between the sample plug and the carrier (which may or may not include reagents). The magnitude of the transient signal recorded is a function of the extent of mixing of these

components. Initially this occurs across the front and back interfaces of the plug, and eventually throughout its volume. Note that (in the absence of a directly detectable analyte) reagents and analyte must come into contact for an adequate time if a detectable *product* is to form. Mixing in FIA thus determines the reaction kinetics and physical dispersion, in what is essentially a 3-dimensional chemical reactor.

1.3.3.1 *Dispersion*

Sample dispersion is a consequence of the internal geometry of the tubing, the flow profile, and molecular diffusion. Excessive dispersion adversely affects detectability and sample throughput: It causes a peak to decrease in height and become increasingly broad with time. Therefore, in FIA studies that involve a chemical reaction, conditions must be chosen that (i) maximize the change in peak response resulting from efficient mixing of the reagent and sample components, and (ii) minimize the reduction of peak height response due to excessive dispersion. The FIA peak profile is dependent on both reaction kinetics and physical dispersion. Physical dispersion produces a concentration gradient of the sample plug within the carrier solution. In 3D, one may view the FIA manifold as an infinite number of small volumes, each of which at any one time contains different concentrations of sample, reagent(s), *etc.* These concentrations change with time and are a function of the flow profile, molecular diffusion, and/or chemical reaction. Directly measurable parameters that affect the concentration gradients lengthwise and widthwise across the tube include flow rate, temperature, viscosity, sample size, internal diameter, and length of tubing.

In characterizing FIA systems, sample dispersion is quantified as the ratio of sample concentrations before and after the dispersion process has taken place. In most FIA methods the analytical read-out is based on measurement of peak height and is therefore dependent on analyte concentration. The maximum of the recorded curve, C^{max}, can be related to the original concentration of the injected sample solution, C^{o} by the relationship:

$$D = C^{o} / C^{max} = H^{o} / H^{max} \qquad (1.1)$$

where D is the dispersion number, H^{o} is peak height of the undiluted sample, and H^{max} is the peak height of the dispersed sample. This assumes that $H \alpha C$, and for absorbance to be proportional to H (using photometric detection system), Beer's law must hold.

Ruzicka and Hansen [1] have categorized the degree of mixing and thus dispersion as either limited (D = 1 to 3), medium (D = 3 to 10), or large (D > 10). The extent of mixing can be selected to match the chemistry of the system under investigation and can be reproducibly controlled by suitable selection of values for the system parameters (flow rates, coil length, *etc*).

Limited dispersion is desirable if the aim is to present samples (without chemical modification) to such detectors as electrodes and atomic absorption spectrometers. With limited dispersion one can best determine a property (*e.g.*, pH, pCa, conductivity) of a sample solution in its original form, as these conditions ensure that the original sample composition transported through the flow cell has undergone minimal dilution. Thus, a short coil length, large sample volume, and/or high volumetric flow rates are desired. Conveniently, these result in high analytical rates.

Medium dispersion can be applied to attain a wide variety of chemical processing steps such as buffering, formation of some detectable entity such as a colored, fluorescent, or electroactive product. In these, the sample plug must be efficiently mixed with the carrier stream and sufficient time allowed to produce the desired product. Also, conditions must be chosen such that the increase in peak height due to greater chemical reaction (arising from increased mixing of reagents and sample) must be greater than that of decrease in peak height that would be caused by dispersion alone.

Large dispersion can be utilized to give a substantial degree of mixing between an injected plug and its carrier stream so as to form a well-developed concentration or pH gradient. This finds application where peak width measurements are necessary;

e.g., (i) continuous flow titrations; (ii) investigating the chemistry at the sample-stream interface in which the injected sample has to be greatly diluted so that the resulting signal can be accommodated within the dynamic range of the detector. This can be achieved with long reaction coils, gradient dilution chambers, zone sampling, *etc.*

As more recent developments and innovative FIA configurations show, the *limited*, *medium* and *large* dispersion boundary values listed above are not absolute. For example, one can specifically design manifolds which give good chemical reaction, and have $D < 2$. Similarly, flow systems which incorporate (*e.g.*) solvent extraction or sorbent extraction can sometimes be operated under conditions that give an "effective" D value of less than 1.00 (*i.e.*, they pre-concentrate the analyte).

1.3.3.2 *Importance / use of alternative FIA readout*

A FIA *readout* can be obtained in several ways with different advantages. The transient signal observed by a detector during the passage of the dispersed sample zone has the form of a peak, of which the height (H^{max}), width (W), and area contain the analytical information.

Generally, for FIA systems without chemical reactions (*e.g.*, in a simple atomic absorption measurement), when the detector responds linearly and instantly to the injected species, it does not matter whether peak height, area, or width is measured. This is so because they all yield useful information, with the concentration of the injected material being related differently to each of these parameters. A brief summary of the various measurement modes is given below.

Peak height is the most commonly measured peak dimension in FIA. This is because of its simplicity (peak height is the most convenient parameter to locate on a chart recorder trace) and has a direct relationship to detector responses, H, such as absorbance, potential, current, *etc.* For each of these, as a first approximation, one can write: $H = a C + b$, where a and b are slope and intercept constants. Vertical measurements can

also be taken at any part of the ascending or descending peak profile, taking advantage of the reproducible nature of the dispersion profiles in FIA. This is sometimes necessary if measurements at peak maximum fall outside the dynamic range of the detector response, and / or additional information is required not only at one detector channel, *e.g.*, a fixed wavelength, but by scanning an entire spectrum.

Peak area is, similarly, directly related to the detector output (Area = a C + b). It can provide improved sensitivity over peak height since it involves integration over a larger number of data points. Its use is, however, somewhat restricted by the difficulty in eliminating baseline noise and determining accurately the beginning and ending boundaries of the peak.

Peak width is proportional to the logarithm of concentration and therefore offers a wider dynamic range for determinations. It yields a readout as a time difference (Δt) between two corresponding points on the rising and falling edges of the peak profile. However, it is less precise than either peak height or area, and cannot be related directly to spectra. Peak width measurements have been used in specialized applications such as titrations and other peak-width-based FIA applications. These are gradient techniques that rely on horizontal peak dimensions, which can be located at any height on the FIA peak.

1.3.3.3 *Gradient methods*

A sample plug injected into a continuously flowing carrier stream forms a well-defined and reproducible concentration gradient. This generates an infinite number of elements of fluid which contain different concentration *ratios* of sample and carrier. These concentration gradients have been exploited in several analytical applications.[1] This added dimension allows elements of fluid that have suitable dispersion number to be conveniently selected by locating the analytical readout position at appropriate points across a peak.

Gradient techniques have found wide applications in procedures such as (i) gradient

dilution in which a suitable element of the dispersed sample zone (not the peak maximum) is selected as the source of the analytical readout, (ii) gradient scanning; an extension of gradient dilution which utilizes a dynamic detector to continuously measure a physical parameter by repeatedly scanning over a certain range, and (iii) gradient calibration; an extension of the gradient dilution technique which relies on the strict reproducibility of the same phenomenon. This aims at avoiding the usual repetitive calibration procedures which involve serially diluting and injecting solutions. It takes advantage of the fact that the sought information is already contained within some of the segments of fluid originating from a sample zone of the most concentrated standard sample material, *etc.*

These techniques find applications in reaction rate measurement by stopped flow.[26, 27] Also, the techniques of merging-zones are based on exploitation of the concentration gradients formed. Two (or several) zones are injected (usually, but not necessarily) simultaneously and then allowed to merge (or penetrate into each other). Thus, a composite zone that is information rich and capable of yielding multiple readouts, is created from a single injection.

1.3.3.4 *Basic models and equations*

An exact mathematical solution for chemical reaction in even a simple single-channel system is a non-trivial task. This is because of the many complex interacting physical and chemical parameters (flow profile, tee-pieces, mode of addition of reagent(s) to analyte, molecular diffusion, chemical reaction, *etc.*). Reaction conditions within an ideal flow injection system can be predicted if the manifold design is simple, and the temperature, viscosity, sample size, and tube dimensions are held constant. Real systems however, are complicated by (i) effects which are always present and a direct result of the manifold and materials used (*e.g.*, the non-ideal flow patterns generated by peristaltic pumps, the effects of connectors and the detector geometry), (ii) effects which are intermittent and result from aging of certain system components (*e.g.*, pump tubing wears,

electrode detectors can become poisoned), and (iii) chemical effects such as precipitate build-up within the tubes, and air bubbles.

Physical dispersion occurs partly by longitudinal flow convection (which results in a parabolic head and tail profile), and partly by radial diffusion. For a flowing stream in a tube of circular cross-section, the velocity of molecules at the wall of the tube is zero, and that at the center is twice the mean flow velocity.[28] The forward movement of sample elements is retarded when they move away from the central streamline, and it is accelerated when they move toward it. Thus, a sample plug which initially has a "square" profile when injected (t = 0), assumes a parabolic shape at t > 0 by the process known as "convection". The velocity profile acquires a parabolic centrosymmetric distribution;

$$F_i = 2\bar{F}\,(1 - r_i^2/r_o^2) \qquad (1.2)$$

characteristic for Poisseulie flow, where F_i is the velocity of the individual streamlines, r_i is an individual streamline's distance from the central streamline, $\bar{F}$ is the average flow velocity, and r_o is the radius of the tube. Molecules situated on the walls, however, do not stay there infinitely (otherwise the plug would have an infinitely long tail). Instead, they diffuse away from (and back to) the wall, and thus gain some longitudinal motion as they join the main stream. Forces that promote radial dispersion facilitate repositioning of elements of sample materials from the original stream line. Manifold elements such as "single bead string reactors" and "knotted tube reactors" are particularly efficient at this.

The diffusion can be longitudinal, *i.e.*, in the direction of the flow (axial) or perpendicular to the direction of the flow (radial). Taylor[28] showed that (under FIA conditions) while these processes always occur simultaneously, dispersion by longitudinal molecular diffusion can be ignored relative to that caused by the main flow pattern, whereas radial diffusion is always important in narrow tubes; at low flow rates, it may even be the major mechanism for dispersion. This should be expected as flow in straight tube FIA systems is laminar, as indicated by typical values for the Reynolds number (R_e).[16]

Even in systems which use coiled tubes, the flow is not thought to be turbulent, but deviations from truly laminar behavior are explained by "secondary flow" phenomena.

The Reynolds number may be calculated as;

$$R_e = 21.2\,Q / d \qquad (1.3)$$

where **Q** is the flow rate in ml. min^{-1}, and **d** is the internal diameter of the tube in centimeters. The onset of turbulence usually occurs at a R_e of 2000, which for a 1 mm i.d. tube would require a flow rate of 94.4 ml. min^{-1}, a highly unlikely flow rate in FIA systems. However, in high-pressure systems, turbulence can be caused by use of coiled tubes, in which a R_e value of 2000 is approached. [1]

The relative weights of these processes depend on flow rate of carrier stream, radius of tube, residence time of the sample, and magnitude of the diffusion coefficient(s). The peak profiles obtained generally fit the C-curve equation; [16]

$$C_n = 1/(2\ \pi\ \delta)\ \exp\text{-}\{(1\text{-}t/t_{mean})^2/4\delta\} \qquad (1.4)$$

where C_n is the concentration (mol. l^{-1}), δ is the dispersion number (dimensionless), **t** is the time from injection (s), and t_{mean} is the mean residence time (s). The value for δ may be calculated empirically from dispersion measurement with dyes. Under purely radial diffusion controlled dispersion conditions, Taylor's equation applies, i.e.,

$$C = (m/\pi\ r^2) * 1/(2(\pi\ \delta\ L^2)^{1/2})\ \exp\text{-}\{(1\text{-}x)^2/L^2 4\delta\} \qquad (1.5)$$

where m is the mass of injected material, L is the total length of tube (cm), and **x** is the distance from the peak maximum (cm). $\delta = \underline{D}\ t/L^2$, where $\underline{D}$ is axial dispersion coefficient ($cm^2\ s^{-1}$). Equation (1.5) only holds when $t_{mean} \geq r^2/3.8^2\ D_m$, where D_m is the molecular diffusion coefficient ($cm^2\ s^{-1}$). Values for D_m have been tabulated. [29]

Since $m/(\pi\ r^2\ L)$ = total concentration, C_{total}, and $C/C_{total} = C_n$, the normalized concentration, substitution and re-arrangement in equation (1.5) gives;

$$C_n = 1/(2(\pi\ \delta)^{1/2}) \exp-\{((1-x)/L)^2/4\delta\} \qquad (1.6)$$

Equation (1.6) is similar to equation (1.4), except that equation (1.4) describes concentration profiles in terms of time to peak mean, while equation (1.6) uses distance from the peak mean.

These expressions, however, are inadequate in completely explaining the complex physical and chemical variable interactions that contribute to the typical FIA peak profiles observed. Besides, FIA is a 3-dimensional chemical reactor - and these are 1-dimensional models. It has proven impossible to probe various points within this reactor space with the present detection systems (although a spatially-resolved two-laser double-excitation molecular fluorescence experiment might achieve this). It is our hope that results from the multiple response surface mapping studies reported in this desertation will complement these theoretical studies and further our understanding of these complex chemical and physical interactions.

1.3.3.4.1 *Tanks-in-series model*

The model is based on the concept that the liquid elements act as if they flow through a series of well-stirred tanks. [16, 30] It postulates that the tube, between the points of injection and detection consists of a number, N, of imaginary well stirred tanks (the actual "size" of each tank is a function of tube dimensions and flow rate). These are in series and the simple mathematical model used to account for the distribution of a sample introduced into the first tank can be used to account for the physical dispersion of the sample into further tanks as a function of time. This is exactly analogous to the concept of the height equivalent to a theoretical plate (HETP) model of chromatography. The mathematical model is as shown in equation (1.7) below;

$$C = (1/t_i)\ (t/t_i)^{(N-1)} * 1/(N-1)! * \exp-(t/t_i) \qquad (1.7)$$

where t_i is the mean residence time in one tank, N is the parameter model, *i.e.*, number of imaginary tanks through which an element of fluid flows between injection and detection (*i.e.*, number of mixing stages (dimensionless)). For high N, the shape becomes Gaussian, but for low N the shape is skewed. Therefore, one can grasp why long narrow tubes result in symmetric peaks, whereas shorter tubes give asymmetric profiles. If the tube is equivalent to 1 tank, there is an exponential rise and fall, *i.e.*, $C = (1/t_i)\ \exp\text{-}(t/t_i)$. When $t_{mean} = N * t_i$ and $N > 10$, then $\delta = 1/2\ (t_{mean})^2/N$. The application of this model to FIA has led to theoretical calculations of dispersion.

According to Taylor [28] (who elucidated the significance of diffusion), under diffusion-controlled conditions the peak shape should be Gaussian. Typical FIA profiles are skewed. FIA generally is carried out just outside Taylor conditions. Taylor's argument leads to the following practical conclusions: Mixing will be complete without recourse to mechanical stirring; the concentration gradient for a given sample plug is both reproducible and predictable; and the peak shape will be influenced by differences in the sample and carrier matrices, because the whole of the plug (matrix, and analyte) is diffusing into the carrier (and the carrier into the sample).

1.3.3.4.2 *Random walk simulation model*

The "random walk model" proposed by Betteridge *et al.* [31] gives an explanation for molecular behavior in a simple single-channel FIA manifold which takes into account chemical kinetic parameters, flow parameters and sample volume. A random walk model for diffusion was used by Einstein [32] to explain Brownian motion. Giddings [33, 34] showed that such a model gave a satisfactory account of the chromatographic process. The random walk model as applied in FIA deals with the fate of a finite number of individual molecules. Furthermore, it is much simpler and faster to compute than any attempt at a molecular dynamics solution in which one would seek to solve for the individual behaviors of all molecules within the complete plug using continuous mathematical functions. It uses

discrete mathematics (within a Monte Carlo style simulation) to simulate the behavior of sample molecules (perhaps 1500) within the manifold and passing through the detector. This has greatly simplified investigation of the effect of "real" experimental factors such as sample size, reaction rate, and temperature, which other models have had difficulty in dealing with.[28, 35, 36] Principal advantages are that (1) it can deal with finite sample sizes, and so simulate the effect of sample mixing and reaction rate, (2) the model is conceptually easier to understand than that based on a series of imaginary tanks,[30, 37] since it works in terms of the motion and reaction of individual molecules.

As mentioned earlier, the movement of a molecule in a laminar flow regime can be considered as a combination of the effect of random walk (molecular diffusion) and laminar flow (convection). The random walk model for FIA provides "snap shots" of the system after discrete time intervals. In each time segment, each molecule is moved a distance along the tube which reflects the local flow velocity (nil at the walls, twice the mean velocity in the center) and then takes a random step, the length of which is determined by molecular diffusion. The random walk step length takes into account viscosity and temperature effects on the molecular diffusion coefficient. If after any time interval, local sample and reagent molecule "concentrations" determine that reaction is possible, an appropriate proportion of the molecules are allowed to react. This process is repeated many times. Results obtained by using 10 experimental variables,[31] (*i.e.*, flow rate, tubing internal diameter, sample volume, reaction coil length, reagent concentration, temperature, viscosity, diffusion coefficient, reaction rate, and order of reaction) were in good agreement with the accepted theory and experimental evidence; other predictions were confirmed in subsequent experimental studies.[38, 39] This random walk model was then extended to cover a merging zones FIA system[40] and its predictions were compared with results from a far from ideal experimental system. A good correlation was found. This work indicated the importance of differences in diffusion coefficients[41] between reagent and sample plugs, and discovered an unnoticed pH gradient in the experimental

system.

1.3.4 Applications of FIA

FIA has many features which make it appropriate for automation of wet chemical analysis, and there is now wide use of this technique as an analytical methodology. Early on, it was overshadowed by the air-segmented continuous flow analyzers, such as those produced by Technicon. However, much work has now been done, and there are standard methods for analytes such as glucose, ammonia, nitrates, *etc.* based on FIA. Its versatility and simplicity have led to the development of simple systems which can be started and closed down in a few minutes, and which can be easily switched from one analysis to another. FIA has been demonstrated to be an ideal tool for the rapid handling and pre-treatment of liquid samples prior to their analysis, and because of this, may prove to be a useful complementary technique to laboratory robotics. A recent review article by Clark *et al.* [42] describes the diversity of sample handling and pre-treatment techniques which are possible with FIA. Most of the original FIA applications were centered on reproducible sample introduction into a detector. Examples of these include high speed sample introduction to detector systems, such as flame atomic absorption/emission spectrometers [43] and inductively coupled plasma spectrometers. [44] Many determinations and techniques carried out using FIA are given in reference 1. Most of these exploit reactions across the sample and carrier interface and/or controlled sample dispersion.

FIA has been used to facilitate and enhance sample pre-treatment steps (*e.g.*, solvent extraction, gas diffusion) which are normally performed manually. [45, 46, 47] The advantages of this are speed, reproducibility, and ability to work with smaller volumes of extractants, reagents, and sample. For toxic or pathogenic samples, as are many of industrial or clinical origin, FIA offers the advantage of removing or at least minimizing human exposure by confining the potentially hazardous materials within the inert flow manifold. Common FIA sample handling and pre-treatment methods have recently been

reviewed. [42] The use of flow injection techniques for sample preconcentration and matrix modification is attracting much attention and this is evidenced by the large number of publications in the area of flow injection - atomic spectrometry. [48]

FIA has also been used for kinetics based determinations (*e.g.*, a two point kinetic assay of glucose [49, 50]).

Because of (i) the rapidly increasing number of publications and first class workers active in FIA research, (ii) the adoption of standard methods by governments based on FIA, (iii) the commercial availability of FIA systems for routine analysis in the laboratory and in process control, and (iv) the enormous opportunity for laboratory automation in industry and the analytical service sector, one can be sure that FIA has a very bright future. Automated FIA systems, such as described in the remainder of this thesis, have much to offer and will further expand the boundaries of chemical research attainable by FIA.

CHAPTER TWO

DEVELOPMENT OF INSTRUMENTATION FOR AUTOMATED METHODS DEVELOPMENT FOR FLOW INJECTION ANALYSIS

2.0 Introduction

An automated apparatus to assist in the development of continuous flow (and specifically flow injection) analytical methods is described. The system is capable of controlling and/or monitoring a variety of pumps, valves, and detectors through an IBM PC-AT compatible computer.

Continuous flow methods of analysis, such as flow injection analysis (FIA) [1, 5] and air-segmented continuous flow injection analysis (ASCFA), [51] have become well-established analytical tools. These methods are characterized by their versatility, high sample and reagent throughput rates, precision and simplicity, which make them ideal for routine analyses in many fields. One difficulty with continuous flow methods is that performance factors such as sensitivity and selectivity are difficult to predict because of the complex interaction of dynamics and reaction kinetics. For this reason, empirical optimization methods such as simplex optimization are often used in the course of method development. [3] Such development procedures typically require the manual preparation and mixing of solutions. However, Betteridge *et al.* have shown that use of a computer-controlled continuous flow system can greatly reduce the time and effort required. [52] By placing the computer in control of hardware components such as pumps, valves, and detectors, it is possible to automate solution preparation and measurement of the analytical response. This removes the operator from the optimization loop for more important tasks and improves the speed and reliability of the system.

The use of programmable continuous flow instrumentation has other advantages as well. Chemical response surfaces can be mapped as a function of two or three variables, and with minimal operator intervention. [53] This is important, as such studies normally involve complete factorial designs with a large number of experiments which would take an unacceptably long time to achieve by hand. With an automated system it is also much easier to carry out complex FIA experiments: These also involve include concentration gradients, [54] merging zones, [55] and flow reversals, [56] where reproducible timing is critical.

This present work began in late 1987 when this research group obtained parts of the original prototype automated continuous flow methods development system developed by Betteridge *et al.* [52] These were a five-channel pump unit, interface box, simple photometers, and an autosampler. For other than technical / scientific reasons, the potential of this hardware and approach to automated FIA was never fully realized in its previous laboratory setting. Furthermore, the availability of much more powerful laboratory microcomputers, and our desire to carry out more and more sophisticated experiments, provided an impetus for our construction of a "second generation" programmable analyzer which incorporated pieces of the original.

For this reason, the Commodore PET computer which was originally used to control the system has been replaced with an IBM PC-AT compatible microcomputer (and more recently by an Intel 80386-based unit). This has necessitated total redesign of interfacing hardware. Furthermore, there has been construction of new units (*e.g.*, injection valve controllers), incorporation of different types of pumps, addition of diode array detection, and writing of over 365 Kbytes of software to allow efficient control of the analyzer and communication with each of the devices. It was our desire to redesign the "second generation" system, so that it could be further expanded and capable of controlling additional continuous flow components. Indeed, this has proven possible.

This chapter describes in detail the controlling hardware and software of the current flow injection development and optimization (FIDO) system. This description includes the components of the modified system which were designed as part of this work, as well as the elements of the original system of Betteridge *et al.* which were never presented in detail. Details of interface circuitry are given where appropriate, and have been reported elsewhere. [57] A description of parts of the software has also appeared in the literature. [53,58]

2.1 System components

Table 2.1 lists the continuous flow system components which are part of the current FIDO system which is schematically represented in Figure 2.1. The software, which will be described in the latter part of this chapter, is capable of controlling and/or monitoring three types of pumps, two types of valves, and four types of detectors. Specific descriptions of the major system components is as follows;

Category		*Description*
Pumps	(a)	Multiple peristaltic pump unit (5 independent pump heads, stepper motor driven)
	(b)	Stand-alone peristaltic pumps (2)
	(c)	Syringe pumps (2)
Valves	(a)	Pneumatically actuated six port valves (4)
	(b)	Electrically actuated six port valves (3)
Detectors	(a)	Simple LED-based photodetectors
	(b)	Dual beam filter photometer
	(c)	Diode array spectrophotometer
	(d)	pH electrodes

Table 2.1 Elements of the automated continuous flow system.

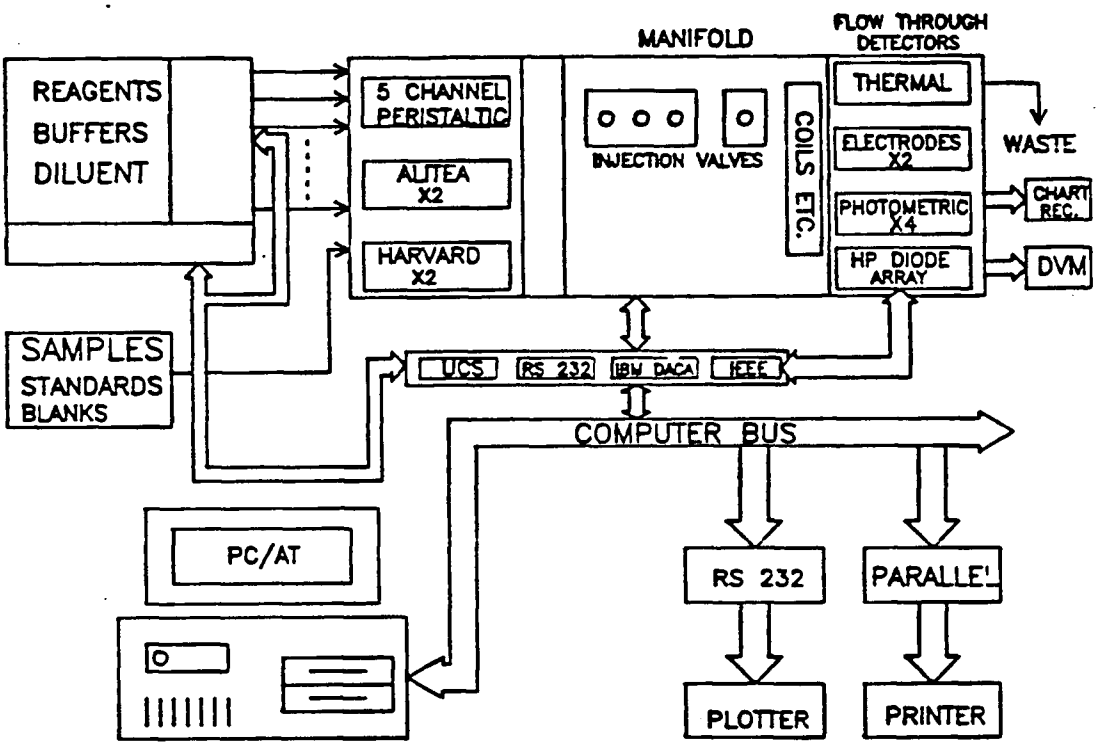

Figure 2.1 Schematic diagram of the Flow Injection Development and Optimization (FIDO) system.

2.1.1 Computer

The "brain" of the FIDO system is the IBM PC-AT compatible computer (Nora Systems, Vancouver, BC) which controls and /or monitors all of the continuous flow system components mentioned above. This computer has a 12 MHz clock speed, 1 Mb RAM, 40 Mb hard drive, 1.2 Mb and 360 kB floppy drives, enhanced graphics adapter (EGA) card and color monitor, an Intel-80287 math-coprocessor and Phoenix BIOS chip set. Communication with FIDO devices is through three interface boards: (1) an IBM data acquisition and control adapter board (Mendelson Electronics, Dayton, OH); (2) an HPIB (IEEE-488) general purpose parallel instrumentation interface (Hewlett-Packard, Palo Alto, CA); and (3) two RS-232 serial ports. Most recent work has shown that control by a much faster Intel 80386-based microcomputer - 20 MHz with Intel-80387 math coprocessor is accomplished without any problems by transferring the interface boards to the newer computer. Thus an upgrade route to PC's which are compatible with the original IBM PC interface bus is readily available.

2.1.2 Pumps

The system is capable of controlling a five-channel peristaltic pump unit, two higher precision peristaltic pumps and two "pulse-free" syringe pumps. Most applications will not require all of these pumps, but the variety of available units increases flexibility and thus makes it possible to select a configuration that is appropriate for a given application. A brief description and discussion on the use of each of the system pumps is given below.

The five-channel peristaltic pump unit is that constructed by Betteridge *et al.*,[52] with circuit modifications to allow the first of the five pumps to be reversible. The unit consists of five independent pump heads (Ismatec, Zurich, Switzerland, Type mini-micro 2/6) housed in a standard 19" rack and driven by independent stepper motors (Impex type). Driver boards (McLennan, Camberley, Surrey, UK, Type EM127) provide the necessary phasing and current forcing circuitry to drive the stepper motors. The speed of these

pumps can be varied from 0 to 76 revolutions per minute, with a resolution of 1 part in 255.

Because the 8-bit speed resolution and 7° per step rotation increment of the multiple pump unit is not suitable for some applications, the system is also capable of controlling two higher precision peristaltic pumps (models C4V and C6V, Alitea USA, Medina, WA) which have a resolution of 1 part in 4095 (*i.e.*, 12-bit speed resolution). The range over which this resolution is obtained can be adjusted on the front panel of the pump, and the rotation of the pump heads at low speeds is much smoother than for the multiple pump unit. The direction of these pumps can also be controlled by the computer. Control is via the IBM DACA board, and details of the interface circuitry are given later.

Finally, for applications where an accurate knowledge of the volumetric flow rate is required without gravimetric flow calibration, or pump pulsations must be minimized, two syringe pumps may be employed. These are dual syringe units (model 22 infusion pump, Harvard Apparatus, South Natick, MA, USA) which are capable of reversible operation, and are controlled across the two RS-232 interfaces.

2.1.3 Valves

Both electrically and pneumatically actuated valves can be accommodated by the modified FIDO system. The original system used only a single motor-driven valve. While electrically actuated motor-driven valves (with rotary action) have the advantage of requiring no compressed gas supply, they generally respond much more slowly than those with pneumatic actuation. Of course, micro-solenoid valves such as Instac types manufactured by The Lee Company (Westbrook, CT) are very rapid (ms), do not require a compressed air supply, and can be used for many low pressure applications. Such units can be controlled by the same circuits as developed for FIDO. The current system permits more than one valve of either type to be used.

The principal injection valve control unit in FIDO includes three pneumatically actuated six-port valves (type 50 valves with model 5701 actuators and model 7163 solenoid

valves, Rheodyne Inc., Cotati, CA, USA) which are mounted in a single case. An additional single valve unit of the same design can be run by a separate controller.

A less preferred alternative is to use electrically actuated six-port valves (model 86916 with motor drivers, Hamilton Valve Co., Reno, NV, USA). These are mounted individually on their controllers. The control circuitry for these was designed in house, and provides integrated timers for the FILL and INJECT positions which allow multiple replicate injections to be made without further communication from the computer.

2.1.4 Detectors

Three different (spectro)photometric detectors are available to meet the varying demands of flow injection experiments. The first is based on a previous design by Sly *et al.* [59] and was used in the original system. [52] This employs a light emitting diode (LED) source and phototransistor detector mounted transversely across optically transparent tubing. This design is simple, inexpensive, and quite effective for many applications, but the short pathlength, broad source spectrum (band width $\approx$ 40 nm), and limited number of available wavelengths restrict its capabilities. An alternative is a detector based on the design of Patton *et al.* [7] This detector, in its normal configuration, employs a quartz halogen source with interference filters and an axial geometry, ensuring a greater range of applications. It is also possible to use these units with LED light sources and in the absence of filters. Finally, a diode array spectrophotometer (model 8452A, Hewlett-Packard, Palo Alto, CA) can be used for maximum flexibility and is the detector of choice for most of the work reported in this thesis. Although this instrument is generally too expensive for routine applications, it is ideal for development work and for specialized experiments.

The FIDO system can also accommodate several electrochemical detectors. For pH measurements, two 50 μL flow-through cells with combination electrodes (model GK74350B, Radiometer America, Westlake, OH) are currently available for use. An

amplified and compensated voltage output can be provided by a standard pH meter (model 119, Fisher Scientific, Vancouver, BC.), or by a dual electrode amplifier which was constructed as part of the FIDO system. The dual electrode amplifier allows for use of reference electrodes and will also accommodate ion selective electrodes.

2.2 **Interface circuitry**

This section describes details of the interface circuitry used to control the various elements of the FIDO system. Unless otherwise stated, all integrated circuits were obtained from Active Components, Vancouver, BC, Canada.

2.2.1 System Bus

The original FIDO system was interfaced to a Commodore Pet microcomputer through ports located within the ROM expansion area of the microcomputer's memory. When the system was to be modified for control by an IBM PC-AT compatible, it was clear that the original interface would have to be re-designed. In making these changes, several goals were established: (1) to maintain, as much as possible, compatibility with existing system components, (2) to develop an improved interface which could be easily adapted to future changes in computer hardware, (3) to remove, as much as possible, dependence on external interface elements, and instead rely on more standard commercially available interface boards, and (4) to allow for easy future expansion.

To meet the last three of these goals, it was decided to employ a fairly standard interface board. We selected the IBM data acquisition and control adapter, which has 16 digital input and output lines, four channels of 12-bit analog-to-digital (A/D) conversion, and two channels of 12-bit digital-to-analog (D/A) conversion. There are other boards, or combinations of boards available that also meet or exceed these requirements. The two additional boards incorporated into the FIDO system were commonly available IEEE-488 and RS-232 interfaces. The IEEE card was necessary to communicate with the diode array spectrophotometer and printer. The RS-232 interfaces were for the syringe pumps and

analytical balance. These may be useful in the future for communications with further devices such as autosamplers, flow meters, level gauges, temperature sensors, and even robotic facilities.

Certain components of the automated continuous flow systems, such as the multiple peristaltic pump unit and the valves, require interface circuitry external to the computer. The use of a centralized interface unit (as on the original FIDO) not only increases the complexity of the system, but also makes it difficult to establish simpler but similar automated continuous flow systems, without entirely duplicating the interface. To avoid this problem as much as possible, it was imperative to eliminate external interfaces where possible, or (otherwise) make them self-contained within each device. This has made for much better adaptability.

For those devices which do not require external interfaces, a simple interface bus input/output protocol was established that allows for further system expansion. The configuration of the IBM DACA used for this system is shown in Figure 2.2. The first eight digital output lines (**BO**0 to **BO**7) are used to provide data to the external interface which is addressed with the next three lines (**BO**8 to **BO**10). The output datum is received by the device when the address is valid and the **BO** strobe handshake line then goes high. The three address lines allow up to eight external independently addressable interfaces to be used. Digital outputs **BO**11 to **BO**14 are used to provide direction control for the two Alitea pumps. This control could have been accomplished using an external interface, but this way the pumps can be controlled directly and implementation on other computers is not hindered. The remaining digital output line, **BO**15, is currently unused, but is reserved for error checking such as may be provided by liquid level sensing devices and flow meters. Digital inputs **BI**0 to **BI**6 are used to return status information from external interfaces. To facilitate future expansion, additional DACA cards can be mounted within the same microcomputer. Alternatively, external interfaces can be used which employ tri-state outputs; these outputs become active only when the device is addressed, and so multiple

devices can use the same status lines. Digital inputs **BI**7 to **BI**15 are currently unused, but could be used for error checking such as may be provided by liquid level sensing devices and flow meters. The output of counter 1 (Delay Out) of the 8253 counter/timer on the DACA board is connected to the **BI** strobe input. The output of this counter is also connected to the input of counter 2 (Count In). This configuration provides a convenient means for timing for data acquisition and other applications.

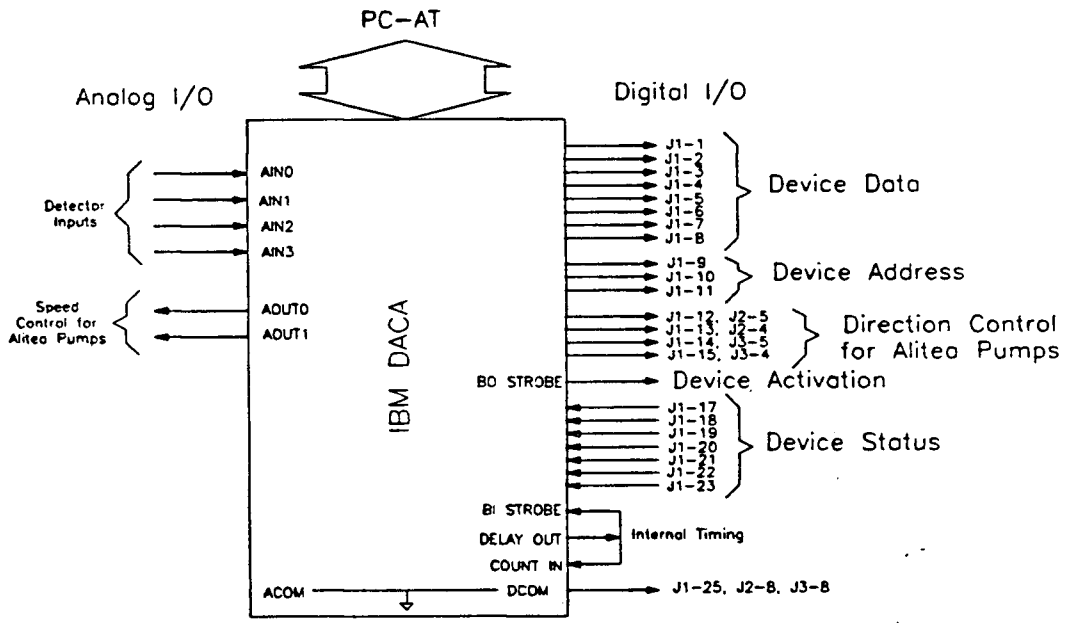

Figure 2.2 Configuration of the FIDO system interface bus. J1 shows the pin connections for a 25-pin D-connector for communication with the external devices. J2 and J3 show pin connections for two 15-pin D-connectors which provide control signals to two Alitea pumps.

The four analog-to-digital converter (ADC) inputs can, in most cases, be connected directly to detector outputs. Differential inputs are used and the voltage range for 12-bit conversion is set at -5V to +5V. Alternative ranges of 0 to +10V and -10 to +10V are switch selectable on the DACA board. Programmable gain is not available with the DACA board, but other data acquisition boards provide this feature as well as a greater number of inputs if these features are important. An external gain control is available with the dual beam photometric detector. The two digital-to-analog converter (DAC) outputs are used to control the speed of the Alitea pumps and have 12-bit resolution and a range of 0 to +10V.

In addition to the standard BNC connectors used for the four analog inputs, three other connectors (**J1** - **J3**) emanate from the DACA board. Connector **J1** is 25-pin D-connector which goes to the external interfaces for control of valve and the five-channel pump unit. Connectors **J2** and **J3** are 15-pin D-connectors which provide control signals to the two Alitea pumps. Connector **J4** is resident on the (modified) original FIDO interface unit.

2.2.2 Pumps

2.2.2.1 *Multiple peristaltic pump unit*

Only a brief description of this unit is given in the original paper of Betteridge *et al.* [52] In this section, full details of the interface are provided. A circuit diagram of the interface is given in Figure 2.3. Timing circuitry is given for one of the pump units (Pump #1). This is identical for all the others, except that Pump #1 has the additional control line (**J4**, pin 6) which is used to toggle the direction of its rotation, but does not affect its speed.

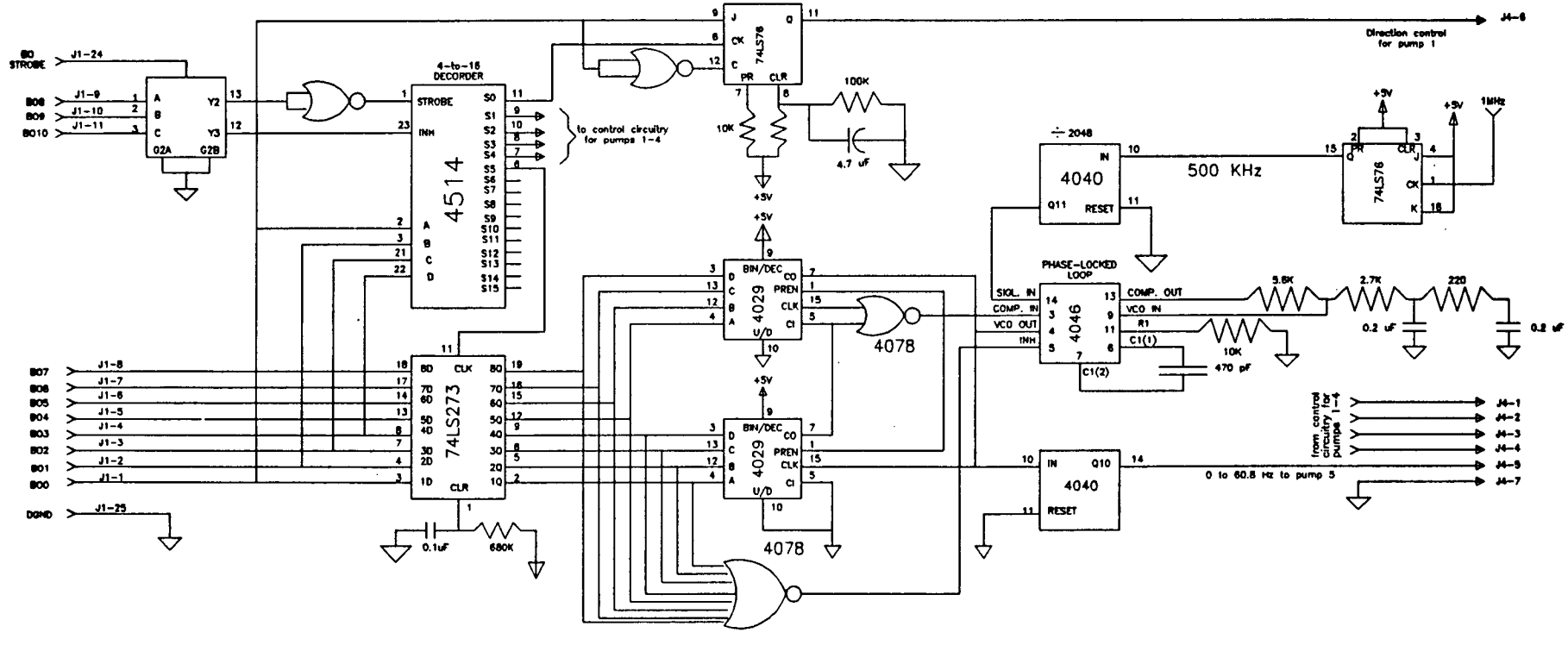

Figure 2.3 Diagram of interface circuit for multiple peristaltic pump unit. The circuitry, shown for pump #1, is the same for all five channels, except that the direction of pump #1 can be reversed.

The pump interface is assigned two addresses on the system bus, one for pump number selection and one for speed selection. The sequence for programming the speed of a pump is as follows: first a pump is chosen by selecting device address 010_2 on the address bus (**BO**8 to **BO**10), putting the pump number (1-5) on the data bus (**BO**0 to **BO**7), and toggling the **BO** Strobe line. This latches the pump number into the 4-to-16 decoder (4514B). The output of the decoder remains low, however, since the INH input is still high. The next step is to select device address three on the address bus, place the pump speed (0 - 255) on the data bus, and once again toggle **BO** strobe. This causes the INH line to the 4-to-16 decoder to go momentarily low, toggling the appropriate output (**S1** to **S5**) and locking the pump speed into the corresponding 8-bit latch (74LS273, Texas Instruments). The outputs from this latch are the preset inputs to two cascaded 4-bit binary counters (4029B, Texas Instruments) which act as a variable frequency divider. The input to the frequency divider is provided by the voltage controlled oscillator output (VCO) of a phase locked loop (4046B, Texas Instruments), whose input is a reference signal of 244 Hz. This arrangement has the effect of multiplying the input frequency by the divider setting to obtain the output frequency (VCO). Additional logic disables the VCO when a speed of zero is specified. Thus, the frequency at VCO will vary from 0 Hz to (255 x 244) Hz in uniform increments. This output is further divided by a factor of 1024 by a binary counter (4040B) before being sent to the stepper motor control circuitry. The control signal varies from 0 to 61 Hz and each pulse corresponds to a 7.5^{o} rotation of the motor. The actual stepper motor driver circuitry is commercially available, so details will not be given here.

The timing circuitry shown in Figure 2.3 for pump 5 is identical to that employed for the other four pumps. Only one decoding circuit is needed. Direction control for pump 1 is available by selecting "pump 0" in the pump addressing cycle. In the speed selection cycle, **BO**0 provides the direction input (1 = forward, 0 = reverse). The direction control is latched into a JK flip-flop (74LS76, Texas Instruments) and sent directly to the stepper motor control circuitry. In the original design, this direction signal controlled all of the

pumps, but flow reversal experiments required that the design be modified so that pumps 2 to 5 are unidirectional. It was felt that this modification provided greater versatility. In principle, it is possible to control the direction of all the pumps independently, but this would have required modification of the original design to provide extra latches and additional lines on connector **J4**.

The additional outputs (**S6** to **S15**) of the 4-to-16 decoder are currently unused, but allow for future expansion. They may be used to trigger external devices (*e.g.*, valves) or to accommodate an additional multiple pump unit. In its current state the multiple peristaltic pump unit has performed without problems for many hours and is the workhorse of the FIDO system. We attribute this to the very high quality of engineering of this unit, for which Timothy J. Sly (Automated Methods Group, University College Swansea) was responsible. [3]

2.2.2.2 *Alitea peristaltic pumps*

Control of the Alitea peristaltic pumps is facilitated through two external digital connections for direction control, and an additional contact for a speed control voltage of 0 to 10V. This voltage is provided by the output of a 12-bit DAC, and gives a speed resolution of one part in 4095. The maximum speed for this voltage range is set on the front panel of the pump. Two DAC's are currently available with the IBM DACA board, allowing control of two pumps. This number can easily be increased by DAC's on additional IBM DACA boards, or by a multiplexer-style interface. The pin connections on the 25-pin D-connectors on the Alitea pumps are shown in Figure 2.2.

2.2.2.3 *Syringe pumps*

The Harvard Apparatus syringe pumps employed in this work are controlled through an RS-232 serial interface. Only pin numbers 1, 2, 3, and 7 of a 25-pin D-connector are used for communications. These connections are straight-through, one-to-one, *i.e.*, pin **i** from the serial port connection is connected directly to pin **i** of the

D-connector on the device. A simple command protocol is used to control flow rate and pump direction, and obtain status information.

The PC-AT compatible computer currently used allows up to four serial ports to be employed for the control of syringe pumps or other RS-232 compatible devices. Further expansion is possible with commercially available boards (which support up to 8 serial ports), or by external multiplexers.

2.2.3 Valves

2.2.3.1 *Pneumatically actuated valves*

The current FIDO system is capable of controlling four pneumatically actuated six-port valves. Three of these valves are mounted in the same controller unit to accommodate special FIA experiments, such as those involving merging zones, which require valves to be in close proximity. The other is mounted independently with its own controller. The design for both controller circuits is essentially the same. The circuit diagram for the three-channel valve controller, showing decoding and control circuitry for valve 1, is given in Figure 2.4. The circuitry for valves 2 and 3 is identical to that for valve 1.

The valve actuators used for this system require positive pressure actuation in both directions, so two 12V solenoid valves (which should always be in opposite states) are needed to alternately switch the compressed air supply to the two sides of the valve actuator. These require a current of 500 mA each and are driven by reed relays (PRMA1A05, Texas Instruments). A metal oxide varistor (18V DC) is used on the output of each relay to suppress transients on the power supply. The relays are driven by complementary outputs of a JK flip-flop through open collector inverters.

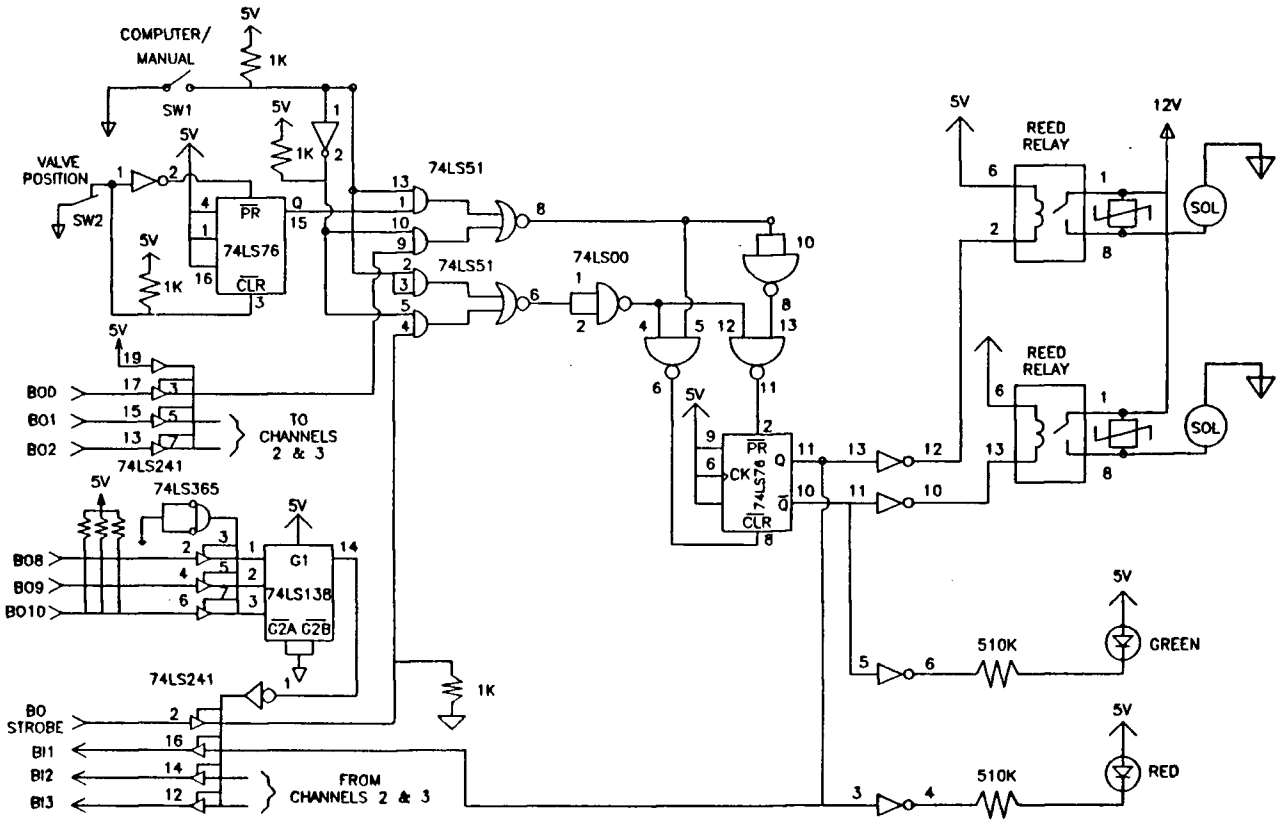

Figure 2.4 Circuit diagram for one channel of the three-channel pneumatic valve controller.

The controller allows both manual and computer control on each channel. In manual mode, switch 1 is open and inputs are provided directly by switch 2. The JK flip-flop (74LS76) at the switch 2 input acts as a debouncing circuit. All succeeding gates are enabled and the JK flip-flop controlling the solenoid valves is either preset or cleared according to the input at switch 2.

In computer control mode, switch 1 is closed, and switch 2 is disabled by the upper And-OR-Invert (**AOI**) gate (74LS51). The controller now responds to the state of **BO**0, but only if the device address is currently set to 1, although this is easily changed. The decoder output controls a tri-state buffer (74LS241) to permit the **BO** strobe signal to reach the controller circuitry and allow the valve position status lines values to appear on the bus. When the device is addressed and **BO** strobe is high, **BO**0 provides the input to the controlling flip-flop. This is latched when **BO** strobe goes low. To ensure correct operation when the computer is disconnected, a pull-down resistor is connected to the **BO** strobe input. The status lines (**BI**1 to **BI**3) are valid whenever the device is addressed and are in the high-impedance state otherwise so these lines may be used by other devices. Channels 2 and 3 of the valve controller are driven by **BO**1 and **BO**2. Identical controlling circuitry is needed, but additional address decoding is unnecessary.

For the single channel valve controller, some modifications were made to reduce the component count. These included: (1) replacement of the 74LS138 decoder with discrete logic, (2) elimination of the 74LS365 line driver, (3) replacement of the 74LS241 line driver with the smaller 74LS125, and (4) use of a double pole relay rather than two single pole relays. In addition, the logic was powered by a 5V regulator to provide better isolation from the solenoid power supply. This single channel controller could be implemented with only six integrated circuit (IC) chips, including the relay (and several such units have now been constructed by this research group). Its mode of operation is essentially the same as shown previously.

Both of the valve controller units have proven rugged and effective. Earlier designs

attempted only temporary solenoid actuation, as this is really all that is required. However, this required more IC chips and was more prone to problems from electrical noise spikes in the system.

2.2.3.2 *Electrically actuated valves*

The electrically actuated six-port valves are driven by unidirectional motors with microswitches to indicate when each of four positions (at 90^{o} increments) is reached. A circuit diagram for the valve controller is given in Figure 2.5. The same controller could also be used for a four-port selector valve.

The position to which the valve is to be driven is specified by a binary value between 00_2 and 11_2. This is provided on the left-hand side of the circuit diagram and comes from one of three sources: a manual switch, a circuit for automatic timing, or the computer. The source of the control is specified by switch 2, which is used to enable appropriate inputs of the two **AOI** gates (74LS54, Texas Instruments).

In manual mode, the position of the valve is specified by switch 1. The setting of this four-position switch is decoded to binary with two **OR** gates (74LS32, Texas Instruments). These two outputs pass through the two **AOI** gates to two **exclusive-OR** (**XOR**) gates (74LS86, Texas Instruments), which compare the requested position with the binary value of the current position decoded from the four microswitches on the motor. The **XOR** outputs will activate the motor through a solid state relay if the two positions are not equal. Additional logic between the **XOR** outputs and the relay input ensures that: (1) the valve position does not change when switching from manual to computer mode, and (2) the motor does not stop while the valve is between positions.

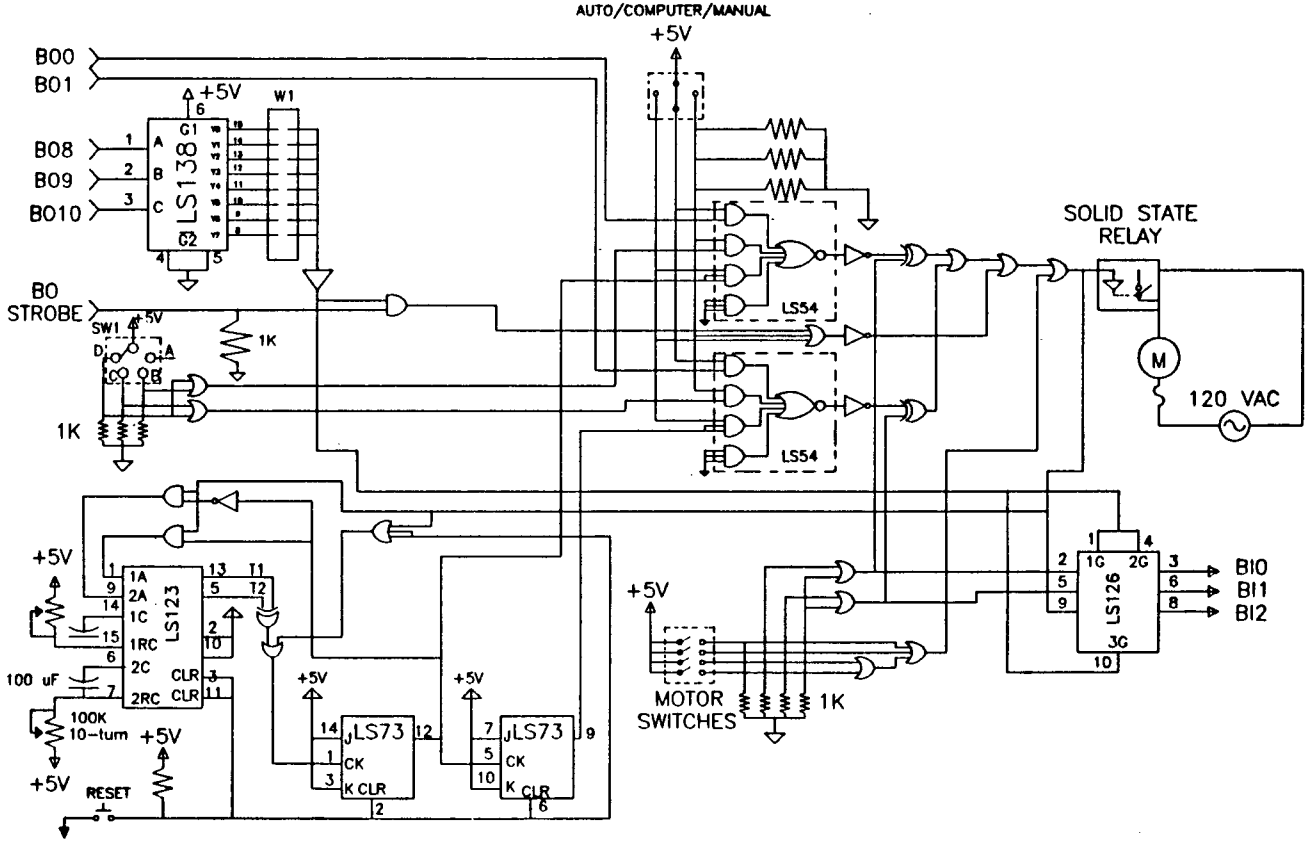

Figure 2.5 Circuit diagram for the electric valve controller.

In automatic timing mode, the two binary outputs which specify the motor positions are provided by timing circuitry shown in the lower left-hand corner of the circuit diagram (Fig. 2.5). The dual JK flip-flop (74LS73, Texas Instruments) acts as a two-bit binary counter and provides these binary outputs. Asymmetric timing is provided by the dual monostable multivibrator (74LS123, Texas Instruments). The two timing periods are adjustable from potentiometers on the front panel and are alternately triggered when the motor stops moving. A reset switch is also provided to initialize the valve sequence. Additional logic on the reset circuitry ensures that the monostable vibrator will continue to receive trigger pulses even if the reset switch is depressed for an extended period. The binary outputs provided by the automated timing circuit are processed in the same manner as for the manual circuitry.

For computer control, the binary outputs which specify the valve position are provided on the system data bus. In this mode, a two-input **AND** gate (74LS00, Texas Instruments) and a three-input **NOR** gate (74LS27, Texas Instruments) prevent the motor from moving until the controller is enabled, *i.e.,* until the device address appears on the address lines and **BO** Strobe goes high. The controller must remain enabled until the motor reaches the desired position. A 3-to-8 decoder (74LS138) is used to decode the jumper-selectable address. A tri-state buffer (74LS126) returns the controller status on the system bus whenever the address is selected. Two status bits indicate the motor (valve) position; a third is set if the motor is currently activated.

2.2.4 Detectors

2.2.4.1 *Spectrophotometric detectors*

The two simpler types of photometric detectors which are part of the current FIDO system were constructed in our laboratory. The designs for these have been reported elsewhere [7, 59] and so will not be repeated here. In each case, the output of the detector is connected directly to one of the ADC inputs of the IBM DACA board. The system can

accommodate upto four such detectors detectors without further multiplexing or DACA boards.

The diode array spectrophotometer has been the most widely used detector in this laboratory. It is specially suited for methods development due its flexibility. It can capture full spectra over the wavelength range 190 - 820 nm (across 316 diodes), and can perform multiple absorbance measurements at one or several wavelengths at preset acquisition rates. Additional options available include calculation of variance in absorbance measurements at each wavelength, and making absorbance (or transmittance) measurements with the shutter closed or open during repeated measurement cycles. These latter two options determine the sampling interval (time between repeat measurements) and integration time. Since shutter processing takes *ca.* 0.5 s, the sampling interval must be greater than the integration time plus the 0.5 s, otherwise a run-time error results. When variance data is to be calculated, the time taken by the instrument to calculate these values must also be considered. Using a data acquisition routine [58] (see below), a sampling interval of as little as 0.6 s is possible for a full spectrum without variance data. A minimum time of 1.8 s is needed per full spectrum if variance data is required. Data points can be acquired every 0.3 s across 35 diodes without variance information with shutter closed between measurement cycles (the sampling interval is at least 0.2 s, and integration time 0.1 s). Information on more than 35 diodes can be obtained at the expense of the peak profile resolution because of the lower acquisition rate possible. Acquisition of data (without variance) may be achieved for up to 6 diodes with the shutter open at a rate of 0.1 s.

Control and monitoring of the diode array spectrophotometer is achieved through an IEEE-488 parallel instrumentation interface card. The IEEE-488 driver routines provided by Hewlett-Packard permit direct communication with the instrument from the FIDO software. These are installed by inclusion of the command; DEVICE = C:\UV\HPIB.SYS in the computer's CONFIG.SYS file, which is accessed

whenever the computer is turned on. The length (in bytes) of each record (of data plus other information) transferred across the HP-IB is dependent on whether variance information is calculated, and is given by:

$$\textit{Length in bytes} = \#\ \textit{of diodes} * (\textit{data point size} + \textit{variance data size}) + \textit{header size} + \textit{endline bytes}$$

2.2.4.2 *Electrochemical detectors*

Capability for pH and ion selective electrode detection on the FIDO system is provided in two ways. First, a separate pH / mV meter with amplified outputs may be employed. The meter currently used (Fisher Scientific, Type 119) has the capability, with amplification, to provide an output of 0.1 V per pH unit. This is connected directly to an ADC input of the IBM DACA board.

A second means of amplifying the signal from the detector electrode is to use the electrode amplifiers which were constructed as part of the original FIDO system. These differential amplifiers were intended as a low cost alternative for monitoring multiple potentiometric sensors. Their design is relatively simple and is shown in Figure 2.6. Differential inputs are provided for detector and reference electrodes, and are buffered with high impedance voltage followers (TL082, Texas Instruments). Often, as with combination electrodes, a reference input is not needed and so this input can be connected to "common" (0V). A capacitor is used on the reference channel input to reduce noise, but is not included at the signal channel where it would increase response time. The buffered differential inputs are fed into an instrumentation amplifier (AD524A, Analog Devices, Norwood, MA). The gain of this amplifier is switch selectable between 10 and 20. The amplifier output may be connected to any of the unused ADC inputs on the IBM DACA board. Slope and offset compensation for the electrode are not available, but these are not essential and can be performed in software if needed. Currently, there are two electrode amplifiers in the FIDO system, but this number can be easily expanded as the need arises.

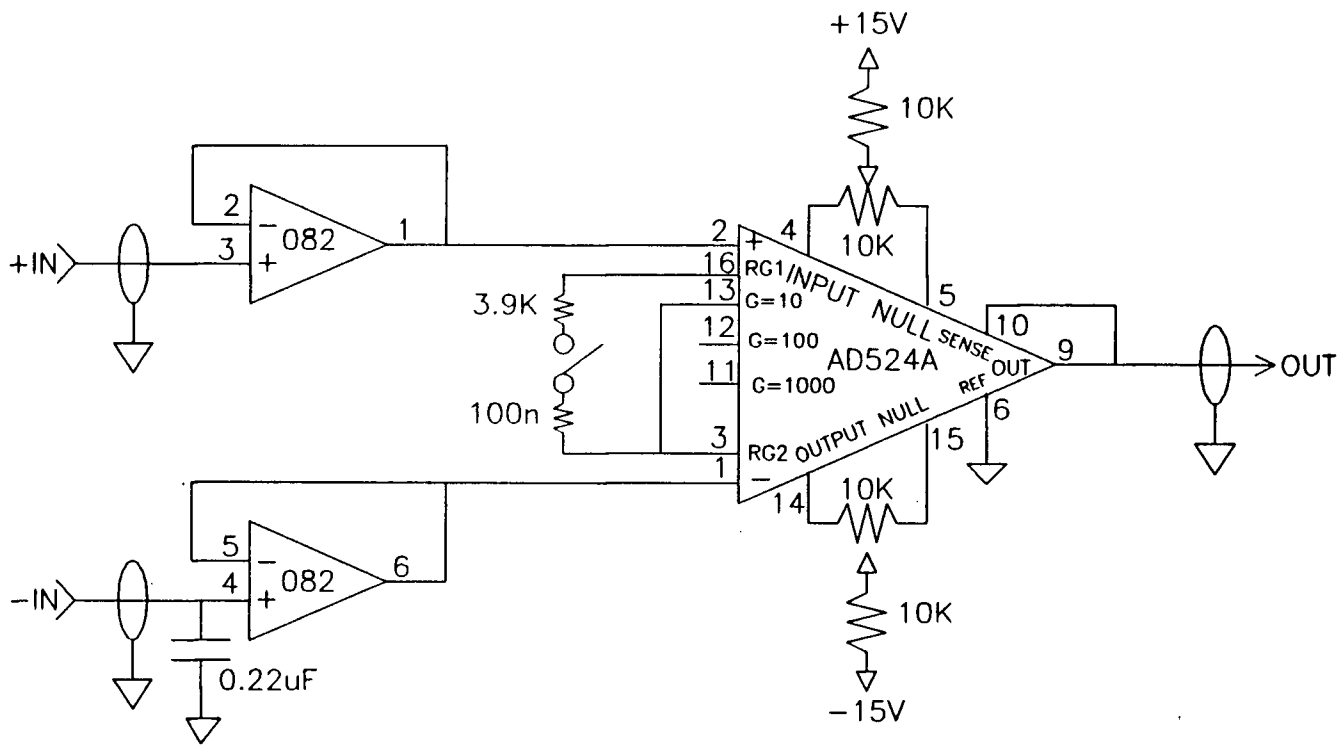

Figure 2.6 **Differential amplifier for electrode circuits.**

2.3 Software

The Flow Injection Development and Optimization (FIDO) software was written in our laboratory in a compilable, structured form of the BASIC programming language (Microsoft QuickBASIC version 4.0 (MSQB4), Microsoft, Missisauga, ON). The design and development of the software to its present level was made possible by several members of this research group, namely; Dr. P. D. Wentzell (a postdoctoral fellow in our laboratory), Ron M. Ree (an undergraduate summer student), Dr. A. P. Wade, and myself. The software is still being expanded as needs arise (*e.g.*, one version now supports a fast transient digitizer card). It currently consists of about 365 Kbytes of source code, excluding external libraries. The main FIDO program was designed for the automated development and optimization of FIA methods. The FIDO software facilitates specification of the system pump configuration, pump flow rate calibration, direct control of the hardware components, display of peak profiles from previous experiments, simplex optimization and response surface mapping studies. Further capabilities are presently being added. Because of the large size of the source code, it was necessary that the code be subdivided into three modules. These are; **FIDO.BAS, SIMPLEX.BAS**, and **CALIB.BAS** (with **FIDO.BAS** as the original main module). This allows for easier future expansion and provides efficient operation without overloading the 640 Kbyte RAM memory limitations of DOS and MSQB4.

System banners plus instructions for the user are printed to the screen via the **FIDO.BAS** module. It also provides the user with the capability of making a selection out of the six available options (*i.e.*, setup, calibration, optimization, control, display or exit) via the **FIDOMENU** subroutine. All user defined subprograms, the Hewlett Packard Interface Bus (HP-IB) library subprograms, HP-IB driver variables, and user defined common variables are declared in the **FIDO.BAS** module. The HP-IB library subprograms, and subprograms which plot data to the screen are contained in one user defined library named

FIDO.QLB, which is present as a QuickLibrary* and must be invoked at the time of execution (if running directly from the Quickbasic environment) by the command;

QB FIDO /L FIDO.QLB

Alternatively, it may be compiled along with the **FIDO.BAS** module by the commands;

BC FIDO.BAS

LINK FIDO.OBJ + FIDO.OBJ,,,;

to form the **.EXE** version of the program, **FIDO.EXE**, which may then be executed directly from DOS, without switches or external libraries.

Both the **SIMPLEX.BAS** and **CALIB.BAS** modules share the same **FIDO.QLB** library. All user defined subprograms available with the **FIDO.BAS** program and their interconnections with the rest of the modules are schematically represented in the flow diagram shown in Figure 2.7.

---

* A QuickLibrary is a collection of user written or/and commercial routines available for common use with other algorithms.

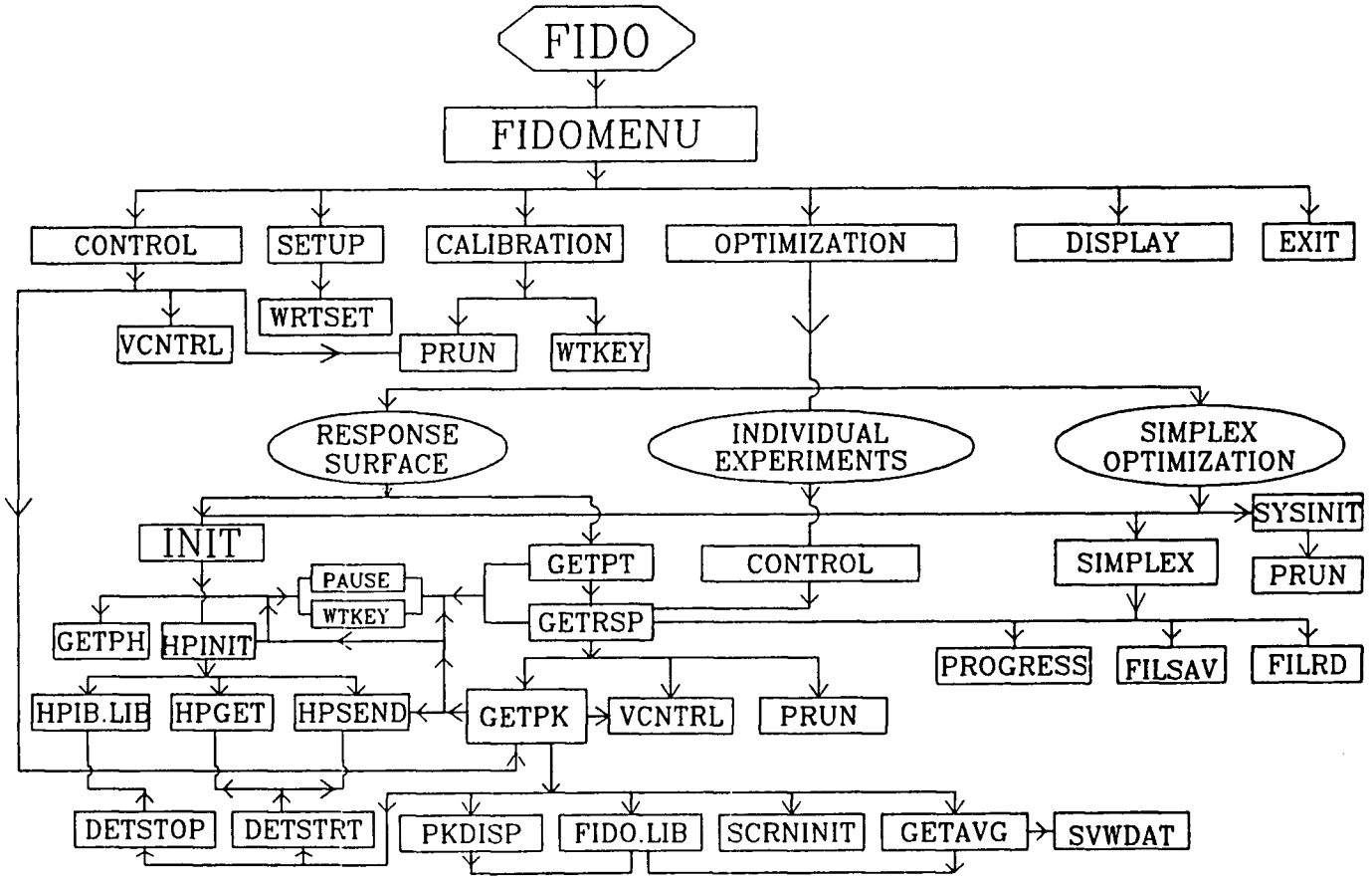

Figure 2.7 Flow diagram of the FIDO control software.

2.3.1 Software Operation

Details of operation and requirements of the major subprograms are given below.

2.3.1.1 *Pump configuration and system setup*

Information on the system pump configuration is required for both the automated simplex optimization and response surface mapping studies. In addition to variable and fixed flow rates, a fixed total flow rate from two pumps can be obtained by "buddying" [60] a variable pump to an appropriate diluent stream. This allows the system to vary chemical concentrations (by flow rates) without changing sample residence time. Appropriately sized pump tubings must be chosen to deliver the flow rate ranges desired.

System pump configuration is achieved via the **SETUP** subprogram of the **FIDO.BAS** module. The process involves the following: (1) specification of the total number of pumps to be used (including the pump channel for the sample stream); (2) assignment of unambiguous physical pump numbers to these pumps; (3) entering into the computer the total number of variables to be investigated together with their chemical names (*e.g.*, Na-SCPAR reagent, diluent, hydroxide, buffer; these names are then assigned to the individual physical pump numbers); (4) specification of the modes of operation for the rest of the unassigned pumps (which operate either at fixed flow rates, or as "buddy" pumps). The pumps designated to provide fixed flow rates have their corresponding flow rates specified; (5) specification of the type of detector to be used (simple photometric detectors [59], diode array spectrophotometer, pH detector, *etc.*); and (6) indication of the number of replicate injections required. All this information is stored in a "setup file" (with the extension, **.SUP**) for use with later optimization studies.

2.3.1.2 *Calibration of flow rates*

Calibration routines are included in the **CALIB.BAS** module. Pump configuration information for a flow system which has been previously stored in a **.SUP** file is first loaded into the computer's memory for use with the calibration routine. The manufacturers' flow rating for the pump tube to be used with each pump channel (if different from that previously stored), the physical pump numbers for pump channels to be calibrated, the pump speeds for calibration for every channel, and the time to run the pumps are then entered. A facility to purge the manifold of air, air bubbles or previous solutions is also available, and may be called upon as necessary. The actual volumetric flow rate (in ml. min^{-1}) is then established gravimetrically for every channel using an analytical balance and water. A pump calibration file (with extension **.CAL**) is thus generated. An option for recalibration of pump(s) is available.

2.3.1.3 *Optimization of analytical procedure*

Modified simplex optimization, response surface mapping studies, and individual confirmatory experiments can all be performed once **.SUP** and **.CAL** files have been created.

The SIMPLEX subroutine is based on the algorithm previously developed by Betteridge *et al.*[3] The version of the original software written in BASICA by Dr. Wade was translated into MSQB4. Details of the simplex optimization software operation are omitted for reasons of brevity but are discussed in detail elsewhere.[9, 61] Information on a previous uncompleted simplex optimization experiment may also be accessed for the purpose of continuation. A session file (**.SES**) containing information on various simplex operations performed, their corresponding experimental conditions and responses, and some statistical results (*e.g.*, mean, standard deviation, relative improvement), is generated. Results may also be stored in any of the three data file types summarized in Table 2.2.

File type	.LOG	.EXP	.RNG
Data Stored			
Experiment #	X	X	-
Experimental conditions	X	X	X
Average response for each point	X	X	-
Response at each vertex of present simplex	X	-	-
Average response for simplex points	X	-	X
Relative standard deviation in response			
Response RSD(%) for present simplex vertices	X	-	X
Simplex cycle number	X	-	X
Relative improvement[a]	X	X	-
Time of peak detection	X	X	-
Type of simplex point	X	-	-
Minimum vertex response[b]	X	-	X
Maximum vertex response[b]	X	-	X

Table 2.2. Information stored in data files produced by simplex optimization.

[a] Relative improvement of present best response over initial conditions.

[b] Minimum and maximum responses for each simplex after a complete cycle.

A hardcopy of the performed experiments can also be obtained if needed, provided a printer is connected to the appropriate parallel port on the PC-AT microcomputer.

Response surface mapping is achieved via the **RSMAP** subroutine. This can be used to map the effect of one to three variables. In addition to information stored in the **.SUP** and **.CAL** files, the user inputs the search range for each variable and the number of steps between its upper and lower limiting values. For example, one might specify a sodium hydroxide concentration (M) range from 0 - x with increments of δx. For a two variable system, different experimental conditions are obtained by keeping the first variable fixed and then changing the value of the second variable systematically from the lower limit value to the upper limit value in the number of steps specified. Then the value of the first

variable is incremented, and the above procedure repeated. This is continued until all requested values of the first variable have been investigated, at all requested values of the second . The flow rates of selected variables are automatically and systematically varied by the microcomputer and the resulting spectrophotometric responses and / or pH values are monitored over the course of each experiment.

Data from these mapping experiments can then be imported into a suitable 3-D plotting package. In this work we have used SURFER (Golden Software, Golden, CO, USA) for three dimensional and contour map plots. Various types of file formats are possible, and selectable by the user. Examples of the different file formats available are given in Table 2.3 below.

File Type	.STD	.REP	.SHP	.WTS
Data Stored				
Experimental conditions	X	X	X	X
Response for each experiment	X	-	-	-
Average response	X	X	-	-
Peak detection time	X	X	-	-
Relative standard deviation	-	X	-	-
Experiment Number	X	-	X	-
Data points as f(time)	-	-	X	X
Data points as f(lambda)	-	-	-	X

Table 2.3. Information stored in data files from response surface mapping.

The user then decides which of the four types of data file summarized in Table 2.3 should be produced. The standard file has the extension .STD, repeatability information is stored in a .REP file, .SHP records peak shapes at a single wavelength and .WTS contains information on absorbance at multiple wavelengths *vs.* time.

2.3.1.4 *Other available options*

The other two additional options available from the main menu are **CONTROL** and **DISPLAY.** The **CONTROL** subroutine provides a means for direct control of the various hardware components. Valves can be switched to either inject or fill positions, pump speeds can be set to desired values, and detector response(s) can be monitored continuously (*e.g.*, to observe baseline stability or instability under different flow regimes). One can determine the baseline relative standard deviation for detection limit calculations. All these actions may sometimes be necessary, either during optimization procedures or at other times. The **DISPLAY** subroutine facilitates the display of previously acquired peak profiles and information pertaining to them, such as stream flow conditions, peak absorbance, and baseline standard deviation. Such information may be necessary for within-run comparisons.

The efficient functioning of the FIDO software is made possible by the presence of the wide range of user-defined subroutines. Figure 2.7 is a schematic of the software flow diagram. As can be seen, many subprograms are used by several of the higher level routines. Because of the large number of subroutines available, a detailed description of the functions of every one of the subroutines is omitted

2.3.2 Detection Strategies

As mentioned, the FIDO software can acquire and display data for an FIA peak from the three different types of photometric detectors. It is also capable of detecting a peak maximum (negative or positive) and providing its corresponding adjusted absolute peak height (measured at peak maximum relative to the baseline then in effect), peak height relative standard deviation, average time to peak detection, and the baseline standard deviation. We have not made use of peak width or area calculations, although these should be readily obtainable.

2.3.2.1 *Peak detection algorithm*

The peak detection algorithm is used by response surface mapping and simplex optimization routines. The algorithm stores incoming data values (absorbances at a single wavelength) in the array, **SIGNL(5000)**. Its algorithm processes the data being stored in **SIGNL()** to detect several types of events: *e.g.*, the start of rising or falling edge of peak, a peak maximum found, a negative peak found). The peak status can have one of several values:

-1 indicates that the system is waiting for baseline to stabilize. This is the initial status value before the baseline has stabilized;

0 shows that the initial baseline data points are being acquired and that the system is waiting for a peak to appear;

1 indicates that the leading edge of a positive peak has been detected and the algorithm is waiting for the peak maximum to occur;

2 shows that the leading edge of a negative peak has been detected and arrival of peak minimum is anticipated;

3 indicates that the trailing edge of a positive peak has been located;

4 indicates being on trailing edge of a negative peak has been located.

It uses two other arrays, **PEVENT%(30)** to store the type of events detected, and **EVNTPT%(30)** to store their positions in **SIGNL()**. These arrays are updated every time there is a change in peak status.

The baseline is considered stable when its drift does not exceed a certain preset value. It uses two variables to help determine this drift; these are **NBSEG%**, the number of baseline segments for which local baseline values are to be calculated, and **NBASE%**, the total number of points of baseline acquired. First, **NBSEG%** segments, each of (**NBASE%/NBSEG%**) points, are read and the mean values in each segment are calculated. These values are then compared to check for the drift: The slope is calculated

between the means of each segment and is compared to a threshold value. This process uses a FIFO (first in - first out) buffer of length **NBSEG%**. As a new segment is acquired, the oldest segment is "pushed out" (*i.e.*, forgotten).

After the baseline has stabilized, the peak status is set to 0, and the last segment is used in calculation of baseline parameters, *i.e.*, the mean baseline reading and its standard deviation. The leading edge of the first peak is determined by a consecutive series of first-derivative values which steadily increase (in a positive or negative fashion). This triggers a change from status 0 to status 1 or 2.

A change to status 3 or 4 (from 1 or 2) is triggered by the first-derivative value passing back through zero. This signifies that a peak maximum (or minimum) has been detected.

On return to baseline conditions, the peak status again becomes zero. The process can then occur again. Changes to status 0, 3, and 4 initiate a count-down to stop acquisition. Data acquisition stops when either a preset time limit is exceeded, a peak is detected, or an "S" (for stop) key is struck by the operator. When acquisition is stopped, the event buffer is checked for the location of peaks, as indicated by a change in status to 3 or 4. Points on either side of the indicated event are checked to find the true peak maximum. The index of the peak with the largest absolute maximum is then returned as the peak height. The data sampling frequency is typically 5 Hz.

The sequence of identified events is more complex (*i.e.*, more events are identified) in the case of peaks which have more than one maximum (or minimum), or which have pronounced shoulders. Such peaks can sometimes be identified by the fact that the signal has not truly returned to the baseline.

After acquisition has stopped, all events indicated to have had a peak status of 0 which changed from a status of 3 or 4 are processed as peaks. In any case, the software reports the largest peak found.

Noise sources such as pulsation from peristaltic pumps, the presence of small air bubbles in tubes, or electrical interference can all contribute to FIA peak characteristics. Study of their effect on peak shape readily reveals that the noise observed is invariably at a much higher frequency than the more slowly time-variant actual analytical peak profile. Thus, algorithms which smooth peak profiles can help reduce noise. However, smoothing also results in a slight broadening of the observed peaks.

In this work, an 11-point Savitsky-Golay derivative filter [62] is used to estimate the slope of the acquired data points. Since it takes into account more than just two consecutive points, it also acts as a way to reduce noise in the first-derivative. The filter used is of order 2 (a quadratic polynomial) with coefficients as -5, -4, -3, -2, -1, 0, 1, 2, 3, 4, and 5, and a corresponding normalization factor of 110. Since 5 values are obtained every second (this number is variable), a further normalization factor of x 0.2 s is applied.

Currently, the maximum slope allowed for a baseline to be considered stable is set at 2.0 ADC units s^{-1}. The threshold for detection of a leading edge is usually set at 6.0 ADC units s^{-1}. These values can be changed, depending on how stable a baseline is required (or obtainable), and how steep one expects the slope of the leading edge of detectable peaks to be. Too large a value for leading edge detection can result in the inability of the algorithm to detect small peaks. If the value is too small, then baseline features due to noise will be falsely identified as the start of a real peak. In any case, data acquisition is terminated after a time corresponding to the transit time of the sample through the analytical manifold, and the value reported as the peak maximum value is the maximum found within the data acquisition window that has been recorded.

CHAPTER THREE

BASIC METHODS DEVELOPMENT AND CHARACTERIZATION

3.1 Introduction

The literature reveals that many manual methods have been adapted to FIA. [1, 42] Indeed, FIA has been described as "a chemical reaction system where the chemistry factors are manipulated so as to overcome problems which may otherwise inhibit the analysis". [42] While it is (usually) relatively simple to take a fast, colorimetric chemistry and make it occur reproducibly within the confines of a flow system, one cannot overemphasize the importance of obtaining a proper understanding of the chemistry involved. Without this, full advantage cannot be taken of the chemical and physical interactions that are characteristic of FIA systems. From a research perspective, scientists would like to achieve an in-depth understanding of these effects; an automated flow injection analyzer is a rapid and efficient way to gain such insight.

In manual wet chemical analysis, one must consider the mutual effects of inter-dependent chemical variables such as pH, reagent concentrations, ionic strength, *etc.* Continuous flow methods are even more complex, because each of these variables may interact with the additional (physical) variables of flow rate, length of tubing between injection and detection, sample volume, inner diameter of reaction coil, *etc.* Even the simplest single channel manifold will have at least five different variables, whereas in more complex systems such as in a solvent extraction system, up to 12 variables have been studied [61]. Thus, full development of an FIA procedure must include proper establishment of optimum physical and chemical conditions. The literature reveals that for a given procedure, conditions adopted by different workers (or some workers on different occasions) and described by them as optimum may vary appreciably, [16] depending on the optimization procedures (or lack of) which they used.

Various theories [1, 30, 35, 63-64] exist that are valuable and provide useful guidelines to the selection of experimental conditions; they all have their limitations. These theories are mainly derived from the studies of Taylor [28, 65] and Levenspiel [37] in which sample dispersion is treated as a purely physical phenomenon. In FIA, one must also

consider deviations from theory due to chemical interactions between sample matrix and carrier. The geometry of the sample injection device and detector(s) also has a significant effect on dispersion [66, 67] as can the rate of chemical reaction. [68] Thus, because of the complex nature of the interactions possible in a FIA system, multivariate optimization approaches are desired. These must be reliable, fast, and preferably less tedious than extensive sets of (usually manual) experiments called for by a full factorial design.

3.2 **Optimization procedures**

3.2.1 Selection of Appropriate Optimization Procedures

The selection of the best method for optimizing a particular system requires consideration of the factors shown in Table 3.1.

Number of maxima	none	one	many		
types of factor	continuous		discrete		
time required per expt.	negligible		short	medium	long
number of variables	1	2	3	4	5 ...
amount of noise present	negligible		low	medium	high
type of response surface	continuous		discontinuous		bounded
interaction of variables	absent		present (simple or complex)		

Table 3.1. Factors to be considered in selecting best optimization method.

For example, hill-climbing methods may be inadequate where more than one maximum exists, since they are not guaranteed to find the highest maximum; algorithms which use mathematical extrapolation or interpolation of values for variables are unsuited to systems with discrete factors (*e.g.*, solvent selection in HPLC); systems which require a long time

per experiment (*e.g.*, agriculture) will be far better addressed by parallel optimization methods than by sequential; exhaustive search (pattern search, grid methods, *etc.*,) are impractical for more than 3 variables; evolutionary methods, such as simplex optimization, may not work in high-noise situations; methods based on model functions will not be well suited to response surfaces with discontinuities; univariate methods are insensitive to variable interactions. Some of these methods and their strengths and limitations are now discussed in more detail.

3.2.2 Optimization Methods

3.2.2.1 *Standard univariate approach*

Until the early 1920's, experiments designed to investigate the effects of several factors (variables) on a response were based on the one-factor-at-a-time (univariate) approach. In these experiments, all factors but one are initially held constant. Responses are then evaluated at various levels of this first factor and the level which gives best response is determined. Sucessive factors are then allowed to vary in a similar manner, each time holding the previous factors at their optimized levels. At that time, the prevailing idea was that if the factors were varied simultaneously, then the effects of the factors would be hopelessly intermingled.[69] This however had the disadvantage of ignoring factor interactions that could exist, in addition to being tedious and time consuming.

Such a sequential single-factor approach is probably the most common method of optimization in analytical chemistry. Unfortunately, it does not guarantee that an optimum will be located, especially when the response surface contains a ridge which is diagonal to the factors' axes. This is unsatisfactory,[72] since, although an improvement over the initial conditions may be obtained in the presence of such a ridge, the approach is likely to yield a false optimum which may be far from the true optimum. For example, ridges are known to exist frequently in chemical systems and result from interdependence of optimum values of

the chosen variables. [73] It is important that ridges be identified, since they indicate the presence and nature of such interactions to the analyst. For response surfaces of this nature, most rapid improvement is possible if the variables are changed together in the direction of the axis of the ridge. This is not possible with a univariate search. Thus, designs that can take into consideration such multi-factor interactions are inherently more efficient and should be employed.

In general, one cycle of varying the factors is not sufficient to precisely locate the optimum. Thus, an iterative approach is often used where more than one cycle of some or all factors is performed.

3.2.2.2 *Iterative univariate method*

In contrast to the standard univariate approach discussed above, each variable can be considered several times. In systems where the variables do not interact (*i.e.*, where the response can be expressed as the sum of independent functions of each variable) this approach is quite successful and very efficient. However, interactions between variables may still cause the method to fail. [3]

It is now generally held that univariate methods are inadequate for multi-factor experimental optimization of analytical chemical methods. Indeed, significant errors can result from their use where complete knowledge of which variable interactions determine the response is not initially available.

3.2.2.3 *Factorial designs*

Recognizing the importance of identifying variable interactions, Fisher [70] advocated the use of factorial design approaches, in which all variables are varied simultaneously. Friedman and Savage [71] pointed out the following deficiencies of factorial design methods when used for the purpose of multi-factor optimization:

(i) The factorial design neglects the fact that some factors are continuous (*e.g.*, samples can be of any size) and some, though they may be discrete, are ordered (*e.g.*,

different solvents may be ranked by their polarity). Factorial designs are most powerful when used to detect differences caused by two or more discrete possibilities. However, if a factor is continuous, then the results are highly dependent upon the choice of levels tested. There is a very real possibility that the levels of the factor might be set either too close together in which case the effect might not be statistically significant, or too far apart in which case an optimum might be missed entirely and possibly no significant effect would be found. Figure 3.1 illustrates some of these possibilities.

(ii) Factorial design can explore either a small region comprehensively or a large region superficially. In the former case, the design might give at best an indication of the direction to move to conduct a new set of experiments. If, on the other hand, the factorial design explores a large region, then an optimum, if found, would be known so imperfectly that further experimentation would be required.

(iii) The factorial design explores regions that might ultimately be of no interest because they are far from an optimum. Friedman and Savage [71] thus suggested a "sequential one-factor-at-a-time" (iterative univariate) search over the classical factorial design.

3.2.2.4 *Evolutionary operation methods*

Multi-factor response surface designs to cope with systems of interacting variables were first advocated by Box. [69] These "evolutionary operation" (EVOP) methods use factorial designs combined with regression techniques to estimate the direction of steepest ascent and to locate the optimum region of a response surface. [74-77]

3.2.2.5 *Basic simplex optimization*

For response surfaces which are continuous, fairly smooth, have a single optimum, and do not suffer from excessive noise, the sequential simplex method (also called the fixed-size or basic simplex method) introduced by Spendley *et al.* [78] can rapidly determine the experimental optimum. It does this through calculations and rules-based decisions that

are rigidly specified; this makes it particularly attractive for automated optimization. Several variables are changed simultaneously in what is essentially a "hill climbing" approach to the problem. The use of simplex designs in analytical chemistry has been reviewed by Deming and Morgan, [79] who pioneered this approach in analytical chemistry. Simplex optimization [78] can also be considered a multivariate "evolutionary" technique (in the Darwinian sense), since points with low merit lose their place in the current simplex (*c.f.* becoming extinct) as they are replaced by points of higher merit.

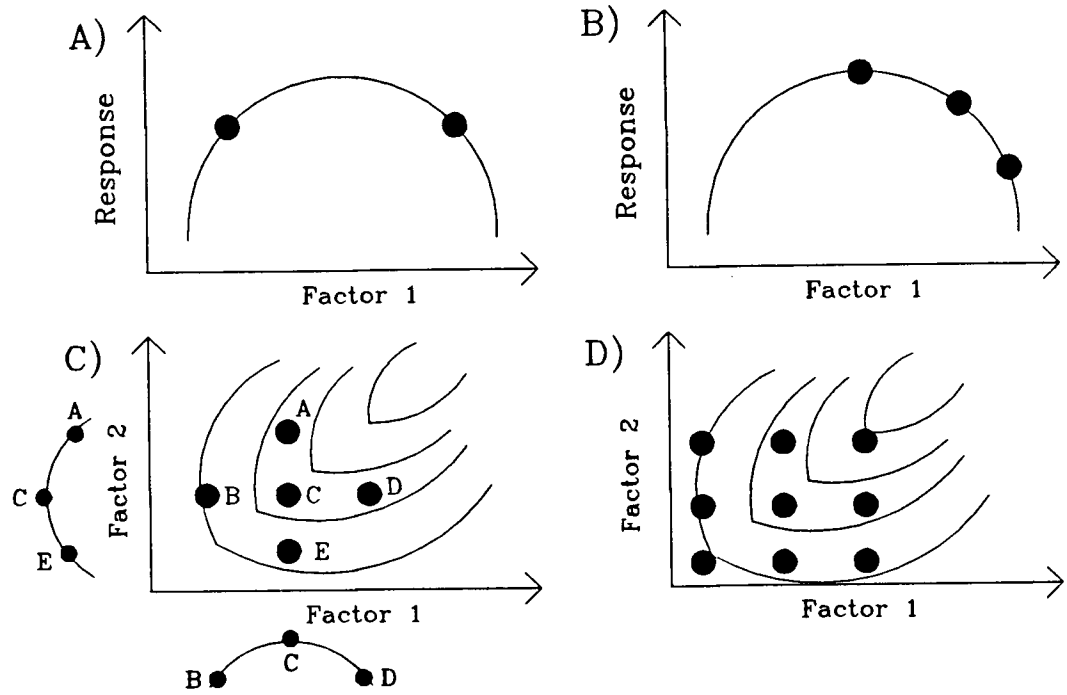

Figure 3.1. Possible effects of different level factorial designs on determining optimum conditions.

(a) A 2-level 1-factor design fails to detect the optimum. This predicts that factor 1 has no effect on the response.
(b) A 3-level 1-factor design (too closely spaced) fails to detect the optimum. It may predict highest response at low values of factor 1.
(c) A "partial" 3-level 2-factor design fails to detect interaction of factors 1 and 2.
(d) A "full" 3-level 2-factor design which detects interaction of the factors and that the optimum likely lies outside of its boundaries.

Let us consider a chemical system which has n factors (n = 1, 2, ...) for which we wish to find the optimum values of all the factors. The n variables can be thought of as n orthogonal axes with each experiment represented by one point in this "factor space". A simplex is defined as a regular geometric figure consisting of $(n+1)$ vertices; thus, for a 2 factor system the simplex will be a triangle, and for a 3 factor system, a tetrahedron, *etc.* For n variables, $(n+1)$ experiments are required to construct the first simplex.

To start a simplex optimization procedure, we first define the range in each variable for the simplex to explore. The initial simplex shape is then set up such that it initially covers a reasonable proportion of the space available (30% in our studies). Experiments are then carried out at conditions corresponding to the simplex vertices, their responses recorded, and then ranked in order of merit. To illustrate in detail further operations for this basic simplex optimization method, a hypothetical two variable system is chosen and the process demonstrated using Figure 3.2. The points labelled **B**, **N**, and **W** represent the ranks of the responses at the simplex vertices and correspond to "Best", "Next-to-best", and "Worst" respectively. By reflecting the point (**W**), through some point (**P**) at the center of the opposite face of the simplex (**B-N**), its reflection (**R**) is generated.

Experiments are then performed under the new experimental conditions corresponding to the point (**R**) and its response compared to the previous responses. The idea is that, since we are moving away from (**W**), a point of poor response, in a direction known to give a better response, it is likely that (**R**) might yield further improvement. By rejecting (**W**) and replacing it with (**R**), a new simplex of the same size is formed. By repeating this procedure, the simplex "climbs" the response surface, and thus finds the optimum conditions. This approach is the "fixed-size simplex method."

The purpose of simplex, just like other pattern search methods, is to "zero in" on the optimum region of the response surface from a given subregion by forcing the pattern to move in the direction of steepest ascent as estimated by response measurements at the points in the pattern. The optimum thus obtained will in general be a local optimum.

Assurance that it is the global (overall) optimum can be increased if the search is repeated starting at different initial regions of the factor space. If more than one local optimum is found, the best can be taken as the "global" optimum.[+]

The fixed size simplex is limited due to its inability to adapt quickly (in few experiments) to the shape of the response surface and inability to accelerate across the response surface when responses indicate this is favorable. This arises from the fact that, if initially a large simplex size is chosen, then the optimum will be reached quickly, but will not be known with good precision. If however, a small simplex size is used, then the final optimum would be known more precisely, but it would take more experiments to get there.

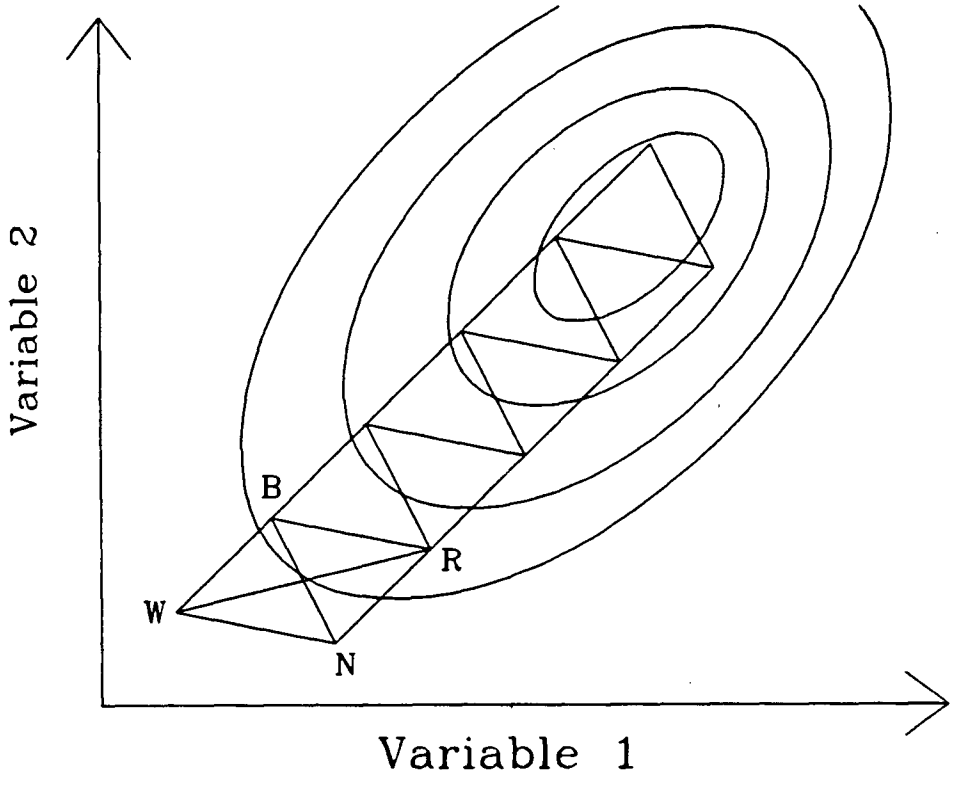

Figure 3.2. A simplex for two factors, showing "best" vertex **B**, "next-to-best" vertex **N**, "worst" vertex **W**, and reflection vertex **R**.

[+] Although not part of the simplex procedure itself, given enough data points spread across the response space, it can be possible to construct a global system model surface from the data obtained.

Figure 3.3 is a diagramatic representation of the simplex procedures for 2, 3 and N dimensional systems. The left hand column shows the array of simplex points which are stored in computer memory. The central column indicates the dimensionality of the simplex and search space. The right hand column shows (where possible) its progress towards the optimum.

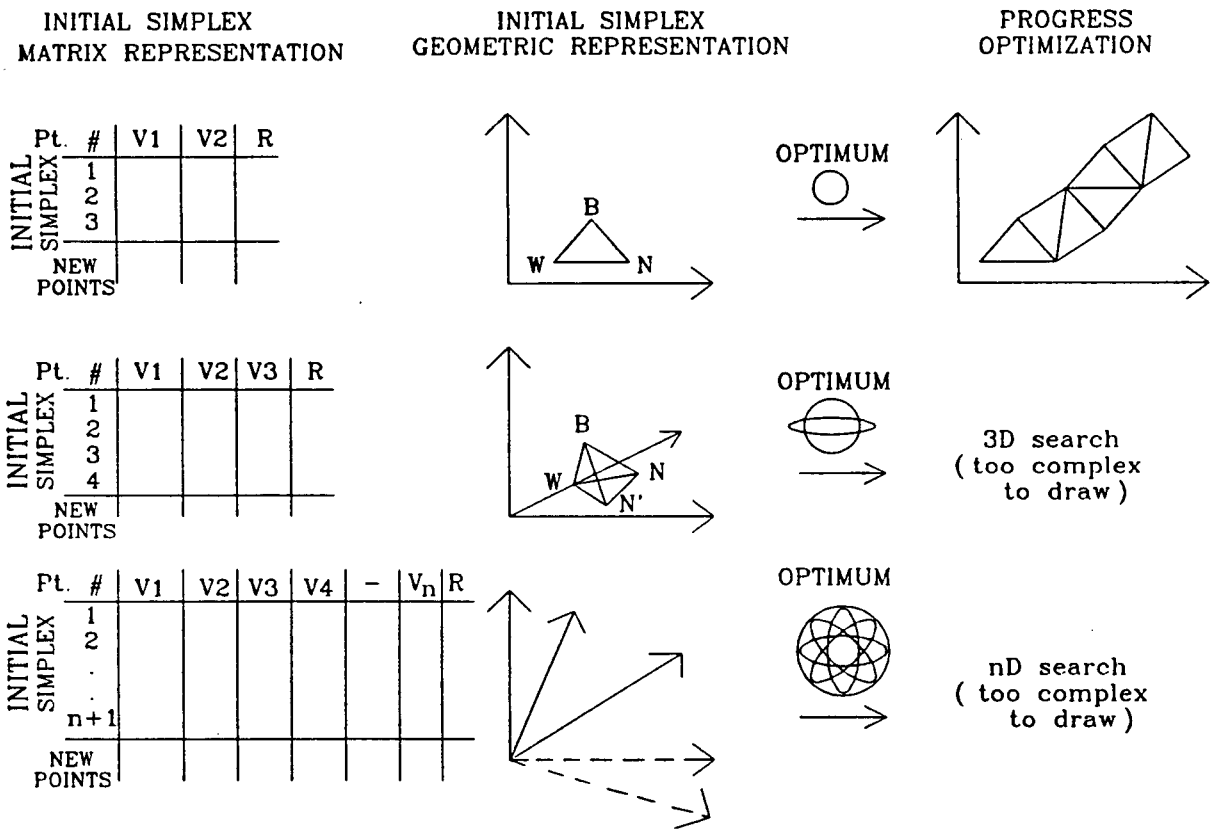

Figure 3.3. Two, three, and *n*-dimensional representations of simplex matrices and their corresponding simplexes.

3.2.2.6 *Modified simplex optimization*

The limitations discussed above gave rise to several more flexible simplex procedures which allow the simplex to expand and contract in a manner determined by the local topography of the surface being investigated. The first of these methods was by Nelder and Mead [80], who provided the capabilities of acceleration in directions that are favorable and deceleration in directions that are unfavorable. This "modified simplex method" is a logical extension to Spendley's algorithm and consists of rules for reflection, expansion, contraction and massive contraction. The introduction of expansion and contraction of the simplex has resulted in faster optimization as the simplex expands up the response peak and then contracts onto the top. A detailed discussion on the procedures of this approach has been given by Morgan and Deming. [72] Since then, various further modified versions have been suggested, each aiming to improve the speed and reliability of optimization. These have been contrasted elsewhere. [61]

3.2.2.7 *The composite modified simplex method*

Used in this work is a further modified version, as described by Betteridge *et al.* [3] Their algorithm includes;

(a) weighting the centroid, **P**, toward the better (n-1) points,

(b) a Lagrange interpolative fit (subject to certain conditions) wherever a maximum is suspected to lie within the current simplex,

(c) a procedure to aid in the detection and avoidance of the problems caused by two or more maxima being present,

(d) provisions to help prevent loss of dimensionality,

(e) prevention of simplex oscillation setting in,

(f) consideration of the amounts by which experimental variables can be measurably varied, and

(g) treatment for boundary conditions.

On average, about two experiments are needed per complete cycle, where a cycle is defined as the number of experiments required to generate a new simplex. At the minimum, a cycle is one experiment, *i.e.*, the reflection is accepted. The usual maximum is three experiments, *i.e.*, reflection, expansion, or contraction, Lagrange fit.

The process is terminated when either the optimum is reached, the procedure fails, the operator considers the current rate of improvement not to be worth the effort (cost) involved, or a pre-specified number of experiments (or cycles) have been carried out. The optimum may be defined as either the point at which further adjustments to the variables would require smaller alterations than are experimentally possible or where the same result is obtained within the limits of experimental accuracy.

3.2.3 Automated Methods Development for FIA using the Composite Modified Simplex

This chapter illustrates the automated optimization of FIA conditions for the determination of palladium and persulphate ions. The Composite Modified Simplex optimization algorithm of Betteridge *et al.*, [3] is employed to optimize the various relevant chemical and flow conditions. While this approach can rapidly locate an optimum, it provides limited information about the global nature of the response surface [81] and so is supplemented by a response surface mapping procedure. This carries out multiple experiments in a regular square pattern (as in a full 2-factor 8-level factorial design) and so better characterizes the experimental variables under study. It provides the experimentalist with evidence of the stability of the analytical performance of different sets of operating conditions, and therefore acts to guarantee the experimental repeatability of the analytical method. It does this at the expense of more experiments and perhaps less information about the region of the optimum. These advantages and disadvantages are discussed in detail elsewhere. [73]

The FIDO system detailed in Chapter 2 is employed to facilitate these approaches to automated methods development by appropriate control of injection/stream switching

valves and variable speed pumps. The automated flow injection analyzer's high degree of computer control is employed and its capabilities for "soft automation" (whereby the function of the analyzer is in part specified through software, and thus may be modified in real-time) are tested. Simplex optimization and response surface mapping are implemented on this automated hardware to facilitate operator-unassisted methods development.[3, 52] These approaches provide a means to obtain optimum flow conditions as well as to better characterize the chemistry which occurs in the analytical systems. Results from both studies are compared and contrasted.

3.3 Spectrophotometric determination of Palladium with sulphochlorophenolazorhodanine by flow injection

3.3.1 Introduction

Until recently, little attention has been given to development of flow injection procedures for palladium. This is somewhat surprising in view of the commercial value of palladium and its wide use in catalysts and alloys. Palladium and its sister metal platinum are widely used as catalysts in several industrially related productions, *e.g.*, in catalysts for automobile exhaust gas converters (to reduce pollution from the toxic fumes), dental alloys, relay contacts in sophisticated electronic equipment, *etc.*

Several methods for the determination of palladium have been reported. Gravimetric approaches involving precipitation by suitable chelates have been used extensively over the years. The need for the development of simpler and more reliable methods still exists and has been one of the driving forces behind this present study. Most of the existing practical procedures for palladium determination can be categorized as: spectrophotometric, extraction based spectrophotometric, gravimetric and instrumental methods. These categories will now be briefly reviewed.

Spectrophotometric methods. The bulk of manual methods for palladium determination are spectrophotometric methods, often with liquid-liquid extraction steps. Kai *et al.* [82] proposed use of 4-(3,5-dichloro-2-pyridylazo)-1,3-diaminobenzene as a sensitive and selective reagent for the photometric determination of trace amounts of Pd(II) ion in aqueous solution. They reported a linear dynamic range of 0.05 - 1.33 ppm with minimal interference from other metal ions. Only Cu(II) and Ag(I) strongly interfered at 100-fold concentration level (relative to Pd(II)). However, a minimum reaction time of 5 minutes is required for adequate sensitivity, presumably because the reaction has not

reached steady state absorbance. Marczenko *et al.* [83] reported a flotation-spectrophotometric method for determining palladium using the ion-association complex of pentabromopalladate (II) with Rhodamine 6G. In this, benzene was used for flotation and dimethylformamide for the dissolution of the ion-association complex. They reported a high molar absorptivity value of 3.0×10^5 l mol^{-1} cm^{-1} at 530 nm and Beer's law was obeyed up to 0.3 μg ml^{-1} Pd(II). The disadvantage with this method however, is that after separation of the aqueous phase, the excess of free dye must be removed from the ion-association complex by washing *i.e.*, the benzene phase and the precipitate are shaken with at least three portions of water. The method also has limited selectivity; mercury and molybdenum give positive errors of about 35% when present in 5-fold ratio to palladium. At the 10-fold excess level, gold, bismuth or manganese gives about 10% error, cadmium, a 40% error and gallium a 20% error. Nitrate was also reported to interfere at the 0.05 M level whereas perchlorate interferes even at 5.0×10^{-4} M concentration. Thus, despite its high sensitivity, the method is far from ideal. MacNevin *et al.* [84] used EDTA as a chelating reagent and photometrically determined palladium over a wide concentration range (Beer's law obeyed over the range 5 - 200 ppm Pd(II)) in the pH ranges of 1.6 - 2.0 and 5.0 - 9.0. Limitations to the use of EDTA as a developing reagent are that the pH must be adjusted and kept within limits based on the accuracy desired in the analysis. The least change in absorbance (A) with pH occurs in the regions pH 1.6 to 2.0 and pH 5 to 9, *i.e.*, $\Delta A/\Delta pH = 0.012$ in the neutral range and $\Delta A/\Delta pH = 0.032$ in the region pH 1.6-2.0. Also, other platinum group metals interfere and palladium must be separated by precipitation with dimethylglyoxime prior to the development of color with EDTA. Photometric measurements are also restricted to within 30 minutes after preparation of solution since a precipitate forms in neutral or slightly basic solution on extended aging.

Recently, Liu *et al.* [85] reported a sensitive co-color reaction between Pt(IV) and Pd(II) with 4,4'-bis(dimethylamino)thiobenzophenone (Thio-Michler's ketone) (TMK) in the presence of ascorbic acid and Triton X-100 (a non-ionic surfactant to stabilize the

homogeneity of aqueous solution). They reported a molar absorptivity of 1.96×10^5 l mol^{-1} cm^{-1} for Pd(II) (in the presence of 10 μg ml^{-1} of Pt(IV)) and 2.98×10^5 l mol^{-1} cm^{-1} for Pt(IV) (in the presence of 10 μg ml^{-1} of Pd(II)). The presence of both Pd(II) and Pt(IV) is a pre-requisite for color development, since reaction between either of these with TMK in the presence of ascorbic acid only proceeds when the solutions are boiled in a water-bath for 15-20 minutes. The best Pt:Pd:TMK ratio was reported to be 1:2:12 and Beer's law is obeyed over the range 0 - 0.8 ppm of Pd(II) and 0 - 0.48 ppm Pt(IV) in the presence of 10 μg ml^{-1} of Pt(IV) and 10 μg ml^{-1} of Pd(II) respectively. In this determination, silver(I), arsenic(V), gold(III), bismuth(III), chromium(III), and copper(II) gave serious interferences, with a tolerance of at most 20 μg ml^{-1} for a ± 5% error in determination of both Pt(IV) and Pd(II).

Extraction-spectrophotometric methods. Several sensitive liquid-liquid extraction spectrophotometric methods have been used as separation methods in the analytical chemistry of platinum group metals.[86] Among the sensitive reagents for palladium, 2-pyridylazo dyes seem to be the most promising. The analytical application of 2-(5-bromo-2-pyridylazo)-5-diethylaminophenol (5-Br-PADAP) has been extensively investigated because of the high sensitivity (a molar absorptivity of around 10^5 l mol^{-1} cm^{-1}) of its reactions with metal ions and the detection limits have been further increased by extraction.[87] Gusev *et al.*[88] suggested 5-Br-PADAP as a sensitive reagent for the extraction spectrophotometric determination of palladium in acidic media (0.5-7.0 M acid), with a molar absorptivity of 4.3×10^4 l mol^{-1} cm^{-1} at 575 nm. Beer's law is obeyed for 0.1-3.0 μg ml^{-1} Pd(II) in chloroform. A similar method was described,[89] again with highly acidic solutions and Beer's law is valid for 0-2.4 μg ml^{-1} of benzene. Because of the high molar absorptivity of the Zn(II)/5-Br-PADAP complex,[87] Michaylova *et al.*[90] reported the further sensitivity enhancement of the palladium determination by applying the known metal-exchange reagent Zinc(II) dibenzyldithiocarbamate. They reported very high

sensitivity ($\epsilon \approx 8 \times 10^4$ l mol^{-1} cm^{-1}), and a lower concentration range obeying Beer's law (0.1-1.2 μg ml^{-1} Pd(II)). However, the method is not selective for palladium in the presence of those metal ions which form colored complexes with 5-Br-PADAP and those which give more stable complexes with dibenzyldithiocarbamate than does zinc(II). Mercury(II), chromium(III), silver(I), lead(II), iron(III), and platinum(II) all interfere. Cobalt(II), cadmium(II), copper(II), nickel(II) and manganese(II) interfere strongly. Thus, selectivity is minimal. Watanabe and Hojjatie [91] also reported a sensitive liquid-liquid extraction procedure for the determination of palladium. In their method, the palladium complex of 2-mercaptobenzamide (MBA) was extracted into tributyl phosphate (TBP) forming a Pd:MBA:TBP complex (in 1:2:2 ratio) with molar absorptivity of 1.59×10^4 l mol^{-1} cm^{-1} at 350 nm. Beer's law is obeyed over the range 1 - 35 μl ml^{-1} Pd(II). The RSD% for 15 μg ml^{-1} Pd(II) was remarkably low, at 1.5%. Silver(I), gold(III), osmium(VIII), selenium(IV) and tellurium(IV) at the 100 μg ml^{-1} level caused an error of up to ± 5% and could be tolerated. Other interfering metals such as nickel(II), lead(II), zinc(II), copper(II), chromium(VI) and cadmium(II) could be masked with 1 ml of 5% EDTA.

Although these extraction methods for the preconcentration of the platinum metals offer high sensitivity, they provide limited selectivity and precision (general relative standard deviations are in the range 3-5%) and are generally time-consuming owing to the slow rate of formation of the extractable species from the relatively stable starting chloro complexes. [92, 93]

Gravimetric methods. Gravimetric analysis using dimethylglyoxime (DMG) as a precipitating agent is the most common method for the determination of palladium. Ayres and Berg [94] reported the optimum conditions for the separation of palladium from other platinum group metals by precipitation with DMG. Ayres and Tuffly [95] also used the DMG method to separate palladium prior to colorimetric determination as the bromide

complex. Their method involved digestion of the precipitate with aqua regia followed by destruction of the remaining organic matter with fuming perchloric acid prior to colorimetric measurement. MacNevin *et al.* [84] also used the above method of Ayres *et al.* to separate palladium from large amounts of other platinum metals and satisfactorily determined palladium photometrically using excess amounts of disodium salt of EDTA (after dissolution of the precipitate with *aqua regia*) without treatment with perchloric acid. These methods are both tedious and time consuming.

Instrumental methods. Several instrumental methods exist for palladium determination. Of particular popularity are atomic absorption spectrometry, [96] plasma atomic emission spectrometry, [97] and inductively coupled plasma-atomic fluorescence / emission spectrometry. [98, 99] Lockyer *et al.* [96] reported a method for the quantitative determination of silver, gold, platinum, rhodium, and palladium in concentrations down to 1 ppm in solution. Reproducibility was good, and no inter-element effects were found even when excess amounts of lead and iron were present. Xiandeng and Peifang [98] used the modified simplex method of optimization in the determination of traces of palladium in extraction with 2-mercaptobenzothiozole-methyl-isobutyl ketone and detection by flame atomic absorption spectrometry. A linear range of 0-0.7 μg ml^{-1} palladium, a sensitivity of 4 ng ml^{-1}, and a relative standard deviation of 1.7% for determination of 0.5 μg ml^{-1} was obtained. Skrabak and Demers [99] used a combination of ICP and atomic fluorescence spectrometry in the simultaneous multielement determination of precious metals with no spectral and few other interferences. Excellent detection limits in the low ppb were obtained. Despite the relative sensitivities of these instrumental methods to the other methods described above, they are fairly costly and are therefore seldom used for routine analysis.

Flow injection spectrophotometric methods. For flow injection methods, direct colorimetric methods of analysis are preferred because of their simplicity. Haj-Hussein and Christian [100] reported a direct colorimetric flow injection method for the simultaneous determination of copper, nickel, and palladium. The method made use of the Beer-Lambert law which states that absorbances are additive. It requires sequential measurement of the absorbances of the metal-EDTA complexes at several wavelengths. This provided them with a set of simultaneous equations from which the individual concentrations of the metal ions were evaluated. The method exhibited reasonable selectivity and precision (better than 1%). The limitations to the use of EDTA as a developing agent are that the pH must be adjusted precisely to limit other metals from interfering when present in appreciable amounts.

Sakai and Ohno [101] recently reported a flow injection method with greater sensitivity. In their method, 2-(5-Bromo-2-pyridylazo)-5-(N-propyl-N-sulfopropylamino)-aniline was used to form a water soluble complex with palladium in an acetate-buffered medium. The molar absorptivity of the complex is 9.84×10^4 l mol^{-1} cm^{-1} at 612 nm and Beer's law is obeyed over the range 0.01 - 0.10 μg ml^{-1} Pd(II). The method offered a good detection limit of 0.002 μg ml^{-1} and a relative standard deviation of 0.6% for 0.1 μg ml^{-1}. The sample throughput was 50 hr^{-1}. No other flow injection methods for palladium have been found in the literature.

In response to the limited number of FIA procedures for the determination of palladium, an attempt was made to develop a simple, fast, and sensitive spectrophotometric FIA method using an azo-derivative of rhodanine as a chelating reagent. Savvin and Guereva [102] reported that a number of azo compounds based on rhodanine and thiorhodanine may be used as highly sensitive and selective reagents for the spectrophotometric determination of noble metals. The reaction times cited for maximum color development were typically several hours, but molar absorptivities obtained were as high as 1.2×10^5 l mol^{-1} cm^{-1}. It was thought that acceptable analytical sensitivity might

be obtained using shorter reaction times if the highly repeatable timing of flow injection was employed. Of particular interest was the azo-derivative of rhodanine, sulphochlorophenolazorhodanine (SCPAR) whose structure is shown in Figure 3.4 below. This reagent was reported to form a palladium complex with a high molar absorptivity (1.2×10^5 $l.mol^{-1}.cm^{-1}$). This section reports further investigation of this chemistry and development of a flow injection method for palladium based on this reagent. The synthesis and characterization of the sodium salt of SCPAR (denoted Na-SCPAR) is also given. [60]

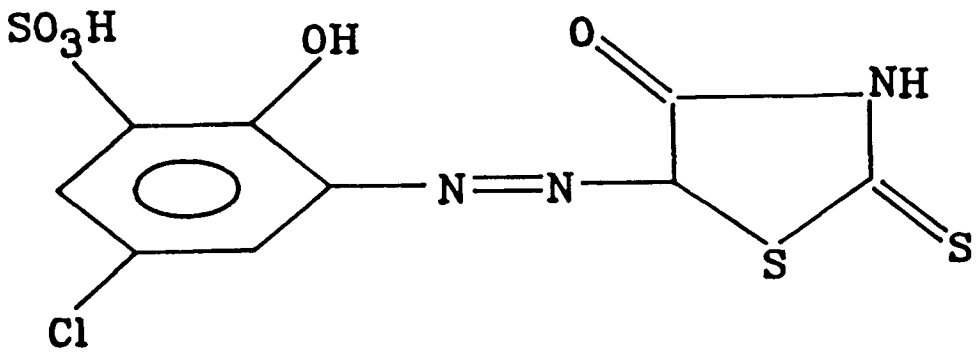

Figure 3.4 Structure of the reagent SCPAR.

3.3.2 Experimental Section

3.3.2.1 *Reagents*

A stock solution of palladium(II) (1.00×10^{-3} M) was prepared by dissolving palladium(II) chloride (Alfa, Danvers, MA), in 0.01 M hydrochloric acid. Sample solutions were prepared by appropriate dilution. Solutions of metal ions for the interference studies were made from the nitrates of copper(II), nickel(II), lead(II), aluminum(III), mercury(II), bismuth(II), silver(I), cobalt(II), rhodium(III), chlorides of iron(II), iron(III), platinum(IV), ruthenium(III), zinc(II), iridium(III), cadmium(II), tin(II), and gold(III), and manganous sulfate. Analar grade salts were used, with the exception of platinum(IV), which was prepared by dissolution of platinum wire in *aqua regia*.

A universal buffer solution [103] at pH 2.0 was prepared for the automated optimization and batch method experiments. Buffer solutions at various pH values above this were then obtained by addition of appropriate volumes of 0.2 M sodium hydroxide.

3.3.2.2 *Synthesis of Na-SCPAR*

Synthesis of the sodium salt of SCPAR (Na-SCPAR) reagent employed a diazotization step followed by a coupling reaction. Details of the synthetic scheme is given below.

3.3.2.2.1 *Diazotization step*

A total of 11 g (0.05 mole) of 2-amino-4-chlorophenol-6-sulfonic acid (ACPS) (ATK Inc., Tokyo, Japan) were dissolved in 100 ml of distilled water. To this was added 20 ml of 12 M HCl; the reaction mixture was then cooled in an ice bath before adding 3.45 g (0.05 mole) of $NaNO_2$. The mixture was then stirred continuously while about 40 ml of water were gradually added over a period of 1 hr. After standing for another hour at 0 °C, the mixture was neutralized by addition of 2.5 g of sodium acetate. The final product expected was the diazonium salt of ACPS.

3.3.2.2.2 *Coupling reaction*

The diazonium salt of ACPS was coupled with rhodanine by adding a solution containing 6.7 g (about 0.05 mole) of rhodanine (Aldrich, Milwaukee, WI) in 150 ml of 1 M NaOH solution to the diazonium salt mixture. This was kept in an ice bath at 0 °C for 1 hr, with the pH maintained between 7 and 9 by addition of small amounts of either dilute NaOH or HCl. As the azo coupling proceeded, the mixture acquired a dark red color. Drops of 12 M HCl were then added until a pH of about 3 was obtained. The product which precipitated out was filtered and washed with small amounts of cold water. The precipitate was then purified. First, it was redissolved in about 200 ml of water and about 3 g of Na_2CO_3 was added. The insoluble residue which remained was discarded. The filtrate was acidified with a few drops of 6 M HCl to precipitate the purified product, which was then filtered off, washed with cold distilled water, and dried in air. The product was a red-orange powder with a yield of about 10 g (54%).

A portion of the isolated product was further purified using preparative column chromatography. Separation of the Na-SCPAR from a minor amount of residual ACPS was carried out on a silica gel column with a mobile phase consisting of 5% methanol and 1% acetic acid in diethyl ether. From this, a 9.44×10^{-3} M Na-SCPAR stock solution was prepared by dissolving 0.3676 g of the purified reagent in 1 l of 0.01 M HCl.

3.3.2.3 *Apparatus*

The automated flow injection analyzer used is described in detail in Chapter 2. The options used were a single 6-port air-driven solenoid-actuated injection valve (Rheodyne 5020P, Cotati, CA) equipped with a 70 μl sample loop, the 5-channel peristaltic pump unit, and 0.42 ml. min^{-1} rated pump tubings. Polytetrafluoroethylene (PTFE) tubing (0.5 mm i.d.) was used throughout. A diode array spectrophotometer (Hewlett Packard 8452A) with a standard 1 cm quartz cell was used for absorption measurements. For the flow injection studies, a 30 μl, 1 cm path length quartz flow cell was used. The pH of

reaction mixtures was determined using a laboratory pH meter (Fisher Scientific, Type 119) and a flow through electrode cell designed in our laboratory.

An infrared spectrophotometer (Perkin-Elmer Model 598) was used to record infrared spectra over the range 200 - 4000 cm^{-1}. Finely ground samples were mulled in Nujol and sandwiched between KRS-5 plates (58% thallium iodide, 42% thallium bromide, Harshaw Chemical Co.). Spectra were calibrated at 907 and 1601 cm^{-1} with polystyrene film. Tabulated frequencies are accurate to ± 5 cm^{-1} for broad bands and ± 2 cm^{-1} for sharp bands.

3.3.2.4 *Software*

The Flow Injection Development and Optimization (FIDO) software used for the optimization and response surface mapping experiments is described in Chapter 2. Additional code that was used for nonlinear curve fitting, factor analysis, and other data processing tasks was written in our laboratory in Microsoft QuickBASIC^{R} version 4.0 (MSQB4). The optimization algorithm used was the composite modified simplex method. [61] Response surface plots were generated using a commercial scientific graphics program (SURFER^{R} version 3.0, Golden Software, Golden, CO).

3.3.2.5 *Procedure*

3.3.2.5.1 *Kinetic studies*

To establish the effect of pH on the rate of the Pd(II)/Na-SCPAR reaction, both manual and stopped-flow studies were carried out. For the initial manual experiments, a 5.00 ml aliquot of 1.00×10^{-4} M palladium solution was added to a mixture containing 15.00 ml of buffer solution and 5.00 ml of 9.44×10^{-3} M Na-SCPAR. After thorough mixing, an appropriate volume was transferred to the cell of the spectrophotometer. Absorbance measurements were initiated 30 s after the start of the reaction and acquired

at 30 s intervals for a period of 600 s over the wavelength range 300 - 750 nm. The pH range of 2 to 11 was examined in this manner.

Once the optimum reaction pH was identified, stopped-flow experiments were conducted to determine kinetic parameters, *i.e.*, the order of the reaction with respect to Pd(II), reaction rate constant, half-life of reaction, the pre-exponential factor, and the constant background term. Buffered streams of Na-SCPAR (3.78×10^{-3} M) and palladium (10^{-5} to 10^{-4} M) were merged at a mixing tee and directed to the flow cell through a 4 cm length of tubing (this being the shortest possible length of tubing that would allow adequate mixing and still minimize time between mixing of the reaction components and detection). Pumps were run at maximum speed to transport the reaction mixture to the cell and then stopped to allow the kinetic measurements. Absorbance measurements at 488 nm were made at 1 s intervals for a period of 200 s after stopping the pumps. The absorbance was found to rise exponentially (see Figure 3.11, discussed later).

3.3.2.5.2 *Automated simplex optimization*

The flow injection configuration used for the automated simplex optimization experiments is shown in Figure 3.5a. The reagent stream consisted of Na-SCPAR merged with distilled water to give a total flow rate of 0.50 ml min^{-1} and a maximum Na-SCPAR concentration of 9.44×10^{-3} M. The buffer stream was allowed to vary in pH during the automated optimization, but was kept at a constant flow rate of 0.50 ml min^{-1}. The carrier stream was maintained at a fixed flow rate of 1.0 ml min^{-1} and merged with the other two streams to give a total flow rate of 2.00 ml min^{-1} at the detector. This ensured a constant sample residence time in the system. Separate pumps were used for each solution. The configuration chosen merges sample with reagent stream rather than direct injection of sample into reagent stream. This was to preclude possible formation of negative response peaks across the sample plug for lower Pd(II) concentrations. This is often observed when the reaction product formed across the sample plug has less absorbance compared to the

carrier stream. During the automated simplex optimization process, the flow rates of Na-SCPAR, NaOH and buffer streams were automatically adjusted so as to attain wide variation in Na-SCPAR concentration and pH.

For each experiment, the required flow rates were established, and the system was allowed to equilibrate. Once a steady baseline was detected, a 70 μl sample of 1.0×10^{-4} M Pd(II) was injected into the carrier stream. Absorbances were measured at 488 nm. The pH of the reaction mixture was measured in a simple flow through cell situated after the detector.

Automated simplex optimizations were carried out at each of five different reaction coil lengths; 50, 75, 100, 125 and 150 cm.

Once the optimum Na-SCPAR concentration, pH, and reaction coil length were established, these were implemented on a simpler flow injection system (Figure 3.5b) which was used for both routine analysis and interference studies. Such routine analyses can be done with a simple flow injection system comprising one pump, two pump tubes and a single injection valve.

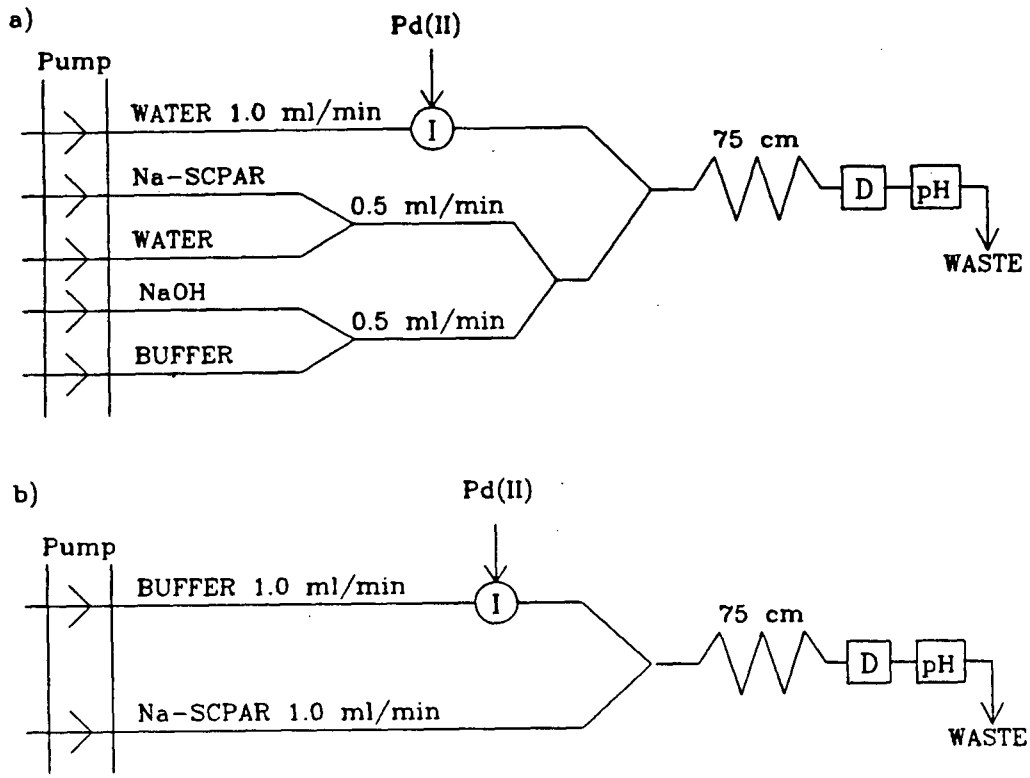

Figure 3.5 Flow injection manifold used for Pd(II / Na-SCPAR study:

(a) manifold for automated optimization and response surface mapping studies; this included an injection valve with 70 μl loop (I), spectrophotometer (D), and pH electrode cell (pH). The carrier stream was of distilled water. The sample was 1.0 x 10^{-4} M Pd(II) in 1 mM HCl. The buffer stream contained 0.2 M sodium hydroxide and universal buffer at pH 2.0. The reagent was 9.40 mM Na-SCPAR in distilled water.

(b) manifold for calibration and interference studies; this included a buffered carrier stream at pH 5.0, an injection valve with 70 μl loop (I), a Pd(II) sample in 1 mM HCl, a 9.44 x 10^{-3} M Na-SCPAR reagent stream buffered to pH 5.0, a spectrophotometer (D), and pH electrode cell (pH).

3.3.2.5.3 *Automated response surface mapping*

The automated response surface mapping experiments were carried out using a flow injection configuration identical to that used for the simplex optimization studies, *i.e.*, Figure 3.5a. System variables (Na-SCPAR and NaOH flow rates), stock solution concentrations, buddy flow rates, and total carrier stream flow rate were as described above.

An 8 x 8 square grid was used, thus providing a flow rate resolution of 1 part in 8. The lower and upper flow rate limits for the Na-SCPAR stream were 0.10 and 0.50 ml min^{-1} respectively, while those for NaOH were 0.00 and 0.50 ml min^{-1} respectively. The 8 x 8 grid represents a total of 64 experimental conditions that were tried. These experiments were carried out in triplicate.

3.3.3 Results and Discussion

3.3.3.1 *Characterization of Na-SCPAR*

The purity of the reagent, Na-SCPAR was investigated after chromatographic separation of possible product impurities. Our own elemental analysis results, and the work by Savvin *et al.*, [102] indicated some difficulty in purifying the Na-SCPAR reagent. Elemental analysis on the reagent, Na-SCPAR, for carbon, hydrogen and nitrogen was conducted and the experimental values found to be: C, 29.79%; H, 2.58%; N, 8.39%. This was not in agreement with the expected values. However, the error may be accounted for by inclusion of acetic acid and methanol as impurities from the purification procedures. Although still unsatisfactory, these results showed an improvement in purity of the reagent over that reported by Savvin *et al.* [102] They never reported purification of reagent using the chromatographic separation process, but the difficulty in the purification was however apparent as had been reported. Our studies also indicated that the reagent was not

SCPAR (as reported by Savvin *et al.*), but was predominantly the mono-sodium salt of the reagent. This was confirmed by flame atomic emission spectrometric (AES) studies using the sodium atomic emission line at 589 nm. A calibration curve was obtained using standard sodium ion solutions (from NaCl), with *ca.* 1% precision. The concentration of sodium ions in a prepared Na-SCPAR solution was then determined by interpolation. The AES results showed an error of +2.56% from the expected value. This confirmed that the purity of the reagent was acceptable. The purified reagent was used as the analytical reagent for subsequent palladium determinations. The absolute purity of the reagent is not essential, so long as prepared solutions are stable. This is because all Pd(II) determinations are done with the aid of a calibration curve, based on Pd(II) standard solutions.

The infrared spectrum of the reagent is shown in Figure 3.6. The assignment of bands in the spectrum was made by comparison of this spectrum with the infrared spectra of the starting reagents used in its synthesis. The complete vibrational assignment of components of the compound is given in Table 3.2.

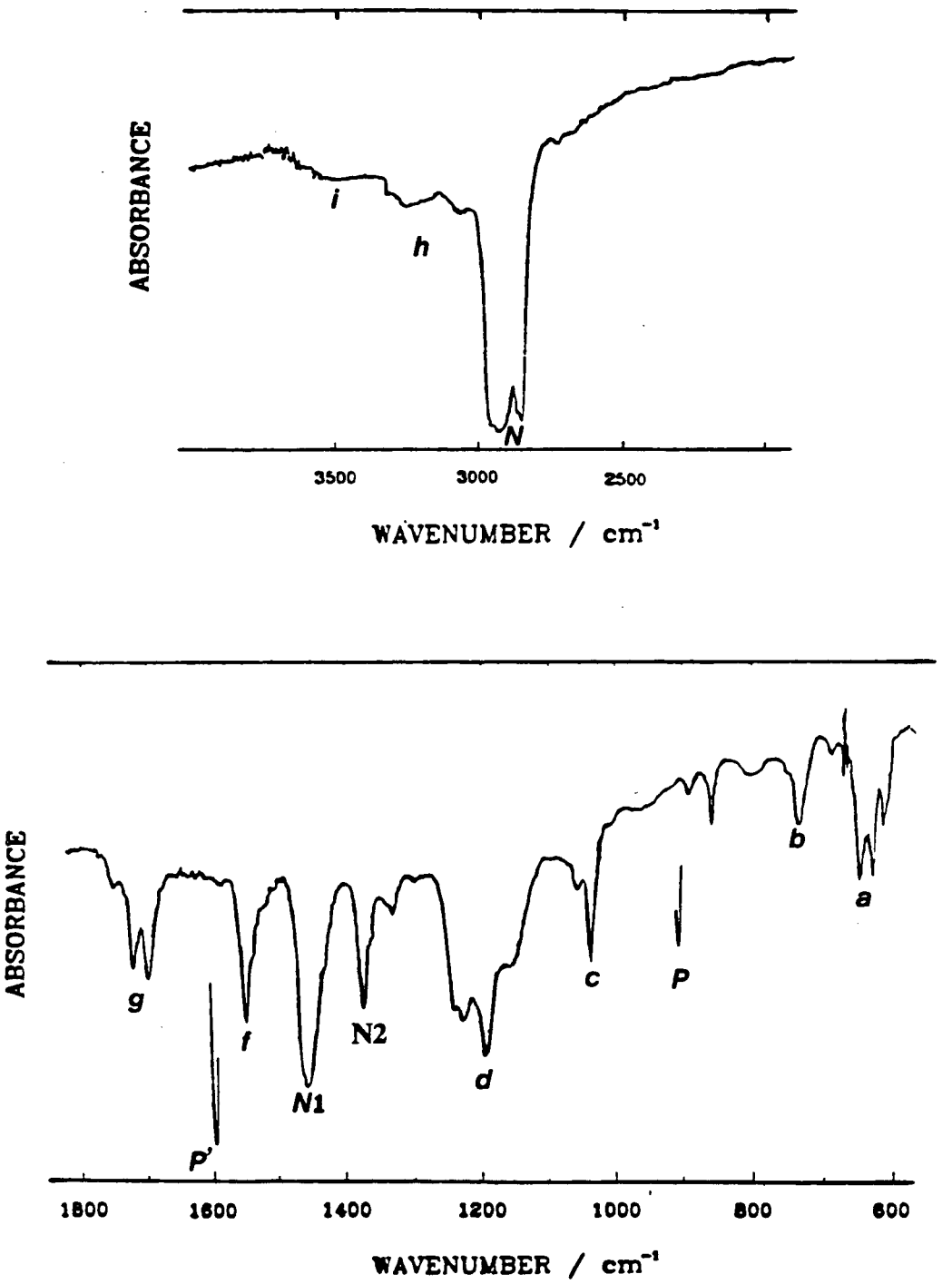

Figure 3.6 Infrared spectrum of Na-SCPAR.

Label	Feature (cm^{-1})	Assignment
a	$600\text{-}650^{M}$	-C-S and $-SO_3$ deformations
b	740^{W}	-C-S stretching
c	1035^{M}	$-SO_3$ symmetric stretching
d	$1150\text{-}1250^{BD}$	$-SO_3$ asymmetric stretching
f	1550^{M}	-N=N- stretching
g	$1675\text{-}1725^{M}$	-C=O (amide group) stretching
h	$3000\text{-}3200^{W}$	-N-H stretching
i	$3200\text{-}3550^{W}$	-OH (phenolic) stretching

Table 3.2. Na-SCPAR infrared vibrational spectrum assignments.

S Strong, **M** medium, **BD** broad, and **W** weak.

P Reference absorption band at 907 cm^{-1} from polystyrene.

P' Reference absorption band at 1601 cm^{-1} from polystyrene.

N Nujol absorption band at 2750 - 3000 cm^{-1}.

N1 Nujol absorption band at 1450 cm^{-1}.

N2 Nujol absorption band at 1370 cm^{-1}.

3.3.3.2 *Effect of pH on Na-SCPAR*

The UV/visible absorption spectra of Na-SCPAR at various pH values are shown in Figure 3.7. In strongly acidic media, absorption maxima occur at 306 nm and 420 nm. The band at 306 nm undergoes a bathochromic and hyperchromic shift as the pH increases to neutral, but there is no effect on the 420 nm absorption. Under alkaline conditions, the absorption band at 420 nm shifts to longer wavelengths with increasing pH (signifying a possible increase in conjugation). These pH effects on the reagent may overall be attributed to either protonation of basic groups, deprotonation of acidic groups, and/or a combination of various tautomeric processes.

The reagent is unstable under strongly alkaline conditions. Above pH 11, decomposition of the reagent follows zero-order kinetics with the rate increasing with pH. This was ascertained from time-based/ multiwavelength absorbance measurements of the reagent solutions under different pH conditions. Equivalent volumes of universal buffer solutions of specific pHs were used to dilute 10 ml volumes of 10 mM Na-SCPAR stock solution by a factor of two. Aliquot amounts of the diluted reagent solutions were then quickly transferred into the sample cell of the diode array spectrophotometer. The spectrophotometer was initially set to start data acquisition after 30 s from the time of mixing the buffer and reagent components. This was to give sufficient time to mix the components, effect their transfer to the sample cell, and provide a uniform starting point for data acquisition. Absorbance data were then acquired every 30 s for 300 s across the 200 to 800 nm wavelength range. These experiments were done in triplicate. The multiwavelength-time curves were analyzed using the UV/visible spectral analysis software from Hewlett Packard. Figure 3.8 shows the change in Na-SCPAR absorbance with time at pH 12.6. A $(1.70 \pm 0.42) \times 10^{-3}$ M s^{-1} zero-order rate constant for the decomposition was calculated. At pH 11.3, a zero-order rate constant of $(3.75 \pm 0.36) \times 10^{-4}$ M s^{-1} was registered, a factor of *ca* 4.5 increase in $t_{1/2}$ of the reagent. There was hardly any change in absorbance with time measurements under pH 7.0 conditions over a period of 10 minutes.

The presence of the -OH, -NH, and sulfonic groups in the reagent increases the solubility of both the reagent and its chelate analogue(s) in aqueous media.

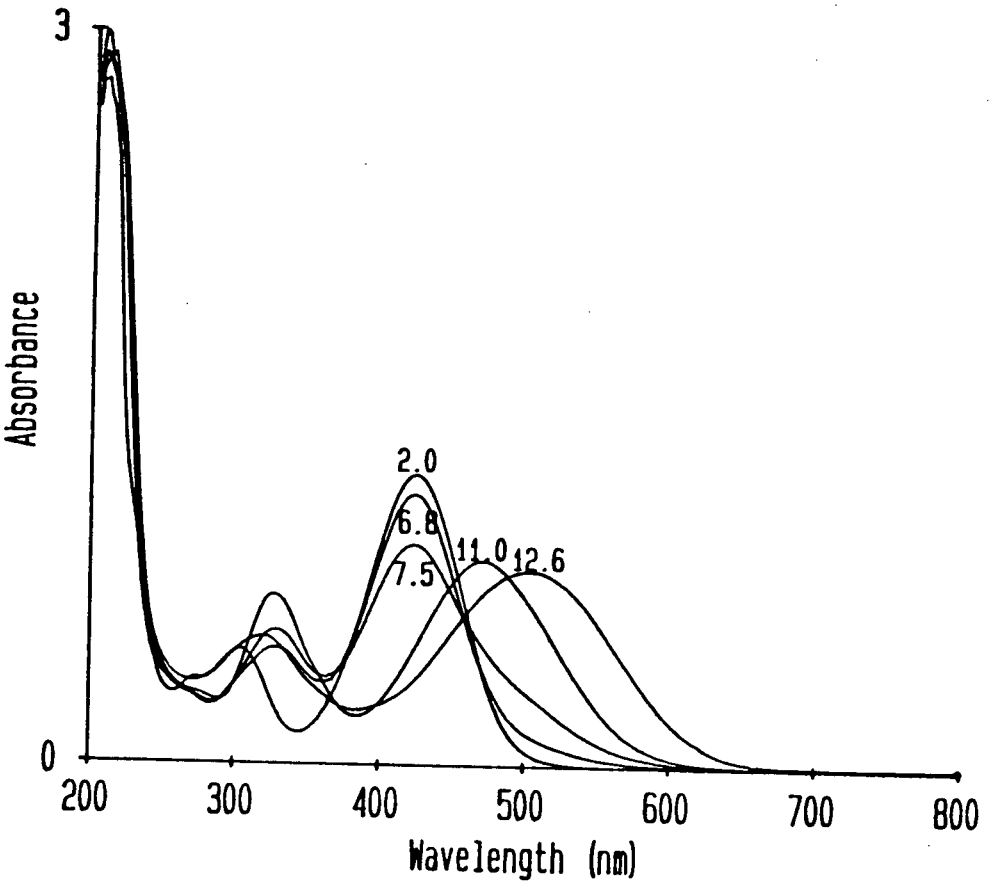

Figure 3.7 UV-Visible absorption spectra of Na-SCPAR at pH 2.0, 6.8, 7.5, 11.0 and 12.6.

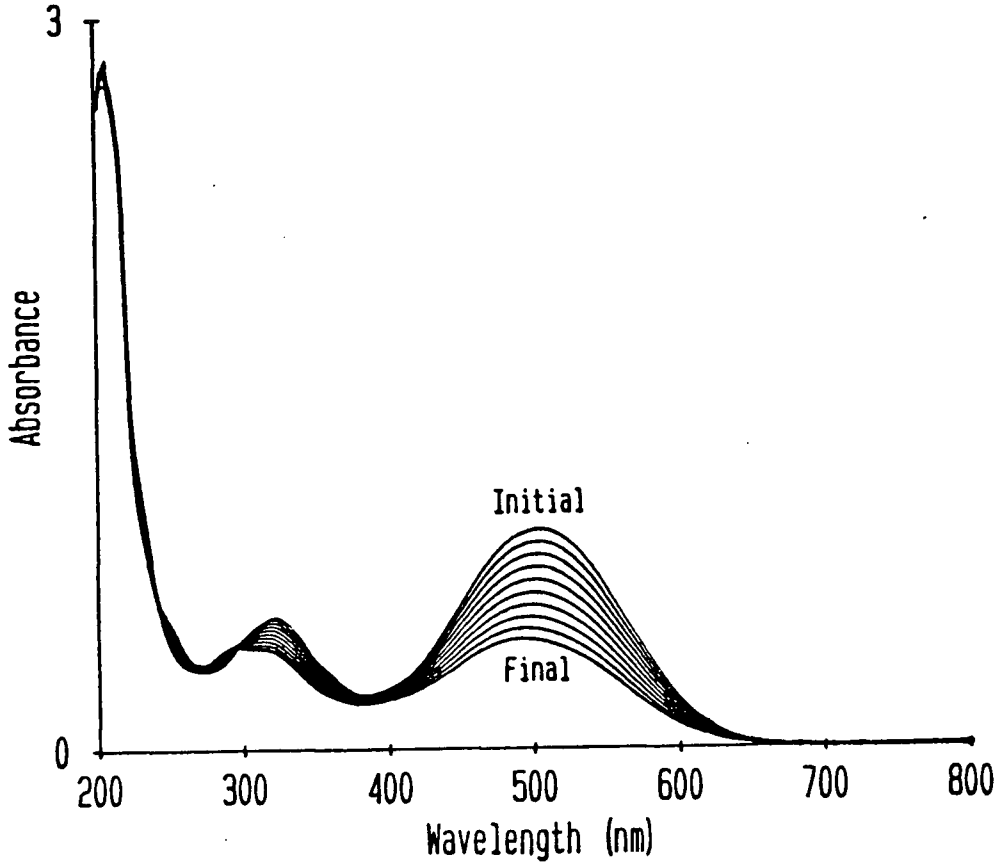

Figure 3.8 Spectra showing that the 500 nm absorbance of Na-SCPAR is unstable at pH 12.6. Measurements were taken at 30 s intervals, starting 30 s after mixing ("initial"), and continuing until 300 s after mixing ("final"). The zero-order rate constant for its decomposition is $(1.7 \pm 0.42) \times 10^{-3}$ M s^{-1}.

3.3.3.3 *Effect of pH on complexation*

The nature of the reagent in solution strongly influences its ability to form metal complexes. The reaction of Na-SCPAR with some noble metals, such as palladium, and some base metals, such as copper, zinc and iron, is known to be highly pH dependent. [102] Experimental results indicated that weakly acidic conditions are optimum for palladium

determination. Reaction product(s) formed under alkaline conditions were less strongly absorbing, and observed to decompose rapidly. Figure 3.9 summarizes the effect of pH on rate of product formation. Absorbance measurements of the reaction mixture were carried out after a fixed period of time (600 s). Optimum pH conditions for the complexation reaction was observed to occur between pH 4.5 and 5.5.

Attempts to determine the stoichiometric reaction ratio of palladium to Na-SCPAR were made without success using the molar-ratio method. With this method, the concentration of Pd(II) was kept constant at 5.0×10^{-4} M, while that of Na-SCPAR was varied from 1.0×10^{-4} M - 5.0×10^{-3} M. This could be attributed to possible formation of a mixture of several complexes (*i.e.*, 1:1, 1:2, and/ or 2:2) of comparable molar absorptivities and close absorbance maxima. This is possible via two chelation sites on Na-SCPAR. These sites are shown in Figure 3.10. Figure 3.10a shows the Na-SCPAR behaving as a tridentate ligand, bonding to the metal ion via the carbonyl oxygen (of the rhodanine ring), the phenolic oxygen and one of the nitrogens of the diazo group, -N=N-. In this way, stable six and five membered rings in a 1:1 type complex are possible, with the complex being either neutral or possessing a single positive charge. Figure 3.10b represents a 1:2 type complex, with coordination via two sets of the carbonyl oxygen (of the rhodanine ring) and the phenolic oxygen of two Na-SCPAR molecules. Coordination is also possible via the two sulfur groups of the rhodanine ring. This would provide a stable bidentate four-membered ring chelate. A combination of the coordination site mentioned in Figure 3.10a and the sulfur coordination site would yield either a 2:1 binuclear chelate or a 2:2 complex as shown in Figure 3.10c. The stoichiometry will most certainly be dependent on solution conditions such as pH and metal-to-reagent ratio. The 2:1 or 2:2 chelates are however less probable under the pseudo-first-order reaction conditions employed in these studies.

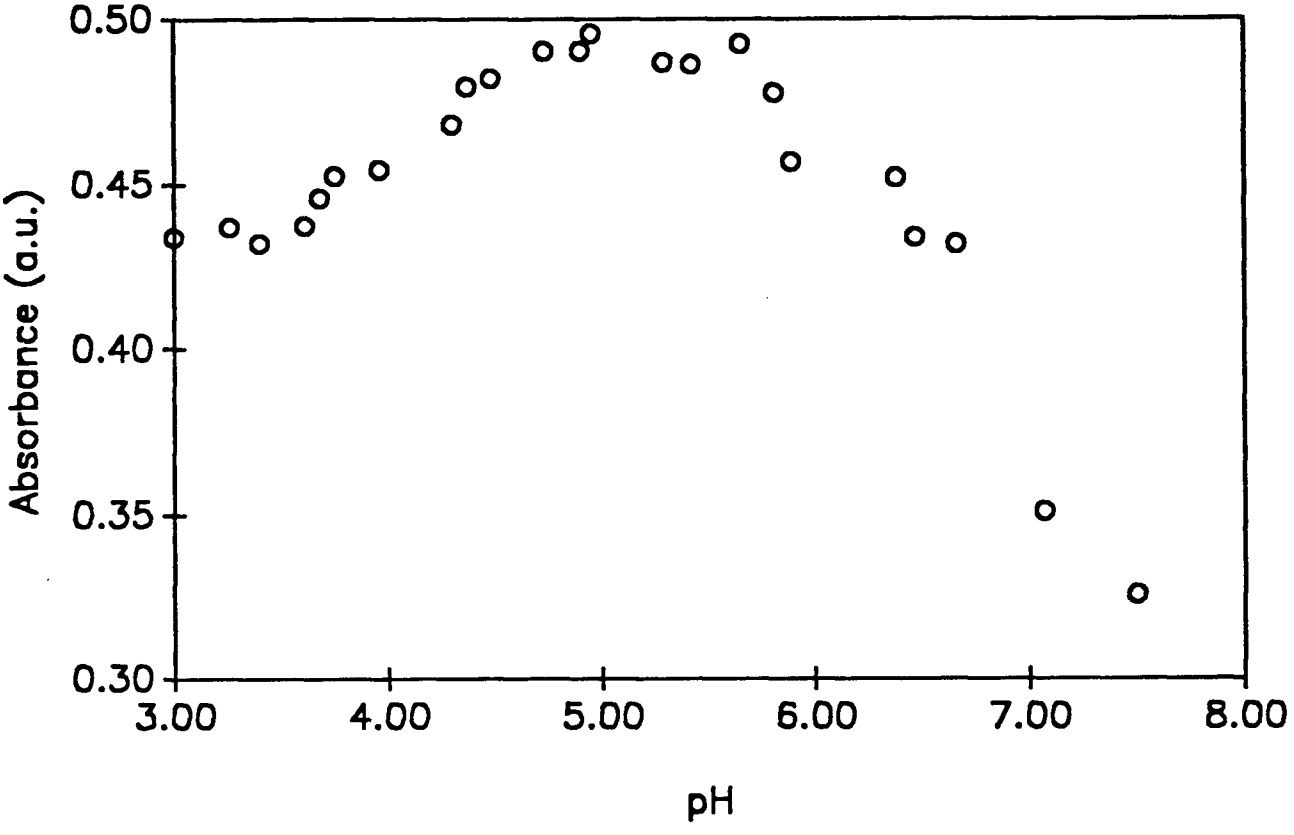

Figure 3.9 Efect of pH on Na-SCPAR/Pd(II) complexation reaction. Absorbance readings taken 600 s after mixing the reaction components. The reaction mixtures comprised of 10.0 ml of 1 mM Na-SCPAR, 5.0 ml of 0.1 mM Pd(II), and 15.0 ml of buffer solutions.

Chelation via the form shown in Figure 3.10a should however be the most favoured path because (a) proton release in the unbuffered reaction mixtures was evident since the pH of reaction mixtures decreased with time, implying that Pd(II) can react directly with the hydroxyl group of the reagent, (b) both O and N are better electron donor groups than S, thus the structure shown in Figure 3.10a would be favoured, and (c) positions of both carbonyl and phenolic oxygens and N of the -N=N- allow formation of five and six membered rings. Under the pseudo-first-order conditions for which these experiments were performed, it is most probable that a 1:1 chelate is the most predominant, and that bonding is via the carbonyl and phenolic groups.

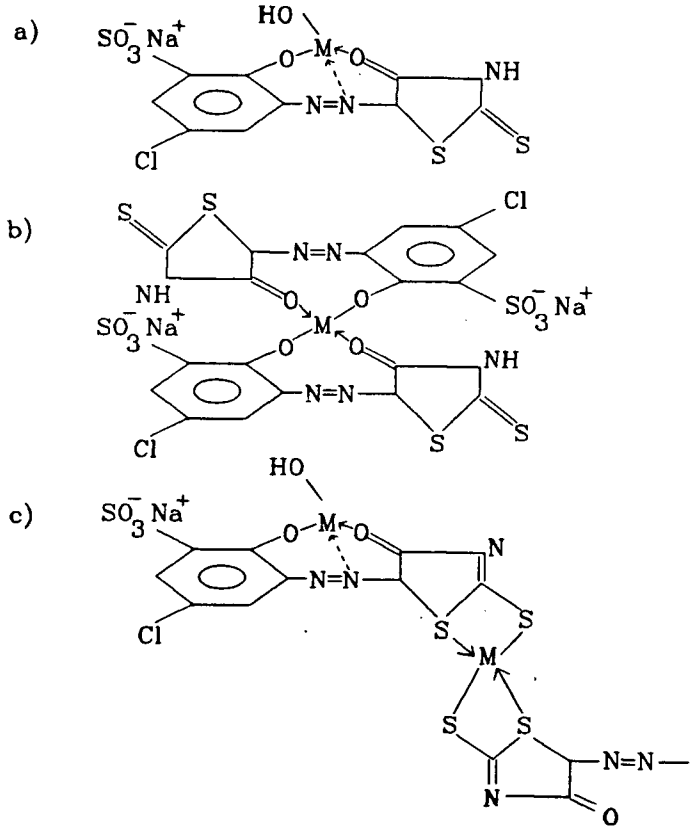

Figure 3.10 Possible products from reaction between Pd(II) and Na-SCPAR.

Reaction kinetics were investigated at the optimum pH (*i.e.*, pH 5.0) under pseudo-first-order conditions with Na-SCPAR in excess. If the reaction is expressed as:

$$\text{Pd(II)} + n\ \text{Na-SCPAR} \dashrightarrow \text{Pd(II)(Na-SCPAR)}_n \qquad (3.1)$$

the reaction rate can be written as,

$$\text{Rate} = k'[\text{Pd(II)}] \qquad (3.2)$$

This assumes that the rate of reaction is first-order with respect to Pd(II), where k' is the pseudo-first-order rate constant.

A nonlinear curve fitting program was used to extract the pseudo-first-order rate constant from the stopped flow data. The equation fitted to the data was,

$$A_t = A_\infty\,[1-\exp(-k't)] + C\,t + B \qquad (3.3)$$

where A_t is the absorbance at time t, A_∞ is the final solution absorbance due to the product, C is a linear drift term, and B is a constant background term. The linear drift term was needed to account for thermal effects on the solution in the cell since the cell was not thermostated. The value of C was generally very small and its value returned by the fitting program was $(1.14 \pm 0.25) \times 10^{-4}$ a.u. s^{-1} (for 10 replicates).

Figure 3.11 shows a typical fit of the model to the data. Good fits were obtained for each of the solutions tested. The pseudo-first-order rate constant extracted from the fitting routine was $0.11 \pm 0.01\ s^{-1}$ at room temperature for 3.78 mM Na-SCPAR. The final equilibrium absorbance due to the product did not change for Na-SCPAR concentrations within the range 1.90 to 7.60 mM, indicating that the equilibrium lies well to the right.

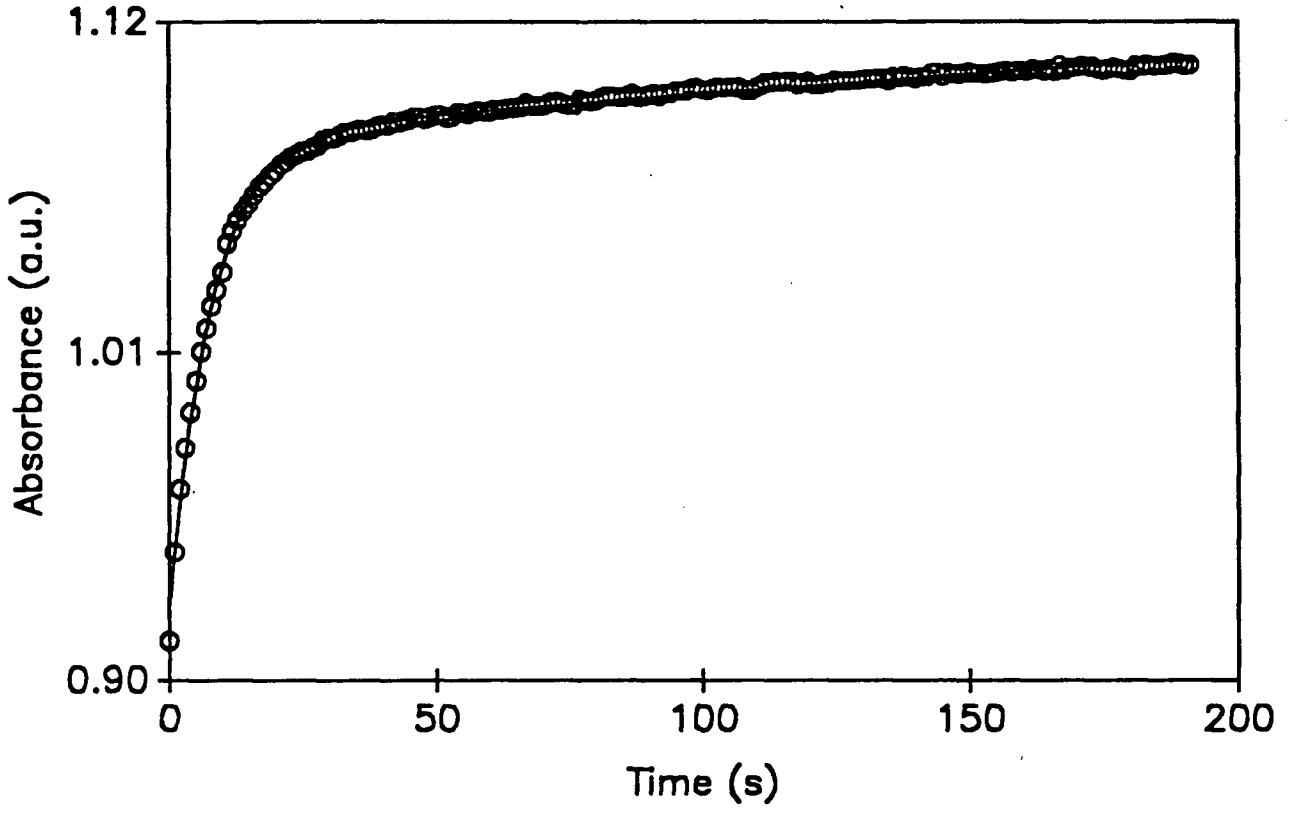

Figure 3.11 Fit of a pseudo-first-order model (solid line) to data collected for the reaction between Na-SCPAR and Pd(II) at pH 5.0.

3.3.3.4 *Confirmation of linear drift term*

Further stopped flow kinetic experiments were performed to ascertain the existence of a thermal effect. Absorbance data from the reaction mixture (minus Pd(II) sample), were acquired at 1 s intervals for a total of 260 s. A typical profile of the results is shown in Figure 3.12. The behavior is linear with a slope of 1.26×10^{-4}, close to the extracted coefficient of drift term, and within the experimental error. This justifies the inclusion of the coefficient of drift term in the expression above.

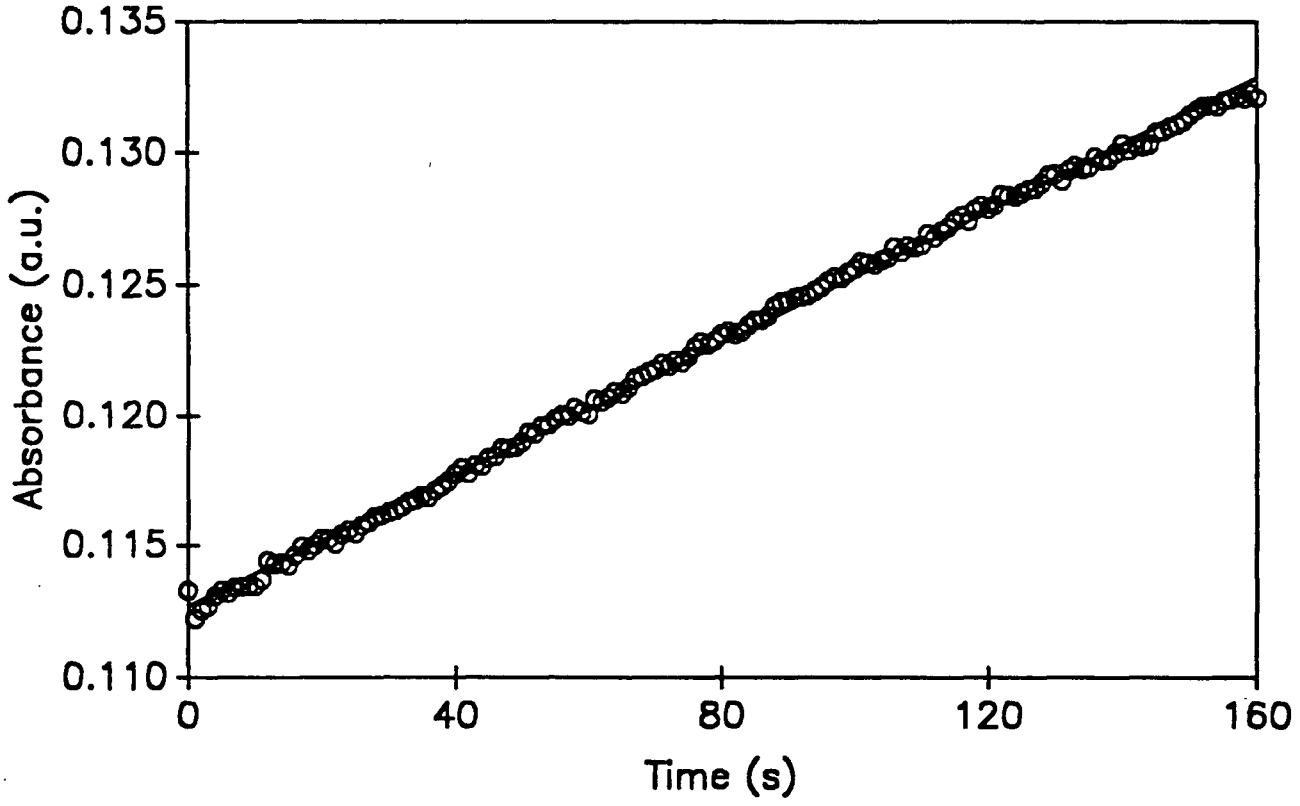

Figure 3.12 Fit of a linear model (solid line) to data collected for the reaction mixture blank (pH 5.0 buffered reagent mixture, minus Pd(II)) to determine the coefficient of drift term. Absorbance readings were made at 488 nm.

For Pd(II) concentrations in the range 5.0×10^{-6} - 1.0×10^{-4} M, the plots of (A_{∞} + B) vs. [Pd(II)] for various Na-SCPAR concentrations were found to be linear. Figure 3.13 shows that for 2.0, 4.0, 6.0, and 8.0 mM concentrations of Na-SCPAR, the slopes of the curves were determined to be 0.9866×10^{4}, 1.0223×10^{4}, 1.0522×10^{4}, and 1.0948×10^{4} respectively. These show a slight progressive increase in sensitivity with increase in Na-SCPAR concentration. These curves can be said to be parallel to each other within experimental error, with an average slope of $(1.039 \pm 0.046) \times 10^{4}$ a.u./ppm. Since sensitivity is dA/dc, this indicates that the sensitivity with which Pd(II) is determined is about the same within the concentration ranges studied. It also proves that it was valid to assume the pseudo-first-order reaction conditions. From the linear behavior of the plots, it is certain that the reaction attains equilibrium by the time measurements are stopped. The average sensitivity value obtained from these experiments is about 2.4 times the sensitivity value obtained from the palladium calibration curve of Figure 3.19. This factor of 2.4 is comparable to the experimental dispersion coefficient, **D** (of 2.8) for the FIA system used for the calibration studies. This is further proof of the validity of these results. Thus, the sensitivity value obtainable from the calibration curve generated using FIA is an apparent sensitivity value, which is lower than the true sensitivity by a factor approximately equal to the value of the dispersion coefficient.

The reaction rate is much higher under the mildly acidic conditions used here than the strongly acidic conditions reported previously. [102] Reaction rates measured in this study indicate the reaction is essentially finished in less than 60 s. The maximum absorbance is found at 488 nm rather than 520 nm. [102]

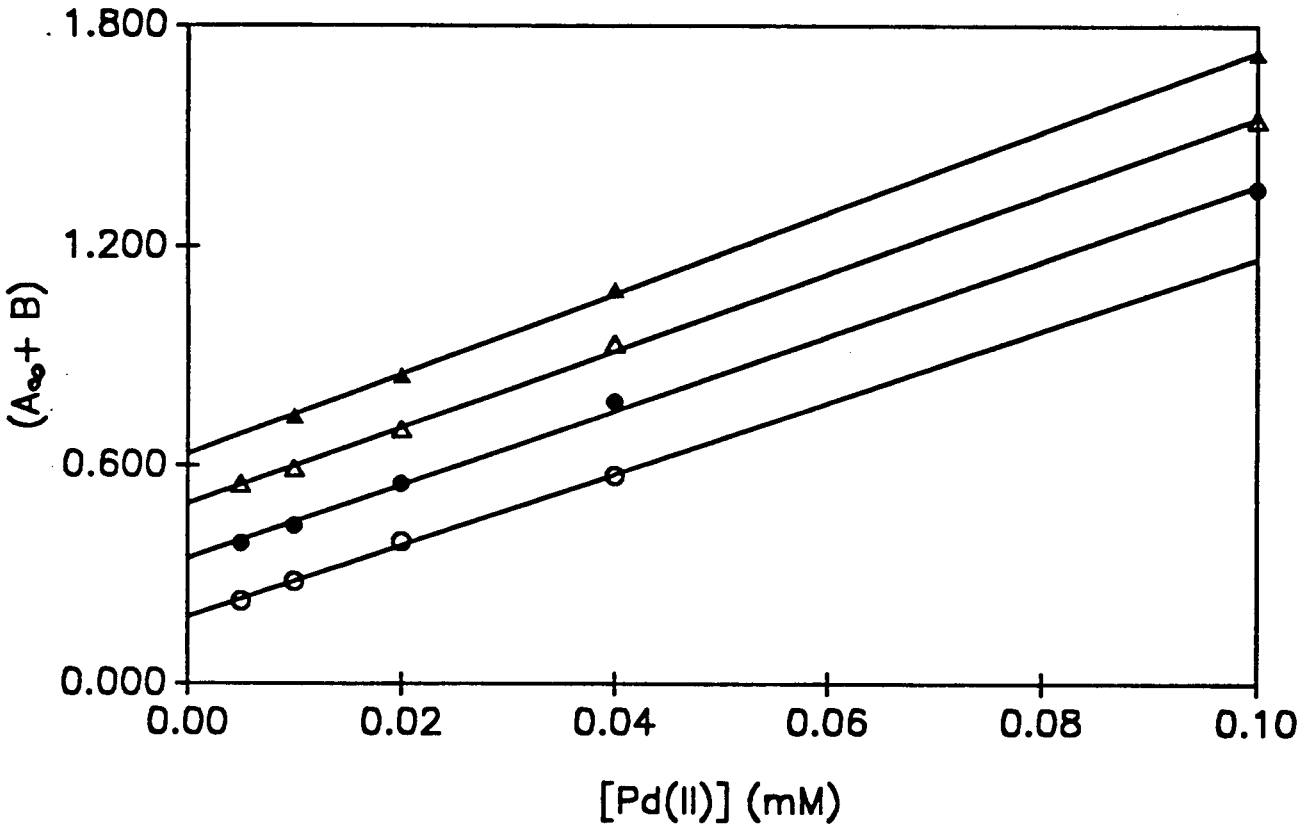

Figure 3.13 Linear dependence of $(A_\infty + B)$ on concentration of Pd(II): ▲, [Na-SCPAR] = 8.0 mM; △, [Na-SCPAR] = 6.0 mM; •, [Na-SCPAR] = 4.0 mM; ○, [Na-SCPAR] = 2.0 mM. Absorbance readings were made at 488 nm.

An attempt was then made to determine the possible number of observable species in the reaction mixture with the help of a chemometric technique called factor analysis. This was done with a hope of getting a better understanding of the reaction mechanism. However, in order for factor analysis to be used, the presumed observables must all (1) absorb radiation within the working wavelength range, (2) be independent of each other, and (3) have different spectra. Treatment of the experimental multiwavelength kinetic curves with factor analysis [104] indicated that a minimum of two components made significant contributions to the observed absorbance-time behavior. That is, the minimum number of factors that were required to reconstruct the original spectrum was two.

Figure 3.14a shows the poor fit observed when an attempt was made to reconstruct the original absorbance-time curve assuming a single factor. A full reconstruction of the original data set was achieved assuming contributions from two factors as shown in Figure 3.14b. This confirmed the existence of at least two observables. One may reasonably presume that these are the Na-SCPAR reagent and the product, since one was identical to the spectrum for Na-SCPAR. However this algorithm is unable to differentiate between a single component and a fast equilibrium, thus it was impossible to reconstruct the individual spectra of the observables or factors with confidence.

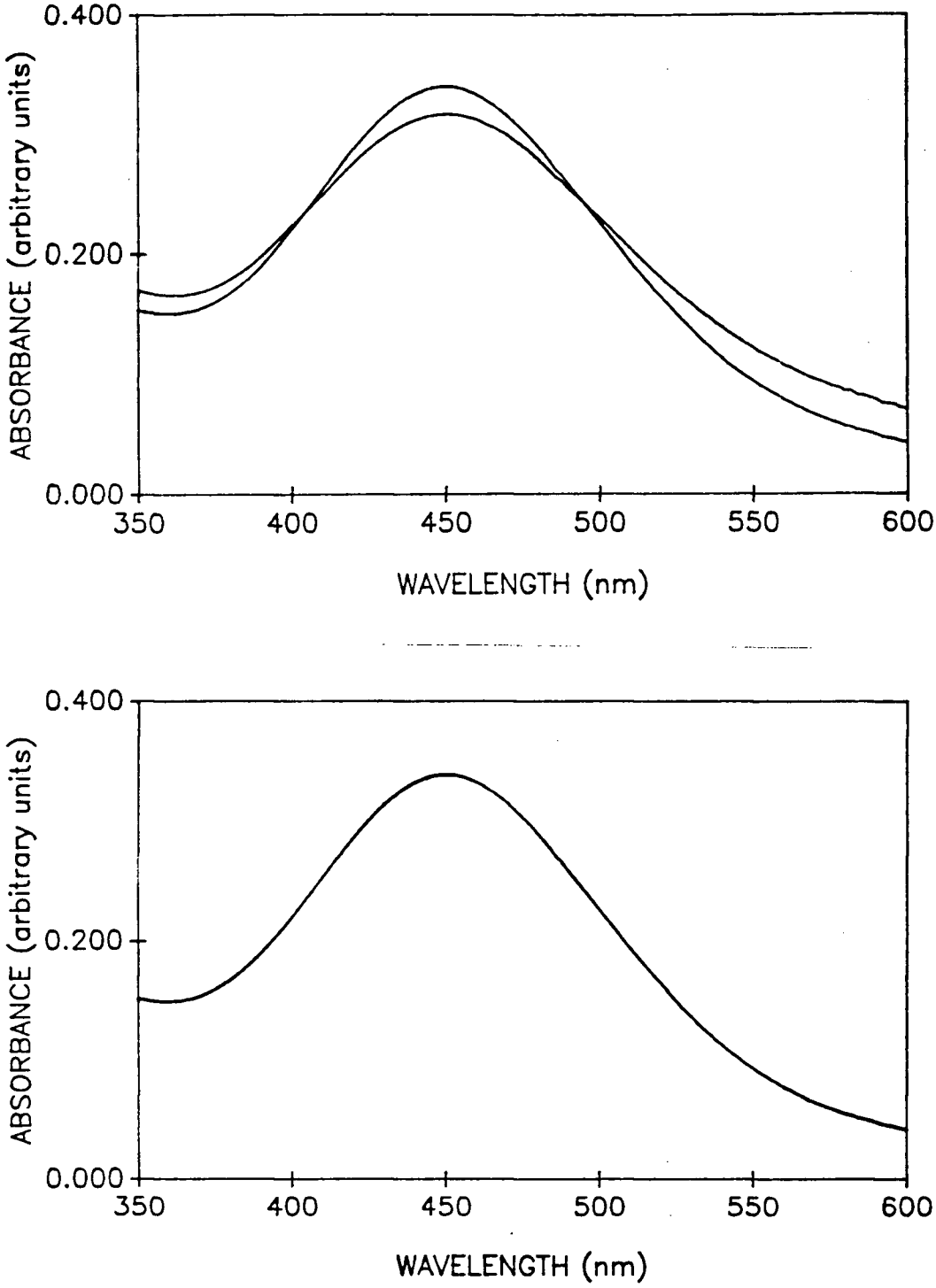

Figure 3.14 Regeneration of experimental data with factor analysis:

(a) assuming only one factor.

(b) assuming two factors.

3.3.3.5 *Automated simplex optimization of the flow injection system*

The optimum pH and reagent concentration for the flow injection analysis of palladium with Na-SCPAR were automatically established using simplex optimization and response surface mapping. An average of 30 experiments were performed during each automated simplex optimization procedure, with four replicate runs for each experiment. In each case optimum flow conditions were achieved in just under two hours.

As shown in Figure 3.4a, the pumps for all streams were arranged to give a fixed total flow rate of 2.00 ml min^{-1}. The reagent stream consisted of 9.44 x 10^{-3} M Na-SCPAR "buddied" to a distilled water stream such that, while relative flow rates of the two streams could change, the total flow rate of the reagent stream remained at 0.50 ml min^{-1}. In this way, the Na-SCPAR concentration could be changed without grossly affecting the total flow rate. Likewise the buffer stream consisted of 0.2 M NaOH "buddied" with a universal buffer of pH 2. The precision with which the individual flow rates were matched so as to maintain a constant total flow rate was good but was limited by the pumps' stepper-motor drivers.[52] Pump tube flow rate calibration data obtained at the start of the procedure were assumed to hold throughout its duration. This assumption could however be eliminated by incorporating a flow meter at an appropriate point in the manifold for in-run checks.

The initial automated simplex optimization showed that the optimum Na-SCPAR flow rate was in the range 0.42 - 0.50 ml min^{-1}. This is as would be anticipated, since the greatest amount of product should be formed when the Na-SCPAR concentration is at its maximum value. This study established the optimum flow rate range for the sodium hydroxide stream to be 0.125 ml min^{-1} - 0.150 ml min^{-1}, which corresponded to pH 4.70 - 5.30. This is consistent with the earlier manual studies of pH effects. The progress of the simplex optimization experiments at the established optimum reaction coil length is illustrated in Figure 3.15.

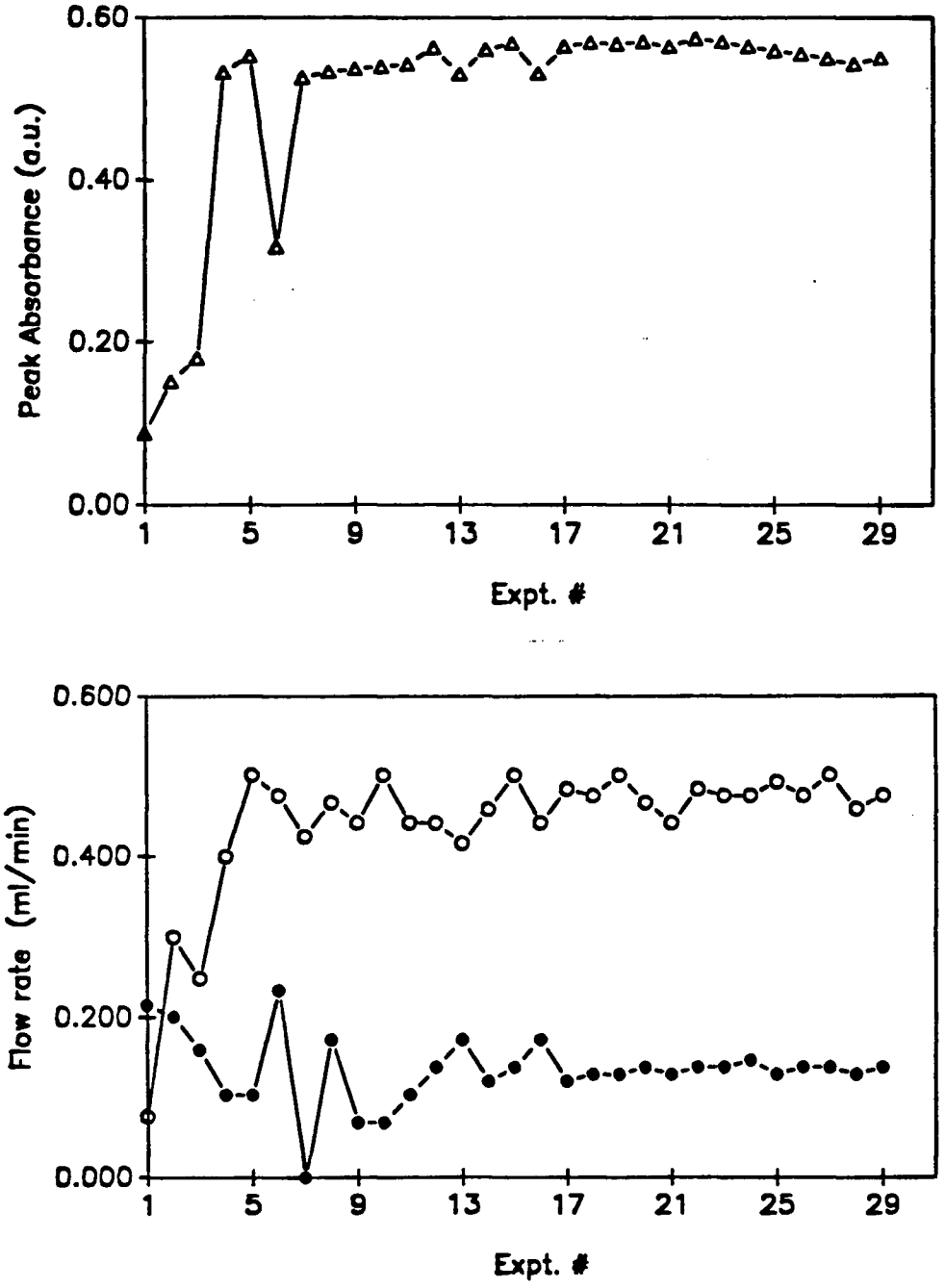

Figure 3.15 Progress of simplex optimization:

(a) peak response (Δ) vs. experiment number.

(b) flow rate of SCPAR (○) and NaOH (•) vs. experiment number.

The figure represents changes in responses as the simplex attempts to "home in" on the optimum conditions by varying all the factors simultaneously, thereby moving in a zigzag manner along the line of highest gradient or steepest ascent that it can find. Simplex optimization results in a rapid initial improvement, corresponding to the movement of the simplex until it reaches the region of a peak or ridge; then follows a slower "fine tuning" stage, as the simplex contracts onto the top of the feature. If it is a ridge, as might be the case with interacting variables, the simplex redirects itself up toward a maximum, and can re-expand.

The greater degree of variation in responses for the initial simplex experimental points is to be expected since the starting experimental points were far from the optimum and lay on a steep gradient. As the simplex "homed in" on the optimum, the variation between responses from consecutive experiments decreased. This also is to be expected, since the algorithm contracts the simplex onto the region of best response. It can be seen that, for this system, the bulk of the improvement was obtained within just 5 experiments and that optimization was essentially complete within 22 experiments.

Plots of responses vs. the two simplex variables are represented as scatter diagrams in Figure 3.16a. These clearly demonstrate the greater density of the points at optimum or near optimum conditions. The plot of peak absorbance *vs.* flow rate of NaOH stream shows a greater point density at flow rates of 0.100 - 0.150 ml. min^{-1}, which correspond to the optimum pH range for the complexation reaction. Stability in responses over the flow rate range 0.400 - 0.500 ml. min^{-1} for the Na-SCPAR stream (as seen in Figure 3.16b) also illustrates that Na-SCPAR is a non-limiting reagent under these conditions.

Both of these scatter plots show the effect of the variable interactions on system performance. The response at the point marked "X" in the figure is lower than that of points having similar Na-SCPAR flow rates because it corresponds to a higher NaOH flow rate. This implies a more alkaline condition. Point "Y" is similarly lower in response due to a lower Na-SCPAR flow rate (*i.e.*, insufficient reagent).

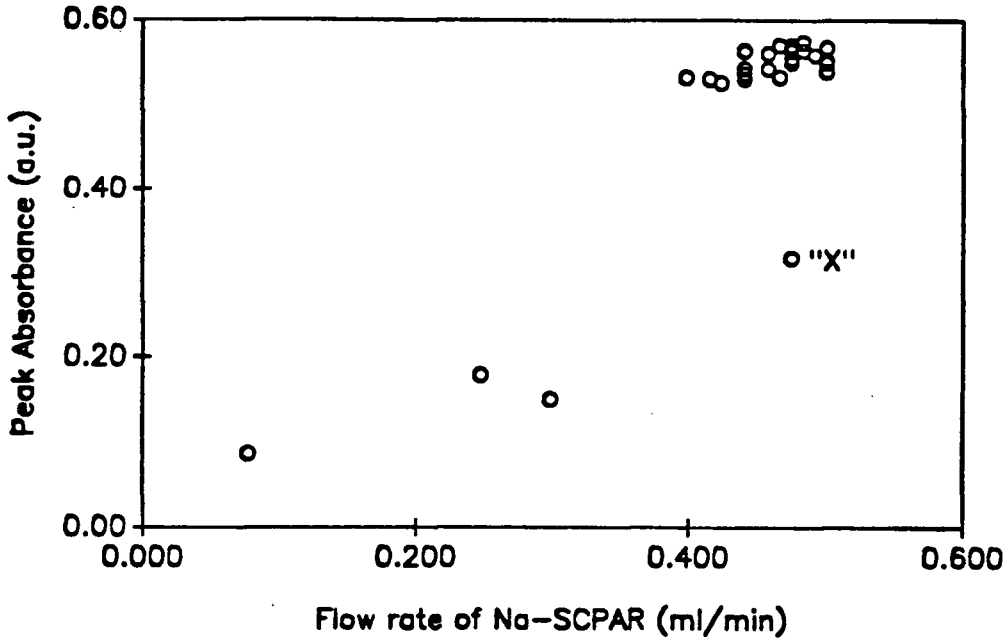

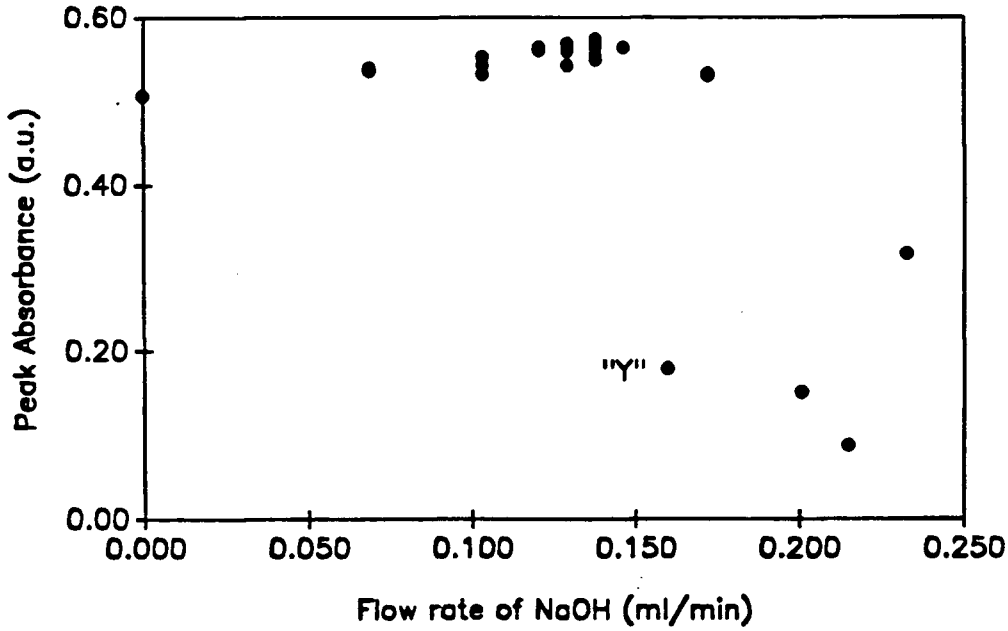

Figure 3.16 Scatter plots for experimental variables:

(a) Na-SCPAR.

(b) NaOH.

The decrease in spread of responses at the simplex vertices after every complete simplex optimization cycle, along the path taken by the simplex algorithm is illustrated in Figure 3.17. This graph shows how the maximum of the responses of the vertices of the simplex compares with both the mean and standard deviation of the vertex responses after every cycle. It is evident that the mean gets closer and closer to the maximum response with increasing number of cycles. This is better illustrated by the progressive decrease in the standard deviation of these vertex responses with cycle number. This may be explained as due to (i) the reduction in simplex size as the optimum conditions are approached, and (ii) the plateau-like nature of the region reached.

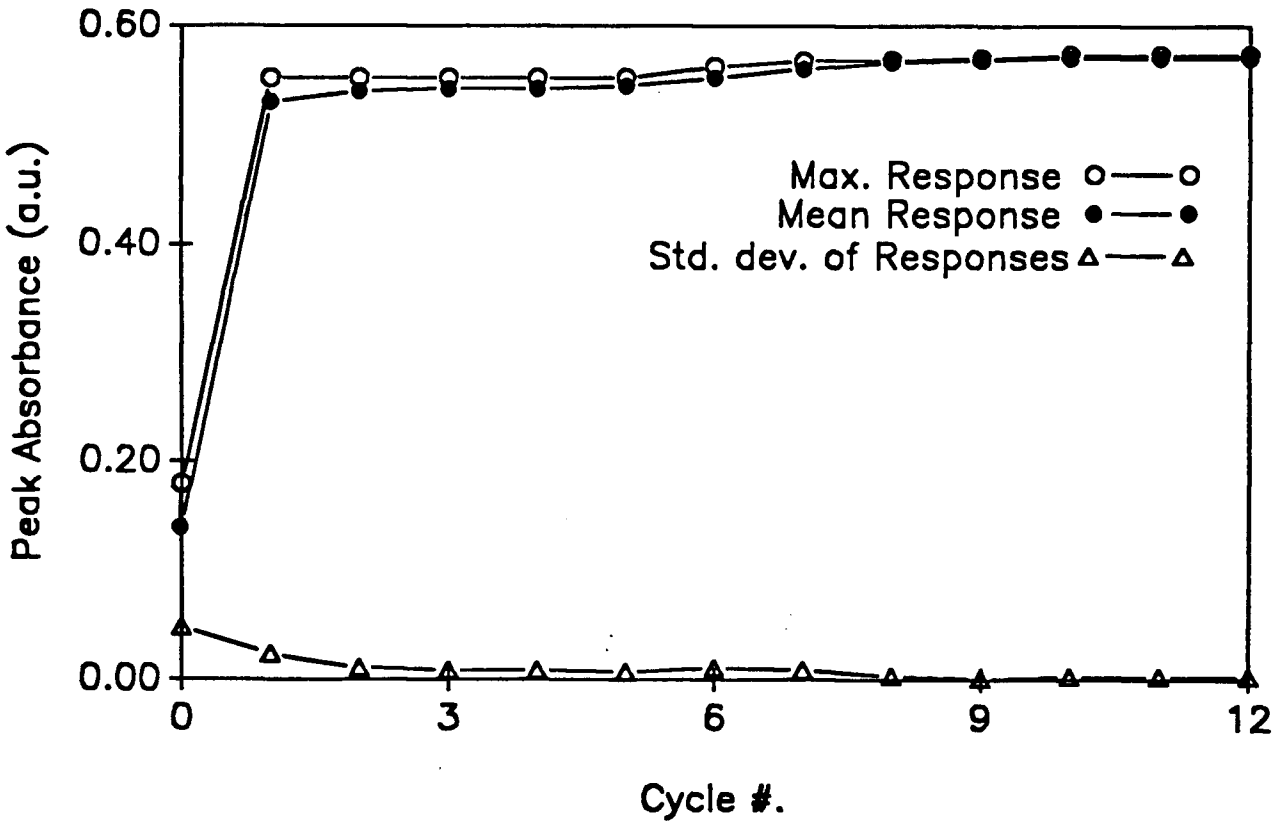

Figure 3.17 Plot of current vertex responses vs. simplex optimization cycle number. Peak absorbance readings were made at 488 nm. Key: Maximum of responses (○); mean of responses (•); standard deviation of responses (△).

The effect of reaction coil length on the sensitivity of the system was determined by performing the automated optimization experiments using several different coil lengths. Optimum performance was observed with a reaction coil length of 75 cm. Both longer and shorter coil lengths resulted in decreased peak absorbance, as is shown in Table 3.3.

Coil Length (cm)	Peak Maximum (absorbance units)	Percent Performance (relative to 75 cm coil)
50 cm	0.451	78.6
75 cm	0.574	100.0
100 cm	0.513	89.4
125 cm	0.448	78.0
150 cm	0.428	74.6

Table 3.3. Best Results from Automated Simplex Optimizations at Different Coil Lengths for Na-SCPAR/Pd(II) Reaction

This can be readily explained by the interaction of reaction kinetics and physical dispersion. [1] There is an optimum coil length, at which reaction product formation and residence time are correctly balanced; *i.e.*, reaction coil lengths which are too short allow insufficient time for reaction to proceed to its maximum, and thus peak height is less than its possible maximum, whereas reaction coil lengths which are too long result in the dispersion effect dominating over improved reaction product formation and thus peak height is again less than its possible maximum.

3.3.3.6 *Automated response surface mapping*

For the automated response surface mapping, a 2-factor 8-level design (8^2 = 64 sets of experimental conditions) was used, with four replicate injections at each point. These experiments took about four hours to complete. The three-dimensional response surface plot and contour map shown in Figure 3.18 indicates how the Na-SCPAR and NaOH flow rates affect system performance, under conditions of fixed total flow rate. The Na-SCPAR flow rates correspond to Na-SCPAR concentrations of 1.90 mM to 9.40 mM in the reagent stream. The NaOH flow rates correspond to an approximate pH range of 3.0 to 11.0. Optimum conditions indicated by this plot are in good agreement with other results obtained in this study. The plateau region found by the automated response surface mapping indicated the developed method to be highly stable if run under "plateau conditions", *i.e.*, in this region its performance is not greatly affected by small changes in pH or Na-SCPAR reagent concentration. Experimental conditions in this region of the response surface are recommended for routine analysis, and were used in interference studies.

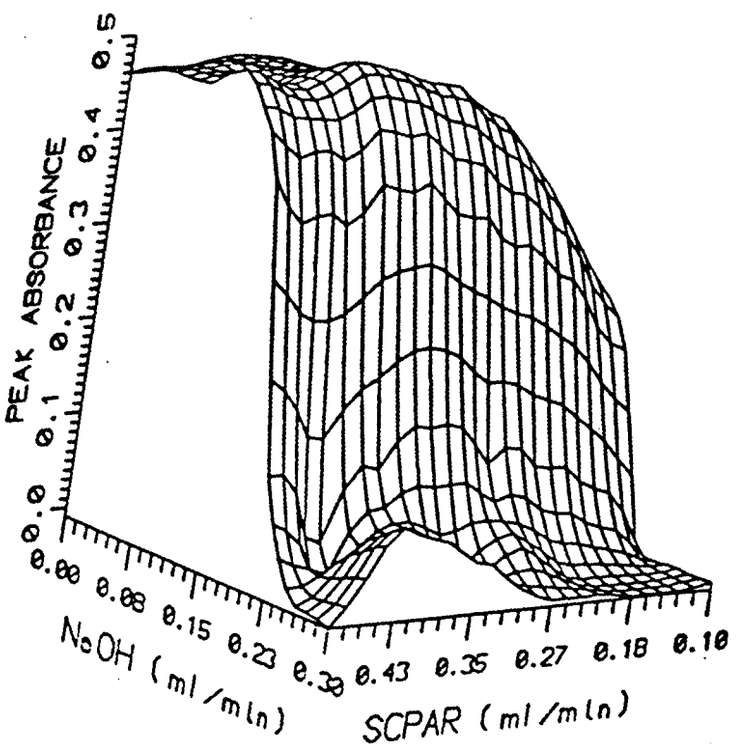

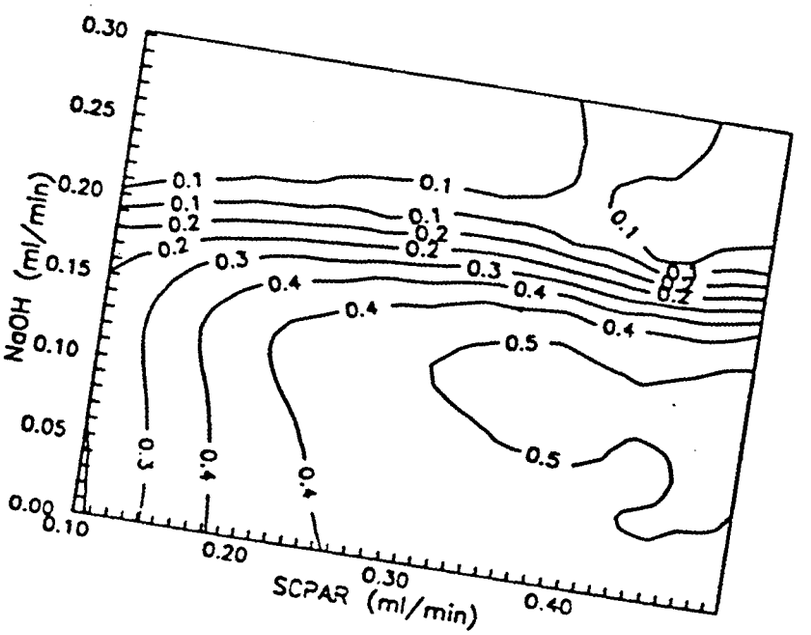

Figure 3.18 The Na-SCPAR-Pd(II) response surface shown as a 3D projection and its corresponding contour map. The response plotted is the peak absorbance at 488 nm. The NaOH and Na-SCPAR flow rates are in ml. min^{-1}.

3.3.3.7 *Interferences*

The effects of various concentrations of other metal ions on the determination of 10 μg ml.$^{-1}$ palladium was examined for this system. Cobalt(II), iron(III), nickel(II), tin(II), ruthenium(III), manganese(II), cadmium(II) and mercury(I) did not interfere at the optimum pH even when present at a level of 0.01 M, *i.e.*, one hundred times the palladium concentration. Interaction of these metal ions with SCPAR under alkaline conditions has been reported. [102] Table 3.4 lists metal ions that were found to interfere. Also listed are sensitivities of the method to the ions, relative to that for palladium, and wavelength maxima observed in the spectra of their complexes. Most of these ions give complexes which have maximum absorbances at wavelengths different from that obtained with palladium (Table 3.4), and thus, where the identities of the interfering metal(s) are known a *priori*, some further selectivity based on multi-wavelength measurements should be possible. [100]

Ion	Relative Sensitivity[a]	Absorbance Maxima (nm)[b]
Rh(III)	0.27	482
Au(III)	0.25	348, 498
Cu(II)	0.24[c]	520
Pt(IV)	0.22	488
Ag(I)	0.18	500
Pb(II)	0.15[c]	294, 472
Fe(II)	0.09[c]	474
Ir(III)	0.08	496
Al(III)	0.07[c]	490
Zn(II)	0.05[c]	334, 520

Table 3.4 Interfering metal ions in the determination of palladium.

[a] Sensitivity at wavelengths shown relative to an equal concentration of Pd(II) observed at 488 nm.
[b] Absorbance for reaction mixture at pH 5.
[c] Can be effectively masked with 10^{-3} M EDTA.

3.3.3.8 *Analytical performance*

For routine analysis, the flow injection geometry shown in Figure 3.4b was employed. The calibration curve obtained with this apparatus (Figure 3.19) was linear in the palladium concentration range of 0.045 - 30 μg ml.$^{-1}$ (4.23 x 10^{-7} - 2.82 x 10^{-4} M) with a sensitivity of 0.04 a.u. / (μg ml.$^{-1}$) (4256 a.u./M). The non-zero intercept observed in the calibration plot results from a refractive index effect due to the injection of the palladium standard into the buffer stream. The detection limit with this system was 0.04 μg ml.$^{-1}$ (3.76 x 10^{-7} M).

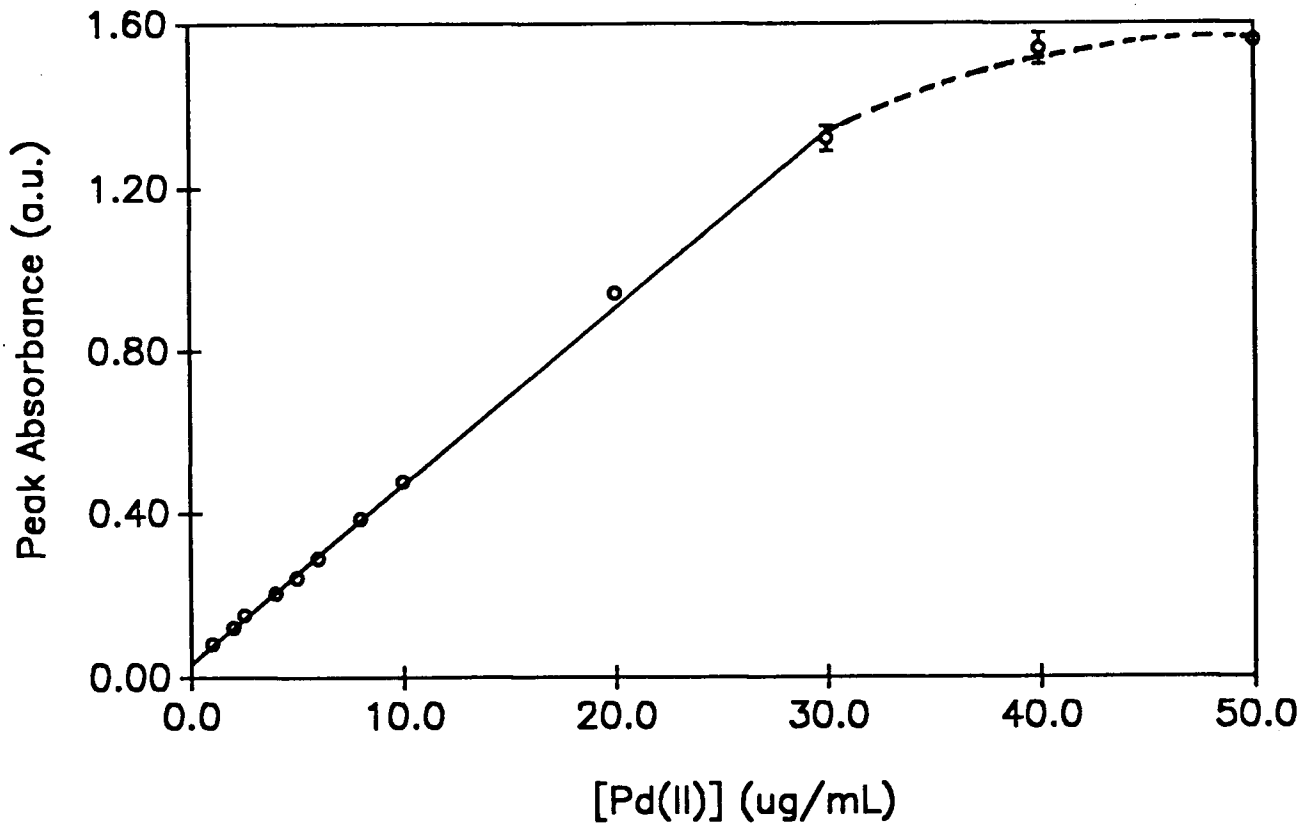

Figure 3.19 Calibration curve for palladium determination. The solid line represents the linear dynamic range.

A molar absorptivity of 4.28×10^4 l mol^{-1} cm^{-1} for the SCPAR-Pd(II) complex was obtained. As such it was unable to reproduce the much higher value obtained by Savvin *et al.* but is significantly better than most absorptometric procedures.[102] At 120 hr^{-1}, sample throughput obtained here was very much higher than obtained by Savvin *et al.* In the unlikely event that even higher sampling rates are needed, an increase in flow rate and/or a decrease in reaction coil length would achieve this, at the expense of sensitivity.

Table 3.5 compares the detection limit, linear dynamic range, and interfering metal ions cited for the two other flow injection methods for palladium [100, 101] with those of the procedure developed here.

Method	Ref.	Detection Limit(ppm)	Linear Dynamic Range(ppm)	Interference
EDTA/Pd	100	not given	9 - 180	[Os(IV), Ru(III), Pt(IV), Rh(III), Ir(III), Ir(IV)][a]
5-Br-PSAA/Pd	101	0.002	0.01 - 0.10	Cu(II)[c], Fe(II)[c], Co(III)[b], Ni(II), Pt(VI)[b], Os(VIII)[b], Ru(II)[b], W(VI)[b,c]
Na-SCPAR/Pd	this work	0.045	0.045 - 30	Au(III), Al(III), Ag(I), Cu(II)[c], Fe(II), Pb(II), Pt(IV), Rh(III), Ir(III), W(VI), Zn(II)

Table 3.5 Comparison of detection limit, dynamic range, and interferences of this work and the other flow injection methods for palladium determination

Footnotes to Table 3.5

a 0.02-1.5 mg permissible weight giving less than 5% error in 1 mg of palladium detection.

b Tolerated up to (1-5 mg l^{-1}) in determination of 0.1 mg l^{-1} palladium

c Tolerated up to (1-10 mg l^{-1}) when 10^{-3} M EDTA added to carrier stream to mask interferents.

The proposed method was used for the determination of 5 and 10 ppm palladium added to a synthetic sample, made up of a mixture of 100 ppm iron(II), iridium(III), aluminum(III), zinc(II), 50 ppm copper(II) and 10 ppm of rhodium(III), gold(III) and platinum(IV). Sample solutions containing 5 ppm palladium(II) was determined with the analytical recovery value of palladium showing +115% in the absence of EDTA and +104% in the presence of 0.001 M EDTA. If no interference is observable, this value should be 100%. The relative standard deviation from 10 replicate samples was 2.8%. The samples spiked with 10 ppm palladium(II) gave a better recovery (+101.5%) in the presence of 0.001 M EDTA, with double the concentration of Na-SCPAR. The relative standard deviation from 10 replicate samples was 1.4%.

3.3.3.9 *Conclusion*

Na-SCPAR is a sensitive and moderately selective reagent for the photometric determination of palladium(II). The FIA method developed is simple and allows the rapid determination of palladium without an extraction step. Additional advantages of this analytical method are those generic to flow injection, and include relatively inexpensive equipment, high precision, high sample throughput, and low sample and reagent consumption.

The results from manual pH studies, and automated response surface mapping and simplex optimization experiments show good agreement. The automated methods development instrumentation provided an effective means to optimize and characterize this analytical method.

3.4 Spectrophotometric determination of peroxydisulphate with *o*-dianisidine by flow injection

3.4.1 Introduction

This section describes the development of an automated spectrophotometric flow injection method for the determination of peroxydisulfate (persulphate) ions. Persulphate oxidizes *o*-dianisidine to form a stable product which has a convenient absorbance maximum at 450 nm. Precise and accurate knowledge of peroxydisulfate ion concentration is critical in industrial polymer production, where it is extensively used as an initiator, *e.g.*, in the production of polystyrene. [107] Its ability to oxidize in either acidic, neutral, or alkali media also makes it widely applicable in many other areas of chemistry. [106]

The persulphate ion is a strong two-electron oxidizing agent

$$S_2O_8^{2-} + 2\,e^- \text{ --> } 2\,SO_4^{2-} \qquad (3.4)$$

with a standard redox potential of +2.01 V in either neutral or alkaline solution. [105]

The literature contains a number of methods for determination of persulphate. Kolthoff and Carr [108] reported several reductometric methods for the volumetric determination of persulphate ions. Of these, the iodometric and ferrometric (titrimetric) methods were the most practicable from the points of view of rate of reaction, accuracy, and simplicity. [108] However, both procedures involve a back-titration step after the redox reactions with persulphate and therefore are tedious to perform in any number. They also require reaction times of at least 15-30 minutes. Amin and Hareez [109] reported a procedure using a combination of titrimetry with alternating current (a.c) polarography. This method is likewise tedious and complex. Amin [110] later reported an indirect amplification method by a.c polarography which enabled measurement of persulphate concentrations as low as 2.6×10^{-6} M with reasonable accuracy. This method however,

involves an extraction step followed by a back-titration. Ion-exchangers are also required to remove metal ions which form water-insoluble iodides that would otherwise interfere. Kolthoff and Woods [111] reported an a.c. polarographic method by which persulphate concentrations in the range 1.0×10^{-4} - 1.0×10^{-3} M could be measured. This method was found to be highly temperature dependent. Substances that have wave potentials close to that of the iodate are known to interfere, [110] (for example, Zn(II) in alkali media or Mo(IV), Cu(II) and Bi(III) under acidic conditions). These examples show that development of rapid selective methods for determination of persulphate has proven to be a difficult analytical problem.

The reaction between persulphate ions and aromatic amines, now known as the Boyland-Sims oxidation, was first reported in 1953. [112] A literature survey found that the reaction of persulphate with the substituted aromatic amine, *o*-dianisidine (ODA) (see Appendix 1 for its molecular structure) had not previously been used for quantitative analysis of persulphate. However, persulphate ion has been used as a spray reagent for detection of aromatic amines and other related compounds in thin layer chromatography. [113] The kinetics of the reaction of *o*-dianisidine with other oxidizing agents such as H_2O_2 are well known. [114, 115]

A report on the automated development of a simple flow injection procedure to determine persulphate ions at low concentrations, with minimal interferences, based on a catalyzed persulphate reaction with *o*-dianisidine is given. The work was carried out on the automated flow injection methods development system, which has been described in Chapter 2 and reported elsewhere. [57] It made use of the simplex optimization and response surface mapping capabilities of this system, and provided another test of their efficacy.

3.4.2 Experimental Section

3.4.2.1 *Reagents*

A stock solution of persulphate (1.00×10^{-2} M) was prepared by dissolving 0.676 g of potassium persulphate (Fisher Scientific, Fairlawn, NJ), in 250 ml of distilled water. Standard solutions were prepared from this by appropriate dilution. A 1.0×10^{-2} M *o*-dianisidine solution (2.443 g/l) (Aldrich, Milwaukee., WI) was freshly prepared daily in a 40 % v/v mixture of acetone in water. Solutions of *o*-dianisidine were freshly prepared every day. A 10^{-2} M copper nitrate stock solution (2.326 g/l) was prepared in distilled water for use as a catalyst.

A buffer solution was prepared from 100 ml of 0.1 M 3,3-dimethylglutaric acid (Aldrich, Milwaukee, WI) in 1 M sodium chloride. [116] The sodium chloride was present to minimize the effect of changes in the ionic strength of the reaction media. Various reaction pHs for the batch method experiments were obtained by adding appropriate volumes of 0.1 M sodium hydroxide to the buffer.

3.4.2.2 *Apparatus*

The automated flow injection analyzer used was as used in previous methods development [53, 60] and discussed in Chapter 2. The options used in this work included the custom-built variable speed peristaltic pump unit containing 5 independent pump heads, a high precision variable speed peristaltic pump (Models C-4V or C-6V, Alitea USA, Seattle, WA), and a 6-port air-driven solenoid-actuated injection valve (Rheodyne 5020P, Cotati, CA) equipped with a 100 μl sample loop. A diode array spectrophotometer (Hewlett Packard 8452A) with a standard 1 cm quartz cell was used for absorption measurements. All the other units were controlled by the same microcomputer as described elsewhere. [57] For the flow injection studies, a 30 μl, 1 cm path length quartz flow cell was used. The pH of reaction mixtures was determined on-line using a flow through electrode cell, an Ag/AgCl electrode (Radiometer America Electrodes Inc.- Model No. GK473901), and a

laboratory pH meter (Model 119, Fisher Scientific, Richmond, B.C.). Polytetrafluoroethylene (PTFE) tubing of 0.5 mm i.d. was used throughout. Code used for nonlinear curve fitting and other data processing tasks was written in Microsoft QuickBASIC^{R} version 4.0. The optimization algorithm used was the composite modified simplex method.[3, 61] Response surface plots were generated using a commercial scientific graphics program (SURFER^{R} version 3.0, Golden Software, Golden, CO).

3.4.2.3 *Procedures*

3.4.2.3.1 *Batch kinetics studies*

A series of preliminary batch kinetics experiments were performed to investigate the suitability of *o*-dianisidine as a reagent for the determination of persulphate ions.

A reaction was first obtained by adding 5.0 ml of 1.0×10^{-4} M persulphate solution to a mixture containing 5.0 ml of 1.0×10^{-2} M *o*-dianisidine solution and 10.0 ml distilled water. After thorough mixing an appropriate reaction mixture volume was transferred to a standard 1 cm cell in the spectrophotometer. Absorbance measurements at 450 nm were initiated 30 s after the start of the reaction and acquired at 10 s intervals for a period of 900 s. The effect of pH on this reaction for the above *o*-dianisidine concentration was then established by adding 10.0 ml of buffer solution at a known pH in place of the distilled water. The pH was varied from 3.00 to 9.00.

3.4.2.3.2 *Stopped flow kinetic studies*

Once the optimum reaction pH was identified, stopped-flow experiments were conducted to determine the kinetic parameters (*i.e.*, final amount of product formed, order of reaction and rate constant, k'). The flow configuration used for the stopped flow experiments is as shown in Figure 3.20. A single Alitea C4V pump was run at maximum speed to merge the reagents and then rapidly transport the reaction mixture to the cell within less than 1 s, from the tee to observation window. The flow was then stopped and

absorbance measurements were made at 1 s intervals at 450 nm for a period of 400 s.

The effect of various metal ions on the kinetics at pH 7 was then established by adding dilute metal ion solutions in place of the 10.0 ml distilled water. A similar procedure was followed using neutral salts to determine the effect of ionic strength on the reaction. Finally, the effect of other possible solvents and solvent mixture compositions on the *o*-dianisidine solution and product stability was determined.

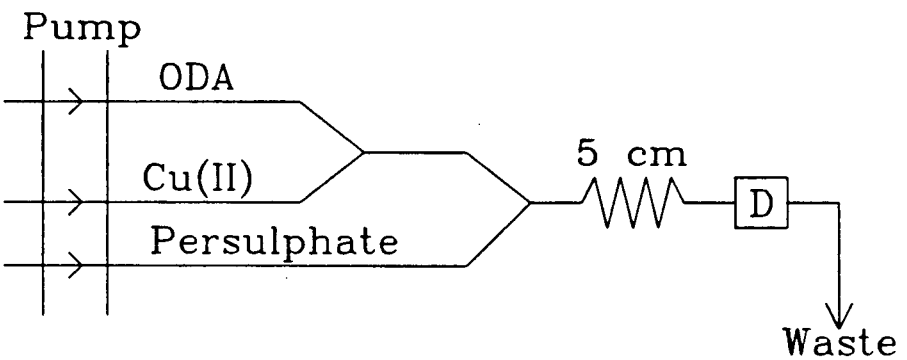

Figure 3.20 Manifold used for stopped flow kinetic studies for the reaction between *o*-dianisidine and persulphate ions. The *o*-dianisidine reagent stream was 1.0×10^{-2} M *o*-dianisidine made in 40 % v/v acetone in dimethylglutaric acid (DMGA) buffer at pH 7.0. A 1.0×10^{-4} M Cu(II) stream was used to catalyze the reaction. A 1.0×10^{-4} M persulphate solution was used. Absorbance measurements were made using the spectrophotometer (D) at 450 nm.

3.4.2.3.3 *Flow injection studies*

The flow injection configuration used for both the automated simplex optimization and response surface mapping studies is shown in Figure 3.21a. The reagent stream consisted of *o*-dianisidine merged with distilled water to give a total flow rate of 1.00 ml. min^{-1} and maximum *o*-dianisidine concentration of 1.0×10^{-2} M. The buffer stream was comprised of 0.10 M 3,3-dimethylglutaric acid in 0.10 M NaCl, and was merged with a 0.10 M sodium hydroxide stream to give a total flow rate of 1.0 ml. min^{-1} and a maximum NaOH concentration of 0.10 M. The carrier stream was made up of 5.00×10^{-4} M Cu(II) solution as a catalyst, flowing at a fixed rate of 1.50 ml. min^{-1}. By allowing the NaOH flow rate to vary from 0.00 - 1.00 ml. min^{-1}, the pH was varied from about 3.5 - 10.0. The flow at the detector was kept at a constant total rate of 3.50 ml. min^{-1}. This ensured a constant sample residence time in the system. Separate pumps were used for each solution. The internal diameter (i.d.) of tubing used for reaction coils was 0.5 mm for all sets of experimental conditions. Before any sample injection was made, the system was allowed to equilibrate to a steady baseline reading. A 100 μl sample of 1.00×10^{-4} M persulphate was then injected into the carrier stream and peak absorbance profile measured at 450 nm. The peak height recorded was taken as proportional to concentration of persulphate. The pH of the reaction mixture was measured simultaneously in a simple-flow through cell placed 5 cm after the spectrophotometric detector.

3.4.2.3.4 *Automated simplex optimization*

During the automated simplex optimization, the flow rates of all the streams save for the carrier stream were automatically adjusted, so as to determine the optimum flow rates for the reagent and NaOH streams. The optimum pH could then be ascertained from the relative flow rates of NaOH and buffer stream.

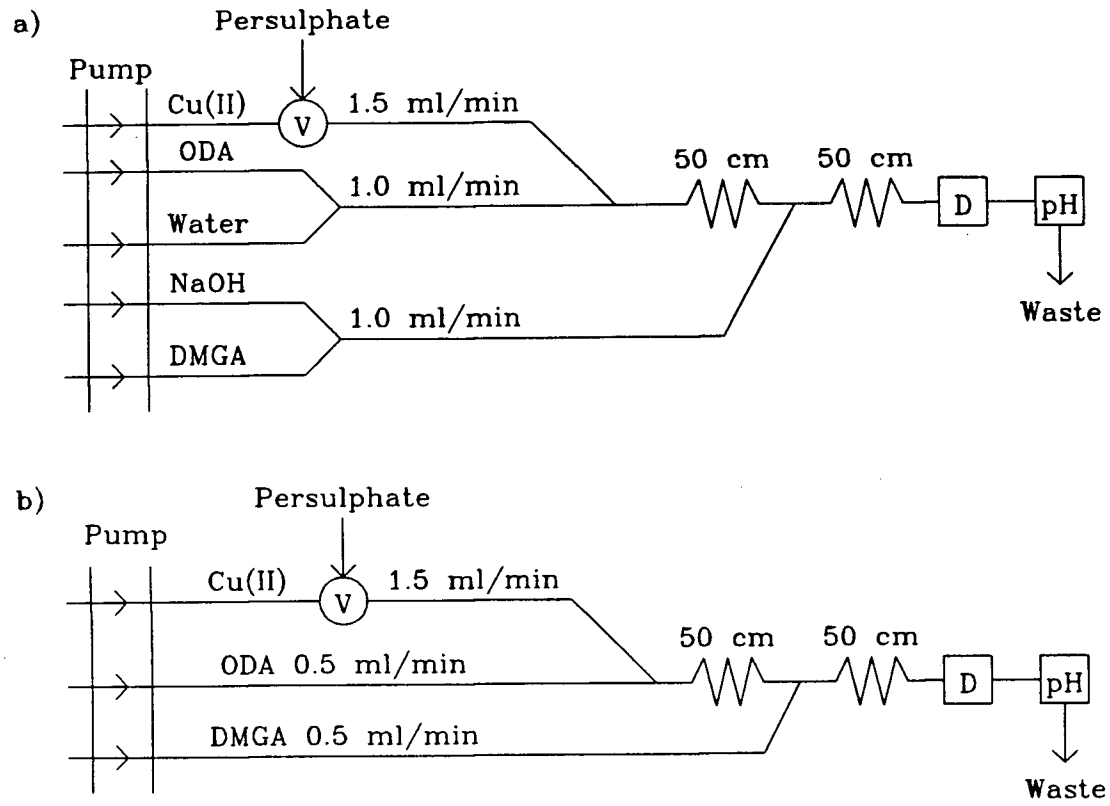

Figure 3.21 Flow injection manifold used for persulphate determination:

(a) Manifold used for automated optimization and response surface mapping studies. The carrier stream was 5.0×10^{-4} M Cu(II) flowing at a constant flow rate of 1.50 ml. min^{-1}. The injection valve (V) was equipped with 100 μl loop, through which 1.0×10^{-4} M sample of persulphate were injected. The reagent and water streams were "buddied" at 1.0 ml. min^{-1}. The buffer stream consisted of NaOH and dimethylglutaric acid (DMGA), "buddied" at 1.0 ml. min^{-1}. Detection was via a spectrophotometer (D) at 450 nm, and a pH electrode cell (pH).

(b) Manifold used for calibration studies and investigation of effect of organic substances. This was comprised of a 5.0×10^{-4} M Cu(II) carrier stream flowing at a constant rate of 1.5 ml. min^{-1}, an injection valve (V) with 100 μl loop, a 1.0×10^{-2} M *o*-dianisidine reagent stream flowing at 0.5 ml. min^{-1}, a dimethylglutaric acid (DMGA) buffer stream at pH 7.0 flowing at a constant 0.5 ml. min^{-1}, a spectrophotometer (D), and a pH electrode cell (pH).

The initial experimental conditions and the best experimental conditions established during the simplex optimization procedure are summarized in Table 3.6 below. The best conditions obtained correspond to those of experimental point number 7, *i.e.*, *o*-dianisidine and NaOH flow rates of 1.00 and 0.66 ml. min^{-1} respectively, with the pH of the reaction mixture equal to 6.67 as recorded by the pH meter.

Expt.#	Variable # 1 (ODA) / ml. min^{-1}	Variable # 2 NaOH / ml. min^{-1}	Response[a]	pH	%RSD
1	0.400	0.400	0.071	4.42	1.5
4	0.840	0.672	0.198	5.75	0.3
5	1.000	0.807	0.198	7.5	1.6
7	1.000	0.664	0.211	6.67	0.7
8	0.763	0.775	0.190	7.12	1.0
12	1.000	0.585	0.189	5.26	0.6

Table 3.6. The response, pH, and the percent relative standard deviation (%RSD) of the initial (expt. #1) and the five best simplex experimental conditions. The total number of experimental points was 20.

[a]Responses were measured as peak absorbance.

Once the optimum conditions were established, these were implemented on a simpler flow injection system shown in Figure 3.21b. This was comprised of two pumps, three pump tubes and a single injection valve, and was used for subsequent routine analysis, calibration and studies on the effect of organic substances. Alternatively, a single pump such as an Alitea C6-V could have been employed with the carrier stream channel having a pump tubing which could provide a flow rate that is three times higher than that of the other channels.

3.4.2.3.5 *Automated response surface mapping*

A more thorough investigation of the *o*-dianisidine-persulphate response surface was then made by carrying out experiments in triplicate at each of the 64 sets of reaction conditions. These were regularly spaced across the search space in the pattern of an 8 x 8 square lattice. The average absorbance at each set of conditions was taken as the height of the response surface at that point.

3.4.3 Results and Discussion

3.4.3.1 *Selection of analytical wavelength*

The absorption spectra of 5.0×10^{-3} M *o*-dianisidine in 40 % v/v acetone-water mixture and that of the reaction product formed from the reaction between 5.0×10^{-3} M *o*-dianisidine in 40 % v/v aqueous acetone and 1.0×10^{-4} M persulphate after five minutes as reaction time are shown in Figure 3.22. This reveals that absorbance measurements due to formation of product can be made at 450 nm without interference from the reagent matrix.

3.4.3.2 *Batch kinetic studies*

3.4.3.2.1 *Effect of metal ions*

A number of metal ions are known to catalyze reactions involving persulphate ions. The metal ions studied in this work are given in Table 3.7. Most showed same catalytic activity, but to varying degrees. Both Fe(II) and Cu(II) showed remarkable catalytic activity, even at concentrations as low as 10^{-5} M. Reactions catalyzed by Fe(II) however yielded very unstable products. This was not surprising since the mechanism of the reaction is thought to be via a free radical species [108] which in this case produces Fe(III), which itself formed a colored complex with *o*-dianisidine (as determined experimentally). A substantial catalytic effect was also observed with Pb(II).

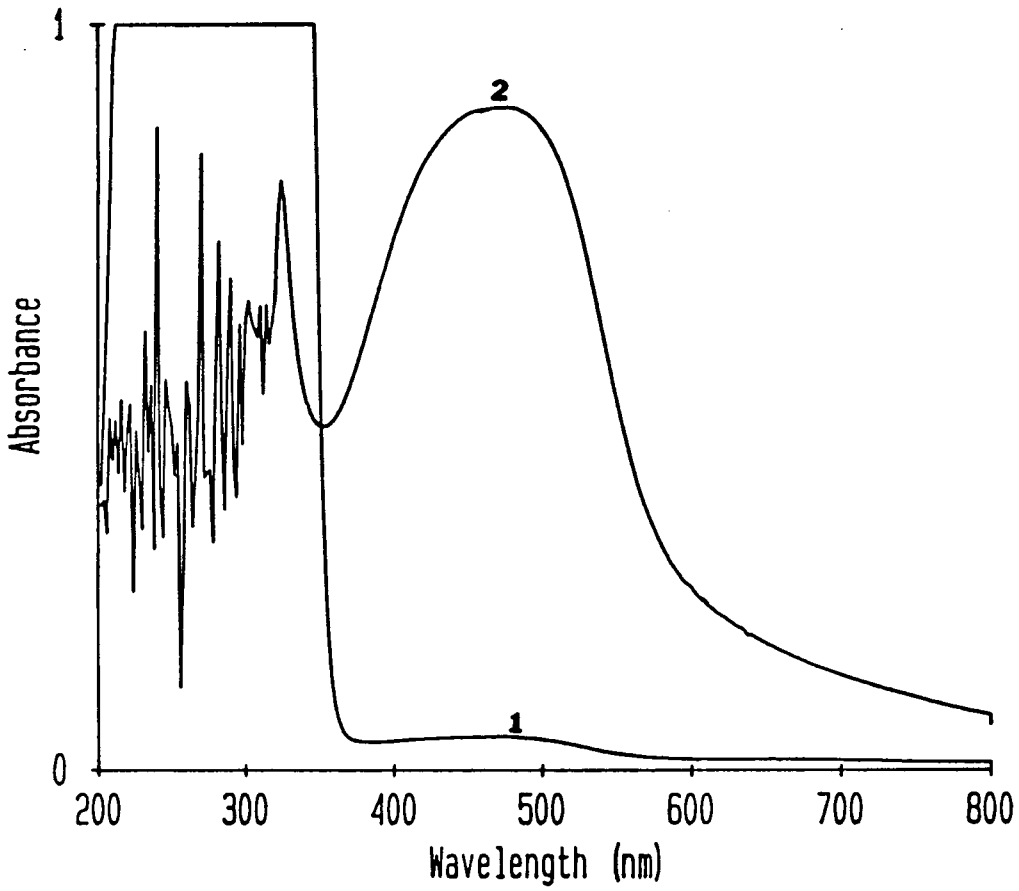

Figure 3.22 UV-Visible absorption spectra of the *o*-dianisidine-persulphate reaction product:

(1) reference spectrum:- reagent blank with water in place of persulphate ion solution;

(2) *o*-dianisidine-persulphate mixture after 300 s with the reagent blank as reference.

The catalytic activities of Mn(II), Co(III), Ni(II), Zn(II), and Mo(VI) were much less than that of Cu(II). About a 100-fold concentration (10^{-1} M) of these metal ions had a comparable catalytic effect to that of the (10^{-3} M) Cu(II). Both Ag(I) and Fe(III) formed colored complexes with *o*-dianisidine directly and thus interfered with persulphate determination.

Further investigation of the suitability of Cu(II) as a catalyst in the *o*-dianisidine-persulphate reaction was then performed. The concentration of Cu(II) was varied from 10^{-7} to 10^{-1} M. At concentrations below 10^{-6} M, the reaction rate was slightly increased relative to the uncatalyzed reaction. For concentrations between 10^{-6} and 10^{-4} M, equilibrium of the reaction mixture was reached between 240 and 90 s respectively, while with concentrations between 5.0 X 10^{-4} and 10^{-1} M, equilibrium was attained within 60 s. A Cu(II) concentration in the range 10^{-3} to 10^{-2} M is therefore recommended. This is a compromise between rate of attaining equilibrium and product instability, since at concentrations above 10^{-2} M Cu(II) instability became more apparent, *i.e.*, product formed was quickly decolorized.

3.4.3.2.2 *Effect of neutral salts*

Ionic strength often varies from sample to sample and so the effects of NaCl, KCl, and KNO_3 concentrations on the *o*-dianisidine-persulphate reaction were investigated. Table 3.8 summarizes the effect of various concentrations of these neutral salts on the rate of reaction. The reported absorbances were measured 300 s after initiating the reactions. All these neutral salts showed a positive effect on the rate of the reaction with increase in concentration. KCl and NaCl showed approximately equal effects, which were greater than that observed for KNO_3.

Potential catalyst	$[M^{n+}]$ /moles l^{-1}	Absorbance	Enhancement factor*	Time (s)
Blank	-	0.747	0.63	300
Mo^{6+}	1×10^{-3}	0.779	0.66	300
Mn^{2+}	1×10^{-3}	0.946	0.80	300
Ni^{2+}	1×10^{-3}	1.040	0.88	215
Co^{2+}	1×10^{-3}	1.038	0.88	200
Zn^{2+}	1×10^{-3}	1.108	0.94	245
Pb^{2+}	1×10^{-3}	1.133	0.96	245
Cu^{2+}	1×10^{-3}	1.181	1.00	85
Fe^{3+}	1×10^{-3}	interferes	-	-
Ag^{+}	1×10^{-3}	interferes	-	-

Table 3.7. Effect of metal ions on the *o*-dianisidine-persulphate reaction. Absorbance measurements were taken 5 min after initiation.

* The enhancement factor is calculated relative to that for 10^{-3} M Cu^{2+} ions. The times shown are those at which maximum absorbance were recorded with [*o*-dianisidine] = 5.0×10^{-3} M, $[S_2O_8^{2-}] = 1.0 \times 10^{-4}$ M, buffered at pH = 7.0.

Salt	Concentration /moles l^{-1}	Absorbance after 600 s	Relative increase (%)
Blank	0.0	0.0932	0
NaCl	1.0×10^{-4}	0.1479	58.69
	4.0×10^{-3}	0.1488	59.66
KCl	1.0×10^{-4}	0.1401	50.32
	4.0×10^{-3}	0.1495	60.41
KNO_3	1.0×10^{-4}	0.1040	11.59
	4.0×10^{-3}	0.1323	41.95

Table 3.8. The effect of neutral salts on the rate of formation of product.

Reaction conditions: 1.0×10^{-3} M *o*-dianisidine;
5.0×10^{-5} M $S_2O_8^{2-}$.

3.4.3.2.3 *Effect of % v/v composition of acetone in water as solvent*

The %v/v composition of acetone in water was varied from 20 to 100%. The lower limit was chosen because of the limited solubility of *o*-dianisidine in distilled water. The results showed a general increase in rate of the reaction with increase in mole fraction of acetone, but product stability decreased. In the presence of 10^{-4} M Cu(II) as catalyst, equilibrium was attained in less than 60 s with compositions above 40%. Product stability however decreased with increase in %acetone composition above 40%. Under similar conditions with 20 - 40% acetone, equilibrium was achieved between 60 and 90 s respectively, with product stability times greater than 300 s (product stability times = time period over which absorbance readings were recorded within ± 0.05 absorbance units). Thus a composition of between 20 and 40% acetone is recommended.

3.4.3.2.4 *Effect of reaction mixture pH*

0.1 M 3,3-dimethylglutaric acid in 1M NaCl and 0.1 M NaOH was used as buffer to vary the pH of the reaction mixtures from 3.5 to 10.0. A high concentration of NaCl was employed to keep the ionic strength of the reaction medium constant. Figure 3.23 shows the responses obtained from the reaction mixtures at various pH values. Absorbance was measured after 300 s of reaction time. From these batch reactions, the maximum response obtained corresponded to neutral conditions, however acceptable sensitivity was obtained between pH 6.5 and 7.5.

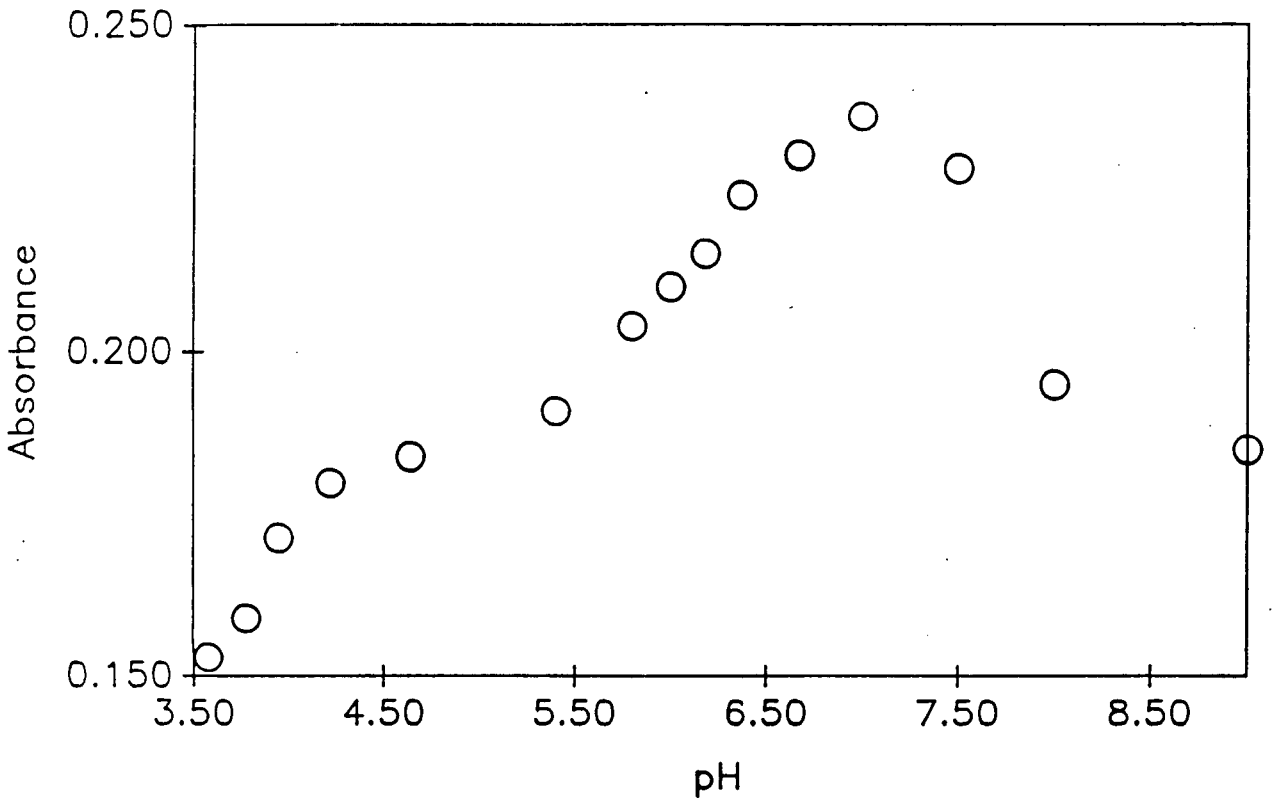

Figure 3.23 Absorbance measured at 450 nm for the *o*-dianisidine-persulphate reaction mixture as a function of pH. The reaction mixture was comprised of 5.0 ml volumes of 2.0 x 10^{-3} M *o*-dianisidine in 40% acetone/water mixture, 1.0 x 10^{-5} M persulphate, and 5.0 x 10^{-4} M Cu(II) and 10 ml of dimethylglutaric acid (DMGA) buffer solution.

3.4.3.3 *Reaction kinetics studies*

The kinetics of the reaction were investigated at neutral pH conditions under pseudo-first order conditions, with *o*-dianisidine in excess. Expressing the reaction as;

$$S_2O_8^{2-} + n\ \text{ODA} \xrightarrow{C_O} \text{Product}; \qquad (3.5)$$

the reaction rate law can be written as

$$\text{Rate} = k_u([\text{ODA}]^l[S_2O_8^{2-}]^m) + k_c([\text{ODA}]^l[S_2O_8^{2-}]^m[C_O]^n), \qquad (3.6)$$

where C_O is the initial concentration of the catalyst, l, m, n are the orders of reaction with respect to *o*-dianisidine, $S_2O_8^{2-}$ and C_O respectively, and k_u and k_c are the rate constants for the uncatalyzed and catalyzed reactions respectively. Assuming that [*o*-dianisidine] > > $[S_2O_8^{2-}]$, $[C_O]$ is constant, and the reaction is first-order with respect to $S_2O_8^{2-}$, this simplifies to:-

$$\text{Rate} = k'[S_2O_8^{2-}] \qquad (3.7)$$

where K' ($= k_u[\text{ODA}] + k_c[\text{ODA}][C_O]$) is the pseudo-first order rate constant.

A non-linear curve fitting program was used to extract the pseudo-first-order rate constant from the stopped-flow experimental data. The equation fitted to the data was,

$$A_t = A_\infty\ [1-\exp(-K't)] + C \qquad (3.8)$$

where A_t is the absorbance at time t, A_∞ is the final solution absorbance due to product and C is a constant background term. The flow through cell was thermostated at 25°C. Figure 3.24 is representative of the fits of the model to the data. Excellent fits were obtained for each of the solutions tested. The pseudo-first order rate constant obtained from the fitting routine was $0.06 \pm 0.01\ s^{-1}$.

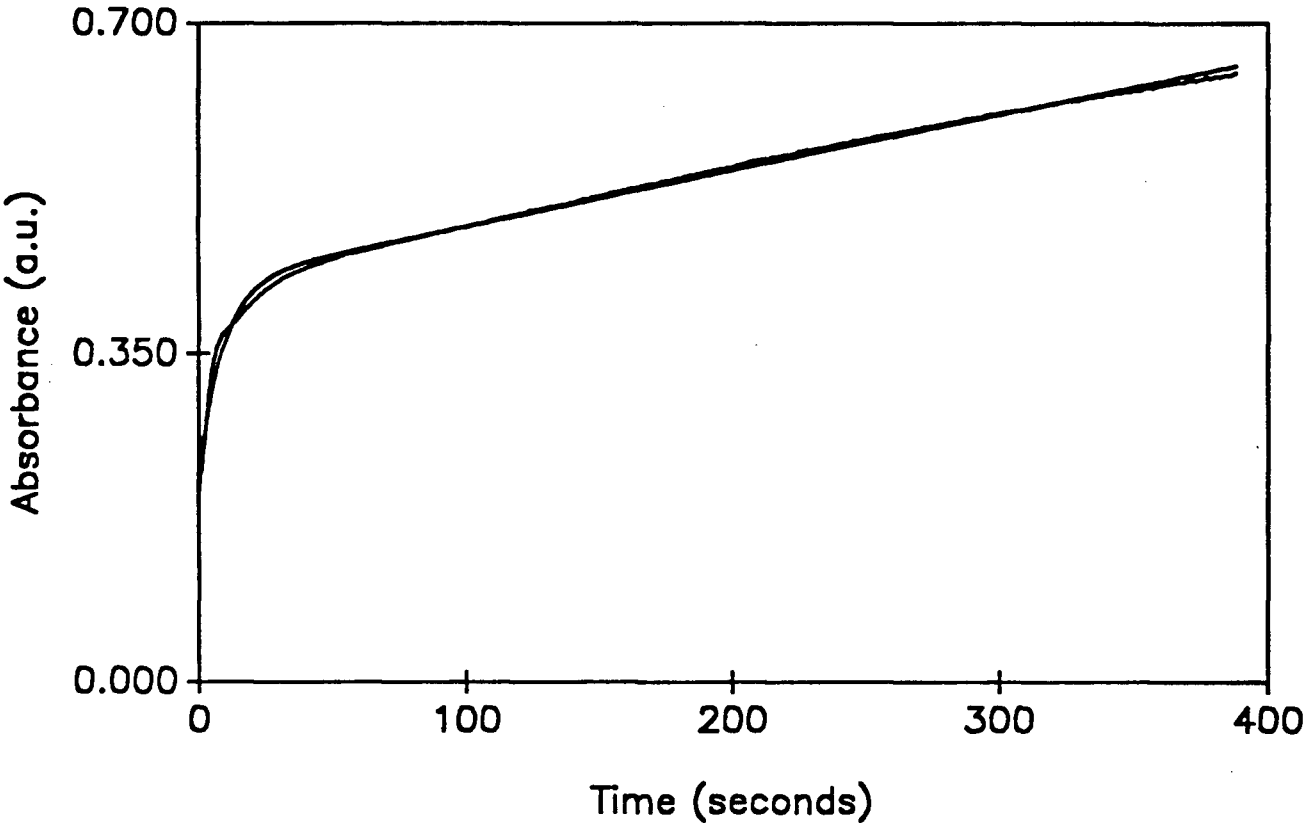

Figure 3.24 Fit of a pseudo-first order reaction model to data collected for the reaction between *o*-dianisidine and persulphate ions at pH 7.0.

The final equilibrium absorbance due to the product remained unchanged within ± 0.01 a.u. for *o*-dianisidine concentrations in the range 0.001 - 0.01 M, an indication that reaction was going to completion. The reaction is essentially finished in less than 90 s.

A possible mechanism for the reaction may be based on that general to oxidations of arylamines or phenols and catalyzed by metal ions. [117] The first step of the oxidation is homolytic:

$$RH + M^{(n+1)+} \dashrightarrow R^{\bullet} + H^{+} + M^{n+} \qquad (3.9)$$

where $R^{\bullet}$ represents an arylamine radical $ArNH^{\bullet}$ or aryloxy radical $ArO^{\bullet}$. This process is permitted by the ready removal of the electron. The radicals are further stabilized by conjugation of the unpaired electron from the N or O with the π-electron system of the aromatic ring. Because of the different ways in which the radical can react further, several final reaction products are possible. These however should depend on the structure, reactivity, reaction conditions, and on the localization of the unpaired electron. [118]

The postulated reaction scheme for the *o*-dianisidine/persulphate system resulting in the regeneration of the catalyst (mechanism for the catalytic cycle) is given below;

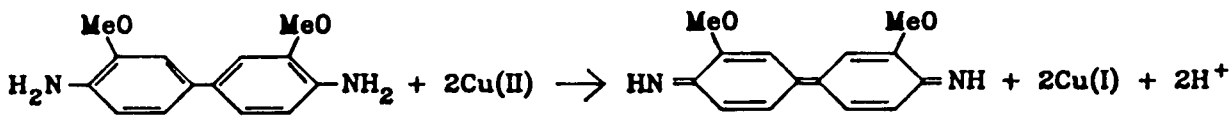

(3.10)

The persulphate dissociates in solution to give sulfate radicals:

$$S_2O_8^{2-} \dashrightarrow 2\ SO_4^{\bullet-} \qquad (3.11)$$

which themselves oxidize the organic compound (*i.e.*, in the uncatalyzed reaction) and also participate in the catalyst regeneration step:

$$SO_4^{\bullet-} + Cu(I) \text{---} > SO_4^{2-} + Cu(II) \qquad (3.12)$$

It is possible that the final product has the structure shown in the right hand side of equation (3.10), or a product of its hydrolysis, especially under neutral pH conditions. Nevertheless, the final product must have increased conjugation compared to the *o*-dianisidine, as is evident from its absorption band in the visible region of the spectrum. The *o*-dianisidine itself absorbs only in the UV part of the spectrum. No further work to isolate and characterize the product was conducted. Several other products are possible from the free radical intermediate, and these may be controlled by the rate of production of the free radical intermediate (this explains why higher concentrations of Cu(II) catalyst produced unstable products in reaction mixture, see section (3.4.3.2.1)).

3.4.3.4 *Automated simplex optimization of the flow injection system*

Simplex optimization was chosen as an optimization procedure because it rapidly optimizes chemical and flow conditions in flow injection systems.[1] Three replicate peaks were obtained for every set of experimental conditions. The total time taken to achieve the optimum conditions by simplex optimization was 2 hr. In all, 22 sets of experimental conditions were tried.

3.4.3.5 *Automated response surface mapping*

For the automated response surface mapping, a 2-factor 8-level design (64 experiments each with three replicates), was used. This optimization process took about 4 hours.

The results of the response surface mapping study are shown in Figure 3.25. The ideal pH for this reaction was established as 7.0, however the pH range 6.0 to 7.5 can be used without great loss in sensitivity. This range corresponded to NaOH stream flow rates in the range 0.30 - 0.80 ml. min^{-1} for the FIA manifold of Figure 3.21. Thus the whole pH range 6.0 - 7.5 is recommended.

3.4.3.6 *Comparison of simplex and response surface mapping results*

The response surface mapping results were in good agreement with those from the simplex optimization procedure. As shown in Table 3.6, the optimum flow rate conditions obtained from simplex experiments fall in the region considered as optimum from the response surface studies. Also the pH's corresponding to the 5 best simplex experimental conditions are within the pH range established as optimum from the response surface studies. The optimum conditions established by the simplex procedure were thus confirmed by the automated response surface mapping studies at the expense of more experiments and somewhat less information about the region of the optimum.

3.4.3.7 *Modelling of response surface obtained*

The absence of diagonal features on the response surface obtained indicated that the pH and *o*-dianisidine were acting largely as independent variables. Visual inspection of the surface suggested that a global system model could be fitted. Peak absorbance increases with increasing *o*-dianisidine flow rate asymptotically, and there is a general rise with NaOH flow rate, but with a pronounced almost Gaussian optimum region at one NaOH value. As a first approximation, the model would be comprised of a dominant exponential term in *o*-dianisidine (ml. min^{-1}), a Gaussian NaOH contribution, a *small* general slope towards higher NaOH flow rate, and a background term.

The model equation actually fitted was of the form:-

Absorbance at Peak maximum (a.u.) =

$$A\,[1-\exp(-\alpha\, f(ODA))] \qquad \text{ODA term}$$

$$+\ B \downarrow \frac{\{f(ODA) - 0.1\}}{s(NaOH)} * \exp[\,-\{\bar{x}(NaOH) - f(NaOH)\}^2 / (2 * s(NaOH))^2\,] \qquad \text{NaOH term}$$

$$+\ C * f(ODA) * f(NaOH) \qquad \text{Cross term}$$

$$+\ D \qquad \text{Background term}$$

where: A, B, C, D and α are constants,

f(ODA) and f(NaOH) are the flow rates of these streams,

$\bar{x}$(NaOH) corresponds to the position of the Gaussian maximum on the NaOH axis, and s(NaOH) expressed as standard deviation.

The best fit values obtained by non-linear least squares fitting were:

$\bar{x}$(NaOH) =	0.50 ml. min^{-1}	s(NaOH) =	0.05 ml. min^{-1}
A =	0.24	D =	-0.05
B =	0.16	α =	1.91
C =	0.05		

The relative magnitudes of the *o*-dianisidine and NaOH terms are shown by constants A and B. The standard error of estimate between the calculated values and the experimental values was 2.58×10^{-2}. The percentage of the residual volume (volume difference between experimental and theoretical response surface) to the original experimental volume was found to be less than 0.5%. The model surface is shown in Figure 3.26 below, and should be compared to the real experimental surface in Figure 3.25.

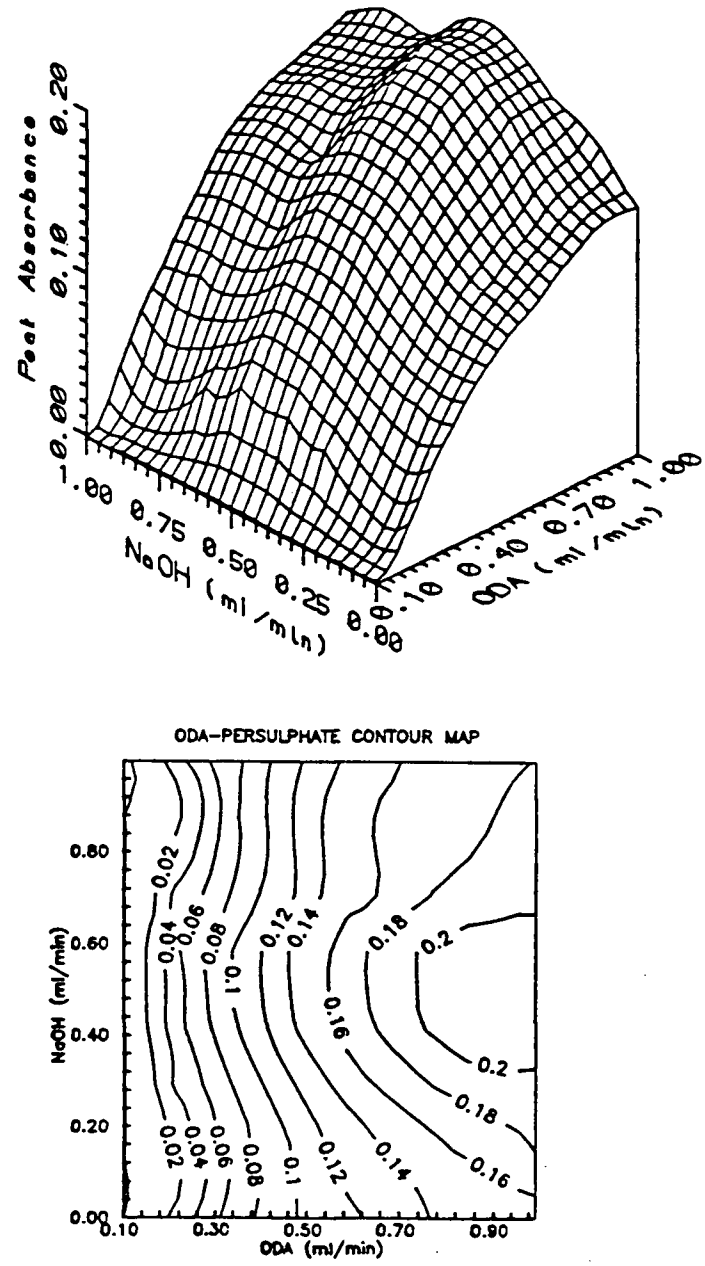

Figure 3.25 The *o*-dianisidine-persulphate response surface shown as a 3D plot and its corresponding contour map. The response shown is the peak absorbance at 450 nm. *o*-dianisidine and NaOH flow rates are in ml. min^{-1}. Stock solution concentrations used were 5.0×10^{-4} M Cu(II), 1.0×10^{-2} M *o*-dianisidine in 40% acetone, 0.1 M NaOH, 0.1 M dimethylglutaric acid in 0.1 M NaCl, and 1.0×10^{-4} M persulphate.

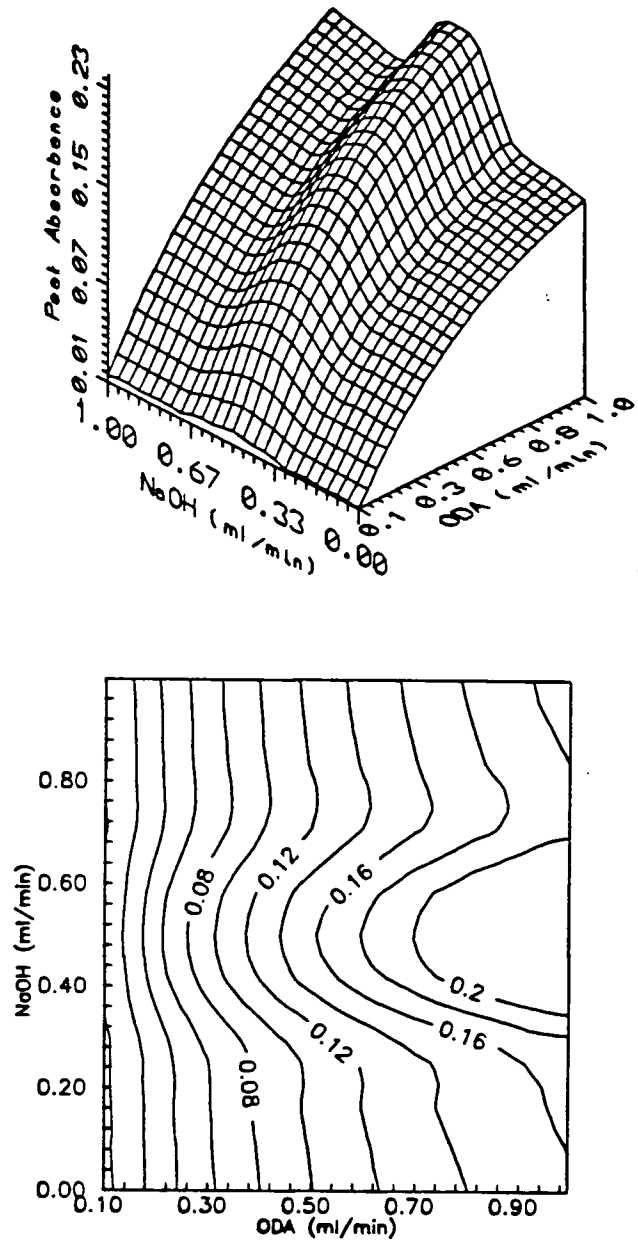

Figure 3.26 The modelled 3D response surface plot for the *o*-dianisidine-persulphate reaction. The response shown is the theoretical peak absorbance at 450 nm. *o*-dianisidine and NaOH flow rates are in ml. min^{-1}. Stock solution concentrations used were 5.0×10^{-4} M Cu(II), 1.0×10^{-2} M *o*-dianisidine in 40% acetone, 0.1 M NaOH, 0.1 M dimethylglutaric acid in 0.1 M NaCl, and 1.0×10^{-4} M persulphate.

3.4.3.8 *Effect of reaction coil length*

The effect of reaction coil length on the sensitivity of the system was determined by performing 10 replicate experiments under the optimum conditions obtained from the first simplex optimization experiment, but with different reaction coil lengths. A 100 cm coil length was established as optimum. Results of these studies are summarized in Table 3.9. Since this value was (fortuitously) that used in the previous automated chemical flow optimization, no further optimization experiments were undertaken. The automated analyzer used does not presently have the capability of automatically adjusting coil length directly, although effective coil length optimization is possible by flow reversal(s) (see Chapter 4 of this thesis, and reference 56).

Coil Length/cm	Peak Maximum (absorbance units)	Performance (%) relative to that for 100 cm coil
55	0.391	77.4
60	0.423	83.8
80	0.466	92.3
90	0.477	94.5
100	0.505	100
110	0.477	94.5
120	0.446	88.3

Table 3.9. Optimization of reaction coil length for *o*-dianisidine-$S_2O_8^{2-}$ flow injection manifold

3.4.3.9 *Interference studies*

In polymerization studies with persulphate as activator, persulphate must often be determined in the presence of various organic substances. Thus the effects of methanol, ethanol, allyl acetate, formaldehyde, ethyl acetate and allyl alcohol on the *o*-dianisidine-persulphate reaction were investigated. Of these substances, methanol and ethanol showed the least effect even at concentrations as high as 1.0 M. Solutions containing 2.5 M methanol and 1.0 M ethanol caused an error of about + 0.22% in the determination of 2.0×10^{-4} M persulphate ions. At 0.25 M concentrations of both allyl alcohol and allyl acetate errors of + 0.50% and - 6.98% respectively were recorded. The worst acceptable interference was obtained with 0.5 M ethyl acetate which gave an error of + 11.80%. Reaction in the presence of formaldehyde resulted in a turbid mixture which then formed a pink precipitate. Formaldehyde thus strongly interferes, and should not be present.

3.4.3.10 *Analytical figures of merit*

The calibration curve obtained with the flow geometry of Figure 3.21b is shown in Figure 3.26. This indicates a linear dynamic range of 2.50×10^{-5} M to 7.5×10^{-4} M, with a sensitivity of 2.4×10^{3} a.u. M^{-1}. The detection limit (3 x the std. dev. of the baseline noise) with this system was 5.0×10^{-7} M. The lower limit of the linear dynamic range was detected with a relative standard deviation of 1.5% from 10 replicates.

3.4.3.11 *Conclusion*

The analytical method developed is both simple and sensitive. Other advantages generic to flow injection techniques include its high precision, high sample throughput rate and low sample and reagent consumption rates. Together these give the analytical procedure reported here many advantages over previous classical, [108, 113] titrimetric, [108] and polarographic methods. [110, 111] While a few organic species and metal ions do

interfere, either the extent of their effects is tolerable, or the interference is usually obvious in the reaction mixture.

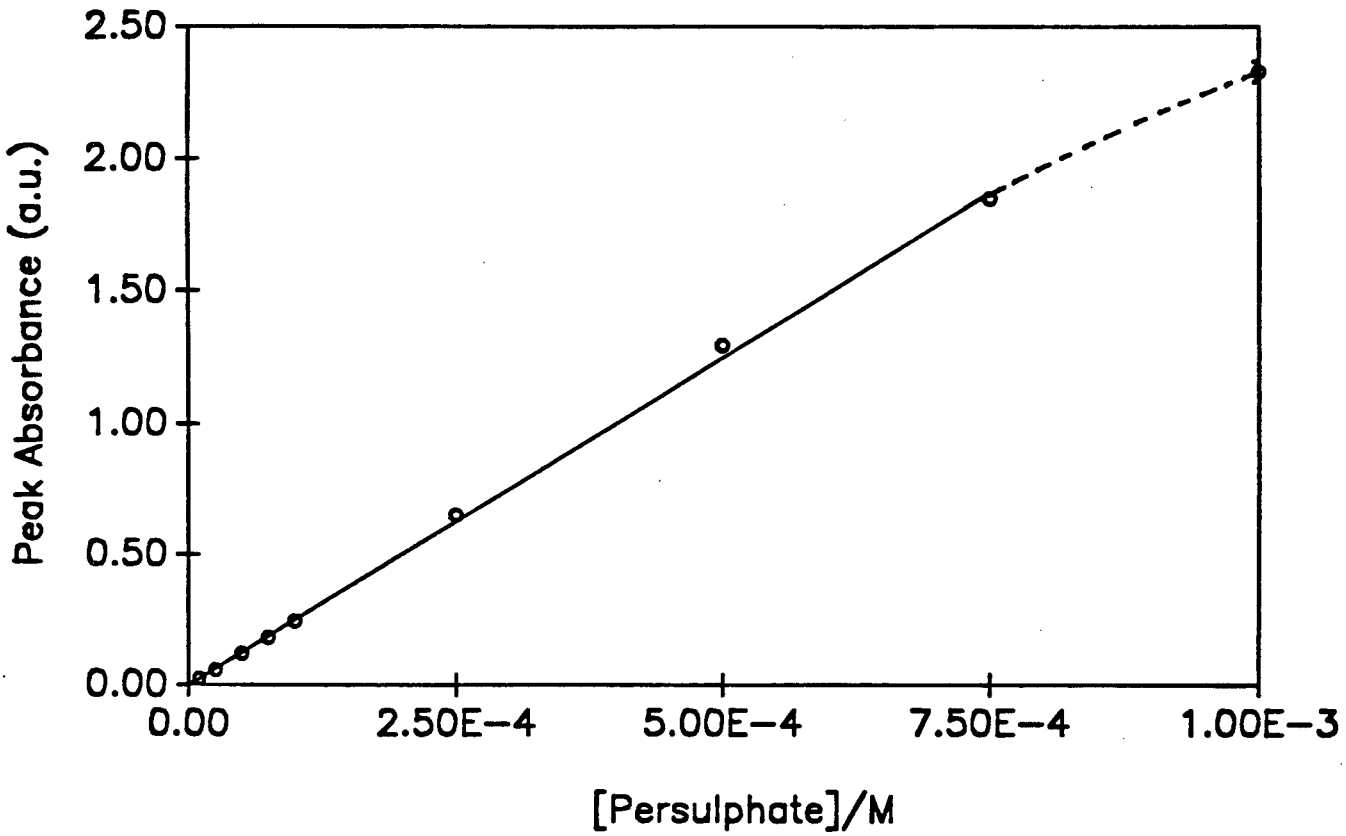

Figure 3.27 Calibration curve for method developed for persulphate determination. The solid line represents the linear dynamic range. The sizes of the error bars are smaller than the symbol sizes shown, except for that corresponding to persulphate concentration of 1.0 mM.

3.5 Conclusions on the methods developed using FIDO

The two methods described in this chapter served to test the apparatus and software. The apparatus is shown to be well suited to automated optimization of FIA methods. Results agree well with manual studies. The automated response surface mapping approach works well and its results agree with simplex and manual methods.

Modelling of the surfaces to fully characterize analytical performance of systems with two experimental variables is shown to be possible. Extension to three variables will be possible with this apparatus. Beyond this, the number of experiments required may become prohibitively high.

Coil length optimization was not automated, but automated optimization was done at various coil lengths.

3.5.1 Caveat

These two systems have involved only single-phases and true solutions. Recent work by Kester *et al.* [119] shows that where precipitation or large changes in refractive index are a problem, the simple response optimized here (peak absorbance) may not be adequate. Other workers have shown previously that for procedures involving a solvent extraction step, the repeatability of peak heights should also be taken into account since conditions can exist which provide high sensitivity but unacceptable reproducibility.[9] Thus one cannot expect the methods proposed here to be applicable in a totally automated fashion to all (more complex) FIA systems without at least some human supervision. However, the methods development strategies proposed and demonstrated would have merit for the majority of FIA methods presently in the literature. More advanced uses of the apparatus are discussed in chapter 4 of this thesis.

CHAPTER FOUR

ADVANCED OPERATION OF THE FLOW INJECTION DEVELOPMENT AND OPTIMIZATION SYSTEM

4.1 Development of catalytic photometric flow injection methods for determination of selenium

4.1.1 Introduction

This Section describes the development of a simple and fast flow injection method for selenium determination which offers good sensitivity, precision and freedom from interferences. Selenium is determined by its catalytic effect on the oxidation of phenylhydrazine by potassium chlorate followed by a coupling reaction with chromotropic acid. Conventional, stopped flow and flow reversal strategies are contrasted for the optimized chemistry.

In recent years, there has been a growing interest in understanding the physiological role of trace selenium in domesticated animals and man. Selenium is essential to life; its deficiency is toxic to animals, [120-121] and has been correlated with diseases such as cardiomyopathy in man. [120, 122] Excessively high levels have been associated with cancer, [123] and a small difference is thought to separate the toxic and essential levels. [120-123] The essential and beneficial roles of selenium in animal and human physiology are documented; selenium is a component of the enzyme glutathione peroxidase, [124] which scavenges the traces of peroxides generated during cellular metabolism before such peroxides can induce oxidative changes deleterious to health. The ability of selenium to reduce the toxicity of heavy metals has been the subject of much study in recent years. [125-126] There are suggestions that selenium combines with mercury (II) and cadmium (II) to give metabolically inert metal selenides in the body. Selenium has also been known to *prevent* several types of chemically induced cancer in animals. [127-128] Shamberger *et al.*, [129-130] noted that human cancer death rates are lower in countries where more selenium occurs in the environment and that human mortality from heart diseases is also lower in the high-selenium areas. The complexity of the above studies calls for the development of more precise and accurate methods for selenium determination in biological, environmental, and/or food product samples. The analytical performance of

existing methods are compared with results from this study in Section 4.3.5.

4.1.1.1 *Instrumental methods for determination of selenium*

Analytical methods already used include gas chromatography (after the formation and extraction of a piazselenol), [131] and electrochemical detection using either differential pulsed polarography, [132] or by anodic [133-134] or cathodic [135-136] stripping voltammetry. Atomic absorption spectrometry (AAS) of the hydride has provided superb detection limits (ng ml^{-1}), especially when combined with cryogenic trapping, [137] and the advantage of sample introduction by flow injection for AAS systems has been demonstrated. [1, 138-139] Other methods make use of special facilities such as neutron activation analysis and X-ray diffraction. These often involve lengthy sample preparation procedures, such as solvent extraction(s) or freeze-drying of the element from water before analysis. Each of the above methods has advantages and disadvantages from the point of view of practicality for routine analyses. Most require specialized apparatus.

4.1.1.2 *Direct spectrophotometric methods*

Several methods for direct spectrophotometric determination of selenium have been suggested and are widely used. These are generally less sensitive, and may still require extensive preparation of real samples (*e.g.*, those of environmental, or biological origin) prior to the determination. The reaction of selenite with 3,3'-diaminobenzidine and related compounds is well established. However these reagents are unstable to light and air. [140] Kamaya *et al.* [141] devised a chemical multiplication procedure to improve the detectability of the reaction of selenous acid with ferrocene. This was based on photometric determination of the iron (III) which is formed from the oxidative decomposition of ferricinium ions by selenous acid, with 1,10-phenanthroline. Despite its chemical elegance, the method is tedious to perform since it involves ion exchange, solvent extraction, and uses very strongly acidic conditions. One of the most commonly used methods is based on the

measurement of the fluorescent piazselenol formed by the reaction of selenite with diaminonaphthalene. [142] Although this method is very sensitive and selective, it also involves a lengthy extraction procedure and requires precise control of pH. [143]

4.1.1.3 *Catalytic spectrophotometric methods*

Catalytic spectrophotometric methods offer excellent alternative choices for the determination of trace concentration of many elements because of their simplicity and specificity. [120, 144-147] Whilst their detection limits are such that they cannot compete with hydride generation AAS, they are still appropriate to meet many analytical needs (especially when properly optimized). West and Ramakrishna reported a method based on the reduction of methylene blue by sodium sulfide. [144] Kawashima and Tanaka [145] proposed a very sensitive procedure for selenium based on the catalytic reduction of 1,4,6,11-tetraazanaphthacene, but the method is subject to interference from several ions.

4.1.1.4 *Flow injection photometric methods*

Recently, catalytic photometric methods for selenium involving flow injection have appeared in the literature. Hwang *et al.* reported a method based on the catalytic effect of this element on the reduction of picrate ion by sodium sulfide. [146] Linares *et al.* [147] reported a method for the simultaneous determination of Se(IV) and Se(VI). In this, Se(VI) is reduced to Se(IV) prior to its determination. This step requires fairly vigorous conditions of temperature (a boiling water bath), hot concentrated HCl, and 5 minutes heating time to give a reduction efficiency of 75%.

4.1.1.5 *Utility of alternative flow injection modes*

Adaptation of a manual procedure to flow injection generally affords many advantages to the experimenter. [1] However, it is evident that the slow rates of many colour-forming reactions involving selenium have precluded wider use of conventional flow injection systems for determination of selenium. Most flow injection procedures use manifolds in which flow rates are held constant both in magnitude and direction. Far less attention has been given to use of manifolds in which flow rates are caused to change within an experiment in a well characterized and repeatable manner. Stopped flow methods [1] are well established in analytical chemistry: In flow injection these have been used most commonly for estimating rate constants, rather than for improving sensitivity *per se*. Flow reversals [56, 148, 149] and other flow paradigms [150] have been demonstrated to have significant advantages. These approaches are now more readily implementable, because of the availability of appropriate computer-controlled hardware such as described in Chaper 2. Of particular importance is that they can provide longer reaction times and alternative mixing conditions, without incurring excessive dispersion.

4.1.2 Experimental Section

4.1.2.1 *Reagents*

All reagents used were analytical grade and their solutions made up in distilled water. A stock solution of 1000 ppm Se(IV) was prepared by dissolving 0.3513 g SeO_2 (BDH Chemicals Ltd, Poole, England) in 250 ml of distilled water. Sample solutions were prepared by appropriate dilution. Stock solutions of 1.00 M phenylhydrazine hydrochloride (PHDZ) (see Appendix 1 for molecular structure) (Eastman Kodak Company, Rochester, NY), 1.00 M potassium chlorate (BDH Chemicals, Toronto, Canada) and 0.50 M 1,8-dihydroxynaphthalene-3,6-disulfonic acid (chromotropic acid (CTA)) (see Appendix 1 for molecular structure) (Eastman Kodak Company, Rochester, N.Y.) were prepared by dissolving appropriate amounts of each of these compounds in water. A 1.20 M HCl

solution was made by dilution of the 12 M acid with distilled water.

Solutions of (potentially) interfering metal ions were prepared by dissolving appropriate weights of their salts in distilled water to give concentrations of 1000 ppm of the metals. The forms used were the chlorides of barium (II), calcium (II), cadmium (II), magnesium (II), mercury (II), tin (II) and zinc (II), the nitrates of aluminum (III), bismuth (III), cobalt (II), copper (II), lead (II), the sulfates of iron (III), manganese (II), nickel (II), and vanadium (V). Chromium (III) was in the form of potassium dichromate and molybdenum (VI) was as ammonium molybdate.

4.1.2.2 *Apparatus*

A diode array spectrophotometer (Model 8452A, Hewlett Packard, Palo Alto, CA) equipped with a standard 10 mm fused-silica cell was used for absorption measurements in manual kinetic experiments. A 30 μl fused-silica flow cell with 10 mm pathlength was used for all studies using flow systems. The automated flow injection apparatus was as described in chapter 2 and elsewhere [57] and used in previous methods development studies. [53, 60, 151, 152] Three-dimensional response surface plots with their corresponding contour plots were generated with a commercial scientific graphics program (SURFER^R v. 3.0, Golden Software, Golden, CO).

4.1.2.3 *Experimental procedures*

4.1.2.3.1 *Manual kinetic studies*

Some preliminary batch experiments were first conducted to ascertain the suitability of this chemistry for adaptation to flow injection. A temperature of 60 °C was used throughout. The effects of reagent concentrations (phenylhydrazine, cromotropic acid and potassium chlorate) on reaction rate were investigated in a univariate manner. A 0.0 - 10.0 ml aliquot of a stock solution of phenylhydrazine (0.25 M) was added to a solution

mixture containing 5 ml of each of 1 M potassium chlorate, 3.17 x 10^{-4} M Se(IV) from SeO_2 (25.0 ppm as Se(IV)), 1.2 M HCl and 0.4 M chromotropic acid. Prior to this last addition, an amount of distilled water was added to the reaction vessel such that the reaction mixture volume would be a total of 30 ml. The mixture was then shaken thoroughly and an aliquot amount transferred into a standard 1 cm cell in the spectrophotometer. Absorbance measurements at 360 nm (λ_{max}, the wavelength at which the product is most strongly absorbing) were initiated 30 s after the start of reaction and data were acquired at 5 s intervals for a period of 5 min. The above procedure was repeated for chromotropic acid, $KClO_3$, and HCl respectively.

The effects of ionic strength and pH at 60 °C. were also studied, since these will vary in real samples. Concentrations of KCl, NaCl, KNO_3, $NaNO_3$, and $NaClO_4$ used were 0.00, 0.03, 0.06, 0.13, 0.20, 0.26, and 0.33 M. Concentrations of HCl used were 0.00, 0.08, 0.16, 0.24, 0.32 and 0.40 M.

Experiments were then conducted in quadruplicate at 25, 30, 35, 40, 50, 60 and 70 °C to establish the effect of temperature on the rate of reaction and in each case the mean absorbance value was recorded. All solutions were kept in a temperature-controlled water bath. Water from the bath was circulated through a thermostated cell holder of the spectrophotometer by use of a peristaltic pump.

4.1.2.3.2 *Automated kinetic studies*

Stopped flow kinetic experiments were conducted to determine the order of reaction and the pseudo-first-order rate constant at 60 °C. The flow configuration used is shown in Figure 4.1a. All streams were propelled at a flow rate of 1.0 ml. min^{-1}. The mixture was transported to the cell via a single bead string reactor (SBSR) of minimum length (0.50 mm i.d., 5 cm length, filled with 0.3 mm diameter glass beads). The SBSR was included to maximize the efficiency of mixing and minimize axial dispersion during mixing (in addition to its interference with laminar and "secondary" flow patterns, the SBSR's glass

beads decrease the volume of solution that can occupy a fixed length of tubing, and this results in a faster stream velocity for the same volumetric flow rate). The flow was then stopped and the absorbance at 360 nm measured once per second for 500 s. This type of study was also used to establish the effect of Se(IV) concentration on the pseudo-first-order rate constant at a given temperature and the effect of temperature on the pseudo-first-order rate constant at several Se(IV) concentrations.

4.1.2.3.3 *Flow injection studies with conventional manifold*

The optimum reagent concentrations were sought in an automated manner. The manifold, shown in Figure 4.1b, merges a carrier stream comprised of phenylhydrazine with a flow of $KClO_3$ to give a fixed total flow rate of 1.0 ml. min^{-1} and a maximum phenylhydrazine concentration of 0.1 M. The other two channels were of HCl (variable flow rate, 0.00 - 1.00 ml. min^{-1}) and chromotropic acid (variable flow rate, 0.00 - 1.00 ml. min^{-1}). All channels used 0.42 mm i.d. poly(vinyl chloride) (PVC) pump tubing except for the HCl channel which required 0.66 mm i.d. Acidflex^R acid-resistant pump tubing. The temperature of the coils was kept constant at 60 °C by the thermostated water bath. All experiments used a 70 μl sample volume. Prior to each injection of Se(IV), the stability of the baseline reading was established by the computer. Readings of product absorbance were taken at 360 nm.

The automatic methods by which optimum experimental conditions for this manifold and chemistry were sought are as described previously, and elsewhere.[53] First, modified simplex optimization was applied to find the optimum values for the chromotropic acid stream flow rate and the best phenylhydrazine / $KClO_3$ ratio (see Figure 4.1b). All experiments were done in triplicate. Then, the effects of phenylhydrazine (and thus the phenylhydrazine / $KClO_3$ ratio) and chromotropic acid concentrations were more thoroughly determined over a wide range of concentrations by response surface mapping. This used a factorial design approach consisting of an 8 x 8 grid (64 experiments)

each with three replicate experiments at each point.

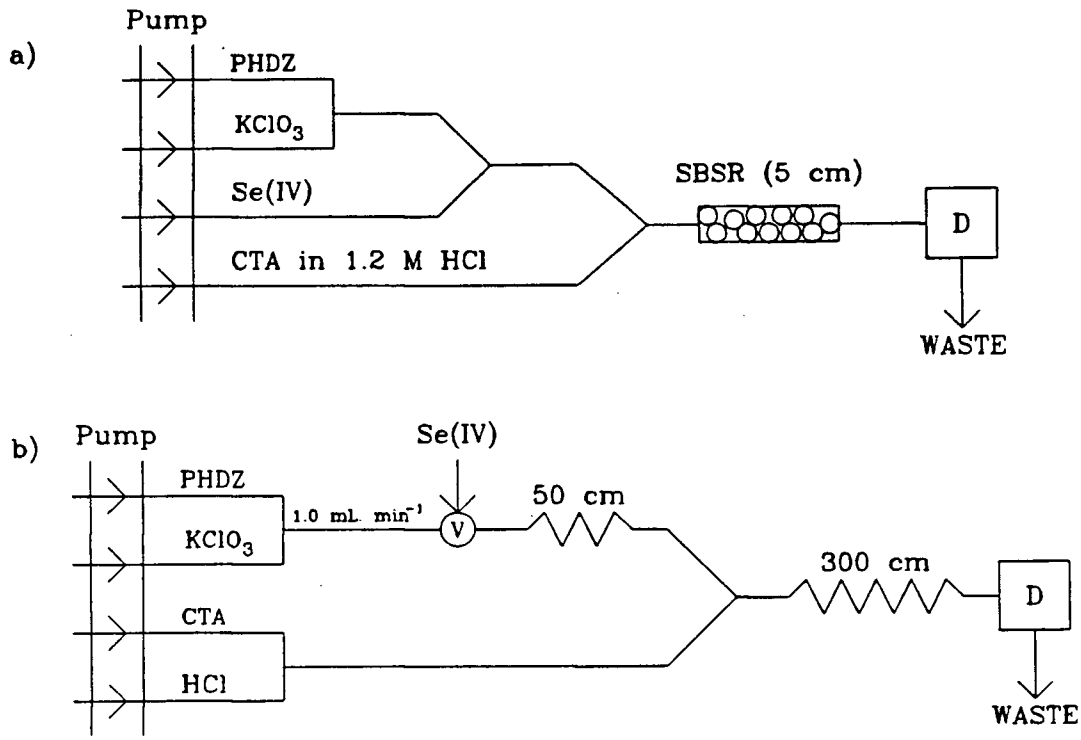

Figure 4.1 (a) Merging stream manifold used for initial stopped flow kinetic studies. SBSR denotes the single bead string reactor. All reagent streams were propelled at a constant flow rate of 1.0 ml. min^{-1}.

(b) Conventional flow injection manifold used for automated optimization and response surface mapping studies.
The merged stream of phenylhydrazine (PHDZ) and $KClO_3$ was kept at a total flow rate of 1.0 ml. min^{-1}. The HCl and chromotropic acid (CTA) streams were variables (each allowed to vary from 0.0 - 1.0 ml. min^{-1}). A 1.0×10^{-4} M sample of Se(IV) was injected into the carrier stream by the injection valve, V. Reaction product was monitored by the spectrophotometric detector, D.

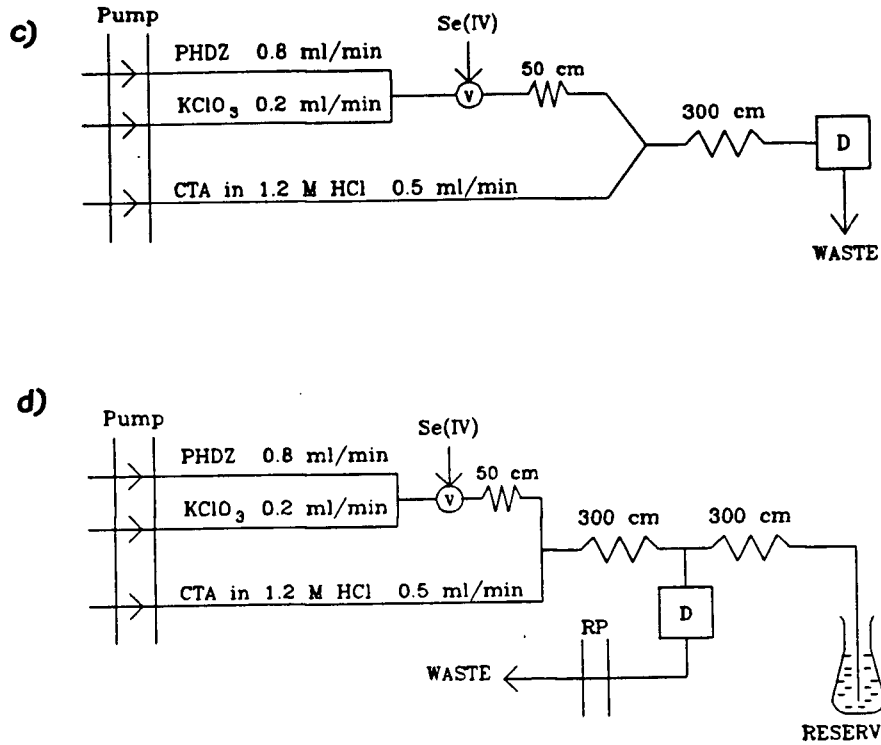

Figure 4.1 (c) Flow injection manifold used for stopped flow studies.
Flow rates were: phenylhydrazine (PHDZ), 0.80 ml. min^{-1};
$KClO_3$, 0.20 ml. min^{-1};
chromotropic acid (CTA) in 1.2 M HCl,
0.5 ml. min^{-1}.

(d) Flow injection manifold used for flow reversal studies.
Flow rates were: PHDZ, 0.80 ml. min^{-1};
$KClO_3$, 0.20 ml. min^{-1};
CTA, 0.5 ml. min^{-1}.

4.1.2.3.4 *Flow injection studies with a stopped-flow flow injection manifold*

In these sets of experiments, improvement in sensitivity of the chemistry was sought by increasing the reaction time of the sample plug, while maintaining both an acceptable amount of dispersion and sample throughput rate. This was effected by stopping the sample plug mid-way between the points of sample injection and detection for some pre-determined period of time. The flow injection configuration used is shown in Figure 4.1c. This differs from that in Figure 4.1b in that the chromotropic acid and HCl were introduced as a single combined solution in one stream. The flow rates used were phenylhydrazine, 0.80 ml. min^{-1}, $KClO_3$, 0.20 ml. min^{-1}, chromotropic acid in 1.2 M HCl, 0.5 ml. min^{-1}, as established as optimum by simplex optimization studies. Before commencement of the experiment, the time interval for stopping the sample plug, the total number of cycles and the number of replicates to be done were entered into the computer. The control options built into the methods development system operating software were used to facilitate stop time intervals of 0 to 70 s in 5 s increments; this corresponded to total time from injection to detection of between 50 and 120 s. Three replicate experiments were done at each stop time.

The position at which the plug was stopped within the 300 cm coil was also investigated. The times used corresponded to the centre of the plug being stopped at distances of *ca.* 5, 50, 150, 250 cm into the 300 cm tube. The 150 cm value was taken as standard for the remaining experimentation.

4.1.2.3.5 *Flow injection studies with a flow reversal manifold*

The flow reversal technique has been described elsewhere.[56, 148-149] This technique was used as a means of achieving longer reaction times (by mimicking longer reaction coil length) and better mixing of the reaction components. The manifold configuration used is shown in Figure 4.1d. Flow rates used were 0.80 ml. min^{-1} phenylhydrazine, 0.20 ml. min^{-1} $KClO_3$, and 0.5 ml. min^{-1} chromotropic acid in 1.2 M HCl,

as established as optimum by simplex optimization studies. The reversal pump, **RP**, was equipped with a larger diameter PVC pump tube (2.0 ml. min^{-1} capacity), so as to be able to pump solution mixtures at a flow rate equal to the total of all the other streams combined. A 3 m coil and a single flow reversal was used to vary the time from injection to detection. At the time of sample injection the flow reversal pump was stopped. The plug was allowed to flow towards (but not enter) the reservoir, **RS**, for some period of time ($t + \Delta t$), where t is the time that it takes for the plug to reach the tee-piece situated just before the detector (as calculated from total flow rate of the stream and tubing internal diameter), and Δt was the additional time allowed before executing the flow reversal. The direction of flow was then reversed, and the product detected as it was swept through the detector. A series of experiments which employed increasing Δt values was automatically achieved.

4.1.3 Results and Discussion

4.1.3.1 *Batch kinetic studies*

4.1.3.1.1 *Effect of reagent concentrations*

The results of univariate studies to find the optimum concentrations of phenylhydrazine, $KClO_3$ and chromotropic acid are summarized in Figure 4.2. The 0 - 10 ml range aliquot volumes shown as the horizontal axis for the three reagents corresponded to 0 - 0.08 M phenylhydrazine, 0 - 0.13 M chromotropic acid and 0 - 0.33 M ClO_3^-. Standard working reagent concentrations were then chosen such that no further substantial improvement in reaction product formation was observed at higher concentrations. Conditions were favoured which minimized both the absolute background and that due to the uncatalysed reaction, which was found to occur slowly with an experimental rate constant of $(1.3 \pm 0.5) \times 10^{-4}$ s^{-1} at 60 °C. An increase in the concentration of $KClO_3$ caused an increase in the catalysed reaction rate. A concentration of 0.50 M $KClO_3$ was chosen as

the working stock solution concentration, partly because of the problems of dissolving higher concentrations of $KClO_3$ and the desire to minimize the background readings due to the uncatalysed reaction. The actual range of ClO_3^- concentrations used in experiments was 0 - 0.33 M. The optimum concentration range for chromotropic acid was 0.02 - 0.05 M. A 0.02 M chromotropic acid concentration was chosen since this maximized the signal-to-noise (S/N) and signal-to-background (S/B) ratios, by minimizing the background absorbance at 360 nm (chromotropic acid is a fairly intensely colored reagent). Figure 4.2 shows that the catalytic enhancement was independent of the phenylhydrazine concentration above 0.05 M. A 0.1 M concentration of phenylhydarzine was considered sufficient for these studies.

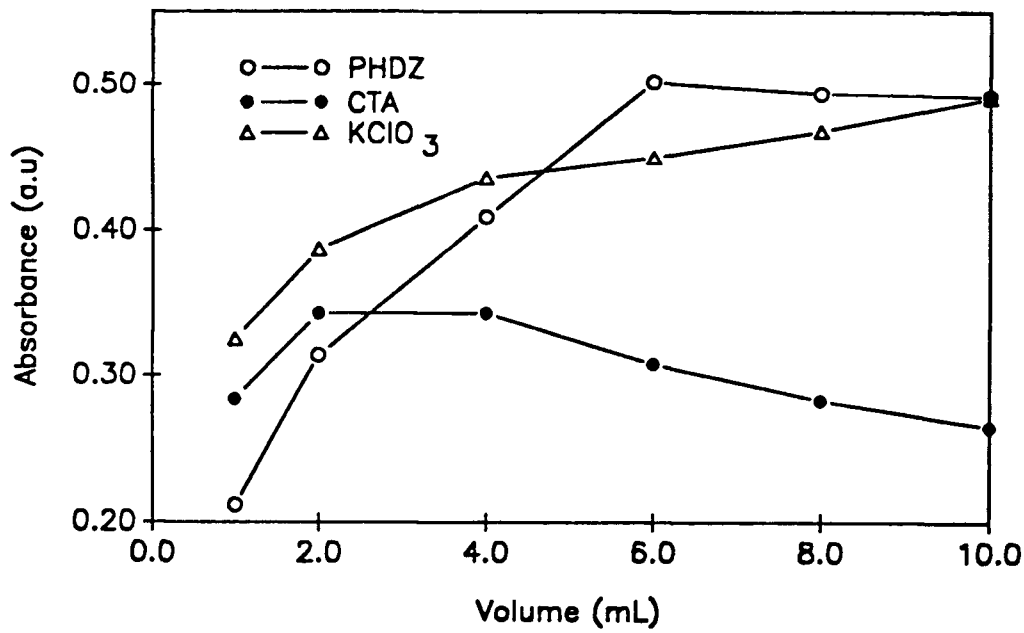

Figure 4.2 Effect of phenylhydrazine (PHDZ), chromotropic acid (CTA) and $KClO_3$ concentrations on absorbance at 360 nm. Higher absorbances correspond to greater reaction rates. Standard conditions required addition of 5 ml of each of 1.0 M $KClO_3$, 0.25 M PHDZ, 0.40 M CTA and 25 ppm Se(IV) solutions, made up to a total of 30.0 ml. Volumes of $KClO_3$, PHDZ, and CTA were independently varied between 0.0 and 10.0 ml, whilst keeping the total reaction mixture volume at 30.0 ml. Absorbance measurements were made at 360 nm after 180 s. Reaction temperature was maintained at 60 °C.

4.1.3.1.2 *Effect of pH*

Figure 4.3 shows a linear increase in response with increase in concentration of HCl, once sufficient HCl is present to establish acidic conditions. In later experiments the concentration of HCl used was kept at 1.20 M, so as to minimize the rate of the uncatalysed reaction.

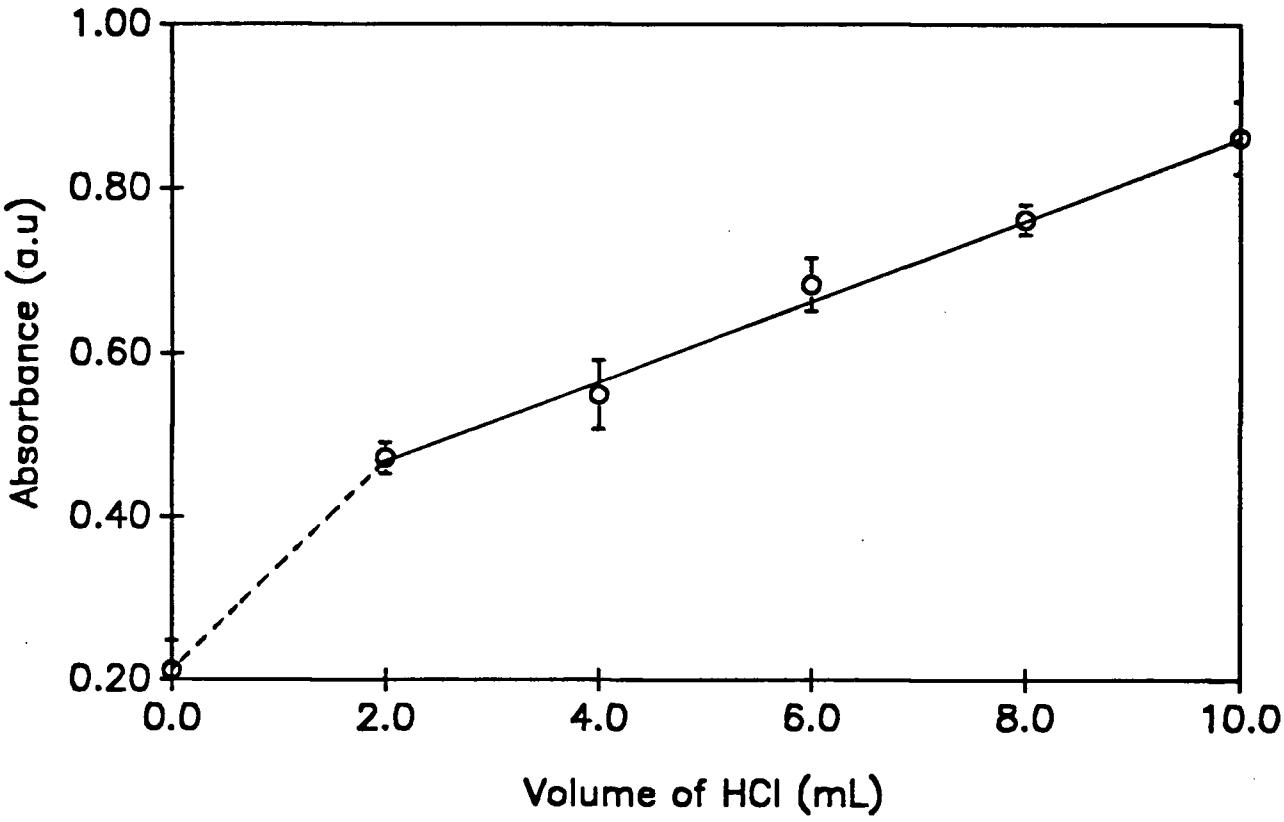

Figure 4.3 Effect of concentration of HCl on absorbance at 360 nm. The reaction mixture was comprised of a mixture of 5 ml of each of 1.0 M $KClO_3$, 0.25 M phenylhydrazine, 0.05 M chromotropic acid and 25 ppm Se(IV) solutions, 0-10.0 ml volumes of 1.2 M HCl and an appropriate amount of water to keep the total reaction mixture volume at 30.0 ml. Absorbance readings were made in duplicate after 180 s of reaction time. All experiments were done at 60 °C.

4.1.3.1.3 *Effect of neutral salts*

Figure 4.4 indicates that addition of NaCl, KCl or $NaClO_4$ enhances the reaction. This behaviour may extend to Cl^- from HCl too (see Figure 4.3). Ionic strength arguments alone are insufficient to explain the general enhancement, since a suppressive effect is observed for higher concentrations of either $NaNO_3$ or KNO_3. It is therefore likely that $[NO_3^-]$ impedes at least one stage of the reaction.

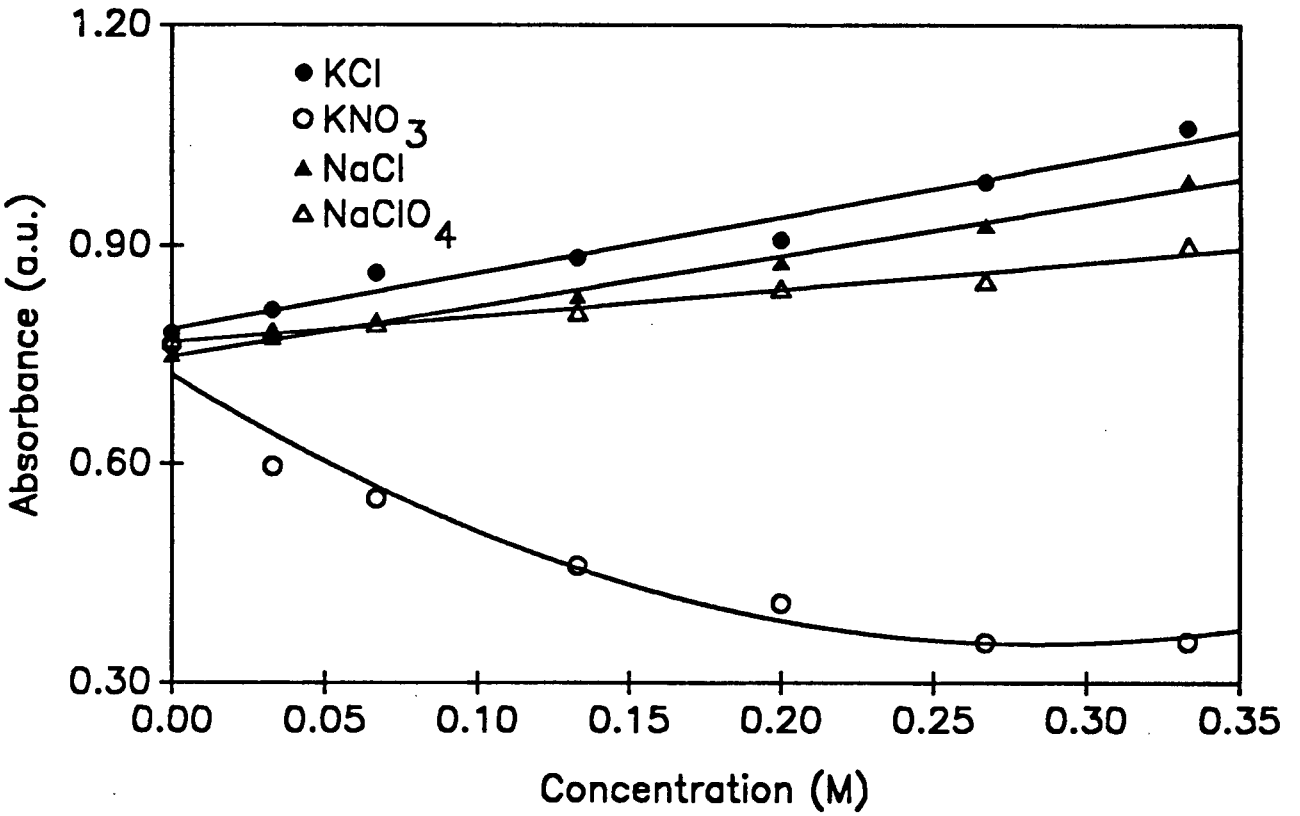

Figure 4.4 Effect of ionic strength of reaction mixture on absorbance at 360 nm. The mixture was comprised of 5.0 ml each of 0.1 M phenylhydrazine, 0.02 M chromotropic acid in 1.2 M HCl 0.5 M $KClO_3$ and 25 ppm Se(IV) solutions, made up to a total of 30.0 ml. Volumes of KNO_3, KCl, $NaNO_3$, NaCl, and $NaClO_4$ were independently varied between 0.0 and 10.0 ml. The total reaction mixture volume was kept at 30.0 ml by addition of appropriate amounts of distilled water (where necessary). Single absorbance measurements were made after 180 s. All experiments were done at 60 °C.

4.1.3.1.4 *Effect of temperature*

The results in Figure 4.5 indicate that at all temperatures there is an increase in the catalyzed reaction rate as the temperature is raised. Two distinct and reproducible line segments are obvious in Figure 4.5. One must stress that the discontinuity seen at around 38°C was reproducible, and is not due to an error in the data for 40°C.

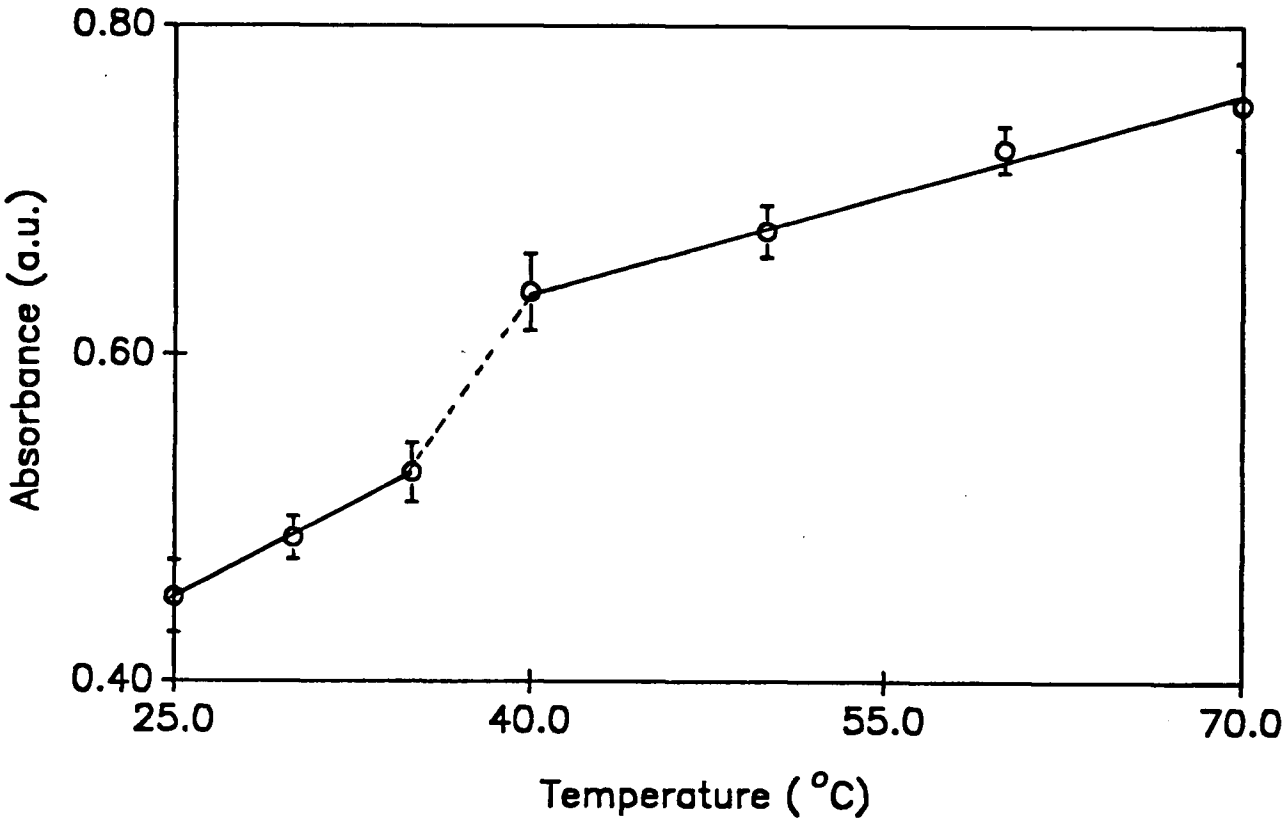

Figure 4.5 Effect of temperature on absorbance at 360 nm at optimum reagent concentrations. The reaction mixture was of 5 ml of each of 0.5 M $KClO_3$, 0.10 M phenylhydrazine, 0.02 M chromotropic acid and 25 ppm Se(IV) solutions. The solutions were always kept in a temperature controlled water bath, from which water was circulated around the cell holder of the detector. Absorbance measurements were made after 300 s.

The origin of the discontinuity becomes clearer when one considers Figure 4.6, which conveys the effect that higher temperatures have on the rate of color development. Increasing the temperature above 35 °C was found to substantially enhance the rate and extent of color development. The second derivative of the absorbance vs. time curves indicates whether there is *positive* or *negative* deviation from a linear absorbance *vs.* time relationship. This proves whether the *rate of increase* in absorbance is rising or falling with time, and was calculated over the time interval 100 - 400 s. At temperatures of 40, 50, 60, 70 and 80 °C, the absorbance vs. time curves exhibit negative d^2A/dt^2 values over the time interval studied, *i.e.*, the rate of increase was dropping off. Results at 35 and 38 °C showed near zero d^2A/dt^2 values, *i.e.*, the absorbance obtained increased linearly with time. Results at 25 and 30 °C showed positive d^2A/dt^2 values over the time interval studied, *i.e.*, the rate of increase was still rising after 400 seconds. This behavior is consistent with a model in which the rate limiting step of the reaction at temperatures below about 38 °C becomes the formation of a (presently unidentified) reaction intermediate. A working temperature 60 °C was chosen, since at this temperature, the uncatalysed reaction was slow enough so as not to substantially interfere.

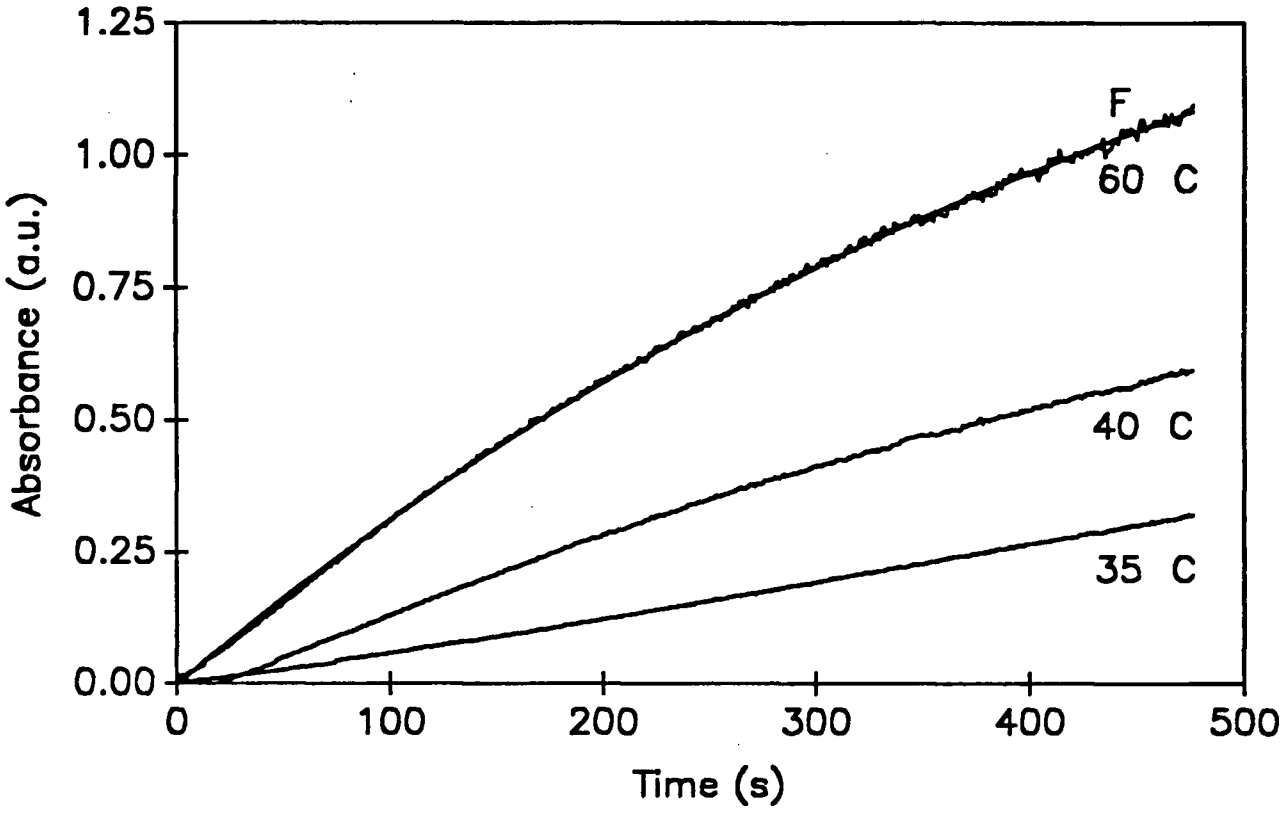

Figure 4.6 Representative plots of absorbance at 360 nm vs. time for the reaction catalyzed by Se(IV) at 35, 40 and 60 °C. The fit of a pseudo-first-order reaction model to the 60 °C curve is shown as the solid line. Data were also obtained at 25, 30, 50 and 70°C; curves for these are similar.

4.1.3.1.5 *Effect of Se(IV) concentration*

The results of Figure 4.7 show the effect of different concentrations of Se(IV) on the rate of reaction. The reaction rate increases with Se(IV) concentration. However, for higher Se(IV) concentrations, the greater absorbance values obtained after long reaction times exhibit more noise. The poorer precision associated with larger absorbance values is due to "0% transmittance noise".

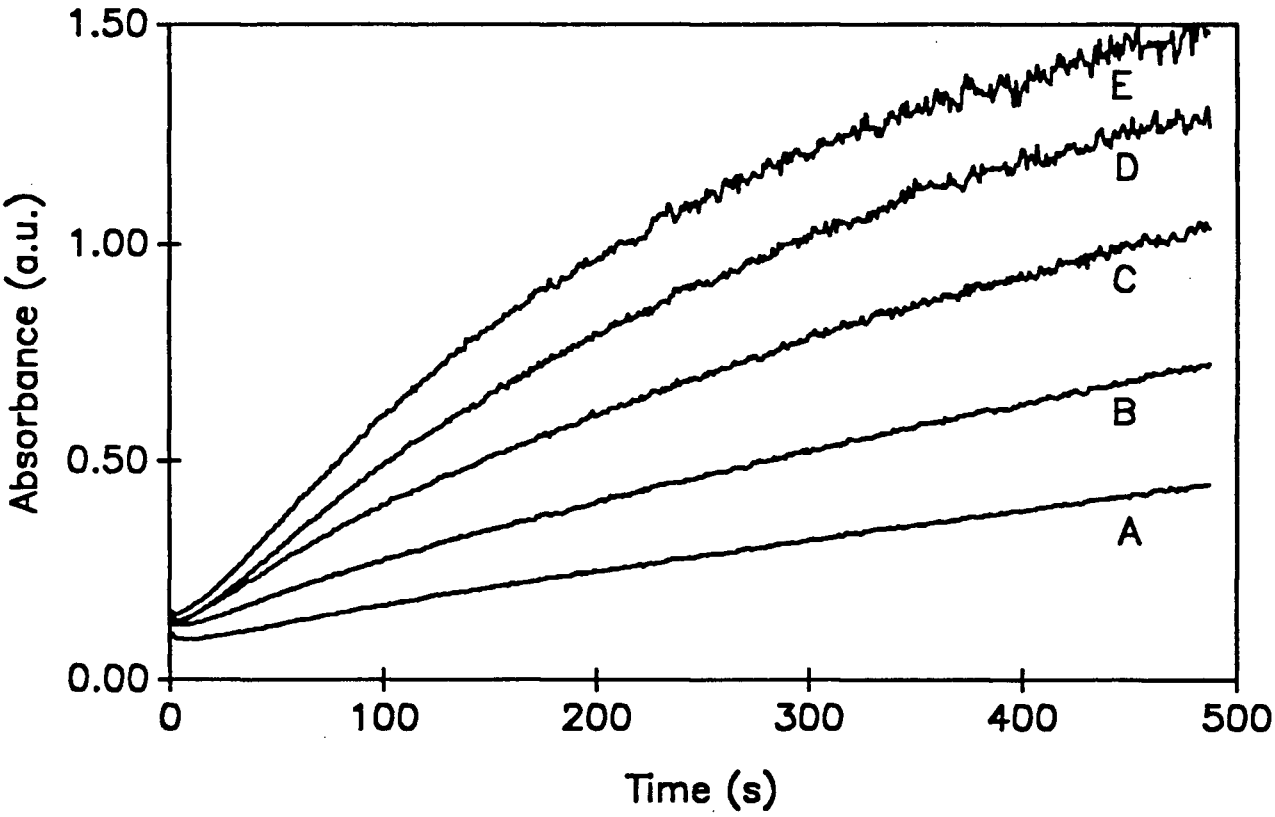

Figure 4.7 Plots of absorbance at 360 nm *vs.* time showing the effect of [Se(IV)] on reaction rate. Measurements were made at 60 ^{o}C. The curves are: A-1.0 ppm Se(IV), B-2.5 ppm, C-5.0 ppm, D-7.5 ppm and E-10.0 ppm.

4.1.3.2 *Stopped flow kinetic studies*

The kinetics of the reaction were investigated using the optimized values for solution concentrations found previously. These conditions were determined to be pseudo-first-order when the concentrations of the reagents were in excess of the concentration of the catalyst. The reaction is thought to proceed in the following manner:

$$ClO_3^- + PHDZ \xrightarrow{C_o} P' \quad (4.1)$$

$$P' + CTA \longrightarrow \text{Colored product} \quad (4.2)$$

where C_o is the original concentration of selenium(IV) responsible for catalysis and P' the intermediate product formed after the catalyzed redox step. The rate law expression for the disappearance of phenylhydrazine, assuming that the concentration of ClO_3^- remains almost unchanged during the course of the reaction, can be described as in Equation (4.3).

$$-d[PHDZ]/dt = k_u [PHDZ] + k_c [PHDZ] C_o \quad (4.3)$$

which simpifies to:

$$-d[PHDZ]/dt = [PHDZ] (k_u + k_c C_o) \quad (4.4)$$

Here k_u is the rate coefficient for the uncatalyzed reaction (including ClO_3^- concentration term), k_c the rate coefficient for the catalyzed reaction (plus some concentration terms), and C_o is the initial concentration of catalyst in the system. This assumes that the coupling step of P' with chromotropic acid is the much faster process, *i.e*, equation 4.1 represents the rate limiting step.

If we define the pseudo-first order rate constant, $k' = k_u + k_c C_o$, Equation 4.4 can be re-written as;

$$-d[PHDZ]/dt = k' [PHDZ] \quad (4.5)$$

This relationship may further be expressed, after integration, as

$$[PHDZ]_t = [PHDZ]_0 \exp(-k't) \quad (4.6)$$

where $[PHDZ]_0$ is the original concentration of phenylhydrazine and $[PHDZ]_t$ is the concentration at time *t*. It represents the disappearance of reactant as a falling exponential. The equivalent expression for formation of product (*i.e.*, a rising exponential) is given in equation 4.7:

$$A_t = A_f [1 - \exp(-k't)] + B \quad (4.7)$$

In this, A_t is the absorbance at any time *t*, A_f is the *final* solution absorbance due to the product, and B is a constant background term. The stopped-flow experimental absorbance measurements were fitted to Equation 4.7 using a non-linear curve fitting program. This successfully extracted values for the pseudo-first-order rate constant, k' and the pre-exponential factor, A_f. Each curve was comprised of 500 pairs of absorbance-time values. Excellent fits were obtained for the solutions tested, as is evident from the standard error of the estimate (SEE) value of $(7.13 \pm 0.05) \times 10^{-3}$. A typical fit of the model to the 60 °C data is shown in Figure 4.6 in terms of its fit residual, $R_{60\,°C}$. The pseudo-first-order rate constant obtained for 5.0 ppm Se(IV) was $(2.05 \pm 0.12) \times 10^{-3}$ s^{-1} at 60 °C. The goodness of fit, demonstrated by the small magnitude and the random nature of the residuals, confirmed that the contribution from the uncatalysed reaction was nearly negligible by comparison.

The Arrhenius equation, given in Equation 4.8, was used to determine the activation energy for the Se(IV) catalysed reaction;

$$k' = A \exp(-E_a/RT) \quad (4.8)$$

In this, E_a is activation energy (in kJ mol^{-1}), *A* is the frequency factor (in s^{-1}), R is the universal gas constant (in J K^{-1} mol^{-1}), and T is temperature (in Kelvin). This may be

A plot of ln(k') vs. 1/T for studies performed at temperatures between 40 °C and 80 °C was linear, and yielded an activation energy value of 25.75 kcal.mol^{-1} (107.7 kJ.mol^{-1}). There was however, a marked reduction in the rate of the reaction at temperatures below 40 °C, unless a higher concentration of Se(IV) was used. This suggests that the activation energy barrier for the rate limiting step becomes significant at lower temperatures where the Se(IV) concentration is 5 ppm or less. Figure 4.7 shows that a general increase in reaction rate occurs with increasing Se(IV) concentration. This is most obvious from the general increase in d(signal)/dt within the first 100 s for all the curves.

Figure 4.8 is a plot of *k'* at 60 °C vs. [Se(IV)].

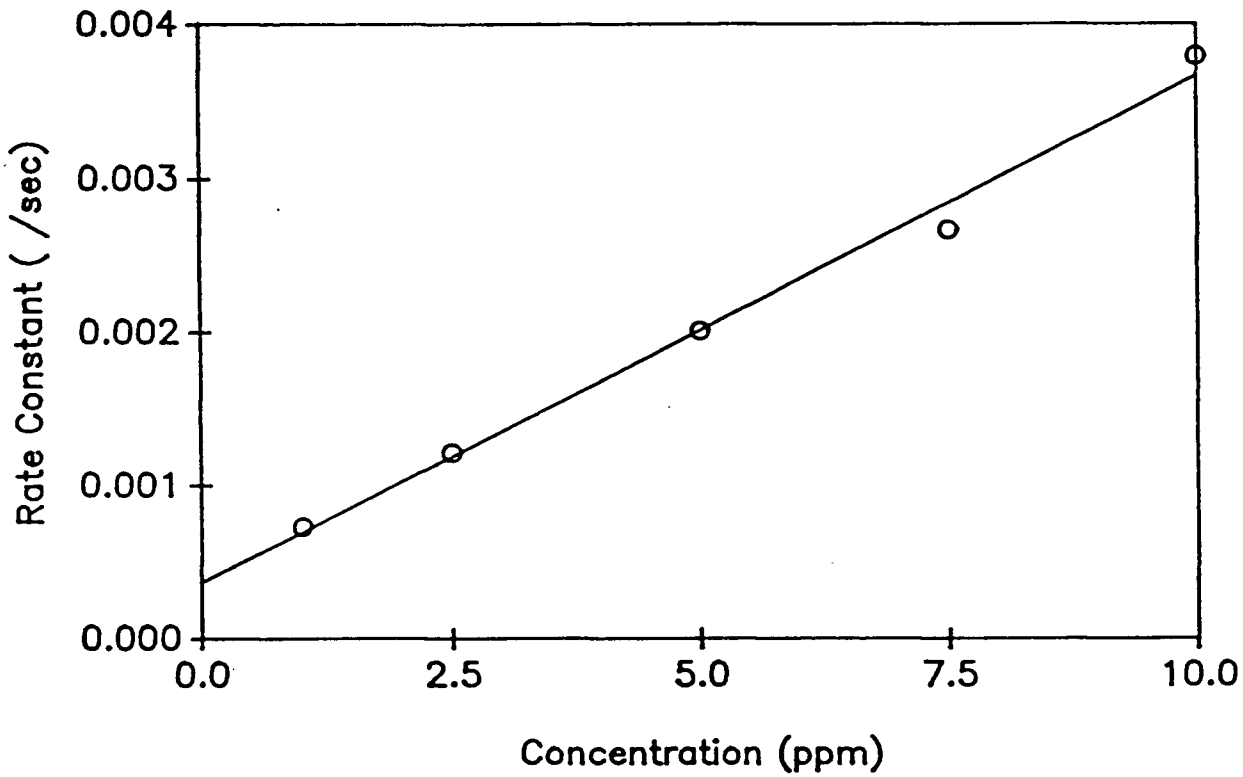

Figure 4.8 A plot of the rate constant *k'* at 60 °C vs. the concentration of Se(IV).

It indicates that the rate of the catalyzed reaction is proportional to C_0, and supports the assumption that the contribution from k_u (*i.e.*, the intercept value) is negligible. This is as a result of the catalytic cycle in which the selenium catalyst species is regenerated after taking part in the catalytic activity. It justifies the assumption that, under these experimental conditions, the redox step (the reaction between potassium chlorate and phenylhydrazine) is rate limiting.

4.1.3.3 *Flow injection studies*

4.1.3.3.1 *Automated simplex optimization of the conventional flow injection manifold*

Table 4.1 shows the initial and best sets of experimental conditions as found by applying the simplex optimization procedure to the manifold shown in Figure 4.1b. The variables optimized were the flow rates of phenylhydrazine, chromotropic acid and HCl streams.

	VARIABLES			RESPONSES	
Expt.#	PHDZ (ml. min^{-1})	CTA (ml. min^{-1})	HCl (ml. min^{-1})	Absorbance @360 nm (a.u.)	RSD (%)
1 (initial)	0.498	0.502	0.498	0.186	0.44
2	0.800	0.502	0.498	0.255	0.73
18	0.815	0.396	0.510	0.234	5.10
16	0.720	0.590	0.611	0.234	1.61
20	0.735	0.528	0.540	0.233	1.50
14	0.680	0.555	0.551	0.228	2.30
7	0.688	0.678	0.563	0.220	6.77
12	0.688	0.408	0.700	0.219	0.40
9	0.617	0.505	0.545	0.217	0.91
10	0.648	0.555	0.563	0.216	5.01
6	0.672	0.810	0.540	0.204	6.07

Table 4.1. Peak absorbances and percentage relative standard deviations (RSD%) for the initial experimental conditions and the ten best sets of conditions found by simplex optimization.

A total of 28 sets of experimental conditions were automatically established and tried, each with three replicates. The whole procedure took just under 4 hours. Sample size and reaction coil length could not be readily modified under computer control within the present experimental apparatus.

For conditions to be considered truly optimal, one should take into account factors other than peak absorbance; these "secondary responses" would include experimental precision (measured as %RSD), time per analysis, cost per analysis, *etc.* Thus, where several sets of experimental conditions give similar high peak absorbance values, some "secondary optimization" can be achieved; the operator can select from among these conditions, the ones which best meet the chosen secondary criteria. In the case shown in Table 4.1, point 12 has an acceptable sensitivity, but uses lower flow rates of the more expensive reagents, and yields a better %RSD value.

4.1.3.3.2 *Automated response surface mapping of the conventional flow injection manifold*

The automated response surface mapping took about 6 hours, and yielded the 3-dimensional response surface plot and contour map of absorbance (360 nm) at peak maximum *vs.* phenylhydrazine and chromotropic acid concentrations shown in Figure 4.9. The contour plot shows the optimum flow rate ranges for phenylhydrazine and chromotropic acid streams to be 0.55 - 0.85 ml. min^{-1} and 0.20 - 0.60 ml. min^{-1} respectively. The response surface shows a well-defined single maximum with minimal chemical interaction of the two variables. The small peak seen in the top left hand corner of the contour plot is due to a single set of experimental conditions and is most likely an artifact. These results were in good agreement with those established by simplex optimization. They allowed selection of conditions which provide a faster determination without greatly compromising the sensitivity of the system.

After optimization of the chemical conditions, the effect of reaction coil length was ascertained. The results are given in Table 4.2. A general improvement in sensitivity was obtained with increase in the reaction coil length for the range of coil lengths studied; about a 20% relative improvement in sensitivity was achieved by varying the reaction coil length from 300 cm to 625 cm. A coil length of 300 cm yielded a sample throughput rate of about 60 hr^{-1}. One should remember, however, that failure to include coil length as part of a true multivariate optimization may result in conditions which are suboptimal. Even so, the improvements obtained here were considerable.

Reaction Coil Length (cm)	Peak Absorbance [a]	Relative Improvement (%) [b]
300	0.248	0.0
400	0.279	12.5
500	0.292	17.6
600	0.293	18.1
625	0.294	18.5
650	0.287	15.7

Table 4.2. Effect of coil length on the sensitivity of conventional manifold.

[a] Absorbances were measured at 360 nm.

[b] Relative improvement is with respect to response using a 300 cm reaction coil length.

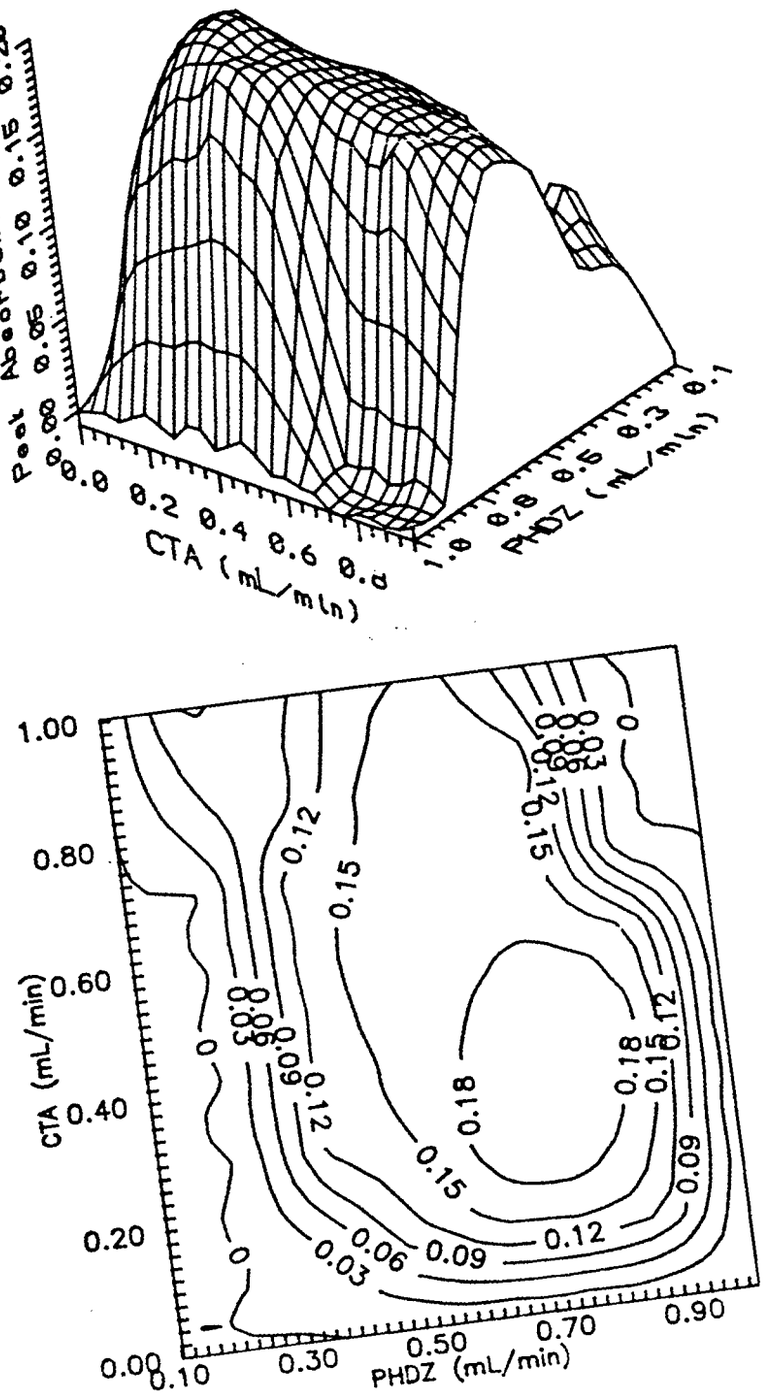

Figure 4.9 (a) The Se(IV) response surface plot shown as a 3D plot. The response is peak absorbance at 360 nm.

(b) The contour map representation of the above surface.

4.1.3.3.3 *Analytical performance*

The calibration graph obtained showed a linear dynamic range of 0.0 - 30.0 ppm Se(IV), with a Pearson's *r* correlation coefficient of 0.9984. The sensitivity (slope of the calibration curve) was 0.025 a.u. / ppm Se(IV). The usable range extended to 55.0 ppm Se(IV). The intercept of the calibration curve was non-zero due to the background absorbance from the uncatalysed reaction which occurs simultaneously with the catalyzed reaction. Injection of distilled water (0 ppm Se(IV)) produced a negative peak because of the relatively high absorbance from the rest of the carrier stream compared to the region of the injected plug.

4.1.3.3.4 *Stopped flow studies*

Despite the evidence that the peak height increase due to greater time for reaction was dominant over the height-diminishing effect of plug dispersion, coil lengths of more than 300 cm are generally considered rather long for routine use, particularly with small sample sizes. Thus, stopped flow studies were conducted using the manifold shown in Figure 4.1c, to seek further improvement in sensitivity by increasing the sample residence time, without incurring as much dispersion.

The results, shown in Figure 4.10, indicate that the peak absorbance, $P_{t,\,360nm}$, increased linearly with stop time, Δt, over the range $0 <= \Delta t <= 70$ s according to the best-fit equation $P_{t,\,360nm} = 0.01\,\Delta t + 0.25$. A value of $\Delta t = 0$ (no stopping) gives the minimum time to peak detection of *ca.* 50 s, and the manifold is then identical to the conventional 300 cm coil length manifold. The sensitivity was almost tripled when the sample plug was stopped for at least 60 s, but this reduced the sample throughput rate to about 30 hr^{-1}. The optimal choice of stop time is thus dependent on whether a high sample throughput rate or low detection limit is desired. A compromise sample throughput rate of 30 - 45 hr^{-1} is achieved with a delay time of between 40 - 60 s. This maintains a relative sensitivity improvement of about 2.5x that of the conventional flow injection manifold with

comparable time to peak detection. Results from this study showed RSD values of less than 2% for times of 71 to 102 seconds.

The sensitivity of this procedure was independent of the distance into the 300 cm coil at which the centre of sample plug was stopped, as long as it was past the point where the chromotropic acid stream was added. The responses corresponding to the 5, 50, 150, and 300 cm lengths were 0.339, 0.342, 0.342, and 0.343 with corresponding relative standard deviation values of 2.82%, 2.33%, 2.58%, and 2.38% (n=5) respectively. Formation of the coloured product requires the presence of chromotropic acid, and so can only occur within the 300 cm coil (see Figure 4.1c). Stopping the plug prior to this might provide a means to study the first step of the reaction.

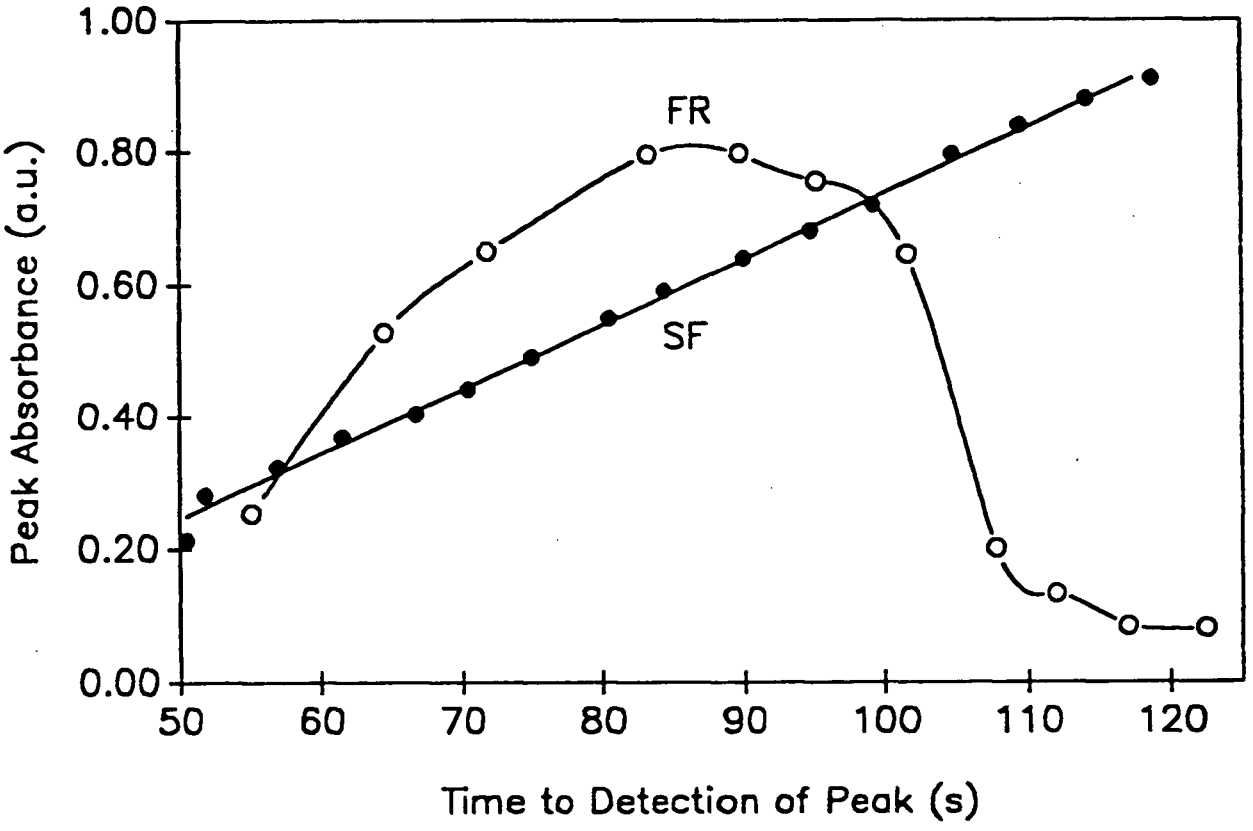

Figure 4.10 Plots of peak height vs. time to peak detection for flow reversal and stopped flow studies.

4.1.3.3.5 *Flow reversal studies*

It was considered valuable to compare the results obtained above with those from a flow reversal manifold, since this approach provides an alternative means of extending reaction time in a flow system of fixed dimensions. Figure 4.10 shows the results obtained using a single flow reversal, and the manifold shown in Figure 4.1d. The point at 55 s corresponded to an experiment *without reversal* of the flow direction, in which the plug travels directly through the 300 cm coil to the detector. The point immediately after this was obtained when the flow was stopped only instantaneously, before proceeding towards

the detector. Flow reversal times of 5 to 30 s, in 5 s increments, allowed the plug to travel increasing distances into the second coil before being caused to flow backwards through the detector. These times to flow reversal corresponded to 60 and 100 s of total time from injection to peak detection.

Correct design of flow reversal systems requires more thought than the other approaches. It is recognized that at low flow reversal times (corresponding to 70 s or less of the time to detection of peak of Figure 4.10), a portion of the tail may remain in coil(s) prior to the flow reversal tee-piece. In simpler flow reversal systems this may be avoided, at the cost of higher dispersion, by causing the flow to reverse back through the injection valve. Addition of chromotropic acid subsequent to reaction and mixing of analyte with phenylhydrazine and $KClO_3$ precluded the latter approach here. At least part of the decrease in sensitivity of the flow reversal procedure for residence times of greater than 95 s is most likely due to loss of the front of the plug into the reservoir. If longer reaction times and better mixing are needed, this artifact could be avoided by use of a longer coil (provided the higher back pressure incurred does not become a problem for the peristaltic pump used), or by multiple reversals with small Δt's within the same coil length.

4.1.3.4 *Comparison of conventional, stopped flow and flow reversal procedures*

The justification for the experimental procedure used must be the sensitivity and repeatability improvements obtained. All three manifolds consume only small amounts of sample and reagents, since their maximum flow rates are 20 ml. hr^{-1} for sample, 48 ml. hr^{-1} for phenylhydrazine and 36 ml. hr^{-1} for chromotropic acid. The chemistry developed provides a simple, sensitive, and selective alternative to existing procedures and offers high precision in response measurements (RSD < = 1.8% for 4 replicates) when used with optimum flow conditions. Just as the stopped flow study improved on the conventional manifold, the shorter duration flow reversal experiments produced an even better improvement in sensitivity whilst maintaining the same sample throughput rate. This is due

to improved efficiency of mixing provided by this design. Table 4.3 shows that the %RSD values obtained using the flow reversal were also generally better than those for the stopped flow procedure for times of less than 95 s to peak detection.

Time (s) [a]	Stopped Flow		Flow Reversal		% improvement of flow reversal [b]
	Absorbance	RSD(%)	Absorbance	RSD(%)	
65	0.403	3.26	0.523	1.15	23
71	0.411	1.52	0.651	1.03	37
83	0.550	1.46	0.796	0.44	31
90	0.640	1.96	0.797	0.22	20
95	0.681	1.65	0.756	2.02	10
102	0.795	1.52	0.646	7.63	-23

Table 4.3. Comparison of the performance of stopped-flow and flow-reversal flow injection manifolds for various times to peak detection.

[a] approximate times to detection of peak.
[b] relative to the stopped flow experiments

Table 4.4 provides a comparison of detection limits and linear dynamic range for the three variations of the present method, along with further details of alternative methods discussed in Sections 4.1.1.1 - 4.1.1.4. The FIA methods developed here have the largest dynamic range, but their detection limits cannot compete with those from atomic absorption techniques.

An interesting and unexpected observation from this present work is that the detection limit for the flow reversal method is better than that for stopped flow, which itself is an improvement over conventional FIA; however, the linear and usable dynamic ranges both show *the opposite trend.* Further improvements in sensitivity could be achieved by increasing sample size and reaction time.

Method	Ref.	Detection limit ($\mu g.\ ml^{-1}$)	Linear Dynamic Range ($\mu g.\ ml^{-1}$)	Usable Range ($\mu g.\ ml^{-1}$)	Reported Interferences
I. Atomic Absorption Spectrometry					
Hydride-generation					
a) with cryogenic preconcentration	137	$3x10^{-6}$	$0-10^{-4}$	-	nitrite [a]
b) with sample introduction	138	$0.6x10^{-3}$	-	-	hydride-forming elements
by flow injection	139	$0.2x10^{-3}$	$(0.2-4)x10^{-3}$		Cu^{2+}, Ni^{2+}, Fe^{3+}
II. Electrochemical Methods					
Potentiometry					
picrate ion selective electrode	145	0.1	0.1-30		Hg^{2+}, Sn^{2+}, Ag^{+}, Cu^{2+}
Stripping voltammetry					
cathodic	135	-	0-0.15		Cu^{2+}, Pb^{2+}, Cd^{2+}, Zn^{2+} [b]
anodic	135	$0.5x10^{-3}$	0-0.08		Cu^{2+}, Pb^{2+}, Cd^{2+}, Zn^{2+} [b, c]
differential pulse (cathodic)	134	-	$0.8x10^{-3}$-0.08		-
III. Catalytic Colorimetric Methods					
a) Manual methods					
methylene blue / S^{2-}	144	0.05	0.1-1.0	-	Cu^{2+}, Ag^{+}, Bi^{3+} [d]
1,4,6,11-tetraazanaphthacene	145	< 0.005	non-linear	0-0.03	Bi^{3+}, Sn^{2+}, Te^{4+}
b) Methods based on flow injection					
picrate / S^{2-}	146	$7.5x10^{-3}$	0.1-1.0	-	Hg^{2+}, Cd^{2+}, Cu^{2+}, Fe^{2+}, Co^{2+}, Pb^{2+}, Ni^{2+} [e]
NH_2NH_2 / ClO_3^-	147	1	1-12	1-12	Al^{3+}, Fe^{3+}, EDTA, VO_3^-, Mn^{2+}, Cu^{2+}, Cr^{3+}
PHDZ / ClO_3^- conventional	(This	0.52	0-50	0-55	Cu^{2+}, MoO_4^{2-}, Hg^{2+} [f]
stopped flow	work,	0.35	0-30	0-40	"
flow reversal	151)	0.15	0-20	0-30	"

Table 4.4. Comparison of detection limits, dynamic ranges and interferences in this work and some other sensitive analytical methods currently used.

[a] Maskable by sulphanilamide.
[b] These metal ions separated by Amberlite IRA-400 ion exchange resin.
[c] Anodic stripping unsuitable for routine determination due to poor reproducibility (ca. 10%).
[d] These metals could be separated from Se(IV) using a 10 cm column filled with Dowex 50W-X2, 50 - 100 mesh.
[e] All masked by cation exchanger, Dowex 50W-X8, 100 - 200 mesh, H^+ form.
[f] These species readily masked by 2.7×10^{-3} M EDTA in carrier solution (see Table 6 for details).

4.1.3.5 *Interference studies*

The selectivity of this chemistry was examined by studying the effect that 100 ppm concentration of various metal ions had on the determination of 5.0 ppm Se(IV). The stopped flow manifold was used for this, since it was thought that the longer residence (reaction) times of this manifold would render these effects most observable. These results, summarized in Table 4.5, show that the method provides excellent precision with RSD values of less than 1.50% in the absorbance measurements (from between seven and ten replicates), except in the presence of a few significantly interfering ions which are now discussed.

The most serious interference arose from the presence of Hg(II). The Hg^{2+} ion at concentrations above 50 ppm forms a white selenide precipitate with Se(IV) solution mixture. This interferent can be removed prior to injection by a sample clean-up column, as per the method of Hwang *et al.* [146]

The ions shown in Table 4.4 were effectively masked by addition of ethylene-diaminetetra-acetic acid (EDTA), without great loss in sensitivity. The initial method of spiking the 5.0 ppm (6.33×10^{-5} M) Se(IV) analyte solution prior to injection with EDTA proved to be unsatisfactory. A 2.69×10^{-3} M EDTA concentration was found to cause an error of about -20% in the selenium determination and so this approach was discontinued.

Then a kinetically favoured alternative was proposed, in which 0.10 M EDTA was added to the phenylhydrazine reagent stream. This worked well, and allowed determination of 5 ppm Se(IV) in the presence of 100 ppm Cr^{3+}, 100 ppm VO_3^-, 100 ppm Fe^{3+}, or 50 ppm MoO_4^{2-}, 50 ppm Cu^{2+} with errors of less than 3%. The EDTA in the absence of other metal ions caused only a -2% error in the determination of 5.0 ppm Se(IV). Unmasked, the Cu^{2+} ion gave a positive error of 85% at a 50 ppm concentration level. The Fe^{3+}, Cr^{3+} and VO_3^- ions interfered significantly at 100 ppm levels, but could be tolerated at levels of up to 50 ppm.

Potential Interferent	Concentration (ppm)	Error (%)	Response RSD(%)
Al^{3+}	100	-0.30	1.02
Ba^{2+}	100	0.60	1.45
Bi^{3+}	100	0.55	1.38
Ca^{2+}	100	-0.30	1.53
Cd^{2+}	100	-6.80	0.95
Co^{2+}	100	0.55	1.30
Cr^{3+}	100	20.0	0.32
	50	0.0	0.43
Cu^{2+}	50	84.7	2.76
	25	39.8	1.03
	5	2.5	0.52
Fe^{3+}	100	54.1	1.72
	50	13.5	1.03
	25	0.83	0.58
Hg^{2+}	-	Interferes	-
Mg^{2+}	100	0.0	0.29
Mn^{2+}	100	-2.5	1.11
MoO_4^{2-}	100	103.0	1.82
	50	22.1	1.23
	25	0.5	0.80
Ni^{2+}	100	2.2	0.62
Pb^{2+}	100	3.3	0.76
Sn^{2+}	100	-0.6	0.26
VO_3^-	100	35.4	0.62
	50	5.6	0.10
Zn^{2+}	100	3.4	0.20
EDTA	0.1 M	-0.48	1.13

Table 4.5. Interference of metal ions on the determination of 5.0 ppm Se(IV).

From these studies, and with reference to Table 4.4, it is obvious that the FIA methods developed here suffer from fewer interferences than the other FIA methods [146, 147] and the electrochemical methods.[134, 135, 145]

4.1.4 Conclusions

This is the first time that the three FIA modes of operation described in this Section and elsewhere [151] have been contrasted. Their implementation on a single apparatus has ensured that the comparisons made are accurate. It is obvious that use of a conventional manifold (even when optimized by simplex or another search method) may not be the best approach. This work has demonstrated that alternative manifold designs and flow programming can provide the analyst with FIA methods of maximum performance.

4.2 Automated exploration and exploitation of flow injection response surfaces

4.2.1 Introduction

This Section reports the use of surface mapping with several *alternative* flow injection responses, which are new to FIA. The data were obtained in four different automated method development studies using the computer-controlled methods development system described in Chapter 2. Simplex optimization and pattern search methods for collecting response surface data are compared. The chemical and physical effects which cause the surface shapes observed are discussed for some surfaces. The utility of vector responses such as peak shape, and those of still higher diamensionality is addressed, as are the experimental limitations of these automated approaches to characterizing chemical systems.

Chemical variables (reagent concentrations, pH, buffer strength, *etc.*), physical parameters (flow rates, reaction coil lengths, sample size), and limitations of experimental apparatus all affect the performance of flow injection analytical procedures. The effects of these variables on the observed analytical signal are not necessarily independent *i.e.*, they can and do interact.[3] Our ability to understand and efficiently optimize flow injection systems has been limited by the lack of convenient means to visualize these multivariate interactions. Three-dimensional (3D) surfaces of absorbance vs. wavelength vs. time data are already used in flow injection and, if the apparatus is equipped with a diode array spectrophotometer, these may be generated within a single experiment. The simultaneous effects that two chemical or flow parameters have on an instrumental response (at fixed values of all other variables) may also be shown as a 3D plot, or "response surface".[60] Such surfaces presently require many experiments to construct, but can provide unique chemical insights into analytical methods. These approaches combines fundamental chemistry, chemometrics and applications-driven analytical methods development.

The most widely used response for flow injection optimization and practice has been peak height at peak maximum, whether from photometric, electrochemical or thermal detection. However, alternative system responses may equally well be chosen, such as peak area, width, and others discussed in this chapter. Each results in a different surface for the same chemical system, and each can convey different information to the chemist. Given a suitably versatile data acquisition strategy, these additional surfaces may be obtained without additional experimental effort, since one just uses more of the data collected, and uses them in different ways. Combination of several measures of performance into a response function [52] serves to indicate compromise experimental conditions which (*e.g.*) minimize the time or cost per analysis while retaining adequate sensitivity. Choice of an appropriate response function is perhaps the most critical step in optimization studies; examples have been given elsewhere. [52] Where more than two variables are of interest, higher dimensionality representations are necessary.

Flow injection systems have previously been studied univariately, *i.e.*, by varying, stepwise, one experimental variable at a time. [3] A linear regression to this data using a simple polynomial equation then provides a quantitative model which is a function of that variable, at the assumed fixed values of all other experimental parameters. Such models help users improve method sensitivity and stability, but usually fail to convey to the chemist the fundamental contribution from each variable *in the presence of others*. Furthermore, information on the kinetics and mechanism of reaction and mixing is difficult to extract. Perhaps seven or more parameters (reagent concentration(s), flow rate(s), coil length(s), *etc.*) should ideally be considered when studying even simple flow injection methods, [3, 31, 153] but only subsets of these have been experimentally investigated at any one time. [3] Global model equations for flow injection systems are still limited to simple manifolds. [153, 154] Accurate theoretical prediction of the optimum operating conditions for complex chemical reactions in flow injection manifolds is still not possible from first principles, and it is generally recognised that empirical optimization by methods such as

modified simplex optimization [3, 52, 60] is beneficial. The complexity of the interaction of chemical and flow parameters has demanded that factors which lead to bifurcated peaks, unexpected tailing, and otherwise non-ideal behavior receive further attention. An improved theoretical understanding is perhaps the most pressing need for flow injection today, [155] but this must be couched in a convenient usable form. Ruzicka [1] and other workers have already established helpful guidelines for design of flow injection methods which go part of the way towards this.

Kowalski *et al.* [156] suggested the term *flow chemography* to describe the use of graphical representation for data taken from flow systems. Since this approach facilitates efficient collection and effective communication of the chemical information it should be more widely used in research and teaching. As will be demonstrated, visual interpretation of such data, when represented as response surfaces, allows the user to rapidly attain qualitative insights into the chemical reaction under study.

A fully quantitative interpretation still requires the design and fitting of *complex* surface models; [157] simple global methods based on polynomials fail to represent more than the gross shape of a response surface, [81] and may be incapable of indicating the presence of more than one maximum. Thus, for other than simple examples, it is better to rely on surface models which are comprised of multiple local models of surface topography. These can be produced by graphics software packages which handle irregularly spaced data points, [158] or by adaptation of simpler surface plotting algorithms. [159] The quality of the local surface model at any point depends on the number and quality of experimental observations in that region. Ideally, where all parts of the response surface are of equal interest, the model should provide a uniformly accurate representation of local response surface contours (and their errors). This generally requires that data points be taken fairly uniformly from all over the surface, and is experimentally intensive, in that several replicate experiments may be needed at each of a very large number of different sets of experimental conditions. [160]

The only realistic way to achieve this goal within a resonable time is by full automation of the experiments, which is the approach used here. As in previous Chapters, the automated FIA instrument is used to mix appropriate proportions of stock solutions, allow the chemical and flow conditions prior to sample injection to reach equilibrium, inject samples, monitor detectors and quantify the response(s) (usually as peak height above baseline). Replicates were run for each set of experimental conditions, and the mean and standard deviation of responses obtained were calculated, before moving on to the next set of experimental conditions.

4.2.2 Experimental Section

4.2.2.1 *Chemical systems studied*

These were for the determination of phosphate by the molybdenum blue (molybdophosphate) method, [162] peroxydisulfate (persulfate) with *o*-dianisidine (ODA), [152, 113] palladium(II) by reaction with the sodium salt of sulphochlorophenolazorhodanine (Na-SCPAR), [60] and iron (II) by reaction with 1,10-phenanthroline. [57, 163] All reagents were of analytical grade. Solutions were made up in distilled water, unless otherwise stated. A summary of the chemical and flow variables studied and their concentration/flow rate ranges is given in Table 4.6. Working solution concentrations were chosen so as to minimize unwanted high background absorbances and maximize detectability. These decisions were based on results from preliminary static experiments and values from the literature data.

System	Variable	Low (ml/min)	High (ml/ min)	Initial conditions (simplex opt.)
Pd(II)/Na-SCPAR	Na-SCPAR	0.10	0.50	0.40
	NaOH	0.00	0.50	0.10
Mo(VI)/PO_4^{3-}	Ascorbic acid	0.00	1.00	1.00
	Molybdate	0.00	1.00	1.00
Fe(II)/Phen.	Phenanthroline	0.10	1.00	-
	Sodium acetate	0.00	1.00	-
$S_2O_8^{2-}$/dianisidine	*o*-dianisidine	0.10	1.00	0.40
	Dimethylglutaric acid	0.00	1.00	0.40

Table 4.6. Low and high flow rate limits used for the optimization procedures, together with the initial simplex optimization conditions.

4.2.2.2 *Molybdophosphate method*

Solutions containing 5.0×10^{-3} M ammonium heptamolybdate (BDH, Toronto, ON) (6.1793 g l^{-1}) in 0.4 M nitric acid and a 0.7% (w/v) aqueous solution of L-ascorbic acid (BDH, Toronto) were prepared. To these were added 1% (w/v) of Brijs' reagent (Fisher Scientific, Richmond, B.C.) to minimize any deposition of precipitate on the walls of the tubing or flow cell. A stock solution containing 100 ppm phosphorus (306 ppm as phosphate) was prepared by dissolving 0.4390 g of anhydrous potassium dihydrogen orthophosphate (BDH, Toronto) in 1 liter of distilled water. This solution was diluted to 1/5th of this concentration for the method development study. The colored reaction product was observed at 660 nm.

4.2.2.3 *Persulphate / o-dianisidine*

A stock solution of persulphate (1.00×10^{-3} M) was prepared by dissolving 0.0676 g of potassium persulphate (Fisher Scientific, Fairlawn, NJ), in 250 ml of distilled water. A sample solution containing 1.00×10^{-5} M of persulphate was prepared by dilution of the stock solution. The *o*-dianisidine (ODA) reagent (Aldrich, Milwaukee., WI) solution used was 1.0×10^{-2} M (2.443 g/l) in 40 (v/v)% acetone/water mixture. Solutions of *o*-dianisidine were freshly prepared each day for reasons of stability. A buffer solution was prepared

from 100 ml of 0.1 M 3,3-dimethylglutaric acid (Aldrich, Milwaukee, WI) in 1.0 M sodium chloride. [103] The sodium chloride was present to minimize the effect of changes in the ionic strength of the reaction media. Various reaction pH's for the batch method experiments were obtained by adding appropriate volumes of 0.1 M sodium hydroxide (BDH, Toronto) to the buffer. The reaction was observed at 450 nm. Further details of this chemistry and method development may be found in chapter 3, section 3.4.

4.2.2.4 *Palladium / Na-SCPAR*

A stock solution of palladium (1.0×10^{-3} M) was prepared by dissolving palladium (II) chloride (Ventron Alfa Products, Danvers, MA) in 0.01 M hydrochloric acid; sample solutions were obtained by appropriate dilution. The Na-SCPAR reagent was synthesized as reported previously. [60] A Na-SCPAR solution (approx. 1.0×10^{-3} M) was made by dissolving 0.3676 g of Na-SCPAR in 1 liter of 0.01 M hydrochloric acid. Sodium hydroxide stock solution (0.20 M) (BDH, Toronto) was prepared from pellets. A universal buffer solution [60] at pH 2 was also prepared. The reaction was observed at 520 nm. Full details of the development of this method appear in chapter 3, section 3.3.

4.2.2.5 *Fe(II)-phenanthroline*

A 1.0×10^{-2} M 1,10-phenanthroline (see Appendix 1 for molecular structure) solution was prepared by dissolving 1.9823 g of the monohydrate (Matheson, Coleman and Bell, Norwood, OH) in 1 liter of distilled water. An acetate buffer solution was made from 0.2 M sodium acetate (Matheson, Coleman and Bell) and 0.2 M acetic acid (BDH, Toronto) solutions. A 1.0×10^{-2} M stock solution of hydroxylamine hydrochloride (Anachemia, Champlain, NY) was used to reduce any ferric ion that might be present to ferrous. The sample was a 1.0×10^{-4} M solution of iron(II) ammonium sulfate (BDH Chemicals Ltd, Poole, England), prepared in dilute sulfuric acid *i.e.*, 2.5 ml. of concentrated (15 M) H_2SO_4 (BDH, Toronto) per liter. The reaction was observed at 508 nm and other wavelengths as shown.

4.2.3 Apparatus

4.2.3.1 *Hardware*

The automated flow injection analyzer, [57] shown schematically in Figure 2.1, was as discussed in Chapter 2 and used previously. [60, 151, 152] A simple photometric detector [59] consisting of a tubular flow cell with a red light emitting diode (660 nm peak, about 40 nm bandwidth) and a phototransistor mounted transversely across the flow stream was used for the phosphate experiments. In all other cases, detection was by the diode array spectrophotometer (Model 8452A, Hewlett Packard, Richmond, B.C.), equipped with a 30 μl, 1 cm path length quartz flow cell. The pH of reaction mixtures was determined at the outflow of the flow cell using a laboratory pH meter (Fisher Scientific, Richmond, B.C.) and a flow-through electrode cell designed in our laboratory. Polytetrafluoroethylene (PTFE) tubing (0.5 mm i.d.) was used for all manifolds. All peak heights reported are relative to stable baseline values obtained just prior to the peak.

The flow injection configurations used in methods development are given in detail in Figure 4.11 (the manifolds shown in Figure 4.11 b,c are repeated from Chapter 3 for reasons of clarity). After automated development of the analytical methods, two of these systems were greatly simplified for routine use; their simplified manifolds are given in Figure 4.12.

4.2.3.2 *Software*

All programs were written in Microsoft QuickBASIC^{R} v. 4.00B. The operating software was significantly more advanced than the version reported previously. [57] Since the enormous amount of data generated would quickly fill the limited hard drive storage capacity of the microcomputer, some data acquisition routines now contain data reduction steps which store only the average value of several replicate responses, peak height rather than peak shape, or absorbance at selected wavelengths rather than full spectra. Storage of full peak shape data is optional.

a)

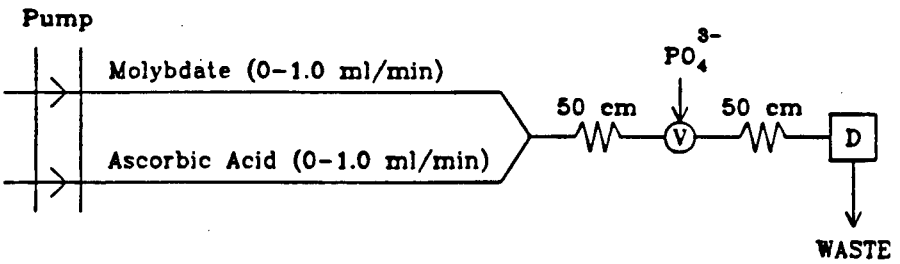

b)

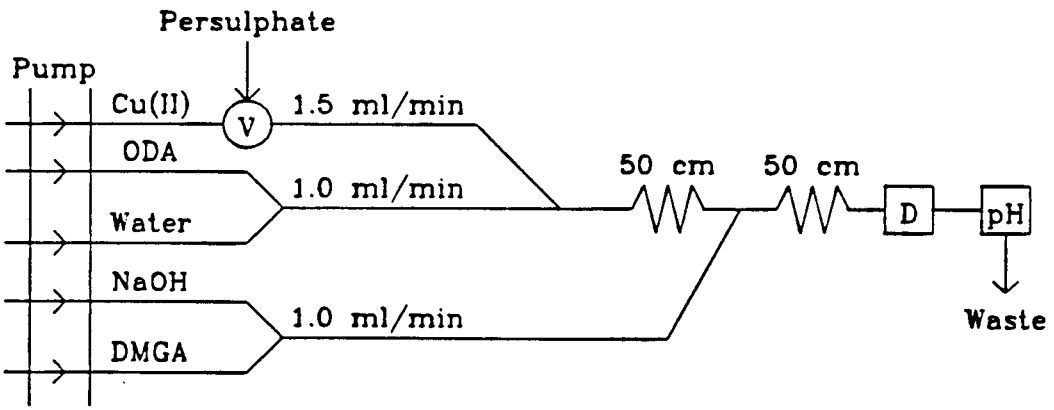

Figure 4.11 Flow injection manifolds used in methods development for;
(a) determination of orthophosphate by reaction with molybdate;
(b) determination of persulphate by reaction with *o*-dianisidine;

c)

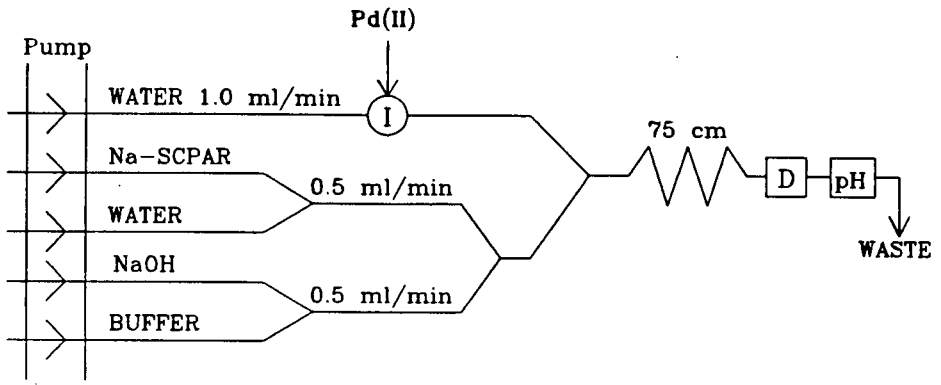

d)

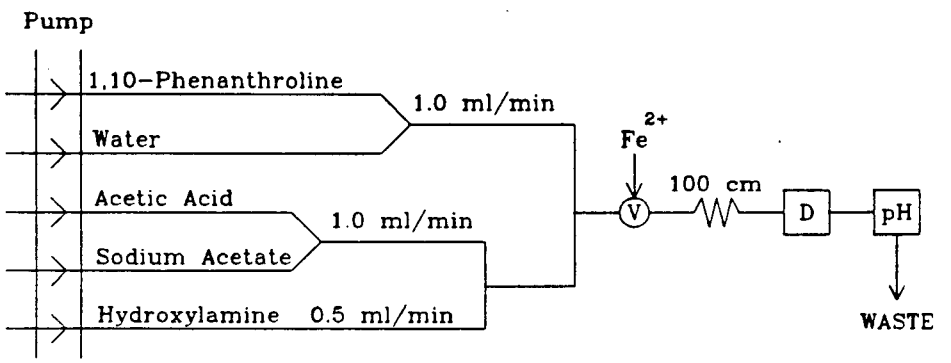

Figure 4.11 (cont) Flow injection manifolds used in methods development for;
(c) determination of palladium(II) by reaction with Na-SCPAR;
(d) determination of Fe(II) by reaction with 1,10-phenanthroline.

a)

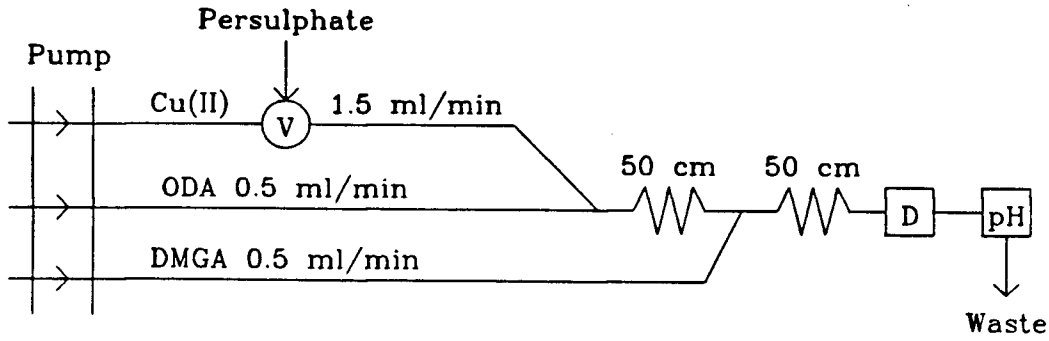

b)

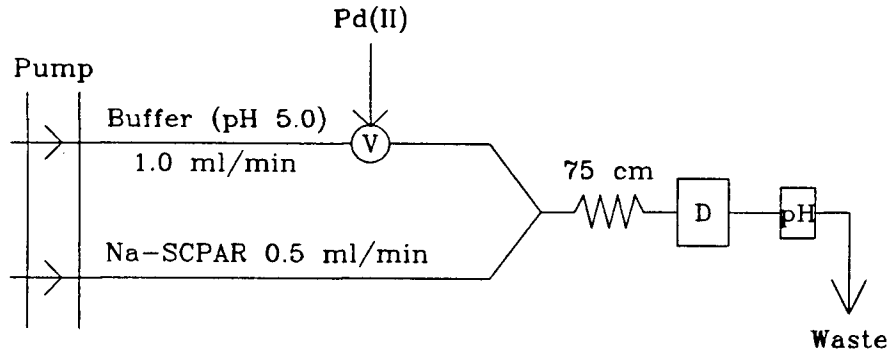

Figure 4.12 Simplified flow injection manifolds used for routine determination of:
(a) persulphate by reaction with o-dianisidine;
(b) palladium(II) by reaction with Na-SCPAR.

4.2.4 Method

4.2.4.1 *Calibration of flow rates*

Calibration routines are included in the operating software. Once the pump configuration for a system was chosen, the manufacturers' flow rating for the pump tube on each channel was entered and the actual flow rate in ml. min^{-1} was established gravimetrically at selected speeds for every channel using an analytical balance.

4.2.4.2 *System initialization*

Prior to simplex optimization and response surface mapping experiments, the selection of pumps and detectors to be used in the method development was entered into the microcomputer, together with the number and names of the variables. The chemical variables were then specified, as shown in Table 4.6. Their flow rate ranges (and hence concentrations) were selected such that the presumed optimum stoichiometry was possible, critical reagent concentrations were always non-zero, and total flow rate through the manifold did not exceed 3.50 ml. min^{-1}. The number of replicate injections required was indicated. Pumps assigned to fixed flow rate streams were identified and their flow rates designated. Pump tubings were chosen to deliver the necessary flow rate ranges. Wherever a fixed total flow rate was desired, so as to ensure comparable sample transit times, variable streams were "buddied" [60, 161] to an appropriate diluent stream. For example, the reagent stream in Figure 4.11c consisted of Na-SCPAR merged with water to give a total flow rate of 0.5 ml. min^{-1} at all times and a maximum Na-SCPAR concentration of 9.44×10^{-4} M. Manifolds without such buddying, such as the one shown in Figure 4.11a, did not provide a constant sample residence time.

Also specified was the distance between the points of sample injection and detection. This allowed the software to calculate the maximum time to wait for the arrival of a peak. This was also used to specify the purging time between different experimental conditions for the system.

4.2.4.3 *Surface exploration by automated simplex optimization*

As before, the optimization algorithm used was the composite modified simplex method. [9, 61] Each new set of experimental conditions was automatically calculated and established experimentally by the microcomputer. The system was allowed to equilibrate to a steady baseline reading before every sample injection. Three to five replicate sample injections were made at each set of experimental conditions to provide an average peak absorbance and an estimate of its repeatability.

4.2.4.4 *Automated response surface mapping*

The user first chooses the number of steps with which to explore each chemical variable. These determine the resolution with which each variable is explored, and together they define the total number of experiments to be carried out. Experiments were done in either an 8 x 8 (64 point) or a 10 x 10 (100 point) grid design. In each case the mapping studies were completed within 2 to 4 hours.

Three dimensional response surfaces (along with their corresponding contour maps) were then generated using a commercial scientific graphics program. [158] The program used the regularly spaced data points from the automated mapping experiments to create 25 x 25 square grids. It interpolated the expected response value for the places which lacked data. The method of interpolation and the number of locations of experimental data used must be carefully chosen in order to avoid artifacts and false detail. This work used the method of Kriging [158] and the 10 nearest actual data points.

4.2.5 Results and Discussion

4.2.5.1 *Mapping studies*

These studies each produced a set of response surfaces (first variable vs. second variable *vs.* response), one for each experimental response or combination of experimental responses. The control and data acquisition software also facilitates a similar process for three or more experimental variables. Studies in three variables provide a stacked set of surfaces (one per value of the third variable). An array of surfaces is generated in the four-variable case. Pseudo-three-dimensional plots, where all points lie along the two axes, can also be used to simultaneously display two experimental responses from a single variable. However, for practical reasons, these data can be shown more clearly as a pair of overlaid graphs. The same logic holds for pseudo-four dimensional representations, which can show two responses and two variables (as a set of "overlaid" surfaces, which are better displayed in a side-by-side fashion) or three responses as a function of one variable (which are better shown as three overlaid graphs). Higher dimensionality is also possible. The accuracy and precision (and therefore the reliability) of the response surfaces obtained is dependent on the accuracy and precision with which each of the variable values can be obtained and the response measured. The response surfaces reported here appear to be well behaved, although as discussed in the latter part of this chapter, Section 4.4.5.3, the molybdophosphate surface (Figure 4.13a) suggests that one data point in the valley at high ascorbic acid and low molybdate concentrations may be high.

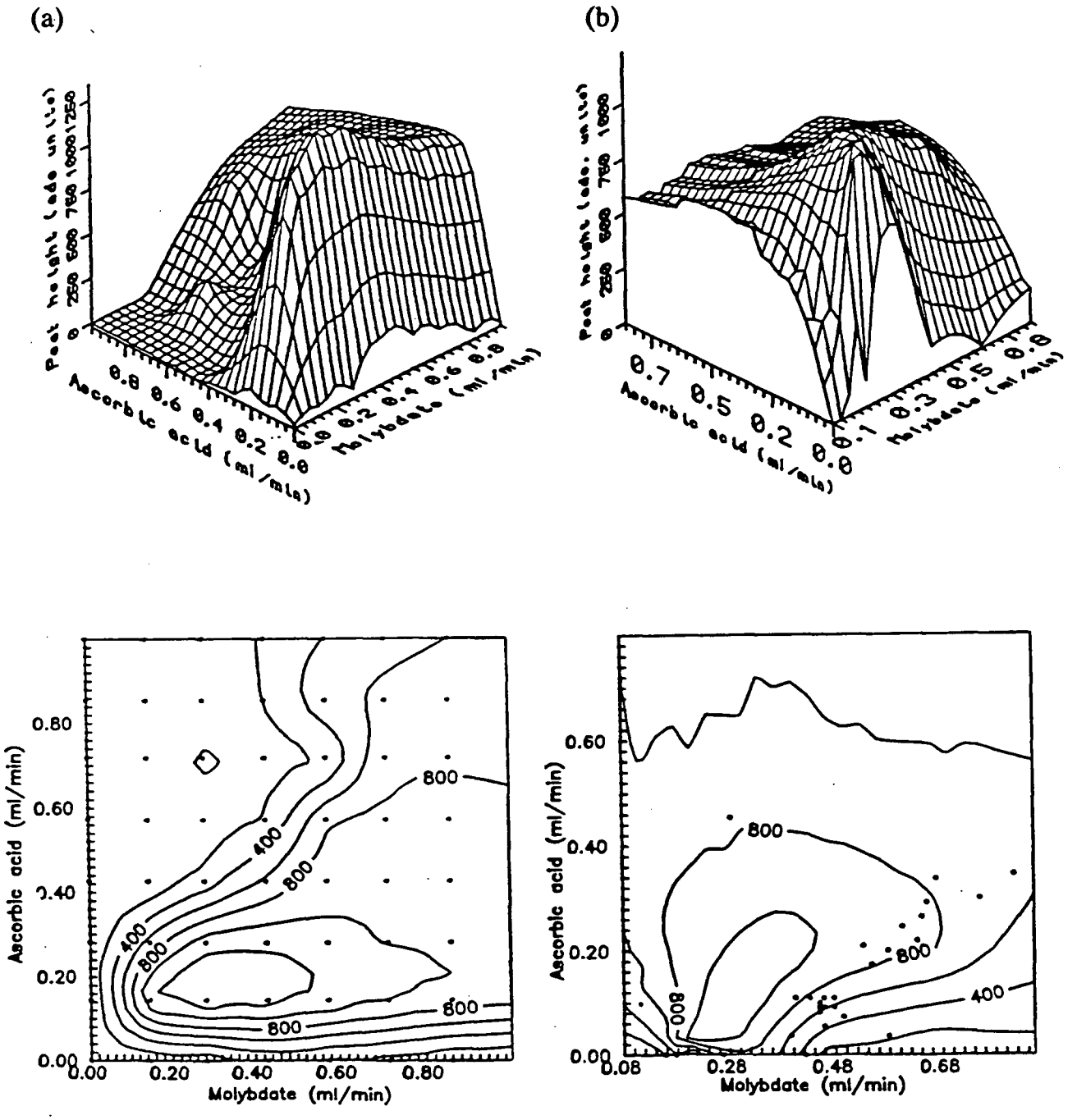

Figure 4.13 Three dimensional response surface plots for molybdophosphate reaction with absorbance measurements taken at peak maximum:

(a) surface generated from 64 regularly spaced data points from grid search optimization for molybdophosphate reaction,

(b) surface generated from 40 irregularly spaced data points obtained by simplex optimization.

4.2.5.2 *Comparison of simplex optimization and grid search methods*

The total number of grid search and simplex experimental points for each system, the maximum response, and the range of responses obtained are shown in Table 4.7. The optimum absorbance values from simplex optimization experiments were in reasonably good agreement with those found by the grid search procedure, and were obtained within 25 - 63% of the number of grid search experiments. This demonstrates the experimental efficiency advantage of simplex over grid search and univariate search procedures. In the case of the simplex optimization of the persulfate system, only 16 experiments were needed to reach the optimum. However, one would doubt the reliability of a surface map based on so few, irregularly spaced, experiments.

Chemical System	Simplex # points	Grid Search # points	Pk. Ht. Simplex	Pk. Ht. Grid Search
Pd(II) / Na-SCPAR	26	64	0.534	0.514
Mo(VI) / H_3PO_4	40	64	0.494$^+$	0.546$^+$
Fe(II) / Phenanthroline	28	64	0.319	0.335
$S_2O_8^{2-}$ / *o*-dianisidine	16	64	0.211	0.226

Table 4.7. Number of sets of experimental conditions tried in simplex and grid search studies, and the absorbances at peak maximum obtained.

$^+$ maximum peak heights were measured as 1236 and 1366 adc units. A reading of 1000 adc units was equal to an absorbance of 0.40.

Figure 4.13 contrasts surface maps generated by grid and simplex optimizations of the molybdophosphate system. In this instance the 64-point grid search found better conditions than the 40-point simplex (see Table 4.7). The spread of data points shown on the contour map in Figure 4.13a indicates that the grid search provides an adequate global coverage and therefore conveys the true general shape of the surface. The locations of the simplex points, Figure 4.13b, show that the simplex gave good coverage close to the maximum, but that contours at higher ascorbic acid flow rates were ascribed on the basis of very little experimental information. Thus, while the plot from the simplex data predicted that there would be a decreased response at high ascorbic acid and low molybdate flow rates, its (extrapolated) values were far too high. A similar effect is seen where the ascorbic acid flow rate is zero.

Simplex optimization, while imperfect, must still be the strategy of choice for optimization of four or more interacting variables where these variables can be rapidly adjusted: The time required to set up the experiment and re-equilibrate should not be much greater than the time needed to take the measurements. In a well behaved five variable system a simplex has been reported to reach near optimum in 35-40 experiments, [3] whereas a grid search of the thoroughness used in this present work would require 8^5 (*i.e.*, 32768) experiments. Simplex methods require that all variables be adjusted when obtaining (almost all) new points. Thus a 40-point 2-variable search requires 80 variable changes. Search methods which require adjustments of only one variable per new experiment are also possible [164] and can sometimes be advantageous. The disadvantages of true univariate search methods have been demonstrated and discussed elsewhere. [3, 9, 61]

Flow injection response surfaces characterized so far have only one or at most two real maxima. Each simplex optimization can home in on only a single maximum, thus surfaces which are suspected of having multiple maxima are best characterized by either by the grid search approach or by multiple simplex optimizations starting from different

regions of the search space. Just as the use of simplex optimization on multimaxima surfaces may not find the global optimum, global models based solely on simplex data will not reflect the presence of an alternative maximum that the simplex has chosen not to explore. Global surface mapping in three or more dimensions using a limited simplex optimization data set suffers from the coverage problems mentioned above, although, given enough experiments, local models based around the optimum are valid. [81]

The grid search method enables the analyst to view the true general profile of the response surface (*e.g.*, Figure 4.13a). This not only provides a better understanding of the interaction of the system variables but also allows intelligent decisions regarding the choice of experimental conditions for routine analysis. Ideally, one would wish to carry out analysis under sensitive conditions which have good stability / tolerance of small variations in the experimental parameters *i.e.*, the middle of plateau regions. Deming *et al.* recommended carrying out an experimental design around the simplex optimum for just this reason. [72] However, other factors such as response repeatability should also be taken into account, as discussed below.

Despite the thoroughness of the grid search approach to mapping, it is possible to miss sharp maxima that might be detected by simplex. The possibility of this happening is greatly increased when the number of data points used to generate the surface diagrams is limited. Practical considerations decree that only a finite number of experiments can be done, but the acceptable number is undoubtedly higher when experiments are automated.

4.2.5.3 *Uses for chemical response surfaces*

4.2.5.3.1 *Establishment of optimum working ranges*

Simplex optimization of the molybdophosphate reaction was begun at at reagent stream flow rates of 0.60 ml. min^{-1} and a detector response of 650 adc units was obtained. Within 27 experiments conditions were found which had a response of 1236 adc units.

Irrespective of the mapping algorithm used, optimum and usable variable ranges can be readily identified from the contour map representation (so long as coverage is adequate). For example, the plateau region shown in Figure 4.13a is at flow rates of 0.10 - 0.30 and 0.25 - 0.50 ml. min^{-1} for the ascorbic acid and molybdate streams respectively.

4.2.5.3.2 *Visualization of non-optimal conditions*

A grid search then showed that the original conditions lay on the side of a steep hill (Figure 4.13a), and that the simplex optimization had found several points on a broad high plateau. Operation in the plateau region resulted in both excellent repeatability and sensitivity in response measurements. Operation on the side of the hill would more noticeably suffer from the effects of small changes in concentrations due (*e.g.*) to flow rate fluctuations or poor mixing of solutions, since these would result in a significant change in absorbance, poorer repeatability, and greater drift in calibration curve coefficients.

4.2.5.3.3 *Understanding chemical and flow contributions*

A qualitative understanding of reaction kinetics, reagent concentration, and time required for reaction may often be obtained by subdividing contour maps into appropriate regions, and then comparing the parts of the surface seen in each. One such approach considers the contour map as comprised of four quarters. The low sensitivity observed in the upper left hand corner of the grid search contour map for the molybdophosphate reaction (Figure 4.13a) may be attributed to a combination of slow reaction due to insufficient molybdate concentration, and both increased dispersion and shorter sample residence times due to high ascorbic acid flow rate (0.50 - 1.0 ml. min^{-1}). The manifold, shown in Figure 4.11a, indicates that the flow rate experienced by the sample is the sum of the molybdophosphate and ascorbic acid streams. In the upper right hand quarter, the molybdate is in sufficient concentration for adequate reaction and the reaction time is even shorter. The lower right hand region sees a decreased total flow rate and an increased

molybdate concentration, this also leading to acceptable conditions for analysis. The response falls off sharply to zero when little or no ascorbic acid is present and when no molybdate is present. This indicates both the necessity of having both reagents present and the absence of other absorbing species or precipitate. The lower left hand region has generally moderate flow rates of each reagent, (0.0 - 0.5 ml. min^{-1}) and includes a well defined optimum for sample residence time and chemical reaction conditions (0.35 ± 0.10 ml. min^{-1} molybdate, 0.25 ± 0.05 ml. min^{-1} ascorbic acid). Users might sometimes prefer the plateau region at faster flow rates since these would provide better sample throughput rates and excellent method stability at a cost of some sensitivity. The surface will change if reaction coil length (and hence residence time) is changed. Since the molybdenum blue product is formed via a molybdenum yellow intermediate, very short residence times are not recommended if detection is at 660 nm.

Another approach for systems with variable residence time is to draw diagonal lines across their contour surfaces which correspond to either (i) fixed residence time, and variable reagent concentration ratio or (ii) fixed (possibly optimum) concentration ratio, and changing residence time. Lines parallel to the axes indicate a simultaneous decrease in residence time with increase in the relative concentration of one reagent. This "line approach" is also valid for systems where, because of buddying, the total flow rate remained fixed. Here, residence time remains constant and the reactant flow rates can be independently related to the absolute concentrations of the reactants. Diagonal lines can indicate the effects of (i) varying the relative concentrations whilst maintaining a fixed total concentration, and (ii) varying the total concentration whilst keeping a known linear relationship between the concentrations. Figure 3.20 shows a surface obtained for the persulfate / *o*-dianisidine reaction using a fixed total flow rate and the manifold shown in Figure 4.11b. This type of surface and the line approach makes more obvious the individual contributions of the hydroxide and *o*-dianisidine: Increasing the reagent concentration increases the absorbance asymptotically and an optimum pH certainly exists.

The wide range of pH values about the optimum value that lie on a nearly flat surface suggests that the method may be suitable for analysis of samples which vary in pH within the allowed range, without strong buffering. The lack of diagonal surface features suggests minimal chemical interaction of the two variables within the ranges studied. Thus their effects were able to be globally modelled largely as independent terms (see Section 3.4.3.7).

4.2.5.3.4 *Example of where a simple global model would be inadequate*

Figure 3.12 shows the peak absorbance response surface obtained by grid search for reaction of Na-SCPAR with Pd(II) under conditions of constant flow using manifold shown in Figure 4.11c. An hydroxide flow rate of less than 0.15 ml. min^{-1} results in acidic conditions and the reaction takes place rapidly. There is a general increase in sensitivity with increase in reagent (SCPAR) flow rate to about 0.30 ml. min^{-1}, above which the surface levels off as reagent is in sufficient excess. A second, smaller, maximum is observed at hydroxide flow rates above that which correspond to the transition from neutral to basic operating conditions. The second maximum becomes more pronounced at even higher pH's, but is unstable due to decomposition of the colored species [60]. Most simplex optimization procedures would either not detect a second maximum or would become stuck on it. While simple quadratic type surface models can be effectively used to describe the general profile of some "well behaved" surfaces, such models would fail to describe this surface. Rowles [165] noted that model equations which adequately describe flow phenomena in open tubes at some conditions may not be applicable at others. Similarly, conventional models for flow analysis will require modification to deal with reactions that are both acid and base catalyzed.

4.2.5.3.5 *Comparison of surfaces for fixed and variable total flow rates*

Figures 4.14a and 4.14b contrast the effect on a response surface of going from the fixed total flow rate manifold discussed above, to one where the total flow rate experienced

by the sample is allowed to vary. The sensitivities for the two systems under their respective optimum conditions are comparable, but the variable flow rate surface is obviously much more complex; the chemical concentrations are no longer independent of other flow rates. Allowed flow rates are shown on the new surface, which retains two chemical features of the fixed flow rate plot, namely the high maximum under acidic conditions, and the secondary maximum under mildly alkaline conditions, but is more difficult to interpret. Significant absorbance is now seen at pH 7. Reaction kinetics, reagent concentration and stability, pH and dispersion effects all have to be addressed. Increasing the flow rate of the hydroxide stream in the range 0.00 - 0.50 ml. min^{-1} now not only affects the pH but causes the flow rate at the detector to change from 1.50 to as much as 2.50 ml. min^{-1}. The residence time and Na-SCPAR reagent concentration are consequently decreased, and both peak height and area are changed as a result of the altered sample dispersion. On moving across the contour plot of Figure 4.14b we pass through regions of best pH, best reaction time, and sufficient reagent.

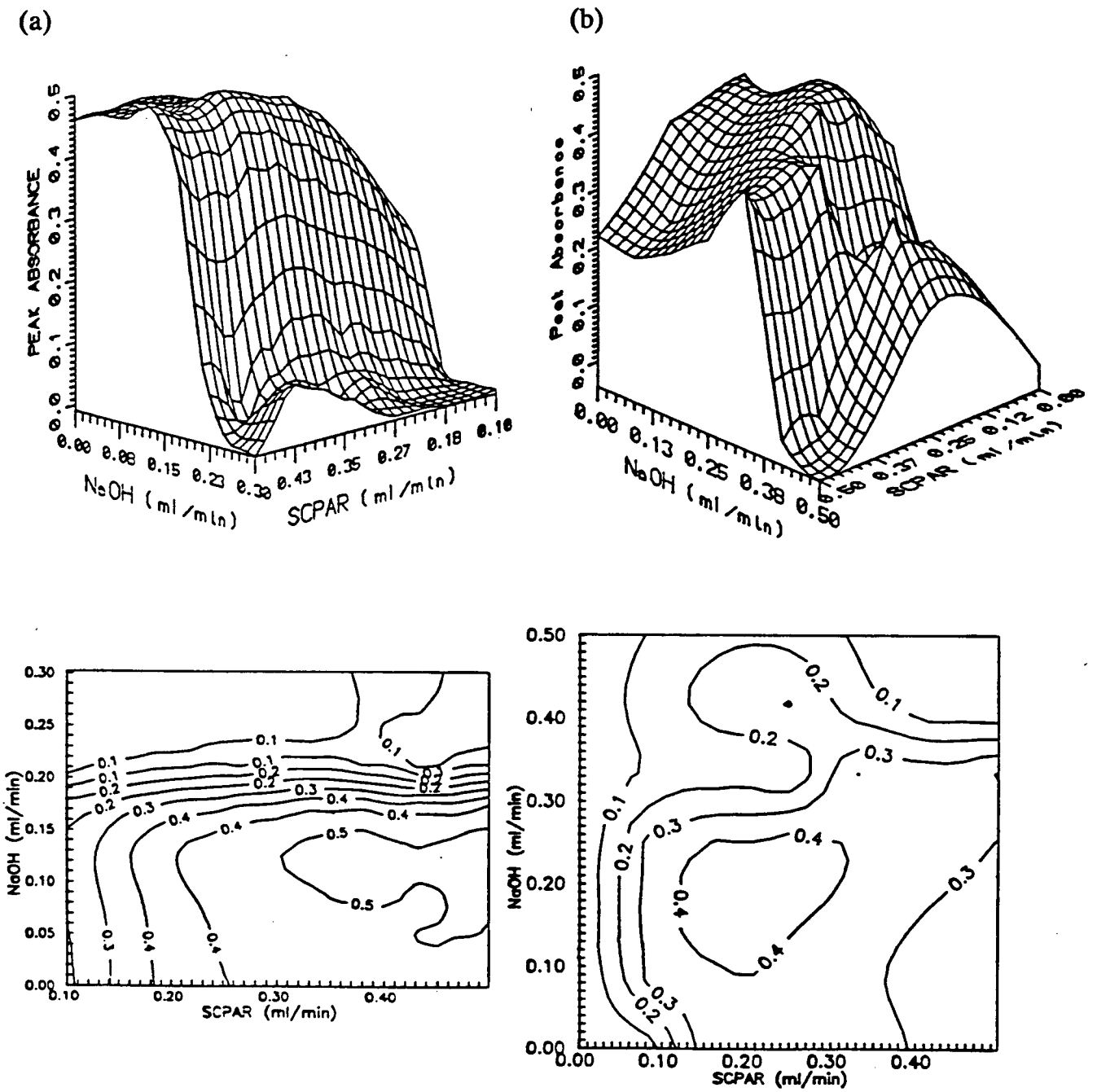

Figure 4.14 Three dimensional response surface plots for Na-SCPAR / Palladium reaction with absorbance measurments taken at peak maximum:

(a) conditions of fixed sample residence time,

(b) conditions of variable sample residence time.

4.2.5.3.6 *Visualizing experimental repeatability*

Most commonly in flow injection methods development, the criterion used for evaluating experimental conditions is sensitivity (as measured by peak height). Failure to also take response repeatability into account can have serious consequences.[69] Repeatability may be quantified by the percent relative standard deviation (RSD%) of replicate peak absorbance responses for each point across the search space. The Fe(II) / 1,10-phenanthroline reaction, whose 3D response surface plot is given in Figure 4.15a was used to show experimental repeatability as a function of flow conditions. Figure 4.15b illustrates the variations in the response RSD% as a function of chemical conditions for the Fe(II) / 1,10-phenanthroline reaction. Overlap of the minimum in the RSD% contour map of Figure 4.15b with the maximum of the corresponding response surface map of the same system shown in Figure 4.15a serves to confirm the best experimental conditions for this system.

The RSD% surface also serves to identify a source of instrumental imprecision for this automated flow analysis system. When run slowly to produce low flow rates, the five stepper-motor driven pumps cause asynchronous flow pulsations, which result in small random fluctuations in chemical concentrations and total flow rate, and hence poorer repeatability. These occur near *all four* corners since at all but the highest reagent flow rates the buddy pumps will still be running slowly.

Other causes of imprecision which will contribute to the height and / or shape of RSD% response surfaces are now listed; (i) the decreased signal-to-noise ratio at suboptimal chemical/flow conditions; (ii) the pump roller positions are not synchronized with injection; (iii) fluctuations in laboratory temperature will affect reaction rate; (iv) flow rates may deviate from calibrated values over the course of an extended run; (v) precipitate or residue may build up from previous experiments, this causing a rising and variable baseline, and possibly flow rate variations. The individual contributions of these effects should certainly be quantified individually in future work. However, such a detailed

understanding is not strictly necessary for routine system optimization, since here one wishes only to establish the best conditions for analysis.

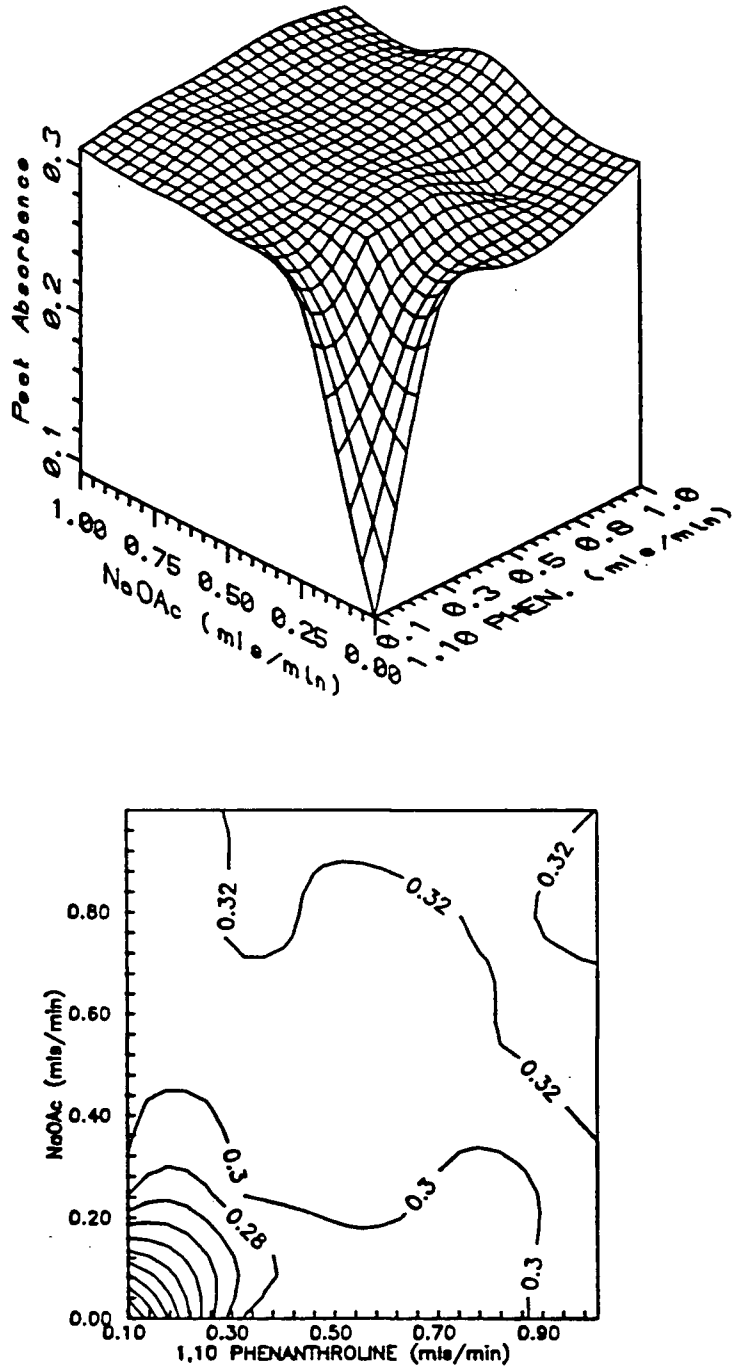

Figure 4.15a Three dimensional response surface plots for Fe(II) / 1,10-phenanthroline reaction showing effect of sodium acetate and phenanthroline concentrations on maximum peak height (absorbance) obtained.

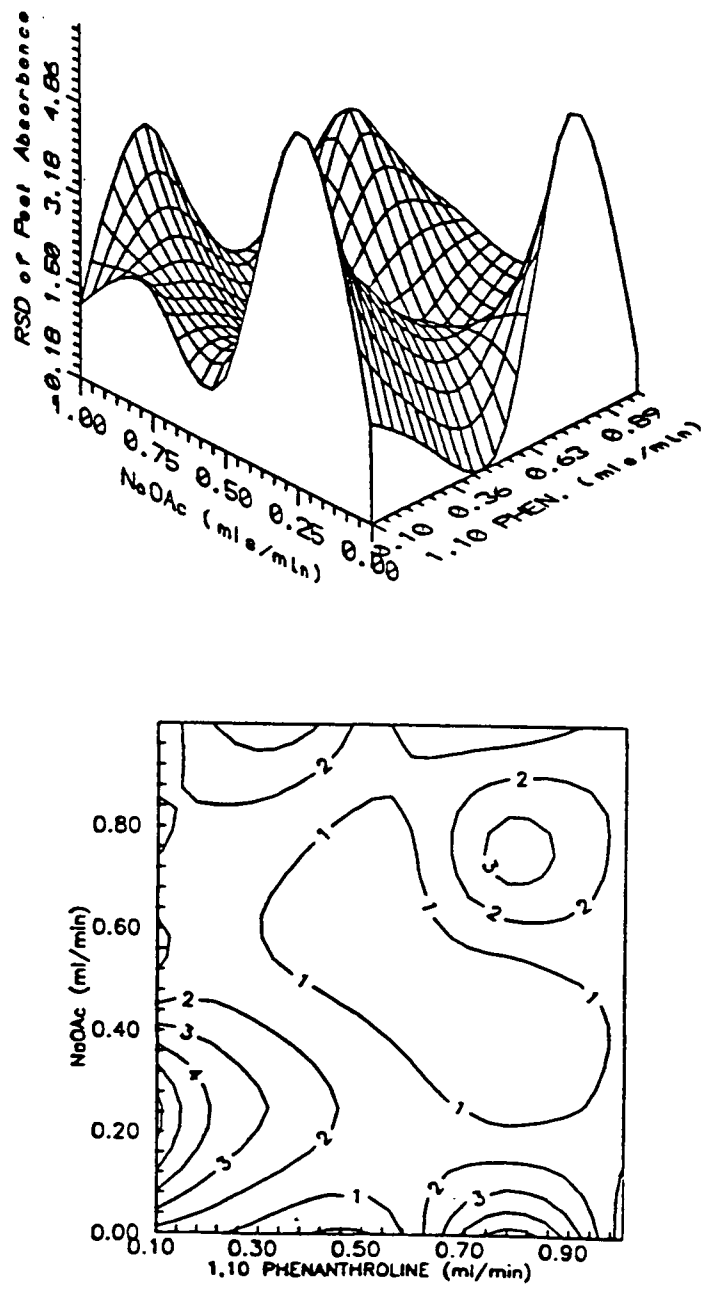

Figure 4.15b Three dimensional response surface plots for Fe(II) / 1,10-phenanthroline reaction showing effect of sodium acetate and phenanthroline concentrations on percent relative standard deviation (%RSD) in absorbance at peak maximum.

Once surface characterization is complete, the flow analysis method may be transferred to a simpler apparatus for routine analysis. This may have fewer (but higher quality) pumps (*etc.*) than the automated methods development system, and certainly will not suffer from buddy pump pulsation, thus the RSD% surface may be even better on the system used for routine analysis. A few manual experiments at maximum flow rates on the routine apparatus would confirm this.

4.2.5.3.7 *Visualizing shifts in wavelength of maximum absorbance*

Traditionally most peak absorbance measurements in flow systems have been made at a fixed wavelength, although some workers [166] have adopted multiwavelength measurements. The single wavelength chosen is assumed to remain optimum over the entire search region, however this generalization is not appropriate for many chemical systems. For example, changes in solvent composition or pH can shift wavelength maxima by several tens of nanometers, which will result in a change in sensitivity at different wavelengths across the surface. Interaction of system variables may cause shifts in the absorption wavelength which are less readily explained in simple terms. Where possible, a multiwavelength method development is therefore advisable. Figure 4.15c shows the distribution of optimum wavelength across the search surface for the Fe(II) / 1,10-phenanthroline chemical system. This reveals that optimum absorption wavelength indeed shifts as a function of the system variables. Thus, carrying out the absorbance measurements only at 508 nm (Figures 4.15a and 4.15b) still does not fully characterize the system. Comparison of Figure 4.15c with a plot of maximum absorbance found anywhere in the spectral region observed provides a way of determining the most sensitive wavelength and conditions.

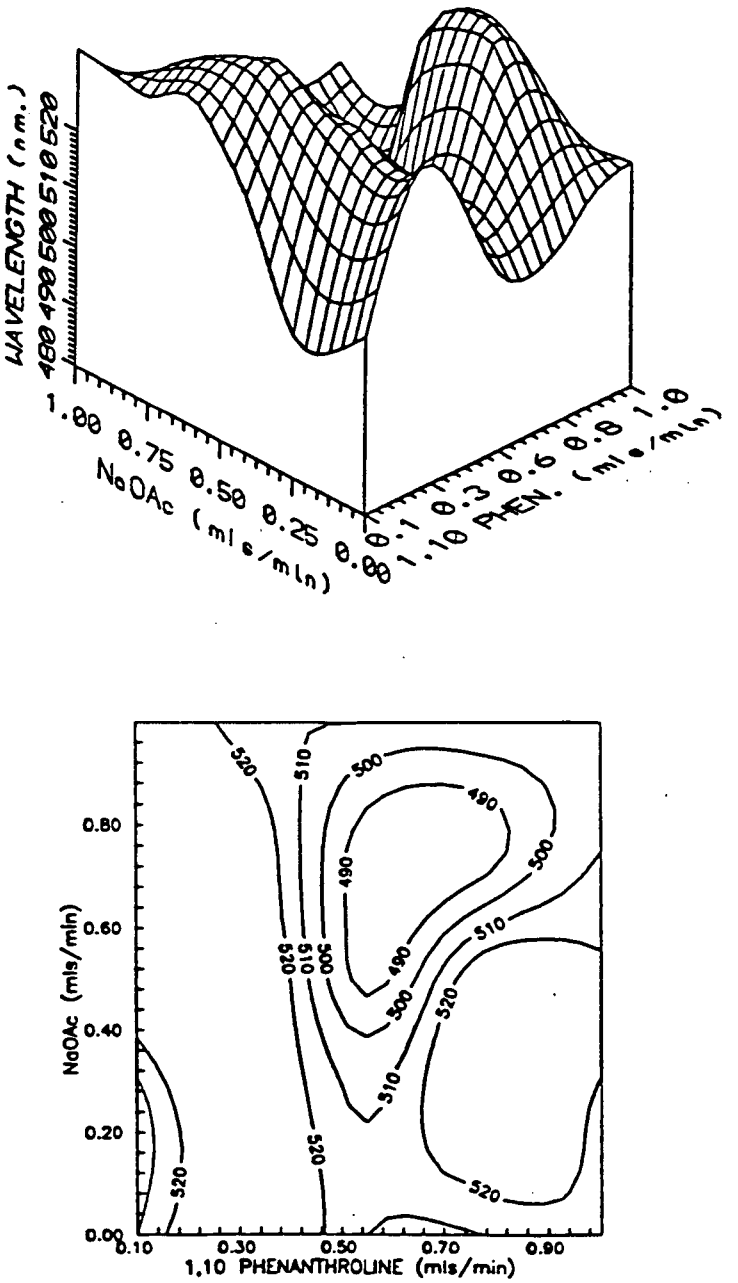

Figure 4.15c Three dimensional response surface plots for Fe(II) / 1,10-phenanthroline reaction showing effect of sodium acetate and phenanthroline concentrations on wavelength of maximum absorption.

4.2.5.3.8 *Visualizing shifts in time to peak maximum*

The systems studied here have all used fixed length reaction coils. For systems in which total flow rate may vary, the minimum residence time per sample and maximum sample throughput rate therefore occurs at maximum total flow rate. It is advantageous to consider the time from injection to detection of peak maximum as a response, and then compare this surface (Figure 4.15d) with those for the other responses (Figures 4.15a-4.15c). Figure 4.15d shows the effect of chemical factors on time to detection of peak maximum. If the time at which the peak maximum will arrive is known, then the control computer can spend time prior to the time of peak detection analyzing data from previous experiments, and once the peak has been measured, flow rates can be increased briefly to sweep the tail of the sample out of the system faster and so improve the sample throughput rate.

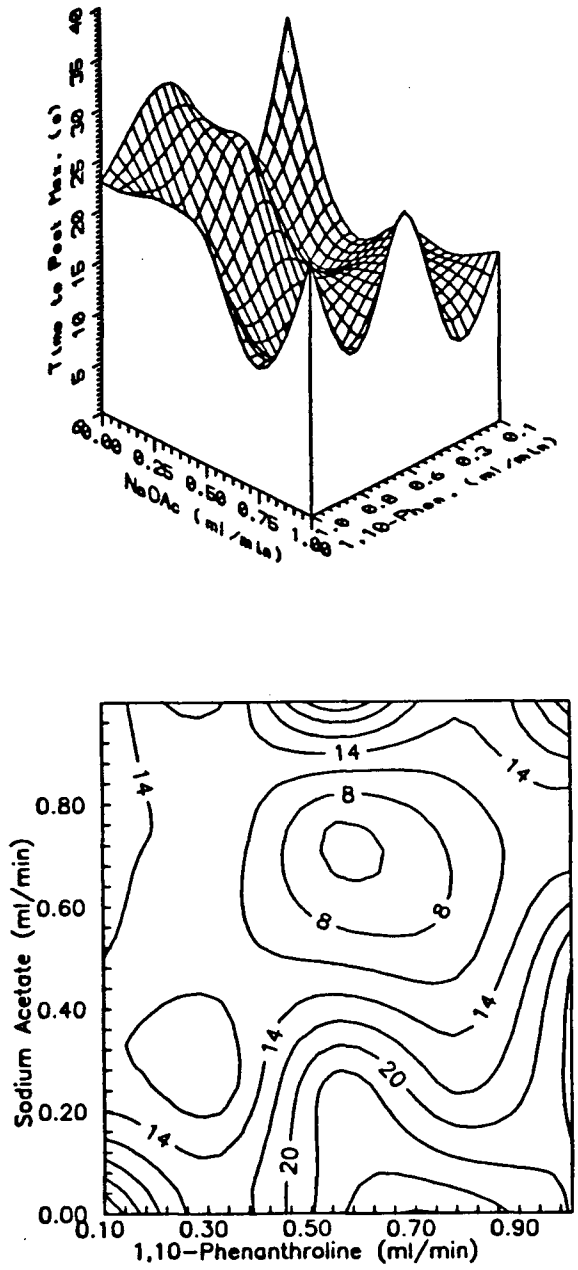

Figure 4.15d Three dimensional response surface plots for Fe(II) / 1,10-phenanthroline reaction showing effect of sodium acetate and phenanthroline concentrations on time to detection of peak maximum.

4.2.5.4 *Further simple responses*

The total dimensionality of the data space to be explored is given by the number of experimental variables studied (here two) plus wavelength, time and the response dimension(s) (absorbance, transmittance, *etc.*). Thus we have what is essentially (atleast) a five dimensional data set to explore and exploit. Response surfaces, spectra, other univariate plots, and even absorbance repeatability data are all subsets of this data space. Measurements from the pH electrode or other detectors provide further information which may be treated similarly. The human mind has difficulty in comprehending more than three (or at most four) dimensions of information at any one time. Where the number of dimensions exceeds three, techniques for dimensional reduction such as principal components analysis, may be appropriate. [167]

Developments in use of descriptive statistics for peak shape analysis will lead to further responses which may be effectively plotted as response surfaces to yield additional information without further experimentation. If one assumes that such computation is carried out on the 12 MHz PC/AT that controls the apparatus, and that a digital signal processing card is not available, this will add not more than 10 s of computation time to each replicate. Of course, more time will have to be spent on data analysis. This work is ongoing in this laboratory.

4.2.5.5 *Higher dimensional representations*

Representation of multidimensional data on a two-dimensional medium such as the printed page is possible but dimensions higher than four require considerable ingenuity. [167] In the remaining examples, Figures 4.16a and 4.16b, the two chemical dimensions plotted are sodium acetate concentration (which may be converted to pH) and reagent concentration. The third dimension of information available is time. This conveys the effects of chemical variables on peak profiles (Figure 4.16a). A fourth (or alternative third) dimension, with the help of a diode array detector is wavelength itself (Figure 4.16b).

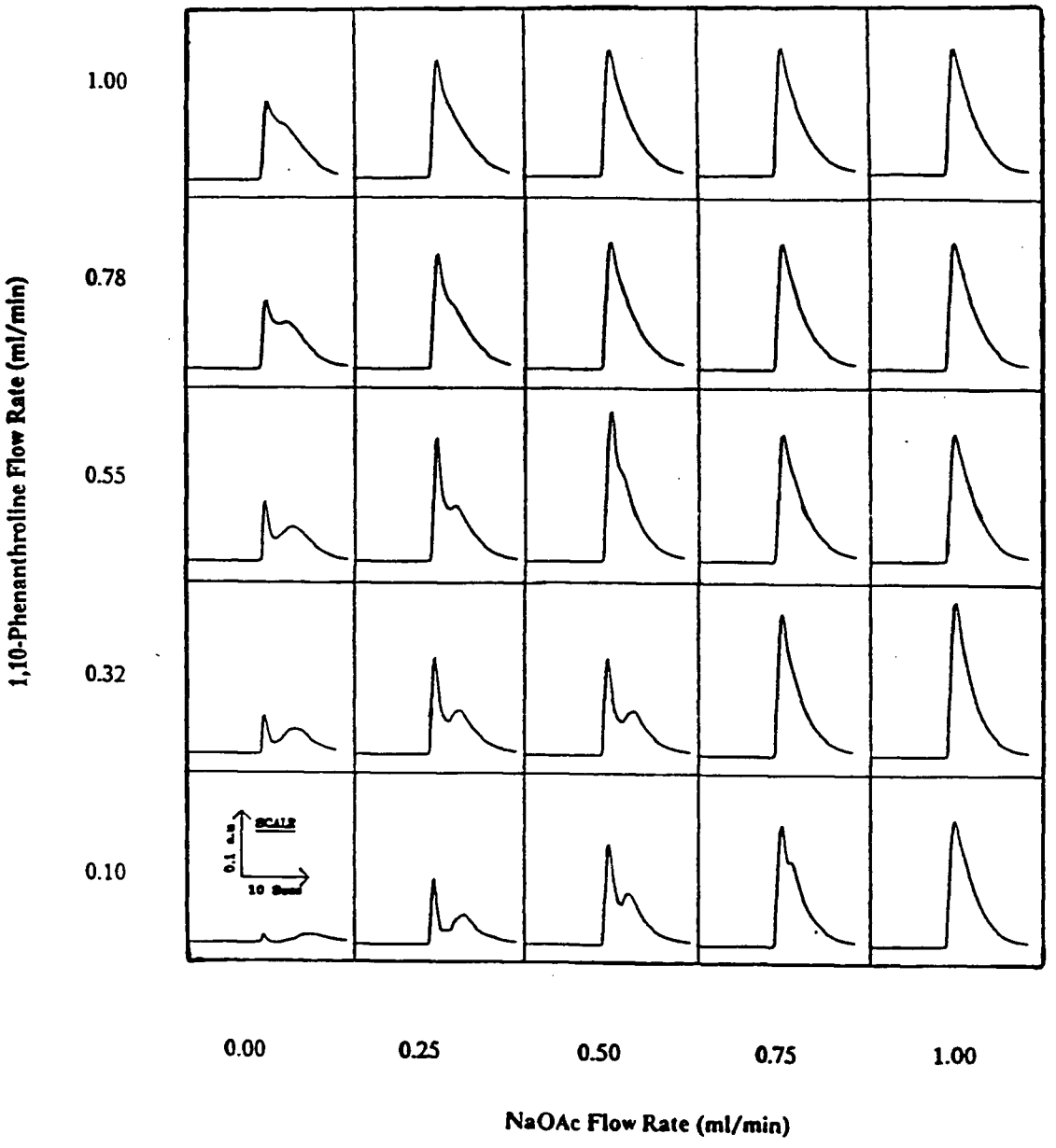

Figure 4.16a Higher dimensional response surface representations showing effect of sodium acetate and phenanthroline concentrations on peak shapes for Fe(II) / 1,10-phenanthroline reaction at 508 nm.

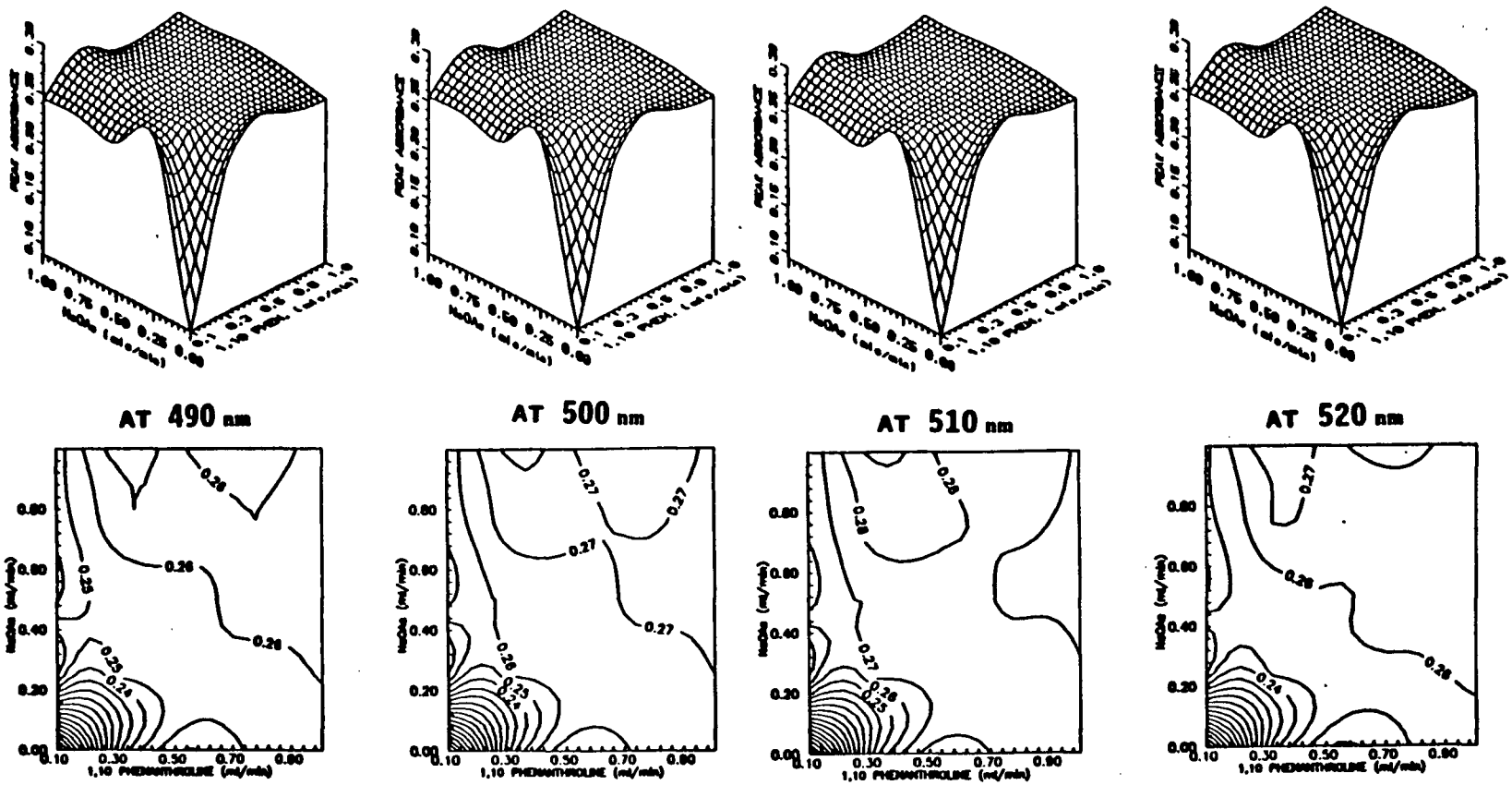

Figure 4.16b Higher dimensional response surface representations showing the effect of sodium acetate and 1,10-phenanthroline concentrations on absorbance at peak maximum response surfaces for different wavelengths for the Fe(II) / 1,10-phenanthroline reaction.

Ideally, one would wish to observe all of these dimensions of data at once, since the UV-visible spectrum observed at the flow cell may itself vary across the peak. [166] This is especially so in flow injection methods which incorporate a pH gradient, asymmetrically merged zones of reagents and sample, or reactions which have kinetics such that absorbance changes significantly whilst the peak is passing through the detector. The analysis of flow injection peak shapes is an area which requires much more work.

4.2.5.5.1 *Variation in peak shape as a function of flow and chemical contributions*

Factors that change the dispersion and reaction of a sample plug in a flow injection manifold will affect both the shape and the height of the transient signal observed. While many flow analysis methods record only maximum peak height (baseline subtracted), a knowledge of both peak shape and magnitude across the search space is useful. Both characteristics should perhaps be used in choosing optimum experimental conditions. Indeed this is commonly already done "by eye", as most flow systems are "optimized" so that they give a high, skewed Gaussian peak shape without shoulders, bifurcation or excessive tailing. Figure 4.16a shows the effect of two chemical variables on absorbance *vs.* time profiles. Since these data were taken using a constant total flow rate it is obvious that a shortage of either reagent results in bifurcated peaks, but that good peak shapes can be obtained at conditions other than those of maximum reagent concentrations.

4.2.5.5.2 *Variation in response surface as a function of best detection wavelength*

Response surfaces which show the effect of two chemical variables and observation wavelength on absorbance are also useful. Photometers which are not strictly monochromatic could be more safely used where the absorbance does not change greatly within a specified wavelength range. Figure 4.16b proves that the shape of the Fe(II)/1,10-phenanthroline surface does not change substantially in the region of 508 nm (the normal analytical wavelength), however such surfaces for other chemistries could show formation of product(s) at some wavelengths and decrease in reagent concentrations at others.

4.2.5.5.3 *Higher-dimensionality representation of simple response surfaces based on coefficients of global models*

The gross features of the surface shown in Fig. 4.15a can be effectively modelled by:

$$\text{Pk. Ht. (a.u.)} = A[1-\exp\{(-\alpha\, f(PHEN) + -\beta\, f(NaOAc)\}] + B \qquad (4.9)$$

where:

Pk. Ht. (a.u.)	is the maximum peak absorbance in absorbance units (at the analytical wavelength),
A	fit constant, for total absorbance due to effects of the products
α	fit constant, showing the magnitude of the f(PHEN) effect
β	fit constant, showing the magnitude of the f(NaOAc) effect,
B	fit constant, for absorbance independent of the reaction (background),
f(PHEN)	flow rate of the 1,10-phenanthroline stream (ml. min^{-1}), and
f(NaOAc)	flow rate of the NaOAc stream (ml. min^{-1}).

The best fit values obtained by non-linear least squares fitting were: A = 0.225, B = 0.092, α = 3.706 and β = 4.525. The standard error of estimate (SEE) between the calculated values and the experimental values was 1.79×10^{-2}. The percentage of the *actual volume* under the response surface which is not accounted for by the model (the *residual volume*, *i.e.*, the difference between the experimental and modelled response surfaces) was 0.15%; this is indicative of the high degree of goodness of fit.

Unlike the example given in Section 3.4.3.7, the model which best fits this surface indicates a strong interaction between the two variables studied. This is obvious, too, from visual inspection of the surface; both the 1,10-phenanthroline and sodium acetate concentrations must be high for optimum analytical performance. If either is decreased, the other must be raised to achieve the same results.

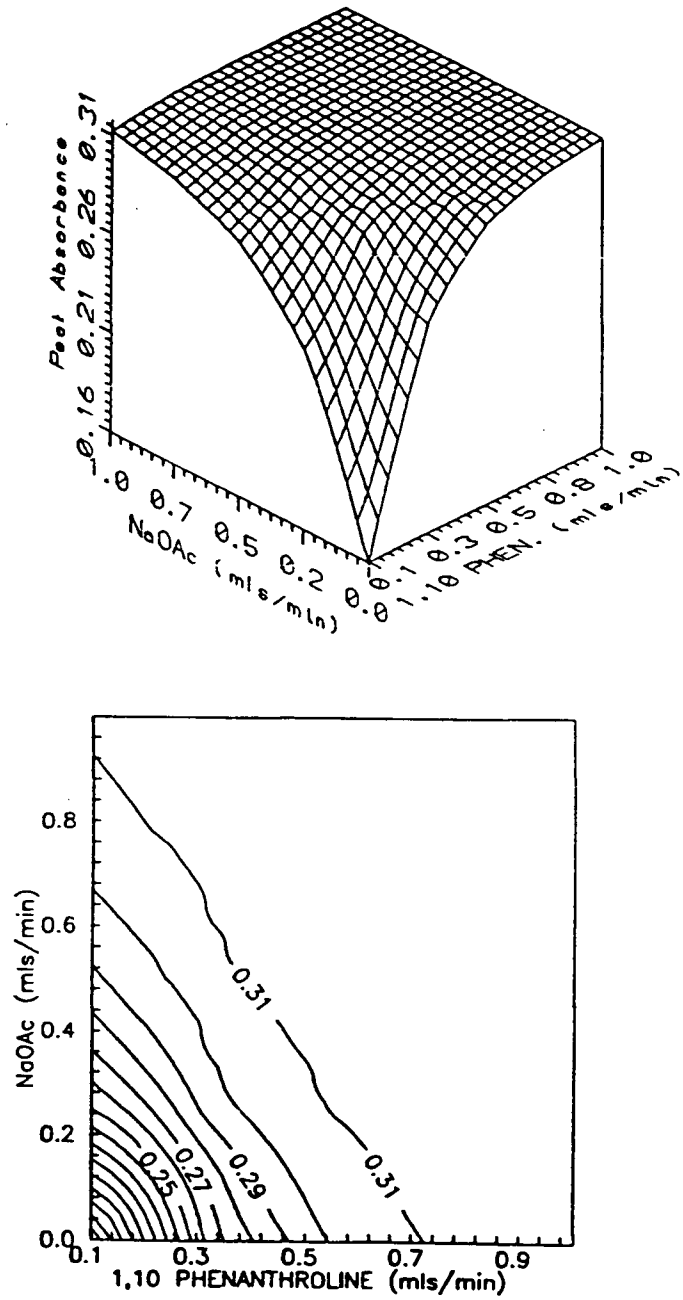

Figure 4.17 Three-dimensional response surface and contour map obtained for the model equation which gave the best fit to the absorbance (508 nm) at peak maximum surface shown in Figure 4.15a

The fit constants themselves may be considered a set of dimensions within which space a whole response surface appears as a single point. The magnitude of "external" factors (*e.g.*, a chemical interference, temperature, the analytical wavelength, *etc.*) which affect the response surface must be evident from changes in the fit coefficients, and thus as a displacement of this point from its normal position within this space.#

To demonstrate this concept, consider the surfaces for this same reaction at four different wavelengths shown in Figure 4.16b. The data set used to create these is shown in Table 4.8. Data for each surface were then fitted to the model given in Equation 4.9. The fit coefficients obtained are given in Table 4.9. From these we see that the coefficients A, α, and β are all at their maximum values at 508 nm (the usual analytical wavelength), and decrease as one moves away from this wavelength. This is a measure of the *generally* greater product detectability under all chemical conditions across the surface at 508 nm (although as shown in Figure 4.15c, the wavelength of maximum absorbance is *locally* dependent on the chemical conditions). The B (background) coefficient, while slightly higher at 508 nm, is not thought to vary significantly.

Noise in the fit constants may prove to be a limiting problem; however, because of the efficiency of the automated approach to data collection, the data used are from multiple replicates taken typically at between 25 (5 x 5) and 100 (10 x 10) sets of conditions, evenly spaced across the entire surface. The number of observations must always greatly exceed the number of parameters (here four) which are fitted. Furthermore, the precision in automated measurements is usually better than in manual. These factors can only help matters.

Recent results from this laboratory confirm similar abilities for selected peak shape analysis descriptors (a 2D analog of response surface modelling coefficients), when applied to the peak shapes shown in Figure 4.16a and others. These suggest that the magnitude of chemical and physical interferences can be observed within appropriately chosen sub-spaces.

Chemical Conditions		Analytical Wavelength, λ (nm)				
1,10-PHEN. ($ml.\ min^{-1}$)	NaOAc ($ml.\ min^{-1}$)	490	500	508	510	520
0.098	0.00	.089	.092	.093	.094	.088
..	0.25	.261	.269	.282	.278	.262
..	0.50	.239	.247	.304	.256	.241
..	0.75	.245	.254	.308	.262	.247
..	1.00	.245	.254	.313	.262	.248
0.328	0.00	.234	.241	.283	.249	.234
..	0.25	.254	.262	.304	.271	.255
..	0.50	.253	.261	.305	.270	.255
..	0.75	.270	.279	.322	.287	.271
..	1.00	.275	.283	.321	.293	.277
0.550	0.00	.271	.280	.287	.289	.272
..	0.25	.257	.265	.310	.274	.258
..	0.50	.257	.266	.313	.275	.259
..	0.75	.263	.271	.315	.281	.264
..	1.00	.259	.268	.324	.277	.261
0.772	0.00	.258	.267	.292	.276	.260
..	0.25	.257	.266	.288	.275	.259
..	0.50	.264	.273	.319	.282	.265
..	0.75	.260	.269	.320	.279	.262
..	1.00	.256	.264	.328	.274	.258
1.002	0.00	.253	.262	.312	.271	.255
..	0.25	.261	.270	.313	.279	.263
..	0.50	.265	.273	.335	.282	.266
..	0.75	.263	.272	.315	.281	.265
..	1.00	.263	.272	.320	.281	.265

Table 4.8 Raw data set of absorbance values at various 1,10-phenanthroline (PHEN) and sodium acetate (NaOAc) flow rates from which the response surface plots shown in Figure 4.16b were generated.

	Analytical Wavelength, λ (nm)				
	490	500	508	510	520
Fit Coeffs.					
A	0.187	0.196	0.225	0.198	0.188
α	2.50	2.500	3.706	2.536	2.500
β	2.50	2.584	4.525	2.599	2.499
D	0.090	0.089	0.092	0.090	0.090
Other Statistics					
Actual Volume	6.27	6.48	6.67	6.49	6.31
SEE	0.0213	0.0218	0.0179	.00165	.0212
Residual Volume	0.0711	.00069	0.150	.0467	.3314

Table 4.9 Fit coefficients obtained by fitting the data shown in Table 4.8 to the global system model (Equation 4.9).

4.2.5.6 *Advantages of the automated approach*

While automated optimization approaches offer a wide range of advantages, including fewer errors due to tired operators, care must be taken with such computer-controlled instrumentation in order to obtain meaningful results. Drift in flow rates may result in erroneous choice of optimum flow rates and "skewed" surfaces. This problem may arise due to aging of pump tubes, poor flow stability in phase separators, or precipitation (and/or clogging) in the manifold. Deterioration of some detector flow cells due to attack by organic solvents or acids may also result in problems. Temperature may vary during the course of a run, and the instability of some stock chemical solutions may limit the time allowed for an experimental run to a few hours, or less. Thus extended use of automated systems (*e.g.*, several replicates at 150 or more sets of experimental conditions) still has its problems. Improved control of instrumentation and in-run flow calibration will help minimize but not completely remove these. Attainment of widely varying flow rates with stepper-motor driven peristaltic pumps is complicated by flow pulsations which are observed most commonly at low flow rates. These result in a degradation of signal to noise ratio, and poorer repeatability, but could be minimized on this apparatus by use of stepper-motors with a finer revolution (*i.e.*, 1.5° per pulse or better, rather than the present 7°).

4.2.6 Conclusions

Flow injection has now reached a stage of maturity where scientists should perhaps change the way they think about developing new analytical methods so as to take advantage of multiple alternative *multivariate* representations of their data. Improved *multidimensional* approaches to handling high quality experimental data are a vital link between optimal experimental practice and improved theoretical insight. Further advances in the theory of flow injection can best be accomplished by use of more than a single dimension of information. Response surfaces (and their higher dimensional analogues) are

a useful way of visualizing the effect of experimental variables on the performance of a flow injection method and apparatus. The surfaces observed for different chemical systems vary greatly in shape and complexity, and the study of several different response surfaces for the same system is highly advantageous. Ultimately such experimental response surface mapping and theoretical models must come together in a unified approach.

This present work has shown that in automated methods development, pattern search methods are to be preferred over simplex-based procedures where three or less experimental variables are to be considered. While they are still experimentally more intensive, their ability to accurately map an entire surface in significantly less time than required for a manual simplex optimization is a great advantage. However, for a detailed automated optimization of systems with four or more variables, simplex may still provide the only presently viable option. For manual development of flow methods one probably still cannot better multivariate optimization procedures such as the modified simplex as they provide the most time-efficient means to improve system performance. The grid search provides more information about the shape of the response surface and for two variables may be accomplished automatically more quickly than simplex can be done manually.

Surface modelling of several system responses, probably most commonly based on multiple local models, will assist in full characterization of flow injection systems. The choice of those models which most efficiently conveys chemical information will depend highly on the chemistry under study and the manifold and apparatus used. Where global models are possible, the effect of external factors on mapping variables will be evident from changes in the relative magnitudes of the various terms in the model. Even for simple surfaces, models require multiple coefficients. Thus these coefficients will provide an additional multivariate window on the effects of external factors.

4.3 Development of a merging-zones flow-reversal FIA system

4.3.1 Introduction

The next logical step is to design new, more capable, FIA experimental techniques which take full advantage of the enhanced data capture and analysis abilities now afforded by laboratory microcomputers and multivariate chemometric methods. This Section presents a novel means whereby the interactions of two components involved in chemical reaction and physical dispersion may be probed. In this, two concentration gradients (*e.g.*, of reagent and sample) are established by conventional injections, made to overlap by the merging zones technique, and varied temporally by flow reversals across one or more fixed flow-through detectors. The result is a complex but reproducible peak profile at each of the detectors and/or detection wavelengths (*etc.*). Theoretically, given the correct amount of initial overlap between injected plugs of species 1 and species 2, the technique could provide maps of the chemical interaction effects between these species, similar to those shown in Figures 3.18, 3.25, 4.9, 4.13, 4.14, 4.15a-d and 4.16b, but generated from a single complex experiment (rather than *e.g.*, 64 or 100 the more conventional ones). This section reports the implementation of such a scheme with the FIDO automated apparatus. It goes on to detail results obtained for two chemical systems and suggest ways in which such complex data sets may initially be interpreted. Finally it tries to evaluate just how well (and for what kinds of chemical system) such an approach will live up to its full "theoretical" potential.

Despite the reality that flow injection analysis is a 3-dimensional-in-space dynamic chemical reactor, typically when we inject a plug of sample (or reagent, interferent, *etc.*) into an FIA system we still make only a single analytical measurement (maximum peak height seen by the detector) and equate this to a single concentration or to the magnitude of a single effect. However, as captured, a FIA peak is comprised of 10^2-10^3 data points at one or more wavelengths (or electrochemical measurements); information present at other

than the peak maximum is usually disregarded.

Several research groups, including this one, have sought ways to break this "information bottleneck". Specialized designs of FIA manifold have been proposed which increase the information obtained from a single sample injection (this is sometimes refered to as "multidetection"), but much more work is needed. The simplest, yet most expensive, way to perform *multidetection* in FIA has been to use multiple detectors of the same [168] or different [169] type(s), which are located either in series [170] or in parallel. [171] Other strategies have used cyclic flow systems, flow reversals, or stopped flow measurements to obtain multiple analytical readings per injection. Thus, the challenge of designing efficient FIA configurations for reproducible multidetection is highly topical and important. Ideally such systems should still require an inexpensive detector and yield multivariate data from a single sample injection.

There is a wealth of information available (or potentially extractable) from peak shapes. The use of pH gradients to generate stepped peaks for multicomponent analysis has been reported. [52] As has been shown (Figure 4.16a), peak shapes are modified by the chemical interaction of species within the FIA manifold. Sometimes interferences can cause depression of the central region of FIA peaks, [172] and thus peak height measurements alone can be misleading.

Since non-conventional peak shapes can contain more information, we decided to investigate manifolds which deliberately result in highly complex profiles. One way to generate novel (non-standard) peak shapes which have a high chance of superior information content and operator understandability is to overlap two or more concentration gradients in a reproducible manner. The rate of reaction, the extent of product formation, and the nature of the product(s) formed will all vary with position along the overlapped zones. The system proposed here combines merging zones FIA with flow reversals (MZFR-FIA) to achieve just this, and employs a diode array multiwavelength spectrophotometer. The two techniques involved here have been used separately before, [1]

with somewhat varied goals.

4.3.2 Merging Zones FIA

Merging zone techniques are based on the exploitation of the overlap and/or concentration gradients formed when at least two zones are injected and then allowed to contact each other. The profiles produced are either partially or completely overlapped (merged).

Merging zones in flow injection was originally developed as a means of conserving both reagent and sample. [1] Small plugs of sample and reagent are injected into separate carrier streams which are then allowed to merge in such a way as to cause their total overlap. Reaction then proceeds in the normal fashion *en route* to the detector. Consequently, these components do not flow continuously but would be injected only when needed.

Ruzicka *et al.* [1] used a novel merging zones technique which required only a single-line manifold; a technique they referred to as *zone penetration*. In this, two separate zones of reagent and sample are injected into the same carrier stream, simultaneously and in close proximity, using a double looped valve. The downstream zone penetrates the upstream zone from behind. Complex concentration patterns are formed on their way to the detector as these zones gradually merge. Such "information rich" composite zones are expected to yield multiple readouts, and have already been used to measure two components in one experiment.[173]

4.3.3 Flow Reversal FIA

Flow reversal techniques, on the other hand, involve the single or repetitive reversal of the flow direction of the sample plug (or a part thereof) across the detector. Betteridge *et al.* [56] used flow reversal flow injection (FR-FIA) as a versatile means for modifying the effective reaction coil length and dispersion characteristics that a sample plug sees in a FIA manifold. The viability of FR-FIA as a regime for multidetection with

the use of a single detector has been proven. [147-149] Rios et al. [148] realized the analytical potential of FR-FIA and effected a repetitive reversal of the flow direction by suitable programming of the electronic control of a peristaltic pump. They sampled a preselected zone of an FIA peak and monitored the processes involving chemical reactions through the disappearance of a reagent or the formation of a product. Applications designed for routine analysis have been published (*e.g.*, ref. 151) but the approach is yet to be extensively exploited.

Different FIA peak profiles are obtained after every reversal cycle. The peak shape becomes more Gaussian and the width at peak base also increases with the number of reversals as the plug has more time to disperse within the carrier stream. More complex shapes should be expected because of the varying degrees of both chemical and physical kinetic interactions.

4.3.4 Merging Zones-Flow Reversal FIA

The simplest possible MZFR-FIA design is where both the sample and reagent are injected into separate carrier streams which are then merged to give a single stream prior to reaching the detector. The direction of the merged stream is then reversed such that the zones move back and forth across the detector several times. This provides controlled dispersion, and facilitates complex chemical interaction across the region of overlap of the offset concentration gradients. The two chemical components can be reagent(s), sample, pH modifiers, neutral salts which determine ionic strength, or interferent(s). Several detectors can be used.

The interplay between two chemical gradients during merging zones and flow reversals generates information which lies on a two dimensional chemical surface, the axes of which are the concentrations of the two injected plugs. A third axis which must also be considered is time, since kinetic considerations dictate that some reactions will not proceed instantaneously. The MZFR-FIA approach provides an excellent opportunity to develop

novel analytical applications. Examples of applications which might benefit from such an approach include; multicomponent analysis, speciation studies, chemical kinetic studies and chemical interference studies.

Wade *et al.* [174] did a computer simulation study which suggested that a combination of several detectors, merged zones, flow reversals, and a pH gradient would facilitate characterization of a pH vs. reagent concentration surfaces within a single injection for use in novel applications. The model simulates the two injected components as initially plug-shaped zones which become Gaussian with time. On merging, reagent concentrations are decreased by the appropriate dilution factor, but pH is assumed to remain constant. They showed that it was advantageous to use multiple detectors, spaced at regular intervals along the tube after the merging tee, since this obtained far greater coverage of the two-dimensional chemical search space. However, this model was limited, as it was only appropriate for very rapid, reversible chemical reactions (*e.g.*, indicators + acid or base).

Stults [175] and Wade then constructed a semi-automated apparatus on which the combined use of the merging zones and flow reversal flow injection analysis techniques was first attempted. This indicated that the MZFR-FIA approach had good potential. However, limitations of their apparatus prevented anything more than preliminary studies. Specifically, available equipment was insufficient for independent control of flow rates and direction, and automated injection of the two components; only a single automated injection valve was available, and this was used to effect the flow reversal. These problems led to poorer reproducibility than is possible (and perhaps necessary).

It was therefore of considerable interest to us to utilize the capabilities of the FIDO analyzer to continue these exploratory MZFR-FIA studies, and so circumvent the earlier problems caused by lack of automation. Indeed, the three-valve injection unit on the FIDO analyzer was constructed with this use in mind. It has allowed different experimental profiles to be generated under different merging zone conditions and reversal times. Examples are provided and their multivariate nature shown.

4.3.4.1 *Experimental section*

4.3.4.1.1 *Reagents*

All reagents used were analytical grade and their solutions were made up in distilled water (unless stated otherwise). A 0.5% (wt./v) stock solution of bromothymol blue (Matheson Coleman & Bell Co., Norwood, Ohio, USA) was prepared by first dissolving 0.5 g of the solid in 25.0 ml of absolute ethanol, and then making up the volume to 100 ml with 0.01 M sodium tetraborate solution (BDH Chemicals Ltd, Poole, England). Working solutions of bromothymol blue (0.01% wt./v) were obtained by appropriate dilution with 0.01 M sodium tetraborate solution.

4.3.4.1.2 *Software description*

The complexity of these experiments has required the development of an Automation Command Language (ACL) for the FIDO system, details of which are given in Appendix 2.

Details of the specific program (REVMERG.BAS) used to control MZFR-FIA experiments on the FIDO system are given. The timing of actions such as flow reversals, injections, *etc.*, must be exactly known and be totally reproducible so as to ensure identical plug shapes for replicate experiments. Thus, these can only be obtained by use of a fully computer-controlled instrument. This program consists of about 83 Kbytes of source code and was written in Microsoft QuickBASIC version 4.0. It contains routines necessary to control one Alitea high precision peristaltic pump (expandable to two), two syringe pumps, the 5-channel peristaltic pump unit and the injection valves.

For the sake of standardization and efficient operation, different pumps have been assigned specific tasks. Physical pump numbers 1 and 2 of the 5-channel peristaltic pump unit (or any combination of pumps of the 5-channel peristaltic pump unit) have been designated to fill the two injection valve loops. The syringe pumps initially propel the respective carrier streams for zone merging. The Alitea pump performs the flow reversals.

To set up MZFR-FIA experiments, the user enters a sequence of events to be executed. This includes information on the device(s) (*e.g.*, pump, valve) involved in each event, the actions to be taken, and the time of the action. The user is first prompted for the number of flow reversals to be executed and their corresponding times. The times and durations for the injection of the respective plugs, the type of detector(s) to be used, and duration of the experiment are then entered. The REVMERG.BAS program sorts the events according to their timing sequence, and then executes them.

Initial Conditions

The start of an experiment is at time, t = 0.

Valves are both initially in the fill position.

The Alitea pump will first run in the forward direction, but is stopped.

Both syringe pumps are stopped.

Irrespective of the detector chosen (diode array, simple photometer or pH electrode), data points are acquired at the rate of 5 Hz. Real time display of the acquired data points on the computer screen is provided. Currently, only data points from one detector output can be displayed in real time on the screen, but this can be increased as the need arises.

4.3.4.1.3 *Manifold configuration*

The MZFR-FIA manifold used is as shown in Figure 4.18. The distances from V1 and V2 to the merging tee are identical. All coil lengths were fixed, and were of 0.8 mm i.d. PTFE tubing. The injected volumes of S1 and S2 were *ca.* 70 μl. The 500 cm and 300 cm coils were knotted so as to minimize axial dispersion and maximize radial mixing. Their lengths were chosen so as to allow up to 3 reversals across the detector (D), without loss of portions of the plugs out of their ends. Greater lengths than these resulted in increased back-pressure, which caused problems with pumping. The two reservoirs shown

are to ensure a constant pressure within the system (at constant flow rate) and to prevent the reversal pump (RP) from pumping air.

4.3.4.1.4 Types of experiment

Several types of experiment are possible with this configuration because of the independent operation of all valves and pumps. If the flow rates C1 and C2 are identical, and S1 and S2 are injected simultaneously, then a symmetric overlap of the injected plugs is accomplished. Offset (incomplete overlap) of the two plugs is achieved if C1 differs from C2 or injections of S1 and S2 are not simultaneous, but are separated by some user-defined time interval.

Alternatively, different overlap can be effected by physically modifying the manifold (as was done by Stults[175]). This entails insertion of a delay coil length just before the confluence point in one of the carrier streams, and/or use of different injection loop sizes.

Several other MZFR-FIA manifold designs are also possible. For example, one can effect flow reversals by use of valve(s), rather than by reversing the pump direction. [175] Furthermore, these and previous studies have all used fixed flow rates. Incorporation of flow programming (continuously variable velocity *vs.* time profiles) will provide a further dimension of flexibility.

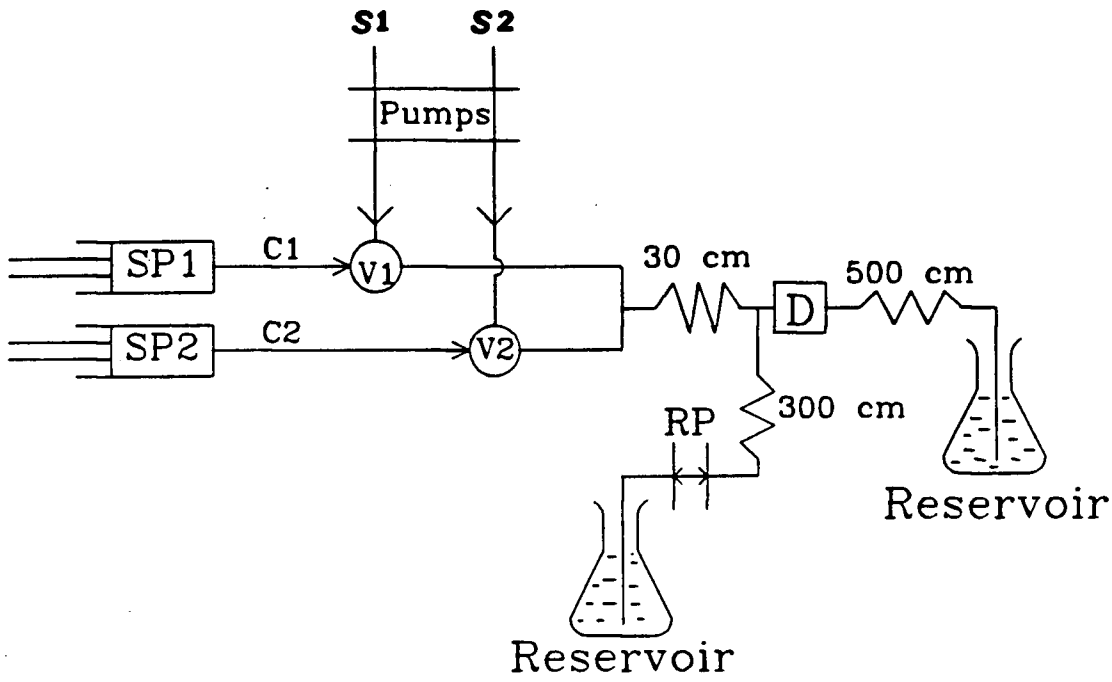

Figure 4.18 FIA configuration used for merging zones-flow reversal experiments. This is comprised of syringe pumps SP1 and SP2 propelling carrier streams C1 and C2 at a flow rate of 0.50 ml min^{-1}. V1 and V2 are six way injection valves equipped with 70 μl loops. RP is the pump used for reversal of direction of flow, and D is a single colorimetric detector.

4.3.4.1.5 *Dispersion calibration*

Calibration experiments were carried out so as to properly characterize dispersion in the system. These allowed prediction of the shape of various chemical concentration and pH gradients. The MZFR-FIA system configuration used is given in Figure 4.18. Distilled water was used as carrier streams C1 and C2 respectively, each flowing at 0.5 ml. min^{-1} to give a combined total flow rate of 1.0 ml min^{-1}. The separate streams merged at the tee-piece. The resulting stream was allowed to move towards and past the detector, D. The flow directions were reversed every 40, 50, 60, or 80 s intervals

respectively for a predefined number of cycles after the syringe pumps were stopped. The reversal pump, RP was used to effect the changes in direction of flow. The experiments were performed in triplicate.

The dispersion characteristics of both arms of the manifold under these conditions were determined separately. A 0.01% (wt./v) solution of bromothymol blue was first injected as S1 into carrier stream C1, and the detector response recorded. At this time, no injection was made in the second carrier stream, C2. Once the dispersion characteristics of the first stream was obtained, the same procedure was repeated, except that S2 was injected into the carrier stream C2, with no injection of S1 into C1. Profiles from the two sets of experiments were then compared to ascertain the degree of overlap between the respective plugs. Finally, both S1 and S2 plugs were simultaneously injected into their respective carrier streams (theoretically, the result obtained here should be the sum of those from the previous two sets of experiments).

Similar experiments were carried out in which overlap between the plugs was asymmetric. This was effected in an automated manner by offsetting the injections of the respective plugs by some time interval.

4.3.4.2.*Results and discussion*

4.3.4.2.1 *Symmetric overlap*

Figure 4.19a shows typical peak profiles observed as a result of three reversals carried out at intervals of 40 s. Figure 4.19b shows the same, but at intervals of 60 s. The peak maximum in each set of curves occurs at the same time (within experimental error), thus indicating complete overlap. The peak maximum for S2 (Figure 4.19a,b (II)) was found to have a higher peak magnitude than S1. This is due to an unexpected difference in volumes of sample loop injections.

Figures 4.19 a,b (III) are the experimental "composite traces" obtained when the two plugs are injected simultaneously. As expected, good agreement is seen between curve III

and the sum of curves I and II.

By plotting the absorbance values shown in Figure 4.19a (I) against those in Figure 4.19a (II), for all times, we can obtain a two dimensional representation of how S1 concentration varies with S2 concentration during the experiment shown in Figure 4.19a (III). Figure 4.20 represents the two surfaces obtained from the Figure 4.19 data. Since the plugs were meant to be of identical size, and were injected simultaneously, complete overlap should result. This should be seen on Figure 4.20 as a series of overlapped straight lines of 45^{o} slope, one per passage of the plugs (or parts thereof) across the detector, with the extent of the line decreasing with the flow reversal number. Such results are obtained perfectly by numerical simulation; [174] the present setup could not reproduce this perfectly because of the asymmetry which arose from the loop sizes for S1 and S2 being slightly different (simulation results similar to the experimental results are obtained when this effect is included). Thus, the first important result from this study is that plots such as given in Figure 4.20 allow the degree of symmetry of merging zones FIA systems (including contributions from flow rates, coil lengths and loop sizes) to be determined.

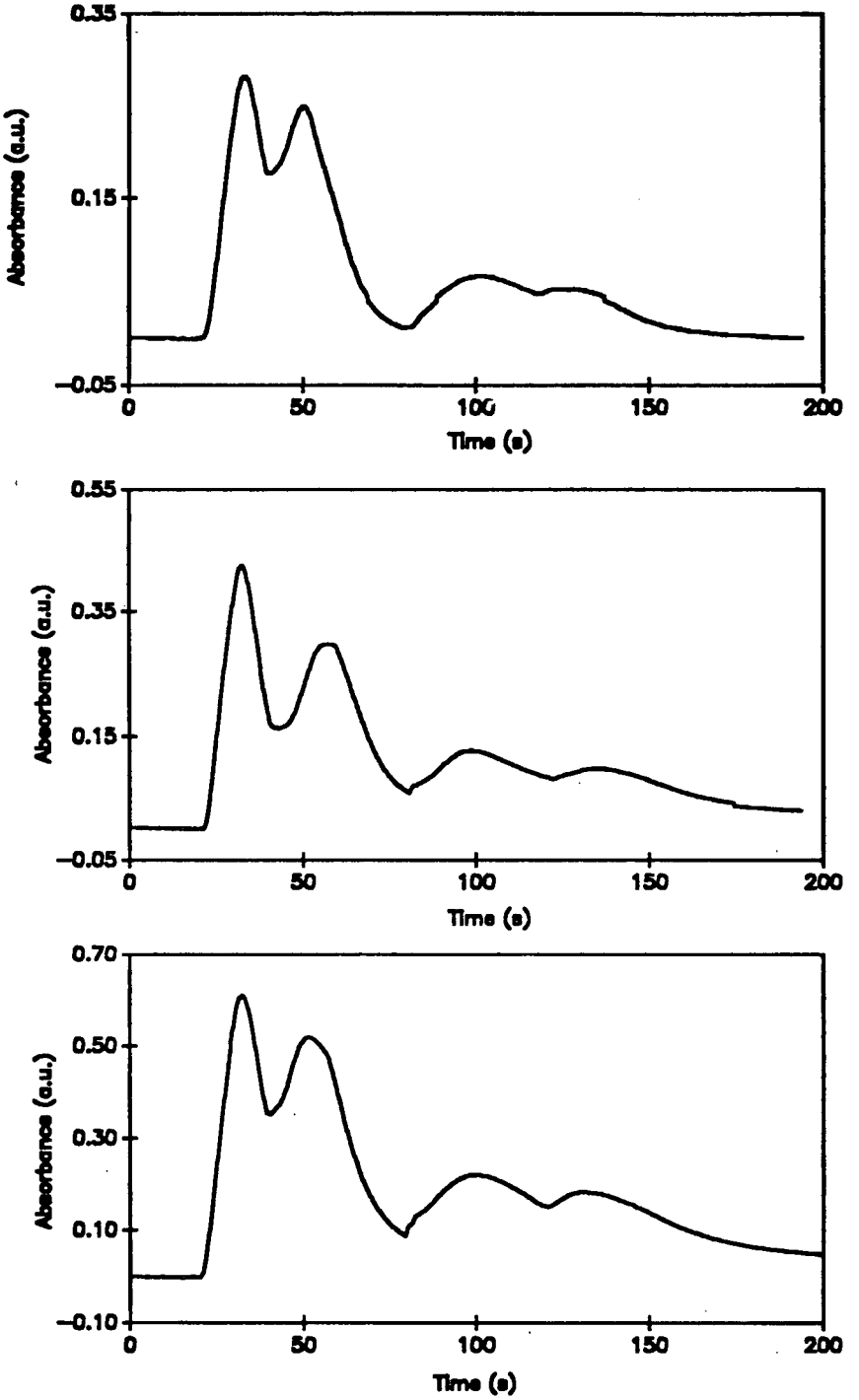

Figure 4.19a Typical FIA profiles for three reversals carried out every 40 s following injections of; I - S1 only, II - S2 only and III - injection of S1 and S2 simultaneously. Double peak seen in the figure is because the plug is not completely over the detector after the first 40 s.

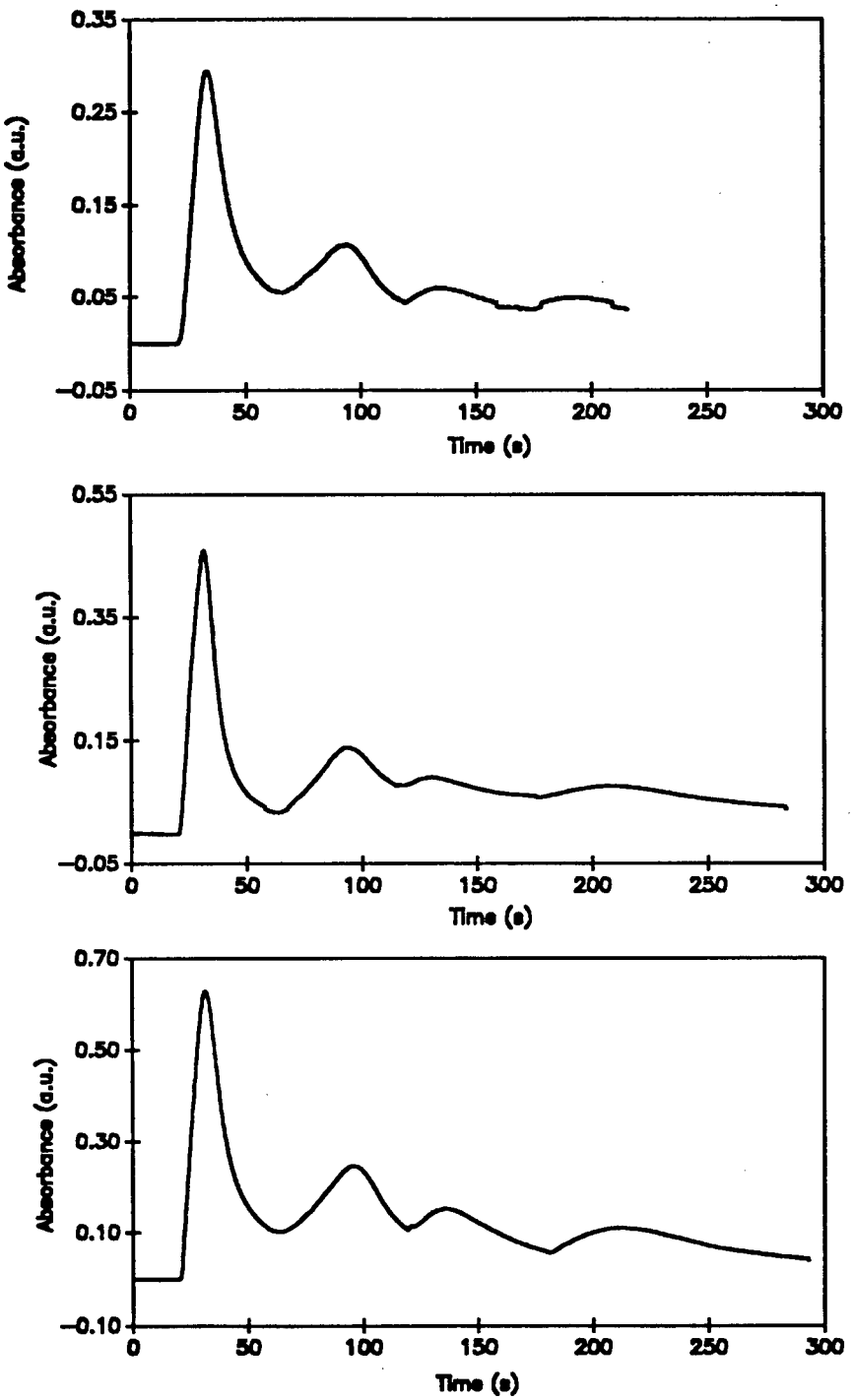

Figure 4.19b Typical FIA profiles for three reversals carried out every 60 s following injections of; I - S1 only, II - S2 only and III - injection of S1 and S2 simultaneously.

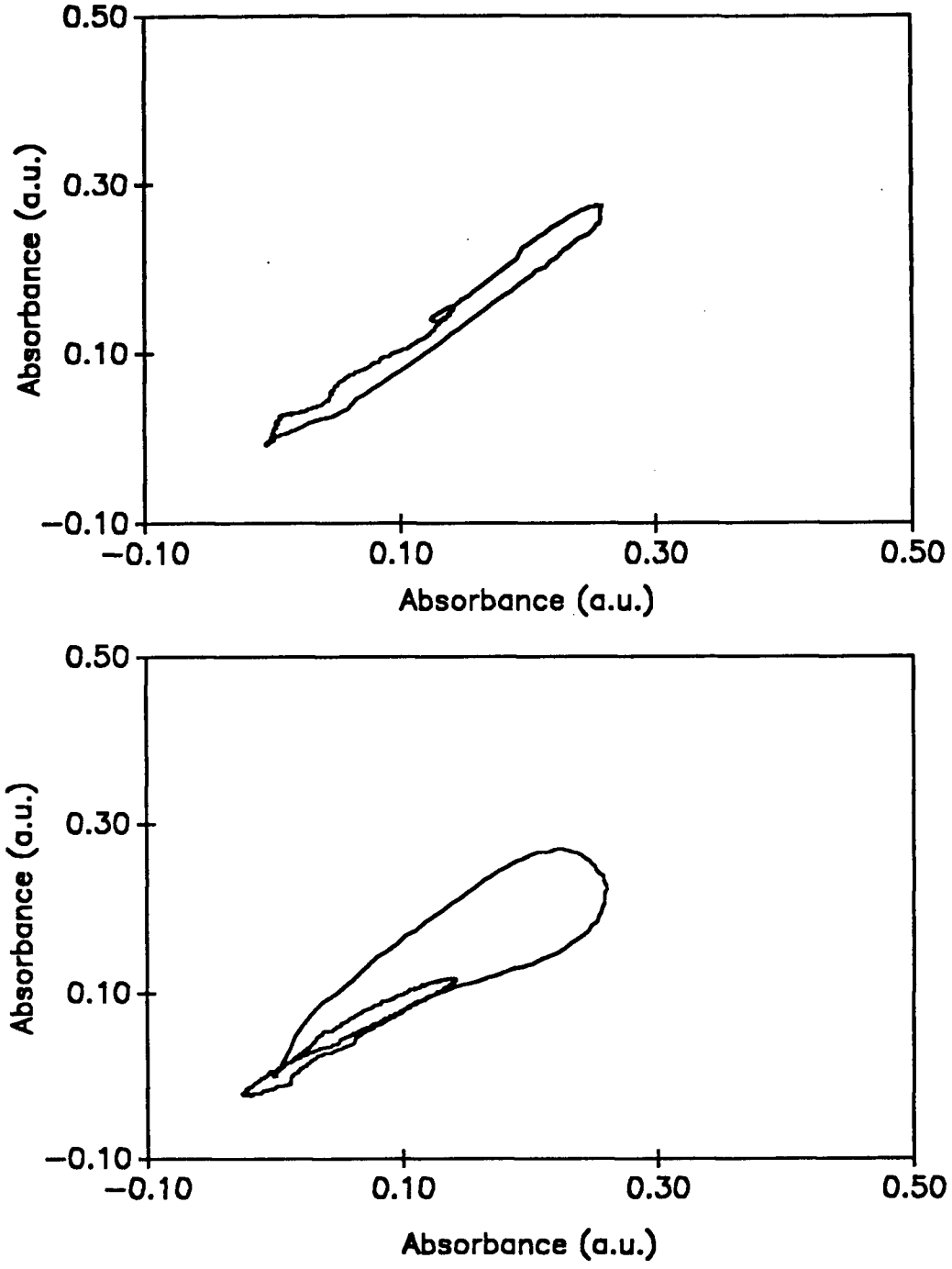

Figure 4.20 Two-dimensional plots of S1 absorbance vs. S2 absorbance after simultaneous injections of S1 and S2:
a) from reversals at 40 s intervals;
b) from reversals at 60 s intervals.

4.3.4.2.2 *Asymmetric overlap*

The effect of offsetting the injection of the two dye plugs causes a significant increase in the coverage of the 2D surface. Some elements of the dye plug S2 were caused to arrive at the detector earlier than those of S1. The extent of the asymmetry obtained may be varied by changing the offset time interval for S1. This alters the extent of overlap and thereby creates alternative experimental conditions. Figure 4.21 shows the changes in the 2D representation observed with varying offset injections times. The initial portion of each of these curves lies parallel to the S2 axis. This is due to initial sensing of S2 only by the detector. Thereafter the detector sees conditions of at least partial overlap of the two zones (as is evidenced by the more central locations of the points on the 2D surface. Just as with the "lines" in the "symmetric" example, each elipse results from one flow reversal. The contraction in size of the ellipses is due to the increased axial dispersion. Thus these points on the surface represent regions of efficient mixing between the injected components. Because of the Beer's Law of additivity of absorbances, for these calibration experiments the surface obtained is planar, and sloped with increasing concentration of S1 and S2.

At each point on the ellipses, we have a measurement of absorbance seen by the detector. However, in the present studies a large gap in information exists between the elipses. Simulation studies have shown that this is because of the use of a single detector, and that multiple detectors can provide additional ellipses which lie between those observed experimentally. However, with the help of a surface fitting routine which uses continuously adjustable weighting factors, one can interpolate a good fit over the entire 2D surface. Thus better visualization of the effect is possible.

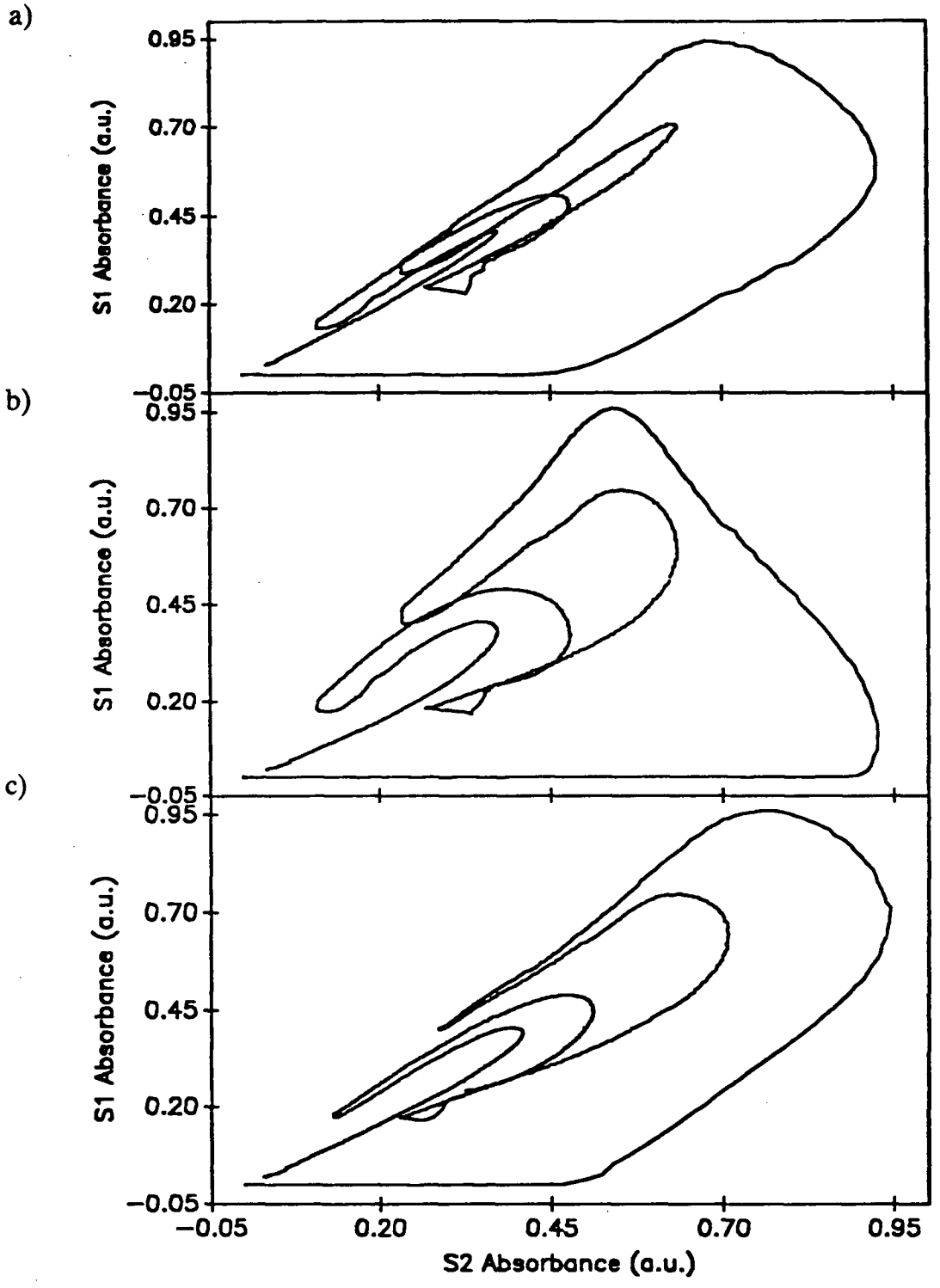

Figure 4.21 Two-dimensional plots of absorbance of S1 vs. absorbance of S2 for three reversals;

(a) with injections of S1 and S2 after 10 and 5 s respectively;
(b) with injections of S1 and S2 after 15 and 5 s respectively;
(c) with injections of S1 and S2 after 15 and 10 s respectively.

The MZFR-FIA studies presented above indicate what is observed in the absence of a chemical reaction, for two components of equal absorptivity and at a single wavelength. In order to use this system to study real chemical systems, S1 and S2 are different chemical species and reaction is present. From this, more complex response patterns are expected, which also will differ with overlap.

4.3.4.3 *Extension to a chemical system*

The MZFR-FIA experiment reported below illustrates that such profiles can be generated. A pH-dependent complexation reaction was chosen to test the efficient operation of the developed software and apparatus. The chemical system chosen was the determination of Fe(II) with the reagent 1,10-phenanthroline, as discussed earlier in this Chapter. Optimal and suboptimal pH conditions for this reaction were generated using the configuration given in Figure 4.22 by means of a pH gradient. Symmetric overlap between an Fe(II) sample concentration gradient and a reagent-pH gradient was initially investigated, with the intention of then going to asymmetric overlap.

4.3.4.3.1 *Experimental section*

4.3.4.3.1.1 *Reagents*

A HCl/KCl solution at pH 2 was prepared by diluting a solution mixture of 25.0 ml of 0.2 M KCl (BDH Chemicals, Toronto, Canada) and 6.5 ml of 0.2 M HCl (BDH Chemicals, Toronto, Canada) to 100 ml with distilled water. A 0.1 g 1,10-phenanthroline reagent solution was made in 100 ml HCl/KCl (pH 2) solution. A more alkaline solution of the 1,10-phenanthroline was made by dissolving 0.1 g in 100 ml solution of 1.0 M sodium acetate (Matheson Coleman & Bell Co., Norwood, Ohio, USA) made in water. An aqueous solution of Fe^{2+} was prepared by dissolving 0.07 g ferrous ammonium sulphate (Matheson Coleman & Bell Co., Norwood, Ohio, USA) into 1 L solution containing 2.5 ml concentrated sulphuric acid (15 M) (BDH Chemicals, Toronto, Canada) and 10 g hydroxyl ammonium hydrochloride (Anachemia Ltd, Montreal, Canada).

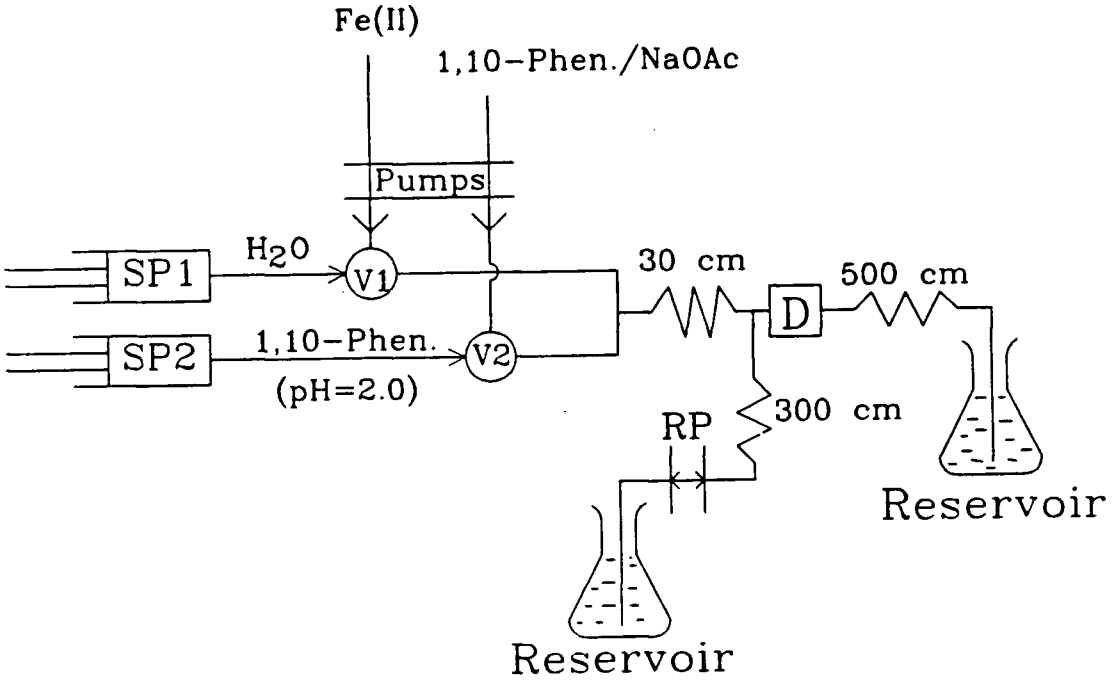

Figure 4.22 FIA configuration for the merging zones flow reversal experiments used with the Fe(II)/1,10-phenanthroline chemical system. This is comprised of syringe pumps SP1 and SP2 propelling water and 1,10-phenanthroline respectively at flow rates of 0.50 ml min^{-1}. V1 and V2 are six way injection valves equipped with 70 μl loops. RP is the pump used for reversal of direction of flow, and D is a single colorimetric detector.

4.3.4.3.1.2 *Manifold configuration*

In the configuration shown in Figure 4.22, 70 μl of 1.0 M sodium acetate solution (pH 10) containing 1,10-phenanthroline solution was injected into a carrier stream of 1,10-phenanthroline made up in a HCl/KCl buffer solution of pH 2.0. This created the pH gradient (at a constant reagent concentration), which was then symmetrically merged with a 70 μl plug of acidified Fe(II) in distilled water. The flow direction of the merged plugs was reversed once across the detector, after a predetermined time interval, Δt. Several different Δt values were studied.

4.3.4.3.2 *Results and discussion*

Figure 4.23 shows the profiles generated for each Δt value. A characteristic feature of these plots is the overlap of high pH conditions with maximum product formation. The increase in peak area after the first flow reversal is from increased product formation (at greater *t*). This suggests that this approach may have value in studies of chemical kinetics.

The pH and absorbance profiles are not perfect. The photometric and pH cells have 30 μl and 50 μl volumes respectively. These contributes to peak broadening. An offset is caused by the two cells being separated by *ca.* 5 cm; in an ideal MZFR-FIA system they would be at the same point. The pH profiles are also broader than they should be, because the electrode has a slower response time. The pH-cell acts as a mixing chamber and causes a decrease in the detectability of rapid changes in pH seen by the chemistry.

The multiple shoulders evident in the peak profiles after reversal are due to the effect of pH on the reagent / analyte interaction. Attempts to explain the origins of the small humps in Figure 23d,e,f have so far failed; because of this, the more complex *asymmetric* studies have not been done. A more complete knowledge is needed of the interaction of the kinetics of reaction and mixing in these systems. Combination of extensive further simulation and experiments may allow the curves to be fully understood. Such a study is beyond the bounds of this present thesis, but should be attempted.

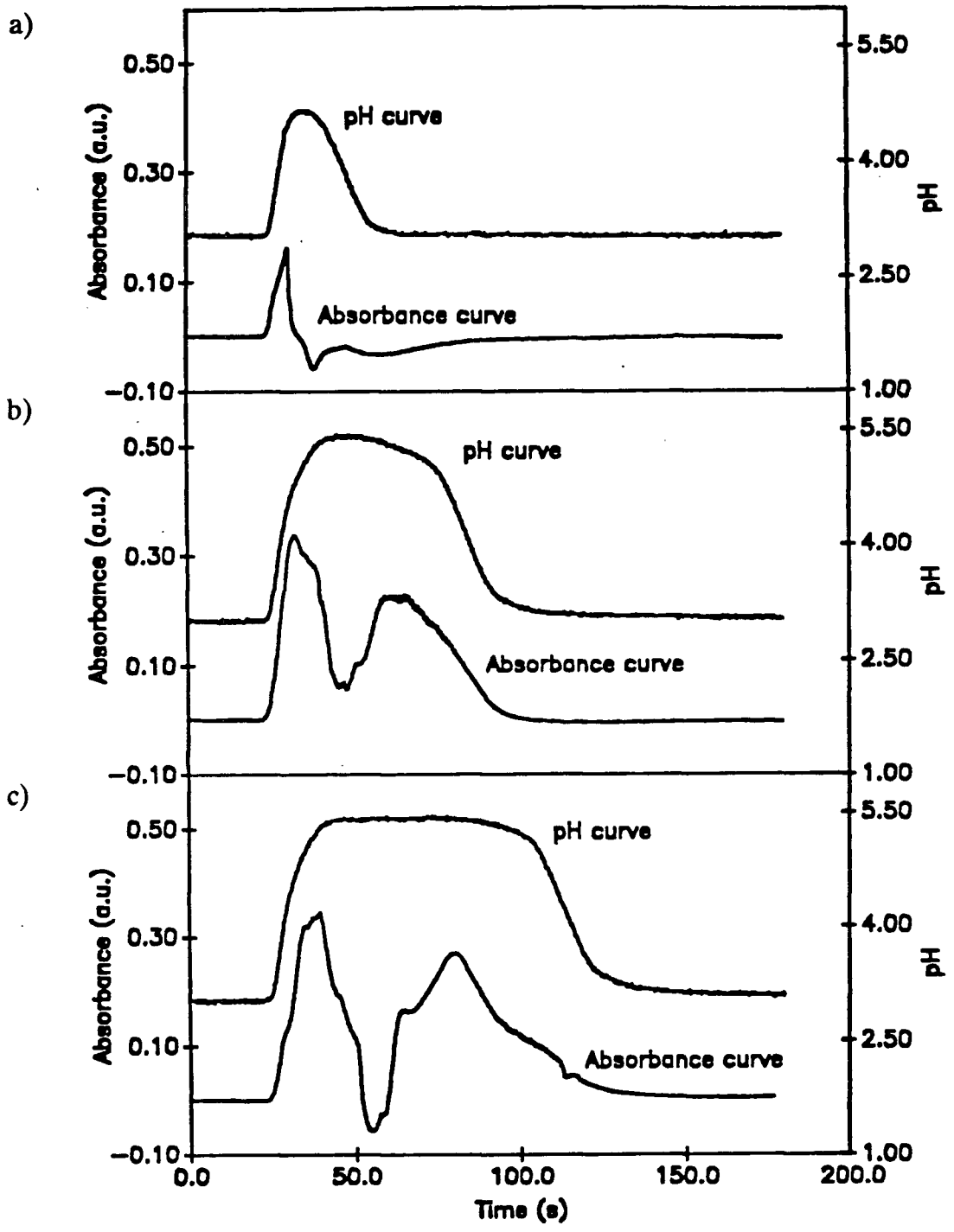

Figure 4.23 Composite absorbance (a.u.) and pH profiles for the Fe(II) / 1,10-phenanthroline chemical system following reversals at intervals of;

(a) 30 s, (b) 40 s, (c) 50 s.

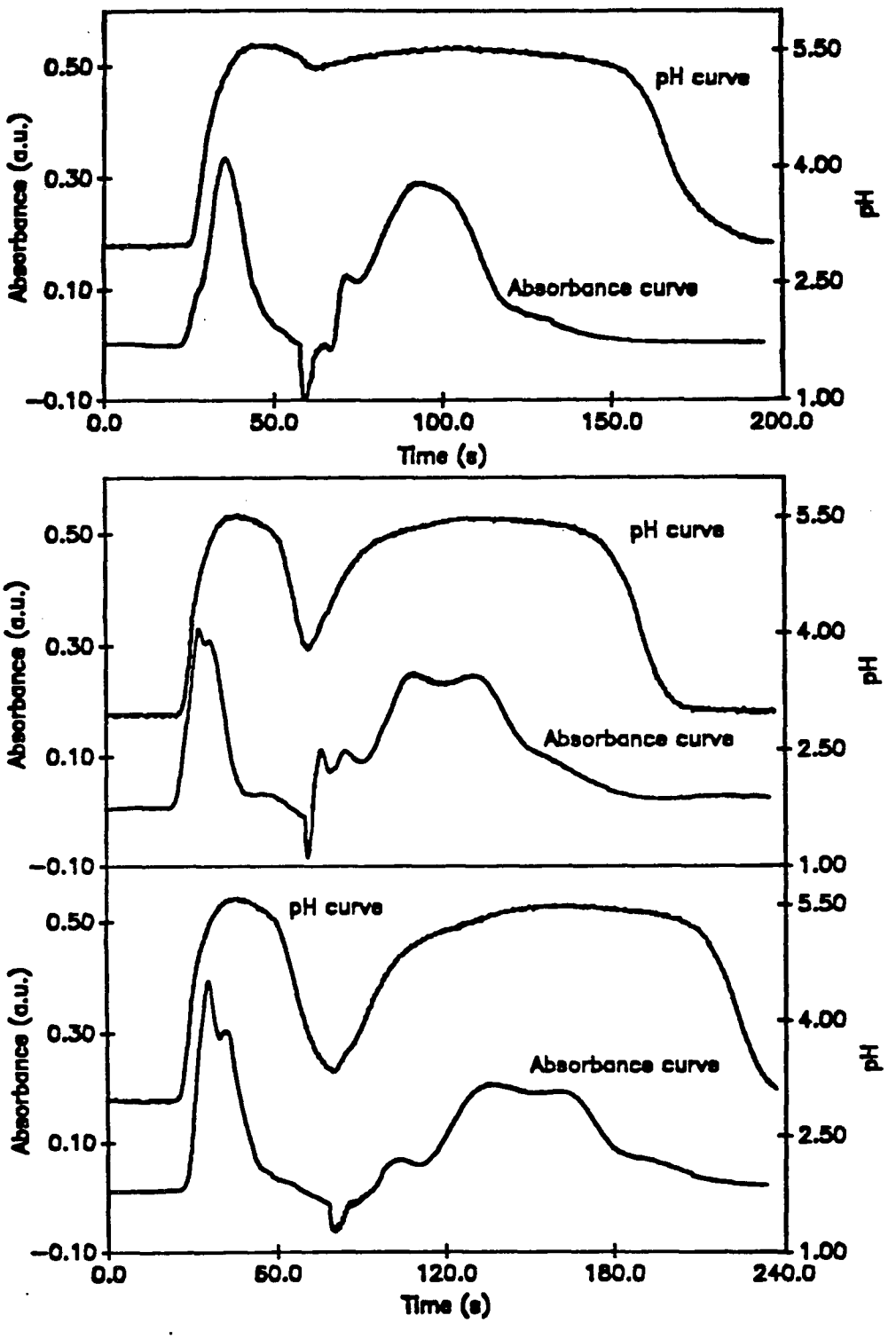

Figure 4.23 Composite absorbance (a.u.) and pH profiles for the Fe(II) / 1,10-phenanthroline chemical system following reversals at intervals of;

(d) 60 s, (e) 70 s, and (f) 80 s.

4.3.4.3.3 *Conclusions*

A significant improvement in automation and reproduciblity of the observed peak profiles over the previous attempt [175] was obtained. The previous study [175] used two photometric detectors but did not include direct measurement of pH. Our use of a pH cell confirmed that the pH gradient was being formed reproducibly; however, the offset (between photometric and pH cells) and the additional dead volume are disadvantages. Another limitation of the present MZFR-FIA system is the lack of multiple detectors along the flow manifold, which would provide more data points across the 2D surfaces.

The dye calibration experiments showed that overlapping chemical concentration gradients can be generated, *and subsequently modified* in a reproducible manner, using the combination of merging zones and flow reversals.

The Fe(II)-1,10-phenanthroline study showed promise for *in situ* evaluation of optimum pH (of course, this could be achieved with a simpler manifold). Suggestions for further development of this "2D-FIA" approach are given in chapter 5.

These studies have verified that the software and apparatus were adequate for operation of one of the most complex FIA experiments ever proposed in an efficient and reproducible manner.

CHAPTER 5

SUGGESTIONS FOR FURTHER WORK

5.0 Introduction

There are still many ways in which the capabilities of the FIDO system can be improved to increase its flexibility and measurement precision. Some of these advancement strategies and suggestions are detailed below:

5.1 Improvements to FIDO hardware

Pumps. The 7° stepper motors on the 5-pump unit should be upgraded to 1.5° or 0.75° motors, perhaps with a gearing system. Use of peristaltic pumps with more rollers and 12-bit speed selection (*e*.g., Alitea, rather than Ismatec) would improve pump speed precision and reduce pulsation effects. Addition of sinusoidal-flow syringe pumps [150] will facilitate rapid development of robust FIA methods for process control. The present ancient sequential autosampler should be updated to a random-access robotic autosampler.

Manifolds. A stream switching manifold based on miniature electrically actuated valves with all-Teflon interiors should constructed to assist in development of parallel analyses and to enable more frequent running of calibration standards. Incorporation of a 6-way stream selection valve would provide greater flexibility on reaction coil length, or use of multiple reagents.

Sensors. Additional detection systems, such as acoustic and thermal sensors, should be incorporated. This will expand the range of chemical reactions that can be studied. An array of single wavelength (or bi-color light emitting diode) detectors would facilitate better characterization of dispersion in FIA manifold. In-line flow meters (with feedback) should be added to allow frequent flow rate validation, correction, and/or recalibration. This will be particularly important for runs of more than a few hours.

Control. The control computer should be updated to an Intel 80486 to allow faster data analysis and multitasking. Data acquisition at a faster rate would allow greater signal

averaging, and so enhance the signal-to-noise ratio of the measurements. As the number and types of diagnostic sensors and detectors increases, the faster processor will become more important. It would particularly be useful for expert system and simulation studies which can be computationally intensive. A data acquisition board with 16- or 24- bit precision and software-programmable gain/offset would allow better measurements from the flow through detectors. This should have direct memory access (DMA) capability, since this would free the computer to do other tasks (*e.g.*, diagnostics or simulation) during peak acquisition.

5.2 Improvements to FIDO software

Communications and control. The operating software is becoming due for a major overhaul; its size is becoming unwieldy and it is becoming difficult to make new additions run within the available memory. Further "modularization" of the code will make it easier to load into memory only those routines that are needed. Furthermore it will be simpler to provide "cut back" versions of the code for use on "routine" analyzers which share the same interface design but which do not need all of FIDO's capabilities. Library routines which "bullet proof" software operation by checking common computer errors *(e.g.*, disk full, disk not present, file not found) are now available, and should be utilized. An on-line help utility should also be provided. Routines to handle new diagnostic information from flow meters, level detectors, *etc.* must be written and integrated. The control software for the diode array spectrophotometer should be expanded so as to provide greater diagnostics capabilities. Examples of problems which should be detected automatically include low (or no) light source intensity, jammed shutter, and communication problems. The kinetics fitting, graph plotting and surface plotting routines should be merged with the FIDO software. They are presently separate.

Peak shape analysis. Routines which use alternative quantitative measures of the observed signal should be developed and implemented. A knowledge base for peak shape classification should be constructed in which descriptions of peak shape and baseline abnormalities are stored. Chemometric techniques such as multivariate pattern recognition, factor analysis, principal component analysis, and knowledge-based methods would be used to determine which of the multiple time and frequency domain descriptive functions best characterize the peak shape data. The apparatus would then be capable of recognizing bad peaks and would correlate with either instrumental problems (low intensity or absence of a light source, the presence of air bubble(s) in a cell, worn pump tubing, tube blockage, leakage, *etc.*), or chemical effects (low reagent concentrations, abnormal sample pH, precipitation, reagent degradation with time, high sample concentration relative to reagent, unmatched refractive indices, *etc.*). While new to FIA, this idea has been used successfully in acoustic emission studies in our laboratory.

Expert sytem. An expert system should be developed to enable more intelligent real-time control and diagnostic decisions to be made. Such an approach has not yet been applied to FIA, and would provide (pseudo-)expert interpretation of the vast data sets which can be generated by automated systems. More advanced adaptive control algorithms could be applied, including "on the fly" wavelength selection. Such a system would improve reliability (through fault diagnostics) and efficiency (through *e.g.*, correct automated dilution steps), but would require extensive work.

5.3 "New" types of experiments

3-D layered surfaces. The effects of three chemical variables (*e.g.*, pH, reagent concentration, ionic strength) should be characterized for several analytical systems. These studies will yield multiple 3D chemical response surfaces (*c.f.*, Figure 4.16b) which are 3D layers of the 4D surface. This can be done with the present FIDO software.

Modelling of FIA response surfaces. Ways should be found to model the more complex response surfaces. Several surfaces can be obtained per reaction (as many as there are detectors and alternative responses (see Section 4.2)). From this we may get a better insight into the nature of the complex variable interactions present in FIA systems.

Comparison of surfaces obtained by FIDO and by simulation. Comparisons of response surfaces generated by computer simulation (random walk and other models) with those obtained experimentally would go a long way in providing an in-depth understanding of the complex variable interactions. This should help users in design of FIA manifolds and choice of appropriate operating conditions.

The original random walk simulation of Betteridge *et al.* [31] has recently been re-programmed to run on an 80386-based microcomputer. This has resulted in a more than 10-fold increase in the number of "molecules" that can be simulated, and an enormous increase in speed. The program should now allow simulation of pH effects, sequential reaction steps, chemical interferences, ionic strength effects, *(etc.)* which were not computationally feasible before. These systems more closely represent real systems encountered.

MZFR-FIA. Further characterization and development of the MZFR-FIA procedure has the potential of providing chemical information unique to FIA. Once present data analysis problems have been solved, extension to kinetics, speciation studies, multicomponent analysis, and other domains should be pursued. A distinction between non-equilibrium and equilibrium type reactions should be possible with the appropriate design. Recently, Agudo *et al.* [176] used a laborious flow programing flow injection method to generate conditions for formation of ML, ML_2, and ML_3 type complexes. Calatayud et al. [20] had earlier proposed a flow injection method to determine the stoicheiometry of several complexes. Similar determinations would be possible from a single sample injection using MZFR-FIA with a multiwavelength detection system.

Non-"plug" injection. Several alternative sample "injection" profiles (*e.g.*, sawtooth wave, staircase, Gaussian) can be achieved by appropriate flow-programmed pumping. These should provide alternative means for handling highly concentrated samples, help detect and possibly minimize chemical interference effects, and assist in determining reaction stoichiometry.

5.4 "New" chemistries

Speciation and multicomponent analysis. The simultaneous quantitation of various components in the same sample has major advantages over their sequential determination in separate manifolds. It may avoid tedious chemical separation or masking stages. Use of multiple detectors, including diode-array detection, makes multivariate determinations more possible. Kinetic gradients (in which different parts of the injected sample see different reaction times) can be formed. This, in partnership with appropriate multiwavelength data plus multivariate chemometric techniques, will allow determination of two or three component mixtures.

Automated study of unstable intermediates. An automated study of the formation and kinetics of unstable intermediates should be done using the present apparatus (see ref. 151).

Kinetic studies. With an appropriate FIA design, different solution elements can be made to have different residence (reaction) times. This should yield kinetic information, such as rate constants, and further facilitate multicomponent analysis based on kinetic discrimination. Initial studies should use model chemical systems for which rate constants have already been well established.

CHAPTER SIX

CONCLUSIONS

6.1 Conclusions

Development of a versatile automated continuous flow analyzer has been completed.[57] The apparatus has enabled the rapid development and characterization of six FIA methods, [53, 57, 60, 119, 151, 152] (five of which are reported in this thesis). It has captured data which allowed the operator to view the performance of FIA systems in novel ways.[53] It has allowed comparison of three different FIA modes, [151] and study of a new one (MZFR-FIA).

Much of the developmental work on the apparatus so far, has involved the use of simplex optimization and response surface mapping for optimization and characterization of FIA-based analytical schemes. It is an example of "soft automation", in that once an FIA manifold is attached, its mode of operation is determined by software. Practically, the apparatus has provided the analyst with the ability to explore as many as five dimensions of chemical information (*e.g.*, absorbance as a function of two (or more) chemical variables, wavelength and time) with unparallelled speed and efficiency.

Availability of code and circuitry schematics

Copies of these may be obtained via Dr. Wade, c/o The Laboratory for Automated Chemical Analysis, at the Chemistry Department, The University of British Columbia.

REFERENCES

1. J. Ruzicka and E. H. Hansen, in "Flow Injection Analysis", 2nd edn., John Wiley and Sons, New York, NY., 1988.

2. L. R. Snyder, J. Lavine, R. Stoy and A. Conetta, *Anal. Chem.*, 942A, **48**, (1976).

3. D. Betteridge, T. J. Sly, A. P. Wade and J. E. W. Tillman, *Anal. Chem.*, 1292-1299, **55**, (1983).

4. C. W. McLeod, P. J. Worsfold and A. G. Box, *Analyst*, 327-332, **109**, (1984).

5. D. A. Burns, *Anal. Chem.*, 1403A-1418A, **53**, (1984).

6. L. R. Snyder, in "Advances in Automated Analysis", Technicon International Congress, 1976, Vol. 1, Mediad Inc., Tarrytown, NY, (1977), p. 76-81.

7. C. J. Patton and S. R. Crouch, *Anal. Chim. Acta*, 189-201, **179**, (1986).

8. W. B. Furman, in "Continuous Flow Analysis: Theory and Practice", Marcel Dekker, New York, NY, (1976).

9 D. Betteridge, A. P. Wade and A. G. Howard, *Talanta*, **32(8B)**, (1985), 709.

10. L. R. Snyder, *Anal. Chim. Acta*, 3, **114**, (1980).

11. R. L. Habig, B. W. Schlein, L. Walters and R. E. Thiers, *Clin. Chem.*, 1045-1055, 15, (1969).

12. J. Ruzicka and E. H. Hansen, *Anal. Chim. Acta*, 145, **78**, (1975).

13. G. Nagy, Z.S. Feher and E. Pungor, *Anal. Chim. Acta*, 47, **52**, (1970).

14. K. K. Stewart, G. R. Beecher and P. E. Hare, *Fed. Proc.*, 1439, **33**, (1974).

15. J. Ruzicka and E. H. Hansen, *Anal. Chim. Acta*, 1-58, **179**, (1986).

16. D. Betteridge, *Anal. Chem.*, 832A-846A, **50**, (1978).

17. Proceedings of the International Conference on Flow Analysis, Amsterdam, (1979), *Anal. Chim. Acta*, **114**, (1980).

18. C. B. Ranger, *Anal. Chem.*, 20A, **53**, (1981).

19. K. K. Stewart, *Talanta*, 789, **28**, (1981).

20. J. M. Calatayud, P. C. Falco and M. C. P. Marti, *Analyst*, 1317-1320, **111**, (1986).

21. D. Betteridge and B. Fields, *Anal. Chim. Acta*, 139, 132, (1981).

22. K. K. Stewart, J. F. Brown and B. M. Golden, *Anal. Chim. Acta*, 119, 114, (1980).

23. W. E. Van der Linden, *Anal. Chim. Acta*, 91-101, 179, (1986).

24. B. C. Erickson, B. R. Kowalski and J. Ruzicka, *Anal. Chem.*, 1246-1248, **59**, (1987).

25. W. E. Bauer, A. P. Wade and S. R. Crouch, *Anal. Chem.*, 287-288, **60**, (1988).

26 J. Ruzicka and E. H. Hansen, *Anal. Chim. Acta*, **99**, (1978), 37.

27 S. Olsen, J. Ruzicka and E. H. Hansen, *Anal. Chim. Acta*, **136**, (1982), 101.

28. G. Taylor, *Proc. Roy. Soc., (London) Ser. A*, 219, **186**, (1953).

29. R. C. Weast, M. J. Astle and W. H. Beyer, in "CRC Handbook of Chemistry and Physics", 68th edn., CRC Press, Inc., Boca Raton, FL, 1988, p. F-47.

30. J. Ruzicka and E. H. Hansen, *Anal. Chim. Acta*, 99, **37**, (1978).

31. D. Betteridge, C. Z. Merczewski and A. P. Wade, *Anal. Chim. Acta*, 227-236, **165**, (1984).

32. A. Einstein, *Ann. Physik*, 549-560, **17**, (1905).

33. J. C. Giddings, *J. Chem. Educ.*, 588, **35**, (1958).

34. J. C. Giddings, in "Dynamics of Chromatography, Part 1, Principles and Theory", Marcel Dekker, New York, NY, (1965), p. 26-35.

35. R. Tijssen, *Anal. Chim. Acta*, 71-89, **114**, (1980).

36. J. M. Reijn, W. E. Van der Linden and H. Poppe, *Anal. Chim. Acta*, 229-237, **123**, (1981).

37. O. Levenspiel, in "Chemical Reaction Engineering", 2nd edn., John Wiley and Sons, New York, NY, (1972).

38. C. L. M. Stults, A. P. Wade and S. R. Crouch, *Anal. Chim. Acta*, 301-308, **192**, (1987).

39. C. L. M. Stults, A. P. Wade and S. R. Crouch, *J. Chem. Educ.*, 645-647, **65**, (1988).

40. C. D. Crowe, H. W. Levine, D. Betteridge and A. P. Wade, *Anal. Chim. Acta*, 49-60, **194**, (1987).

41. G. Gerhardt and R. N. Adams, *Anal. Chem.*, 2618, **54**, (1982).

42. G. D. Clark, D. A Whitman, G. D. Christian and J. Ruzicka, *CRC Critical Reviews in Anal. Chem.*, 357, **21**, (1990).

43. W. R. Wolf and K. K. Stewart, *Anal. Chem.*, 1201, **51(8)**, (1979).

44. J. A. C. Broekaert and F. Leis, *Anal. Chim. Acta*, 73, **109**, (1977).

45. S. Olsen, J. Ruzicka and E. H. Hansen, *Anal. Chim. Acta*, 101, **136**, (1982).

46. E. Martins, M. Bengtsson and G. Johansson, *Anal. Chim. Acta*, 31, **169**, (1985).

47. B. Karlberg and S. Thelander, *Anal. Chim. Acta*, 1, **98**, (1978).

48. J. F. Tyson, *Anal. Chim. Acta*, 3, **234**, (1990).

49. E. H. Hansen, J. Ruzicka and B. Reitz, *Anal. Chim. Acta*, 241, **89**, (1977).

50. C. L. M. Stults, A. P. Wade and S. R. Crouch, *Anal. Chem.*, **59**, (1987), 2245.

51. W. B. Furman, in "Continuous Flow Analysis", Marcel Dekker, New York, NY, 1976.

52. D. Betteridge, T. J. Sly, A. P. Wade and D. G. Porter, *Anal. Chem.* 2258, **58**, (1986).

53. A. P. Wade, P.M. Shiundu and P. D. Wentzell, *Anal. Chim. Acta*, 361, **237**, (1990).

54. J. A. Horner, A. P. Wade and M. W. Blades, *J. Anal. At. Spectrom.*, 809, **3**, (1988).

55. H. Bergamin, E. A. G. Zagatto, F. J. Krug and B. F. Reis, *Anal. Chim. Acta*, 71, **101**, (1978).

56. D. Betteridge, P. B. Oates and A. P. Wade, *Anal. Chem.*, 1236, **59**, (1987).

57. P. D. Wentzell, M. J. Hatton, P.M. Shiundu, R. M. Ree, A. P. Wade, D. Betteridge and T. J. Sly, *J. Automatic Chem.*, 227, **11(5)**, (1989).

58. P.M. Shiundu and A.P. Wade, *J. Automatic Chem.*, 83, **13(3)**, (1991).

59. T. J. Sly, D. Betteridge, D. Wibberly and D. G. Porter, *J. Autom. Chem.*, 186, **4**, (1982).

60. P. M. Shiundu, P. D. Wentzell and A. P. Wade, *Talanta*, 329, **37(3)**, (1990).

61. D. Betteridge, A. G. Howard and A. P. Wade, *Talanta*, 723, **32(8B)**, (1985).

62. A. Savitzky and M. J. E. Golay, *Anal. Chem.*, **36**, (1964), 1627.

63. J. M. Reijn, W. E. Van der Linden and H. Poppe, *Anal. Chim. Acta*, 105, **114**, (1980).

64. J. T. Vanderslice, K. K. Stewart, A. G. Rosenfeld and D. J. Higgs, *Talanta*, 11, **28**, (1981).

65. G. Taylor, *Proc. R. Soc. London, Ser. A*, 446, **227**, (1953).

66. D. Betteridge, W. C. Cheng, E. L. Dagless, P. David, T. B. Goad, D. R. Deans, D. A. Newton and T. B. Pierce, *Analyst (London)*, 1, **108**, (1983).

67. D. Betteridge, W. C. Cheng, E. L. Dagless, P. David, T. B. Goad, D. R. Deans, D. A. Newton and T. B. Pierce, *Analyst (London)*, 17, **108**, (1983).

68. C. C. Painton and H. A. Mottola, *Anal. Chem.*, 1713, **53**, (1981).

69. G. E. P. Box and K. B. Wilson, *J. Roy. Statist. Soc.*, B. **13**, (1951)

70. R. A. Fisher, in "The Design of Experiments," Oliver and Boyd, Edinburgh, 1935.

71. M. Friedman and L. J. Savage, in "Techniques of Statistical Analysis," in Ch. 13, C. Einsenhart, M. W. Hastay and W. A. Wallis, Eds., McGraw Hill, New York, NY, 1947.

72. S. L. Morgan and S. N. Deming, *Anal. Chem.,* 1170, **46**, (1974).

73. G. E. P. Box, *Biometrics,* 16, **10**, (1954)

74. I. B. Rubin, T. J. Mitchell and G. Goldstein, *Anal. Chem.,* 717, **43**, (1971).

75. G. E. P. Box, in "The Design and Analysis of Industrial Experiments," 2nd edn. O. L. Davies and Hafner Publ. Co., New York, NY, 1963, Ch. 11.

76. G. E. P. Box and N. R. Draper, in "Evolutionary Operation," John Wiley, New York, NY, 1969.

77. R. H. Meyers, in "Response Surface Methodology," Allyn and Bacon, Inc., Boston, Mass., 1971.

78. W. Spendley, G. R. Hext and F. R. Himsworth, *Technometrics,* 441, **4**, (1962).

79. S. N. Deming and S. L. Morgan, *Anal. Chem.,* 278A, **45**, (1973).

80. J. A. Nelder and R. Mead, *Computer J.,* 308, **7**, (1965).

81. P. D. Wentzell, A. P. Wade and S. R. Crouch, *Anal. Chem.*, 905, **60**, (1988).

82. F. Kai, Y. Sakanashi, S. Satoh and S. Uchikawa, *Anal. Lett.*, 1013, **16**, (1983).

83. Z. Marczenko and M. Jarosz, *Talanta*, 561, **28**, (1981).

84. W. M. MacNevin and O. H. Kriege, *Anal. Chem.*, 1768, **26**, (1954).

85. Z. Liu, W. Chang, J. Hong and Y. Ci, *Analyst*, 213, **116**, (1991)

86. F. E. Beamish and J. C. Van Loon, in "Analysis of Noble Metals: Overview and Selected Methods," Academic Press, Inc. (London) Ltd, 1977, Ch. 7.

87. D. Nonova and K. Stoyanov, *Mikrochim. Acta*, 143, **1**, (1984)

88. S. I. Gusev and V. A. Vinkova, *Zh. Anal. Khim.*, 552, **22**, (1967).

89. Z. Xinwei and H. Zhide, *Chem. Abstr.*, 89159d, **102**, (1985).

90. V. Michaylova, B. Evtimova and D. Nonova, *Anal. Chim. Acta*, 373, **207**, (1988).

91. K. Watanabe and M. Hojjatie, *Anal. Chim. Acta*, 111, **218**, (1988).

92. S. J. A-Bazi and H. Freiser, *Solv. Extr. Ion Excl.*, 1121, **4**, (1986).

93. S. J. A-Bazi and H. Freiser, *Solv. Extr. Ion Excl.*, 265, **5**, (1987).

94. G. H. Ayres and E. W. Berg, *Anal. Chem*, 980, **25**, (1953).

95. G. H. Ayres and B. L. Tuffly, *Anal. Chem*, 949, **24**, (1952).

96. R. Lockyer and G. E. Hames, *Analyst*, 385, **84**, (1959).

97. E. Motonori, *Chem. Abstr.*, 142339q, **108**, (1988).

98. X. Xiandeng and X. Peifang, *Chem. Abstr.*, 105545h, **108**, (1988).

99. J. W. Skrabak and D. R. Demers, *Chem. Abstr.*, 30963g, **108**, (1988).

100. A. T. Haj-Hussein and G. D. Christian, *Analyst*, 65, **111**, (1986).

101. T. Sakai and N. Ohno, *Anal. Chim. Acta*, 271, **214**, (1988).

102. S. B. Savvin and R.F. Guereva, *Talanta*, 87, **34**, (1987).

103. D. D. Perrin and B. Dempsey, in "Buffers for pH and Metal Ion Control," Chapman-Hall, London, 1974, p.48.

104. E. R. Malinowski and D. G. Howery, in "Factor Analysis in Chemistry", John Wiley and Sons, New York, NY, 1980.

105. W. M. Latimer, in "The Oxidation States of the Elements and Their Potentials in Aqueous Solution", Prentice-Hall, Englewood Cliffs, NJ, 1952, p.78.

106. W. K. Wilmarth and A. Haim, in "Peroxide Reaction Mechanisms", J. O. Edwards (Ed.), Wiley Inter-Science, New York, NY, 1962, p. 175 - 222.

107. R. B. Seymour, in "An Introduction to Polymer Chemistry", International Student Edition, McGraw-Hill, Kogukusha, Ltd -Tokyo, 1956, p. 157.

108. I. M. Kolthoff and E. M. Carr, *Anal. Chem.*, 298, **25**, (1953).

109. D. Amin and A. K. Hareez, *Analyst*, 1221, **106**, (1981).

110. D. Amin, *Analyst*, 1217, **106**, (1981).

111. I. M. Kolthoff and R. J. Woods, *J. Am. Chem. Soc.*, 13, **88**, (1966).

112. E. Boyland, D. Manson and P. Sims, *J. Chem. Soc.*, 1953, 3623.

113. K. C. Khulbe and R.S. Mann, *Journal of Chromatography*, 554, **150**, (1978).

114. H. Mullu, J. Mattusch and G. Werner, *Mikrochim. Acta.*, 349, **II**, (1980).

115. K. B. Yatsimirski, in "Kinetics Methods of Analysis", Pergamon Press, London, UK, 1966.

116. D. D. Perrin and B. Dempsey, in "Buffers for pH and Metal Ion Control", Chapman-Hill, London, UK, 1974, p.133.

117. P. R. Bonchev, *Talanta*, 499, **17**, (1970).

118. W. A. Waters, in "Mechanisms of Oxidation of Organic Compounds", Methuen, London, UK, 1964.

119. M. D. Kester, P. M. Shiundu and A. P. Wade, "Spectrophotometric Method for Determination of Sulfide with Iron(III) and Nitrilotriacetic Acid by Flow Injection", in press, *Talanta*, (1991).

120. H. Robberecht and R. Van Grieken, *Talanta*, 823, **29**, (1982).

121. E. J. Underwood, in "Trace Elements in Human and Animal Nutrition", 4th edn., Academic Press, New York, NY, **1977**, p. 302-340.

122. J. G. Morris, W. S. Cripe, H. L. Chapman Jr. and D. F. Walker, *Science*, 491, **233**, (1984).

123. E. P. Diamandis and T. P. Hadjiioannou, *Anal. Chim. Acta*, 143, **123**, (1981).

124. C. F. Mills, *Chemistry in Britain*, 512, **15**, (1979).

125. L. Magos and M. Webb, *CRC Rev. Toxicol.*, 1, **8**, (1980).

126. K. L. Nuttall and F. S. Allen, *Inorg. Chim. Acta*, 187, **92**, (1984).

127. G. N. Schrauzer, D. A. White and C. J. Schneider, *Bioinorg. Chem.*, 265, **6**, (1976).

128. G. N. Schrauzer, D. A. White and C. J. Schneider, *Bioinorg. Chem.*, 23, **7**, (1977).

129. R. J. Shamberger, T. L. Andreone and C. E. Willis, *J. Natl. Cancer Inst.*, 1771, **53**, (1974).

130. R. J. Shamberger, *Sci. Total Environ.*, 59, **17**, (1981).

131. C. I. Measures and J. D. Burton, *Anal. Chim. Acta*, 177, **120**, (1980).

132. S. B. Adeloju, A. M. Bond and H. C. Hughes, *Anal. Chim. Acta*, 59, **148**, (1983).

133. C. Chuguo, *Talanta*, 221, **31**, (1984).

134. L. Campanella and T. Ferri, *J. Electroanal. Chem.*, 241, **165**, (1984).

135. S. B. Adeloju, A. M. Bond, M. H. Briggs and H. C. Hughes, *Anal. Chem.*, 2076, **55**, (1983).

136. C. M. G. Van Den Berg and S. H. Khan, *Anal. Chim. Acta*, 221, **231**, (1990).

137. S. C. Apte and A. G. Howard, *J. Anal. At. Spectrom.*, 379, **1**, (1986).

138. M. Yamamoto, M. Yasuda and Y. Yamamoto, *Anal. Chem.*, 1382, **57**, (1985).

139. C. C. Y. Chan, *Anal. Chem.*, 1482, **57**, (1985).

140. K. L. Cheng, K. Ueno and T. Imamura, in "CRC Handbook of Organic Analytical Reagents", CRC Press, Boca Raton, FL, 1982.

141. M. Kamaya, T. Murakami and E. Ishii, *Talanta*, 664, **34**, (1987).

142. J. H. Watkinson, *Anal. Chem.*, 92, **38**, (1966).

143. R. F. Bayfield and L. F. Romalis, *Anal. Biochem.*, 569, **144**, (1985).

144. P. W. West and T. V. Ramakrishna, *Anal. Chem.*, 966, **40**, (1968).

145. T. Kawashima and M. Tanaka, *Anal. Chim. Acta*, 137, **40**, (1968).

146. J. M. Hwang, T. S. Wei and Y. M. Chen, *J. Chin. Chem. Soc.*, 109, **33**, (1986).

147. P. Linares, M. D. Luque de Castro and M. Valcarcel, *Analyst*, 1405, **111**, (1986).

148. A. Rios, M. D. Luque de Castro and M. Valcarcel, *Anal. Chem.*, 1540, **60**, (1988).

149. F. Canete, A. Rios, M. D. Luque de Castro and M. Valcarcel, *Anal. Chem.*, 2354, **60**, (1988).

150. J. Ruzicka, G. D. Marshall and G. D. Christian, *Anal. Chem.*, 1861, **62**, (1990).

151. P. M. Shiundu and A. P. Wade, *Anal. Chem.*, 692, **63**, (1991).

152. P. M. Shiundu, A. P. Wade and S. B. Jonnalagadda, *Can. J. Chem.*, 1750, **68**, (1990).

153. J. T. Vanderslice, A. G. Rosenfeld and G. R. Beecher, *Anal. Chim. Acta*, 119, **179**, (1986).

154. T. Korenaga, *TrAC, Trends in Anal. Chem.*, 323, **8(9)**, (1989).

155. J. Ruzicka, personal communication, September 1988.

156. B. R. Kowalski, J. Ruzicka and G. D. Christian, *Trends in Anal. Chem.*, 8, **9(1)**, (1990).

157. G. E. P. Box and N. R. Draper, in "Empirical Model-Building and Response Surfaces", John Wiley and Sons, New York, NY, (1987).

158. Users' Manual, SURFER^{R} graphics package (version 3.0), Golden Software, Golden, CO, USA.

159. I. O. Angell, "Advanced Graphics with the IBM Personal Computer", Halsted Press, John Wiley, New York, NY, (1985).

160. A. P. Wade, *Anal. Proc.*, 523, **20**, (1983).

161. P. D. Wentzell, *Chemometrics and Intelligent Laboratory Systems*, 283, **8**, (1990).

162. C. C. Kircher and S. R. Crouch, *Anal. Chem.*, 879, **54** (1982).

163. R. A. Day and A. L. Underwood, in "Quantitative Analysis", 5th edn.; Prentice-Hall: Englewood Cliffs, NJ, 1986.

164. S. Greenfield, M. S. Salman, M. Thomsen and J. F. Tyson, *J. Anal. Atom. Spectrom.*, 55, **4**, (1989).

165. R. S. Rowles, Ph.D. Thesis, University College Swansea, (1984).

166. M. Blanco, J. Gene, H. Iturriaga, S. Maspoch and J. Riba, *Talanta*, 987, **34(12)**, (1987).

167. J. Zupan, in "Algorithms for Chemists", John Wiley, New York, NY, (1989).

168. D. J. Hooley and R. E. Dessey, *Anal. Chem.*, 313, **55**, (1983).

169. E. A. G. Zagatto, A. O. Jacintho, L. C. R. Pessenda, F. J. Krug, B. F. Reis and Fº. H. Bergamin, *Anal. Chim. Acta*, 37, **125**, (1981).

170. R. Virtanen, *Anal. Chem. Symp. Ser.*, 375, **8**, (1981).

171. W. D. Basson and J. F. Van Staden, *Fresenius Z. Anal. Chem.*, 370, **302**, (1980).

172. D. Yalvac, "Flow Injection Analysis in Industrial Applications of Process Control and Optimization", presented at the FACSS XVII Conference, Cleveland, Ohio, October 7-12, (1990).

173. J. Ruzicka, personal communication, (1989).

174. A. P. Wade, D. Betteridge and S. R. Crouch, "Flow Reversal FIA for Rapid Speciation and Optimization Studies", presented at the FACSS XIII Conference, St. Louis, MO, October, 2nd, (1986).

175. C. L. M. Stults, Ph.D Thesis, Michigan State University, (1987).

176. M. Agudo, J. Marcos, A. Rios and Valcarcel, *Anal. Chim. Acta*, 211, **239**, (1990).

Appendix 1. Molecular structures of some compounds used

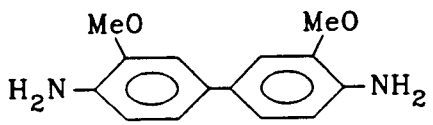

O-dianisidine (ODA)

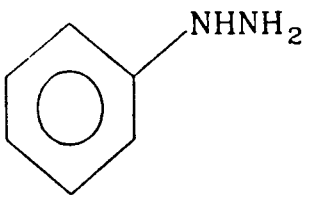

Phenylhydrazine (PHDZ)

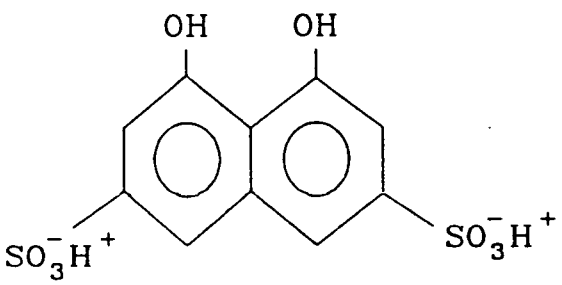

Chromotropic acid (CTA)

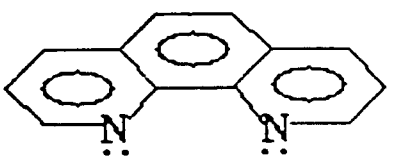

1,10-phenanthroline

Appendix 2. Automation Command Language

The ACL device and event codes used in this description are fairly self explanatory:

Device Codes

AL	Alitea pump #1 (used to effect flow reversals)
SP1	Syringe pump #1 (used to propel carrier stream #1)
SP2	Syringe pump #2 (used to propel carrier stream #2)
V1	The first injection valve on the 3-channel valve unit
V2	The second injection valve on the 3-channel valve unit

Event Codes

FWD	start the Alitea pump in the forward direction
RVS	reverse the flow direction of the Alitea pump
STP	stop an Alitea or syringe pump
RUN	start a syringe pump
FIL	switch a valve to the fill position; next, run a pump to completely fill the loop on the injector, and then stop it.
INJ	switch a valve to the inject position.

Further device and event code types may be easily added; the event codes correspond to MSQB4 subprograms which have the same names.

Typical commands and their timing stored in the event array would be:

20	FIL V1	20 seconds after the start of experiment, carry out actions to fill the loop on injector 1 (see above);
30	RUN SP1	10 seconds later, start syringe pump #1
30	INJ V1	Simultaneously, switch valve #1 to the inject position.
etc.		